Steady State Behaviour
of Stochastically Excited
Nonlinear Dynamic Systems

Steady State Behaviour
of Stochastically Excited
Nonlinear Dynamic Systems

PROEFSCHRIFT

ter verkrijging van de graad van doctor
aan de Technische Universiteit Eindhoven,
op gezag van de Rector Magnificus, prof.dr. M. Rem,
voor een commissie aangewezen door het College voor Promoties
in het openbaar te verdedigen op
woensdag 20 oktober 1999 om 16.00 uur

door

NATHAN VAN DE WOUW

geboren te Eindhoven

Dit proefschrift is goedgekeurd door de promotoren:

prof.dr.ir. D.H. van Campen
en
prof.dr.ir. J.J. Kok

Copromotor:
dr.ir. A. de Kraker

voor Kees en Mijntje

Contents

Abstract

Nonlinear, dynamic systems subject to random excitations are frequently met in engineering practice. The source of randomness can vary from surface randomness in vehicle motion and environmental changes, such as earthquakes or wind exciting high rise buildings or wave motions at sea exciting offshore structures or ships, to electric or acoustic noise exciting mechanical structures. The research goals are, firstly, the computation of stochastic, nonlinear response characteristics (with accuracy and efficiency as important criteria) and, secondly, the investigation and thorough understanding of stochastic, nonlinear response phenomena.

The desire to compute response characteristics, such as the statistical moments and the power spectral density of the response of these systems, leads to the development of methods that can be used to approximate this response. The necessity of approximation is caused by absence of analytical solutions for general, nonlinear systems.

The excitations, that will be studied, are stationary, Gaussian processes. These processes can be white noise processes or processes with band-limited frequency spectra. The nonlinear system, investigated throughout this thesis, is a piece-wise linear system, which exhibits a nonlinearity frequently met in engineering practice. Furthermore, an impacting beam system is studied both experimentally and numerically.

One could classify the approximation methods, developed and discussed in this thesis, as follows: Monte Carlo simulation using numerical integration methods; linear approximation methods; and nonlinear approximation methods. When the excitation is a (Gaussian) white noise process, classical integration schemes cannot be used to obtain sensible results. Suitable integration schemes are based on Itô calculus. These schemes can be used to compute the response very accurately. Therefore, it is an effective method for the investigation of nonlinear, stochastic response phenomena. Methods that are frequently used in literature, such as closure techniques and stochastic averaging, merely pursue information regarding the statistical moments. However, the information in the frequency domain is essential for a thorough understanding of the system's behaviour. Specifically nonlinear response phenomena are non-Gaussian response, multiple resonance frequencies and, for asymmetric nonlinearities, high-energy low-frequency spectral content (outside a resonance range). An improved understanding of these phenomena can be obtained by applying band-limited noise excitations and comparing the resulting response characteristics to the response characteristics of the same system, when excited by periodic excitations. In this way, stochastic equivalents of harmonic and subharmonic solutions can be

perceived. These phenomena can help to understand the occurrence of the multiple resonance frequencies that were observed in the response to white noise excitations. Knowledge on the periodic system behaviour can, therefore, fruitfully support the investigation and understanding of stochastic system behaviour and vice versa.

However, when using numerical integration, extensive CPU-time is needed to reduce statistical errors on the estimated response characteristics. This becomes even more important when MDOF systems are studied.

Therefore, the development of computationally more efficient approximation methods is desirable. The first class of approximation methods, that will be discussed, uses linear models; the response characteristics of a linear model can be evaluated analytically and thus efficiently. A well-known and widely used method is statistical linearization. However, a serious drawback of the method is the fact that, for strong nonlinearities, this method fails to predict the specifically nonlinear, frequency domain characteristics of the piece-wise linear system properly. Consequently, energy estimates produced by this method appear to be structurally too low. This can be dangerous when such estimates are used in system failure criteria. Therefore, a hybrid simulation-linearization method is developed that builds a higher-order, linear model with approximately the same output power spectral density (for a reference excitation) as the original, nonlinear system. This idea was initiated by the knowledge gained while studying the response characteristics of nonlinear systems in the frequency domain. The method makes use of a limited set of simulated data (applying the reference excitation) on the power spectral density of the response of the nonlinear system. Using the method of spectral factorization, a higher-order, linear, stable, causal model can be constructed, which exhibits approximately that same spectral output to the reference excitation. Consequently, the specifically nonlinear frequency domain phenomena, such as multiple resonance frequencies and high-energy low-frequency spectral content, are modelled in a linear fashion. Such a model can, then, be used to estimate the response characteristics of the original, nonlinear system very efficiently in case of other excitations. The method provides more accurate results than statistical linearization.

In order to obtain even more accurate results in an efficient manner, one could consider accepting one extra level of modelling complexity: nonlinear models. The models that are used are finite-order Volterra systems, which can be described using merely polynomial nonlinearities. The response characteristics for such systems can be evaluated efficiently compared to numerical integration. Moreover, using such models the response characteristics of the original, nonlinear system can be predicted very accurately.

Furthermore, the systematic reduction of the original, nonlinear system to linear models or (nonlinear) Volterra systems sheds light on the root of the nonlinear, stochastic response phenomena of the original system and thus enlarges the fundamental understanding of stochastic, nonlinear, dynamic system behaviour.

Samenvatting

Niet-lineaire, dynamische systemen, die belast worden door stochastische krachten, komen veelvuldig in de praktijk voor. De bron van stochasticiteit kan bijvoorbeeld voortkomen uit onregelmatigheden in het rij-oppervlak van voertuigen of uit de willekeurigheid van omgevingsvariabelen, zoals aardbevingen of wind die hoge gebouwen belasten. Ook golven op zee, die schepen of boorplatformen belasten, worden in het algemeen stochastisch gemodelleerd. Verder worden mechanische structuren vaak geëxciteerd door stochastische krachten van akoestische of electrische aard. Dit onderzoek heeft twee belangrijke doelstellingen resulterend in twee onderzoekslijnen. De eerste onderzoekslijn betreft de berekening (approximatie) van de stochastische eigenschappen van de responsie van stochastisch geëxciteerde, niet-lineaire, dynamische systemen, met nauwkeurigheid en efficiëntie als belangrijke criteria. Ten tweede, is het zeer belangrijk om fundamenteel begrip op te bouwen omtrent stochastische, niet-lineaire responsie fenomenen.

De responsie van niet-lineaire, dynamische systemen zal, in het algemeen, benaderd moeten worden, daar analytische oplossingen niet voorhanden zijn. Een belangrijk deel van dit proefschrift zal dan ook gewijd zijn aan de ontwikkeling en studie van dergelijke approximatie methodes. Met deze methodes kunnen dan de stochastische eigenschappen van de responsie, zoals de statistische momenten en de spectrale energie dichtheid, benaderd worden.

De excitaties, die toegepast worden, zijn stationaire, Gaussische processen. Dit kunnen witte-ruis-processen zijn of processen met een beperkte frequentie bandbreedte. Deze excitaties worden onder andere toegepast op een stukgewijs-lineair systeem. De niet-lineariteit in dit systeem vertegenwoordigt een veelvuldig in de praktijk voorkomende niet-lineariteit. Verder wordt ook een experimenteel balk-systeem beschouwd met een lokale niet-lineariteit in de vorm van een elastische stop.

De benaderingsmethodes, die aan bod komen, kunnen als volgt geclassificeerd worden: Monte-Carlo-simulatie (gebruikmakend van numerieke integratie), lineaire benaderingsmethodes en niet-lineaire benaderingsmethodes. Wanneer de excitatie een witte-ruis-proces is, kunnen klassieke integratie schema's niet gebruikt worden om de responsie op een zinnige wijze te benaderen. Geschikte numerieke integratie schema's kunnen in dit geval gebaseerd worden op Itô-calculus. Deze schema's kunnen gebruikt worden om de responsie zeer nauwkeurig te benaderen. Numerieke integratie is daarom ook een zeer geschikte methode om het niet-lineair gedrag van stochastisch geëxciteerde, dynamische systemen te onderzoeken. In de literatuur worden vaak methodes gebruikt, zoals stochastische middeling en sluitings-

technieken, welke slechts informatie verschaffen ten aanzien van de statistische momenten van de responsie. Echter, de informatie in het frequentie-domein (zoals de spectrale energie-dichtheid) blijkt essentiëel te zijn voor een goed begrip van niet-lineair, stochastisch systeemgedrag. Specifiek niet-lineaire, stochastische fenomenen zijn: niet-Gaussische responsie, meervoudige resonantie-frequenties en, voor asymmetrische niet-lineariteiten, veel laagfrequente energie in de responsie (buiten een resonantie-gebied). Het begrip ten aanzien van deze fenomenen kan vergroot worden door de responsie van hetzelfde systeem te bekijken voor excitaties met een beperkte frequentie bandbreedte. Bovendien werkt het vergelijken van de stochastische en periodieke responsie karakteristieken van hetzelfde systeem sterk begripsverruimend. Al doende, kunnen stochastische equivalenten van harmonische en subharmonische oplossingen waargenomen worden. Deze fenomenen werpen licht op het bestaan van meervoudige resonantie-frequenties in de responsie op witte-ruis-excitaties. Geconcludeerd kan worden dat kennis ten aanzien van het periodiek gedrag van een systeem van groot nut kan zijn bij de studie van het stochastische gedrag van dat systeem en vice versa.

Wanneer numerieke integratie wordt toegepast als benaderingstechniek, kan de rekentijd aanzienlijk oplopen om de statistische fouten op de stochastische responsie eigenschappen voldoende te reduceren. Dit probleem wordt nog belangrijker wanneer systemen met meer graden van vrijheid onderzocht worden.

Als gevolg hiervan is de ontwikkeling van (qua rekentijd) efficiëntere benaderingsmethodes noodzakelijk. De eerste klasse van alternatieve benaderingsmethodes, die behandeld wordt, is die van benadering door middel van lineaire modellen. De responsie van een lineair model kan, over het algemeen, analytisch bepaald worden, hetgeen dus rekentechnisch erg efficiënt is. Een zeer bekende lineaire methode staat bekend als statistische linearisatie. Echter, een belangrijk nadeel van deze methode is dat deze, voor het stukgewijs-lineaire systeem, de specifiek niet-lineaire, frequentie-domein fenomenen niet goed kan benaderen (voor sterke niet-lineariteiten). Als gevolg hiervan zijn de schattingen van de variantie van de responsie van dit systeem ook slecht. Deze onnauwkeurigheid kan bijzonder gevaarlijk zijn wanneer deze schattingen gebruikt worden in faal-criteria voor bepaalde systemen. Daarom is er in dit proefschrift een hybride simulatie-linearisatie methode ontwikkeld, waarin een lineair model met een hogere dimensie dan het originele niet-lineaire systeem wordt geconstrueerd. Dit model geeft, bij benadering, hetzelfde responsie spectrum als het originele systeem voor een bepaalde referentie-excitatie, waar het model op gebaseerd is. Het idee voor deze methode is ontstaan door de frequentie-domein-fenomenen van de responsie van het niet-lineaire systeem goed te bestuderen. De methode maakt gebruik van een beperkte set gesimuleerde data van het niet-lineaire systeem voor een bepaalde referentie-excitatie. Gebruikmakend van de methode van spectrale factorizatie kan een lineair, stabiel, causaal, minimum-fase-model (van hogere dimensie) geconstrueerd worden. De spectrale energie-dichtheid van de responsie van dit model benadert dan die van het niet-lineaire systeem voor de referentie-excitatie. De meervoudige resonantie-frequenties en de grote hoeveelheid laagfrequente energie worden hierdoor op een lineaire wijze gemodelleerd. Dit model kan vervolgens gebruikt worden om de stochastische eigenschappen van de responsie van het niet-lineaire systeem op andere stochastische excitaties op zeer efficiënte wijze te benaderen. De

methode blijkt nauwkeuriger resultaten te leveren dan statistische linearisatie.

Met het doel om, met behoud van efficiëntie, nog nauwkeurigere resultaten te behalen is de stap naar benadering met behulp van niet-lineaire modellen gezet. De gebruikte modellen zijn Volterra-systemen van eindige orde. Hierin spelen slechts niet-lineariteiten van polynoomvorm een rol. De responsie-karakteristieken van deze systemen kunnen relatief efficiënt geëvalueerd worden vergeleken met de numerieke integratie-technieken, die voor het het originele, niet-lineaire systeem gebruikt moesten worden. Bovendien, blijkt deze methode zeer nauwkeurige resultaten te leveren. Dit komt doordat de niet-lineaire responsie-fenomenen van het originele systeem ook op een niet-lineaire wijze gemodelleerd worden.

De systematische reductie van het originele, niet-lineaire systeem naar eerst lineaire modellen en vervolgens niet-lineaire modellen verheldert de oorsprong van de niet-lineaire, stochastische responsie-fenomenen van het originele, niet-lineaire systeem. Hierdoor wordt het fundamentele begrip van niet-lineair, stochastische systeem-gedrag sterk vergroot.

Notation

General notation

$\underline{0}$	null vector or matrix
$\underline{I}_n$	$n \times n$ identity matrix
$\underline{A}^T$	transpose of a vector or matrix $\underline{A}$
Trace$(\underline{A})$	trace of a matrix $\underline{A}$
$\det(\underline{A})$	determinant of a matrix $\underline{A}$
$\underline{A}^{-1}$	inverse of a matrix $\underline{A}$
$\underline{A}^*$	complex conjugate of a matrix $\underline{A}$
$\mathcal{F}$	Fourier operator
$\mathcal{L}$	Laplace operator
Re(x)	real part of complex number x
Im(x)	imaginary part of complex number x
erf(x)	error function with argument x
$\mathbb{R}$	collection of real numbers
$\mathbb{C}$	collection of complex numbers
$\dot{a}$	total derivative of a with respect to time t
$E\{x\}$	expected value of stochastic variable x
$x_E(t)$	zero-mean equivalent of the stochastic process $x(t)$

Latin symbols

a	term in a differential equation
$\check{a}$	drift term in an Itô stochastic differential equation
a_i	coefficients of the denominator polynomial of the transfer function
b	term in a differential equation
$\check{b}$	diffusion term in an Itô stochastic differential equation
$b^{(n)}$	stochastic step function
b_i	coefficients of the numerator polynomial of the transfer function
c	damping coefficient
d	force
e	restitution coefficient
$f_X(x)$	probability density function of random variable X
h	distance between the two half spheres of the beam-impact system
h_a	height accelerometer
h_b	thickness beam

h_j	j^{th} order Volterra kernel
h_{tri}	triangular Volterra kernel
h_{sym}	symmetric Volterra kernel
k	stiffness linear spring
k_{nl}	stiffness one-sided spring
l	length beam
l_e	length elastic part of beam
m	mass
m_{eff}	effective mass
m_a	mass accelerometer
m_s	mass half sphere
m_{tot}	total mass rigid part of beam
n	natural coordinates
n_a	order of the denominator polynomial of the transfer function
n_b	order of the numerator polynomial of the transfer function
p	order of a finite order Volterra model
	pressure
p_0	maximum pressure
p_w	weak order of convergence of a stochastic integration scheme
p_s	strong order of convergence of a stochastic integration scheme
q	weighting coefficient
r	radius
r_j	Rayleigh-Ritz coefficients
r_n	Fourier coefficients
t	time
t_0	initial time
u	input
w_b	width beam
x	state variable
x_0	initial state
y	output variable
	prescribed displacement of the rigid frame of the beam-impact system
A	cross-section
	quotient output/input spectrum
$\underline{A}$	system matrix
A_b	cross-section of beam
$\underline{C}$	damping matrix
C_{xx}	covariance of stochastic process $x(t)$
D	intensity of a white noise process
$\underline{D}$	bilinear system matrix
E	expected value operator
E_b	Young's modulus of elastic beam
E_r	reduced Young's modulus
$F_X(x)$	probability distribution function of stochastic variable X
F_c	contact force between the two half spheres of beam-impact system

G_r	Green's function
H	Transfer function or frequency response function
I	Itô integral
$\hat{I}$	Itô sum
I_R	Riemann integral
$\hat{I}_R$	Riemann sum
I_{RS}	Riemann-Stieltjens integral
$\hat{I}_{RS}$	Riemann-Stieltjens sum
I_b	second moment of area for the cross-section of the beam
$\underline{J}$	moment of inertia matrix
J_r	moment of inertia of the rigid part of the beam
J_s	moment of inertia of the half sphere
J_a	moment of inertia of the accelerometer
$\underline{K}$	stiffness matrix
K_H	Hertzian stiffness parameter
M	number of inputs
$\underline{M}$	mass matrix
N	number of state variables
O	object or target function
$\underline{P}$	transformation matrix
R_s	radius half sphere
R_r	reduced radius of curvature
R_{xx}	autocorrelation function of a stochastic process $x(t)$
S	estimate for the standard deviation
S_{xx}	power spectral density of a stochastic process $x(t)$
S_0	constant power spectral density of a white noise process
T	kinetic energy
$\underline{U}$	matrix of eigencolumns
V	potential energy
	variation of a function
W	Wiener process

Greek symbols

α	nonlinear stiffness parameter
β_j	linearization or bilinearization coefficients
γ	skewness
$\hat{\gamma}$	estimate for the skewness
$\delta(t)$	Dirac delta function
δ	displacement elastic beam relative to rigid frame
$\epsilon(-x)$	step function
ε	error
ε_{lin}	error in statistical linearization
ε_{bilin}	error in statistical bilinearization
ζ	dimensionless damping parameter
η_{X^p}	p-th order central moment of random variable X

$\theta(x)$	step function
κ	kurtosis
$\hat{\kappa}$	estimate for the kurtosis
λ	linear system parameter
μ	mean
	hysteresis damping coefficient
μ_{X^p}	p-th order statistical moment of random variable X
μ_D	cubic stiffness parameter of the Duffing system
ν	Poisson's ratio
ξ	white noise process
ρ	mass-density
σ	standard deviation
τ	time variable
ψ	multi-dimensional polynomial function
ω	angular frequency
ω_{min}	minimal angular frequency in a band-limited excitation
ω_{max}	maximal angular frequency in a band-limited excitation
ω_{band}	$[\omega_{min}\ \omega_{max}]$
ω_{bw}	bandwidth of band-limited excitation ($\omega_{max} - \omega_{min}$)
ω_f	undamped angular eigenfrequency of a filter
ω_e	angular frequency of a harmonic excitation
ω_{nl}	(nonlinear) harmonic, angular resonance frequency
Δt	time step
ΔW	step in a Wiener process
Ω	parameter vector
Φ	transition matrix
	phase

Constants

i	imaginary unit
e	natural logarithmic base
π	circumference to diameter ratio of a circle

Abbreviations

CNC	cumulant neglect closure
FFT	fast Fourier transform
LVDT	linear variable differential transformer
MDOF	multiple degree of freedom
ODE	ordinary differential equation
SDE	stochastic differential equation
SDOF	single degree of freedom
psd	power spectral density
pdf	probability density function

1 Introduction

1.1 Objective of the thesis

Thorough understanding of the dynamic system behaviour is of major importance in many fields, such as mechanical, electrical, chemical and civil engineering and the biological and economic sciences. The interest towards this subject stems from the desire to predict the dynamic behaviour of a system. Using this knowledge of the system dynamics, one can either adjust one's actions (think of the weather or economics) or modify or influence the system. The modification of a system may be accomplished in its design process. Thus, dynamics can play an important role in the optimisation part of a system's design. In system's design one can either think of achieving specified, desirable goals (with respect to the system's behaviour) or the minimisation of the probability of system failure. Of course, the understanding of system dynamics is also of major importance for the control of systems. It should be noted that this thesis was written from a background of mechanical engineering. Consequently, the systems that will be investigated stem from this background.

In order to illuminate the scope of the thesis within the research field of system dynamics, one could distinguish, firstly, between linear and nonlinear systems and, secondly, between stochastic and deterministic systems. The research field of linear, deterministic systems (area A in figure 1.1) has been covered extensively by former
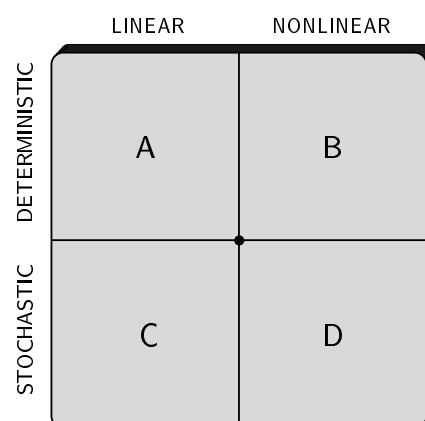
Figure 1.1: Research areas in dynamics.

work [Zadeh and Desoer, 1963; Meirovitch, 1997; Den Hartog, 1956]. The resulting knowledge is generally considered to be well-known.

However, many practical engineering systems exhibit nonlinear behaviour. The source of the nonlinearity can vary from nonlinear springs, nonlinear dampers, dry friction, and backlash to contact phenomena. Examples of nonlinear dynamic system components are aircraft landing gear, ships colliding against fenders, bearings, axle suspensions for vehicles, snubbers in solar panels on satellites, suspension bridges, offshore structures, rattle in cog-wheels and so on. The nonlinearity can change the behaviour of the system dramatically, both in the qualitative and the quantitative sense. Therefore, extensive research has been done in the field of nonlinear dynamic systems subject to deterministic excitations (area B in figure 1.1) [Nayfeh and Mook, 1979; Nayfeh and Balachandran, 1995]. A lot of interesting, nonlinear phenomena can be encountered while observing the response of such systems. Specific nonlinear response characteristics are, for example, harmonic and subharmonic solutions, superharmonic resonances, chaos, bifurcations, multiple (non-unique) solutions and so on [Thompson and Stewart, 1986; Parker and Chua, 1989; Fey, 1992; Van Campen et al., 1997a]. Here, harmonic solutions are not sinusoidal solutions but solutions with the same period time as the excitation. These harmonic solutions are also called period one solutions. Subharmonic solutions are of a higher period than the excitation and are also called higher-period solutions.

An aspect that partly defines the scope of this work is the type of nonlinearities that will be studied. The nonlinearities that will be used are of a physical nature. Consequently, geometrical nonlinearities, which can often be encountered in multibody systems, are excluded from this research. The actual type of nonlinearities will not be limited to the polynomial or even the analytical kind. It can even be discontinuous and, in general, we will not limit ourselves to weak or moderate nonlinearities.

In this thesis stochastic systems will be investigated. The meaning of the word 'stochastic' should be clarified in order to be able to discuss the practical relevance of this field of research. Of course, stochasticity indicates randomness. A very essential distinction can be made between what will be termed fundamental randomness and modelled randomness. Fundamental randomness directs to a true randomness, where modelled randomness is a randomness that is merely used to model a process, which is in essence deterministic, however, too complex to model it as such. An example of the latter form of randomness could be 'rolling the dice'. One could assume that the outcome of a throw would be predictable when all the variables, that influence the outcome, could be incorporated properly within the model. However, one could also assume that mere '(bad) luck', referring to a true randomness from a source beyond rational comprehension, influences the outcome of a throw. However, the well-known luck-factor in the game could again be explained by the fact that the extreme physical complexity of the process of a throw prevents us from building a proper deterministic model. A practical model would then incorporate randomness, either true or merely modelled. Of course, this distinction is an interesting topic for a philosophical debate. However, the subject will be put to rest here. The point is that the stochasticity in a model can either model a physical randomness or model a deterministic process of very high complexity. The former example clarifies the

extensive practical use of stochastic modelling.

The model form of dynamic systems, which will be used throughout this thesis is a continuous one, namely, the differential equation.

The stochasticity can be introduced in the model (i.e. the differential equation(s)) in several ways. Firstly, one could consider a dynamic system with random forcing. These 'stochastic excitations' are often encountered in practice. The source of randomness can vary from surface randomness in vehicle motion, and environmental changes, such as earthquakes or wind exciting high rise buildings or wave motions at sea exciting offshore structures or ships, to electric or acoustic noise exciting mechanical structures. The stochastic excitation exhibits a randomness in time. These kind of uncertainties are generally modelled as stochastic processes. The same kind of stochasticity is introduced when one (or more) of the system parameters is a random process. Often, this can be viewed (mathematically) as a random excitation, either parametric or external. Secondly, consider a system with system parameters or boundary conditions, which are fixed in time, though random. These system characteristics can be modelled using random variables (not processes) obeying a certain probability distribution. In this perspective, one could also consider random initial conditions (of the differential equation). In this thesis, merely the influence of the first type of randomness (the stochastic excitation) on nonlinear, dynamic system behaviour will be studied.

Another important choice will be the assumption that the excitations (forcings, inputs) or system parameters can be modelled as stationary, stochastic processes. Consequently, only the steady state behaviour of the systems will be investigated. The motivation for this choice is that in most practical situations the random excitations or random system parameter variations are stationary or are non-stationary on a large time-scale. This creates the possibility to model these as being stationary.

The kind of practical, stochastic excitations, mentioned before, generally has relatively broad-banded power spectral densities. The major part of this thesis will deal with this kind of excitations. However, one could also think of stochastic excitations that are near-periodic. In system's design, components are often designed to be excited periodically. Examples are engines, rotor dynamic systems such as bearings, components of CD players, and so on. However, in practice these forces often are only nearly periodic due to, for example, inevitable design imperfections or environmental disturbances. Thus, in reality near-periodic excitations are frequently met. The deviation from periodicity can have a significant effect on the response of such systems in comparison to the expected periodic response characteristics. This will be shown to be especially true for nonlinear systems.

Clearly, the introduction of stochasticity within a system model can be necessary in many practical situations. Valuable contributions on the subject of linear, stochastic systems, (area C in figure 1.1), can be found in Kwakernaak and Sivan [1972]; Roberts and Spanos [1990]; Chen et al. [1995]. Generally, linear systems can be investigated using analytical techniques. However, the scope of the thesis lies within research area D (figure 1.1) and thus encloses the topic of nonlinear, stochastic, dynamic systems.

In the following paragraphs, the research goals will be presented. Within the scope defined earlier, these goals can be formulated as follows: the computation,

investigation, and thorough understanding of general, nonlinear, stochastic response characteristics. The first element, 'computation', implies the search for methods (semi-analytical or numerical) that can be used to compute stochastic response features. The response information, which is pursued, is not only information regarding the statistical moments and the probability density function, but also includes the power spectral density of the response (e.g. the energy distribution in the frequency domain). An important feature of a response computation method is its balance between accuracy and efficiency. However, this is not the sole perspective from which these methods will be viewed upon. Other features of these methods are the variety of systems and random excitations, which it can tackle. Moreover, the specific set of stochastic response characteristics that do become available by using the method is an important characteristic of the method.

It should be stressed that the mere computation (including its accuracy and efficiency) represents only a part of the whole objective of this research. The actual investigation of the nonlinear, stochastic response phenomena, that become available through computation, is of major importance. This effort should lead to a thorough understanding of the root of certain nonlinear, stochastic response phenomena. The study of these phenomena can be characterised by two things. Firstly, a great deal of attention will be given to frequency domain characteristics. In literature, often merely the probability density function (and statistical moments) of the response are covered. However, it will become clear that crucial information towards the true understanding of stochastic nonlinear, dynamic behaviour lies in the knowledge of the power spectral density of the response. Secondly, the stochastic response features will be compared to the response characteristics in case of periodic (sinusoidal) excitation. Too often, the fields of deterministic and stochastic excitations are kept separate. A great deal can be learned by observing both simultaneously. Periodic response characteristics can help to understand certain stochastic response phenomena. Conversely, knowledge on the stochastic response features of a system can provide information about the periodic response of that system.

Once a thorough understanding of the stochastic behaviour of a system has been gained, ideas for the development of new response computation methods can be created.

From a more general perspective, the research approach followed, incorporates both a deductive as well as an inductive side. The actual development of response computation methods mainly follows a deductive path. However, the interpretation and the path towards physical understanding of the source of certain nonlinear, stochastic phenomena has both a deductive and inductive side. As mentioned before there can be a fruitful interaction between those two.

1.2 Response approximation methods

1.2.1 Problem definition

In this section, a brief literature survey will be given on the existing methods for the computation of stochastic response characteristics of nonlinear, dynamic systems.

Beforehand, the class of systems and the class of excitations, which jointly determine the class of problems (within area D in figure 1.1) to be tackled, should

be properly defined. Furthermore, the response information that should become available by the application of the methods should be defined. Then, the methods, discussed thereafter, can be judged with respect to their suitability to tackle those problems.

The class of systems, which defines the scope of interest, can be characterised by the following features:

- systems that can be modelled by one or more differential equations;

- polynomial, non-polynomial, and even discontinuous (non-smooth) nonlinearities;

- Multi-Degree-Of-Freedom (MDOF)-systems;

- strong nonlinearities;

- stationary systems.

The choice to aim for methods applicable to systems with a general form of nonlinearity stems from practical considerations. In practice, namely, the form of the nonlinearity is rarely of a purely polynomial kind. Furthermore, discontinuous nonlinearities, which will be studied extensively throughout this thesis, can be found in many engineering systems, for example ships colliding against fenders on quay sides, snubbers in solar panels on satellites, suspension bridges, stops in axle suspensions for vehicles and so on. Moreover, most engineering systems essentially are MDOF systems. However, it should be noted that, when complex nonlinearities are considered, it can be advisable to study a Single-Degree-Of-Freedom (SDOF)-system first. This is surely the case when one is attempting to understand specific, nonlinear, stochastic response phenomena. The decision not to limit ourselves to merely moderate nonlinearities is initiated by the desire to observe, investigate, and understand truly nonlinear behaviour.

The class of stochastic excitations can be defined by the following characteristics:

- Gaussian excitations;

- excitations with broad-banded as well as narrow-banded spectra, either white or non-white;

- external as well as parametric excitations;

- stationary excitations.

In most practical situations, the random inputs can be accurately modelled as normally distributed processes; so, the deviation from normality is not significant. Hereby, we have, thus, imposed a restriction on the probability density function of the excitations. However, a wide variety of spectral energy distributions for the excitations is incorporated within the research scope. Most excitations, which stem from environmental loads acting on mechanical systems, can be modelled by broadbanded random processes. Situations with parametric excitations can easily be encountered when one of the system parameters varies randomly in time.

The desired 'steady state' response characteristics are:

- statistical moments and the probability density function;

- power spectral density.

In literature, the investigation of the stochastic response of dynamic systems is often merely focussed on the statistical moments and the probability density function. Consequently, essential information, regarding the dynamic response, remains hidden. Therefore, it is of the utmost importance that the response information in the frequency domain, the power spectral density function, is incorporated in the investigations. It will become clear, throughout this thesis, that the information in the frequency domain exhibits many interesting, nonlinear, stochastic phenomena. These frequency domain response characteristics can, moreover, help to understand the root of specific tendencies in the statistical moments of the response.

As mentioned earlier, the research scope is restricted to both stationary (time-independent) systems and stationary excitations. We, therefore, are merely interested in the steady state behaviour of the systems.

In the following subsections, several existing methods will be discussed, with respect to their suitability to tackle the problems described above. In the majority of the methods, that will be described, the assumption is made that the excitation can be idealised as Gaussian white noise. The practical validity and effectiveness of 'white noise modelling' will be discussed in chapter 2. Realisations of a white noise process at two distinct points in time are independent by definition, no matter how small the time interval between them. A more formal definition of a white noise process will also be given in chapter 2. When the excitation is a white noise process, the response of the system can be represented by a Markov process. As a consequence, the unnormalized probability density function of the response is governed by a partial differential equation, called the Fokker-Planck-Kolmogorov (FPK) equation [Caughey, 1963a; Lin, 1967; Melsa and Sage, 1973]. The vast majority of the existing methods makes use of the Markov process assumption. In practical applications, the justification of the Markov process assumption is usually based on the following sufficient condition: the increments of the response, during two non-overlapping time intervals, are independent events. This ideal property can never be found in a real physical process. However, when the time increments are viewed as observation time laps, the length of these time laps can be chosen to ensure the independence of the increments. On the other hand, one will have to choose the observation time intervals small enough in order to avoid loss of essential information on the dynamics of the system. As long as there is a randomness in a real physical process, it is possible to select a long enough observation time interval to ensure Markov-like appearance of the observed increments.

1.2.2 Monte Carlo simulation

A method for the estimation of the response statistics of randomly excited, nonlinear systems, within any desired confidence level, is based on random computation experiments, popularly known as Monte Carlo simulation, see Rubinstein [1981]. For a review article on Monte Carlo simulation, see Spanos and Mignolet [1989].

Monte Carlo simulation is generally used to validate the results of other approximation methods, discussed in the following subsections. Namely, Monte Carlo

simulation can provide very accurate results. However, this accuracy can only be obtained at the cost of computational efficiency.

In Monte Carlo simulation, one generates a realisation of the excitation. This realisation of the excitation is used to compute a realisation of the response by numerical integration. Obviously, this approach can be applied to estimate both stationary and non-stationary response statistics. The higher the number of realisations used, the smaller the expected deviation of the obtained numerical values from the theoretical values of the response statistics will be. In order to compute statistical properties of the response accurately, many realisations are required. Therefore, many computationally expensive integrations will have to be executed. Obviously, this method is very inefficient from a computational point of view. This problem becomes even more evident for MDOF systems.

However, the method of numerical integration can tackle problems incorporating the entire class of systems and excitations described in section 1.2.1. Furthermore, both the statistical moments (and probability density function) and the power spectral density can be estimated from the time series of the response that can be computed by numerical integration. This method, thus, answers to all our demands. Unfortunately, these benefits are gained at the cost of computational efficiency.

It should be noted, that the necessity of a large number of records can often be eliminated if the interest is confined to stationary response statistics. In engineering practice, it is quite common to assume ergodicity with respect to a specific statistical moment for stationary processes. This assumption allows the determination of this specific ensemble statistical moment by using its temporal counterpart, which is calculated by using a single sample function of the response.

A subject that should be addressed is that of the numerical integration of the differential equations describing the systems. Excitations with a broad-banded power spectral density are generally modelled as white noise processes. In that case, the differential equation is termed a 'stochastic differential equation' (SDE)– as opposed to an ordinary differential equation (ODE). The concepts of a white noise process and the SDE will be discussed extensively in chapter 2. Furthermore, extensive attention will be given to the numerical solution of a SDE. It will be set forth why classical integration schemes can not be used to solve initial value problems of SDEs. Therefore, other numerical integration schemes are developed. An extensive survey on integration schemes for SDEs can be found in Kloeden and Platen [1992].

1.2.3 Perturbation method

In the classical perturbation method, see Crandall [1963], Lin [1967] and Nayfeh [1973, 1981], the basic idea is to expand the solution to the nonlinear set of equations in terms of a small scaling parameter, which characterises the magnitude of the nonlinear terms in these equations. The first term in the expansion is simply the linear response, which is the response when all the nonlinearities in the system are removed. The subsequent terms express the influence of the nonlinearity. As with perturbation in general, the calculations are usually lengthy and rapidly become more tedious as the order of the scaling parameter increases. In practice, results are usually obtained only to the first order in the scaling parameter. The method is, therefore, only valid for small perturbations. Consequently, the perturbation method

can only be applied effectively when weakly nonlinear systems are considered.

1.2.4 Fokker-Planck equation method

The Fokker-Planck (FPK) equation method can provide information on the stationary (or non-stationary) unnormalized probability density function of the response of a dynamic system. The FPK equation is a partial differential equation for the probability density function of the response incorporating partial derivatives to this response (and time, in case of a non-stationary probability density function). This equation should be solved under appropriate boundary (and initial) conditions. For a more detailed discussion of the Fokker-Planck equation method refer to Caughey [1971] and Dimentberg [1982]. One could distinguish between methods providing exact solutions and methods providing approximate solutions of the FPK-equation.

Analytic solution

An exact, analytic solution of the non-stationary FPK-equation, which shows how the probability density evolves with time, is known only for very special first-order systems, for which the system's response is a scalar Markov process [Caughey and Dienes, 1961].

One of the first to obtain an exact, stationary solution of the FPK-equation for systems with a nonlinear restoring force and linear damping under external random excitations was Kramer [1940]. Caughey [1964], and Caughey and Ma [1983] extended the solutions to include certain types of nonlinear damping, but still restricted to external excitations. Yong and Lin [1987], Lin and Cai [1988] and Cai and Lin [1988b] developed a systematic procedure to obtain exact stationary response solutions for either external or parametric excitations, or both. The class of nonlinear systems, for which this procedure is applicable, is termed the class of generalised stationary potential, and is claimed to be the broadest class of solvable, nonlinear, stochastic systems up to that date. The method is said to be also applicable to MDOF systems. However, the class of generalised stationary potential is too narrow with respect to the class of systems that we strive to cover.

Approximate solution

Another approach to the problem of determining the time-dependent probability density function is to solve the FPK-equation by numerical means. A simple and efficient numerical scheme can be formulated by employing the random walk analogue Roberts [1978, 1981]. This method can only be applied to 1-dimensional FPK equations and is, therefore, not applicable to MDOF systems. The numerical integration of the FPK-equation for MDOF systems quickly becomes very cumbersome, because of the high dimension of the probability space that is to be discretized.

Summarising, it can be concluded, that the Fokker-Planck equation method is not suitable to be applied to a wide class of practical MDOF systems. An even more important shortcoming of the method is that is does not provide information on the power spectral density of the response.

1.2.5 Stochastic averaging

The method of stochastic averaging has proven to be a very useful tool for deriving approximate solutions to problems involving the vibration of weakly damped systems to broad-band random excitation. It was proposed initially by Stratonovich [1963]

for solving problems concerning noise-excited, dynamic systems. Subsequently, Stratonovich's method was justified and interpreted rigourously by Khasminskii [1966] and Papanicolaou and Kohler [1974]. For reviews on the stochastic averaging method see Roberts and Spanos [1986] and Zhu [1988].

The basic idea is to use the Markov approximation for the response, so that the probability density function can be described by the FPK-equation. The stochastic averaging method was devised to obtain the coefficient functions in this partial differential equation. For a rederivation of the formulas required for the application of Stratonovich's stochastic averaging method, see Lin [1986].

The goal of the method is to simplify the FPK-equation, or even reduce the dimension of the FPK-equation [Zhu, 1988]. Thus, by using stochastic averaging methods, the difficulties in solving the FPK-equation are relieved and the range of application of the FPK equation method can be extended.

In random vibration studies, the stochastic averaging method has been applied principally to systems with one degree of freedom. Often, the equation of motion is a one-dimensional, second order differential equation. Then, the stochastic averaging method enables the basic two-dimensional (in mechanical systems often displacement and velocity) Markov process governing the response to be replaced, approximately, by a one-dimensional Markov process governing an envelope amplitude process. The appropriate FPK-equation for the envelope amplitude can be easily solved analytically to yield simple expressions for the stationary probability distribution of the amplitude process. By considering an associate phase process, approximate analytical expressions for the joint distribution of the response displacement and velocity can be derived. The reduction in dimension of the governing FPK-equation, from two to one, also considerably simplifies the computation of non-stationary or transient solutions.

In general, the application of the stochastic averaging method is constrained to weakly damped systems. For the application to systems with high damping, the reader is referred to Sri Namachchivaya and Lin [1988]. Furthermore, the application of the method is generally limited to SDOF systems. The application to MDOF systems is very limited due to the difficulties in solving a multi-dimensional FPK-equation. However, it should be noted that externally as well as parametrically excited systems can be examined.

Furthermore, the standard stochastic averaging method is not particularly useful for examining the effect of nonlinear 'restoring forces'. Namely, the effect of these forces on the probability density function vanishes after averaging. However, in reality the nonlinear 'restoring forces' can markedly affect the probability distribution of the response. An approach to tackle this problem is 'stochastic averaging of the energy envelope' [Roberts and Spanos, 1986], in which the total energy of the system is approximated by a one-dimensional Markov process. Its probability distribution can then be described by the FPK-equation. This procedure is also only applicable to SDOF systems.

Summarising, the stochastic averaging method is not suitable to tackle problems incorporating MDOF systems with nonlinearities of a general form. Moreover, the method provides no information in the frequency domain.

1.2.6 Closure techniques

Closure techniques are also based on the Markov process assumption. A very important tool for the analysis of Markov processes is the Itô stochastic calculus [Itô, 1944, 1951a,b]. Using the Itô stochastic calculus, the so-called moment equations can be derived. The description of the Itô stochastic calculus and the actual derivation of the moment equations will be given in chapter 2. Generally, the moment equations are a set of differential equations in the statistical moments of the response. For stationary problems, the set of differential equations reduces to a set of algebraic equations.

It is well known that the response of linear, time-invariant systems subject to Gaussian excitations will generally be Gaussian too [Schetzen, 1980]. As a consequence, the (Gaussian) probability density function can be described using only the first-order and second-order statistical moments (corresponding to the mean and the mean square of the response). In this case, these moments can be determined by solving two algebraic moment equations.

However, for nonlinear systems the response to Gaussian excitations is generally non-Gaussian [Wiener, 1942]. The corresponding, non-Gaussian probability density function cannot be described using merely the first two statistical moments; higher-order moments become important. These statistical moments are, then, governed by an *infinite* hierarchy of coupled equations. Therefore, some form of a closure scheme has to be applied in order to make the set of moment equations solvable. In stochastic dynamics the term 'closure' refers to a procedure, by which an infinite hierarchy of equations governing the statistical moments of random quantities is truncated and the values of lower-order moments are computed approximately. One can distinguish between 'Gaussian' and 'non-Gaussian' closure.

Gaussian closure

The simplest closure scheme is the Gaussian closure, in which higher moments are expressed in terms of the first-order and second-order moments as if the random processes involved were normally distributed. In order to express these moments of higher order (higher than two) in terms of the first-order and second-order moments a 'cumulant neglect closure' (CNC) scheme is used, see Wu and Lin [1984]. In the Gaussian CNC, the closure of the infinite hierarchy of moment equations is achieved by setting the third-order and higher-order cumulants (also called semi-invariants) to zero; see Ibrahim [1985] or Nikias and Petropulu [1993] for a mathematical definition of the cumulants.

The result of the application of the Gaussian CNC is a closed set of nonlinear moment equations concerning the first-order and second-order moments. It should be noted that this can be implemented for MDOF systems. Moreover, stationary as well as non-stationary problems can be tackled. In the stationary case, the remaining moment equations are algebraic. When non-stationary moments are to be computed a set of differential equations will have to be solved by integration. The approximate moments can be used to form a Gaussian probability density function.

Gaussian closure can yield satisfactory results for systems with weak nonlinearities. However, the response of strongly nonlinear systems subject to Gaussian excitations will generally be non-Gaussian, and can, therefore, not be described

accurately using only the first two statistical moments.

Non-Gaussian closure

To overcome the shortcomings of Gaussian closure, non-Gaussian closure schemes were proposed by Wu and Lin [1984] and Crandall [1985]. In the non-Gaussian closure, non-Gaussian features of the response are taken into account. Mathematically speaking, the Gaussian closure can be generalised by successive inclusions of additional terms, which describe the non-Gaussian features in greater and greater detail. Of course, the complexity of the closed set of moment equations to be solved becomes greater. This becomes even more evident when the system has discontinuous nonlinearities.

Two approaches can be distinguished. In the first approach, the CNC is applied. Since the third-order and higher-order cumulants of Gaussian random variables are zero, successive improvements over the Gaussian closure can be obtained by including additionally the third-order, fourth-order, fifth-order cumulants and so on. For example, one could set the fifth-order and higher-order cumulants to zero. The result is a closed set of nonlinear equations concerning the first-order, second-order, third-order and fourth-order moments. This approach is applicable to MDOF systems with strong nonlinearities. However, the nonlinearities have to be of a polynomial kind. Furthermore, external as well as parametric excitations can be treated and stationary as well as non-stationary problems can be tackled. In the second approach, the unknown probability density function of the response is approximated by a truncated Gram-Charlier or Edgeworth series [Crandall, 1985; Ibrahim et al., 1985; Hampl and Schuëller, 1989], in which the first term is the Gaussian distribution. The coefficients of the finite series are then determined using the dynamic equations of motion of the system. Following this approach, problems which include nonlinearities of higher complexity can be treated as well. However, MDOF systems and non-stationary problems are difficult to treat, due to the difficulties in defining appropriate probability density functions for these cases.

It can be concluded that non-Gaussian CNC can be appropriate to tackle problems concerning MDOF systems and strong nonlinearities. However, the application to systems with discontinuous nonlinearities implies the solution of rather complex nonlinear equations. Furthermore, in Sun and Hsu [1987] it was stated that it might occur that the validity of the results, provided by the non-Gaussian CNC, is restricted to specific areas of parameter values of the equations of motion. In such cases, non-Gaussian CNC would provide erroneous results in certain parameter areas. However, in many cases, the extension to the non-Gaussian closure does lead to an improvement of accuracy of the moments. The most important drawback of the closure techniques, with respect to the aims of this research, is the fact that this method does not provide information on the power spectral density of the response.

1.2.7 Linearization methods

A natural method of attacking nonlinear problems is to replace the governing set of nonlinear differential equations by an equivalent set of linear differential equations; the difference between the sets being minimised in some appropriate sense. The stochastic linearization technique can be considered to be an extension of the equivalent linearization method for the treatment of nonlinear systems under deter-

ministic excitations [Krylov and Bogoliubov, 1943]. Caughey [1963b] was one of the first to apply the stochastic linearization technique to randomly excited nonlinear systems.

The basic idea of the statistical linearization approach is to replace the original nonlinear system by a linear one. This is done in such a way that the difference between the two systems is minimised in some statistical sense. In this way, the parameters of the linearised system are determined. The response of the nonlinear system is approximated by the response of the equivalent linear system. So, the unknown statistics of the response are evaluated approximating the response as a Gaussian process, when the excitation is assumed to be Gaussian. Recently, Roberts and Spanos [1990] provided a comprehensive account on statistical linearization.

The use of the Gaussian approximation for the response suggests that stochastic linearization is very close to Gaussian closure. For externally excited systems, the two approaches provide the same results. However, when parametric excitations are applied, different approaches can be used, which do not all show equivalence to Gaussian closure: linearization of the equations of motion; linearization of the Itô equation of the system; linearization applied to the coefficients of Itô's differential rule [Falsone, 1992]. The Itô equation and Itô's differential rule will be discussed in chapter 2. In Falsone [1992], it is shown that only the third approach is equivalent to Gaussian closure in case of parametrically excited systems. The methods are extended for application to MDOF systems, see Roberts and Spanos [1990] and Falsone [1992].

A feature which distincts statistical linearization from all the methods, discussed earlier (excluding numerical integration), is its capability to provide approximate information on the power spectral density of the response very easily. Moreover, the response statistics can be computed analytically, once the actual linearization has been performed. Consequently, the method is computationally very efficient compared to numerical integration.

The linearization approach can be applied to both white and non-white inputs. Furthermore, Zhu et al. [1993] have investigated a Duffing oscillator subjected to narrow-band excitation by means of simulation. It is well-known, that it is possible for nonlinear systems subjected to sinusoidal excitation to exhibit multiple stable solutions (depending on the initial conditions) in certain parameter areas. For narrow-band stochastic excitation, it is shown in Zhu et al. [1993] that for each combination of the parameters all the statistics of the stationary response are unique and independent of the initial conditions. However, in a certain domain of the parameter space there are two more probable motions in the stationary response and jumps between those more probable motions may occur. This phenomenon only occurs when the frequency band of the excitation is small enough. It was shown by Richard and Anand [1983] that the statistics of these more probable motions can be computed by means of the linearization technique. The 'multiple solutions' computed by the linearization technique correspond, to some extent, to the "local" behaviour of sample functions of the response. The response statistics of the total response can only be computed by linearization when it is known how much time the system spends in the two more probable motions. So, it can be concluded that the linearization can be applied to problems with a wide variety of excitation forms.

Furthermore, it can be applied to systems with non-polynomial and discontinuous nonlinearities.

The main limitation of the method lies in the fact that it will only provide accurate results for (very) weak nonlinearities.

So far, linearization of the equations of motion of nonlinear systems has been achieved by replacing the nonlinear terms in the equations of motion by zero-memory linear terms. This is optimal when the input is Gaussian. However, in the case of a nonlinear system the relevant input to the nonlinear term is the response process, which is often distinctly non-Gaussian (this becomes more evident for stronger non-linearities). So, conventional linearization is not optimal in these cases. Increased accuracy may be obtained through the introduction of memory into the linear substitution. A relatively straightforward approach to introducing memory has been given by Iyengar [1988]. The resulting linear system is of a higher order than the original nonlinear system. Therefore, the approach is called higher-order linearization. Iyengar [1988] has shown that, for the case of a Duffing oscillator excited by white noise, a fourth-order equivalent linear system leads to a significant improvement in accuracy, with regard to the mean square of the response. Moreover, the power spectrum obtained yields an estimate of the power spectrum of the response which shows two peaks, reflecting the existence of subharmonics in the system. This is in reasonable agreement with digital simulations. However, application to systems with discontinuous nonlinearities has not been investigated yet and problems are expected to occur with regard to the analytical computation of the derivatives of the nonlinear terms, which are needed in this approach.

1.2.8 Nonlinear methods

In equivalent nonlinear methods the original nonlinear system is replaced by an equivalent nonlinear system. The replacing, equivalent, nonlinear system should be a system of which the nonlinear stochastic response can be determined rather easily.

In the method proposed by Cai and Lin [1988a] and Cai et al. [1992], the original nonlinear system is replaced by a nonlinear system belonging to the class of generalised stationary potential. As mentioned in subsection 1.2.4, this class of systems is the broadest class of nonlinear systems of which exact solutions for the stationary response can be obtained. In order to choose an appropriate replacement system, in this method, a residual is defined as a measure of the difference between the two systems. This residual is defined as the error in the original FPK-equation, introduced by using the solution of the equivalent system as an approximation for the solution of the original system. The residual is minimised by means of the method of weighted residuals. This results in a set of constraints for obtaining an approximate stationary probability density function. One of the constraints coincides with the criterion of dissipation energy balancing. This criterion implies, that the average energy dissipation is the same for the original as it is for the replacement system. The other constraints are useful to calculate the equivalent conservative force of the equivalent system. When the equivalent system is known, the stationary probability density of this system can be determined and can be used as an approximate solution for the original system. This method can yield results with much higher accuracy than those obtained by statistical linearization. Note that also non-Gaussian proper-

ties are covered (partly), because the original system is not linearised. However, the method is only applicable to SDOF systems and does not provide frequency-domain response information.

Another equivalent nonlinear method is known as partial linearization, see Elishakoff and Cai [1992]. In partial linearization only the damping of the system is linearised. The equation thus obtained is amenable to an exact solution. The equivalent (linear) damping parameter is selected by means of the dissipation energy balancing criterion, see Cai and Lin [1988a] and Cai et al. [1992]. The proposed procedure considerably improves the accuracy of the statistical linearization method and yields simple equations to determine probabilistic characteristics of the system. The results are less accurate than those obtained by the method described above (of which partial linearization is a special case). However, the computational efforts are reduced. Unfortunately, also the partial linearization method is only applicable to SDOF systems.

The main shortcomings of these methods are, thus, the lack of applicability to MDOF systems and the fact that no frequency-domain information can be obtained.

A method that can be applied to MDOF systems and provides information on the power spectral density of the response is equivalent statistical quadratization. The equivalent statistical quadratization method was introduced by Spanos and Donley [1991, 1992] as an extension to the equivalent linearization method. The linearization method often fails to estimate the spectral properties of the response accurately for strongly nonlinear systems. This is sometimes due to the fact that the power spectra of the response of linear systems span only the frequency range of the excitation spectrum. However, significant responses outside this range are possible for nonlinear systems. The quadratization method was developed to overcome this shortcoming of the linearization method and is suitable for application to MDOF systems. In the quadratization method, the nonlinear system is replaced by an equivalent system with polynomial nonlinearities up to quadratic order. Consequently, the solutions of the nonlinear, equivalent system can be approximated using the Volterra series method, see Schetzen [1980]. The non-Gaussian response probability function is approximated by a third-order Gram-Charlier expansion. In Spanos and Donley [1991, 1992], it is shown that the quadratization method provides much more accurate results than the linearization method. It should be noted that the method is also applicable to systems with non-polynomial nonlinearities.

1.2.9 Concluding remarks

A wide variety of methods to approximate the response of nonlinear, dynamic systems to random excitations has been discussed in the former sections. Based on the necessary properties, formulated before in section 1.2.1, for a response approximation method, the potential of all the methods, described before, can be assessed. One of the most limiting demands seems to be the desire to investigate MDOF systems. Moreover, the need for response information in the frequency domain seems to be a very restrictive demand.

Methods which are not in conflict with the criteria, formulated in section 1.2.1, are:

Numerical integration Virtually any problem, within the scope of section 1.2.1,

can be tackled using numerical integration methods. Moreover, any desired level of accuracy can be attained. So, simulation is pre-eminently suitable for the purpose of detailed and accurate investigation of the stochastic, steady state behaviour of strongly nonlinear, dynamic systems.

However, rather extensive computational effort is generally needed to achieve the high levels of accuracy. This problem becomes even more evident for MDOF systems. Here, the second main goal of this research presents itself: the efficient approximation of the response statistics.

Statistical linearization The method of statistical linearization can also be applied to the total set of problems defined in section 1.2.1 and is very efficient. In particular, the stochastic response characteristics of the linear model can be evaluated analytically, once the optimal, linear model has been constructed. However, for strongly nonlinear systems the method is known to lose accuracy fast.

Statistical quadratization The quadratization method incorporates a natural increase of modelling complexity with respect to linearization. It can also be applied to a wide variety of problems.

1.3 Outline of the thesis

Chapter 2 starts with an introduction on the modelling using white noise processes. Consequently, the concept of a SDE will be illuminated. The correct derivation of the SDE from the physical equations of motion will be described. In order to be able to treat SDEs, Itô 's calculus is described. Moreover, extensive attention will be given to tools for the numerical solution of these SDEs. This chapter, thus, provides all the necessary tools to perform numerical simulations with SDEs.

In *chapter 3*, the focus lies on the investigation and understanding of typically nonlinear, stochastic response phenomena. The additive power of these investigations (compared to former research) lies in the fact that a great deal of attention is given to the study of frequency-domain characteristics. Both numerical integration and statistical linearization are used to estimate the response characteristics. These methods are applied to a nonlinear system with a piece-wise linear stiffness term. This system is known to exhibit a wide variety of complex and interesting, nonlinear response phenomena, in case of periodic (sinusoidal to be precise) excitations [Shaw and Holmes, 1983; Fey et al., 1996; Van Campen et al., 1997a]. Firstly, the response of the system to white noise excitations is studied. By gaining insight in the stochastic, nonlinear response characteristics, the shortcomings of the linearization approach can be explained and understood. In this way, ideas for a new response approximation method evolve. In order to explain the source of certain response phenomena (that occur in case of white noise excitations), the response of the same system to band-limited Gaussian excitations is investigated. A natural extension of this research path is to study the response of the piece-wise linear system to very narrow-banded random excitation (nearly periodic). The response characteristics to random excitations are compared to the response characteristics in case of periodic

excitations. It will become clear that a great deal can be learned from the simultaneous study of periodic and stochastic response characteristics. In a qualitative sense, many corresponding characteristics can be found.

In *chapter 4*, a highly nonlinear system is investigated both numerically and *experimentally*. The system is a beam with a nonlinearly elastic stop. The stochastic response characteristics of this system to both broad-banded and narrow-banded noise excitations are investigated experimentally. Many of the general, nonlinear response phenomena, described in chapter 3, are also found in these experiments. The main purpose of chapter 4 is to give the insights gained in chapter 3 experimental backup and to increase the general value of the response phenomena, discussed in chapter 3, by studying another system, which exhibits, moreover, multiple degrees-of-freedom. Both SDOF and MDOF models of the system are investigated through numerical simulations. In the chapters 3 and 4, knowledge on many interesting, nonlinear, stochastic response phenomena is gained. Moreover, the root of the shortcomings of the statistical linearization approach is illuminated using this knowledge. As a consequence, ideas concerning a new approximation method root from this knowledge. The development of other methods to approximate the response statistics is desirable since, firstly, statistical linearization is very inaccurate for strongly nonlinear systems and, secondly, numerical integration techniques appear to be relatively inefficient from a computational point of view.

In *chapter 5*, a new hybrid simulation-linearization method is developed. In this method, a simulation with a reference excitation (for example white noise) has to be performed. The resulting frequency domain response data are, then, used to build a linear model of higher dimension, which exhibits approximately the same power spectral density of the output as the original nonlinear system for the reference excitation. The model is constructed using the spectral factorization technique [Papoulis, 1977]. For this technique, two approaches are developed; one using Fourier theory and one using potential theory. The resulting linear, higher-dimensional model can, then, be used to estimate the response characteristics of the nonlinear system to other excitations (for example non-white excitations) in a very efficient manner. The accuracy of the method is generally higher than that of the conventional linearization approach.

In *chapter 6*, a method that incorporates nonlinear models is developed and discussed. These models are low-order Volterra systems. The response statistics of such systems can be estimated more efficiently than using numerical integration. Using these models certain specifically nonlinear characteristics of the original, nonlinear system can be predicted very well. The accuracy is generally higher than that of the linearization methods. Of course, this is at the cost of computational efficiency. This nonlinear approximation technique (termed bilinearization or Carleman linearization [Rugh, 1981]) is used to construct optimal (in some statistical sense) Volterra models. This method is not developed merely from the point of view of efficiency. The gradual increase of complexity of the approximate models from linear (including models of higher dimension) to nonlinear (Volterra) models provides us with valuable information with respect to what kind of (nonlinear) system-elements are responsible for what kind of response phenomena (discussed in chapter 3 and 4).

In *chapter 7*, conclusions concerning both the knowledge gained on the subject of

general, nonlinear, stochastic response phenomena and the methods used to estimate these characteristics will be given.

2 Stochastic differential equations

2.1 Introduction

The type of systems considered in this thesis can be described by a set of differential equations of the form

$$\frac{d\underline{x}(t)}{dt} = \underline{a}(\underline{x}(t)) + \underline{b}(\underline{x}(t))\,\underline{u}(t), \qquad t \geq t_0,\ \underline{x}(t_0) = \underline{x}_0, \tag{2.1}$$

in which $\underline{u}(t)$ is an M-dimensional column-vector with excitations that evolve in time t and $\underline{x}(t)$ is an N-dimensional column-vector with state variables. The N-dimensional column-vector $\underline{a}(\underline{x}(t))$ and the $N \times M$ matrix $\underline{b}(\underline{x}(t))$ do not depend explicitly on time. So, only stationary systems are considered. The differential equations treated in this thesis exhibit two very important features:

1. $\underline{a}(\underline{x}(t))$ (and/or $\underline{b}(\underline{x}(t))$) are nonlinear functions;

2. $\underline{u}(t)$ is a stochastic process, which represents an external excitation when $\underline{b}(\underline{x}(t))$ is constant and a parametric excitation when $\underline{b}(\underline{x}(t))$ depends on $\underline{x}(t)$.

Now, if $\underline{u}(t)$ is a white noise process $\underline{\xi}(t)$, equation (2.1) is termed a stochastic differential equation (SDE). Such a SDE can be interpreted in the sense of Itô or in the sense of Stratonovich [Arnold, 1974, 1998; Kloeden and Platen, 1992; Oksendal, 1998]. Both interpretations provide mathematically valid formulations for SDEs. In section 2.3, the Itô formulation will be discussed thoroughly. Moreover, the difference between the Itô and Stratonovich interpretations of the SDE will be discussed briefly.

2.2 Stochastic processes

Before we go any further, the concept of a stochastic process should be introduced. It is important to clarify the difference between a random variable and a stochastic (random) process. A random variable X (on $\mathbb{R}$) is defined by its probability distribution. The probability distribution $F_X(x)$ of a random variable X can be defined as

$$F_X(x) = \text{probability}(X \leq x) = P(X \leq x). \tag{2.2}$$

Moreover, the probability density function $f_X(x)$ of a random variable X can be defined as

$$f_X(x) = \frac{dF_X(x)}{dx}. \tag{2.3}$$

Now, the p-th statistical moment μ_{X^p} $(p = 1, 2, 3, \ldots)$ of a random variable X can be written as

$$\mu_{X^p} = \mu_p = E\{X^p\} = \int\limits_{-\infty}^{\infty} x^p f_X(x) \, dx, \tag{2.4}$$

whereas

$$\eta_{X^p} = \eta_p = E\{(X - \mu_X)^p\} = \int\limits_{-\infty}^{\infty} (x - \mu_X)^p f_X(x) \, dx \tag{2.5}$$

is termed the p-th central moment. In (2.4) and (2.5), $'E'$ is the expected value operator, which is defined by

$$E\{g(X)\} = \int\limits_{-\infty}^{\infty} g(x) f_X(x) dx. \tag{2.6}$$

In order to be able to give meaning to the concept of a stochastic process the joint distribution function of a sequence of random variables $X_1, X_2, \ldots, X_n$ should be introduced:

$$F_{X_1 X_2 \ldots X_n}(x_1, x_2, \ldots, x_n) = P(X_j \leq x_j, \ j = 1, 2, \ldots, n). \tag{2.7}$$

A sequence of random variables $X_1, X_2, \ldots, X_n, \ldots$ may describe the evolution of a stochastic system over discrete instants of time $t_1, t_2, \ldots, t_n, \ldots$: $X(t_1)$, $X(t_2), \ldots$, $X(t_n), \ldots$. This is called a stochastic process. The totality of its joint distribution functions $F_{X_{j_1} X_{j_2} \ldots X_{j_k}}$ $(j_k = 1, 2, \ldots$ and $k = 1, 2, \ldots)$ is termed the probability law of the stochastic process. Hereafter, we will write these distributions as $F_{t_{j_1} t_{j_2} \ldots t_{j_k}}$ to emphasise the role of the time instants. When all the joint distribution functions are Gaussian we call the process a Gaussian process.

As mentioned before, the stochastic processes, considered in this thesis, are stationary processes. This is an interesting class of processes since they represent a probabilistic equilibrium (*steady state*). This means that the specific point in time, on which the process is examined, is not relevant. A process is *strictly stationary* if its joint distribution functions are all invariant under time displacements:

$$F_{t_1 + \Delta t, t_2 + \Delta t, \ldots, t_n + \Delta t} = F_{t_1, t_2, \ldots, t_n}, \qquad n = 1, 2, 3, \ldots . \tag{2.8}$$

When the mean $\mu_X = \mu_1 = \mu$ and the variance $\sigma_X^2 = \eta_2$ are constant and the covariance function satisfies $C_{XX}(t_j, t_k) = E\{(X_j - \mu)(X_k - \mu)\} = C_{XX}(t_j - t_k)$, the process is termed *wide-sense stationary*. The latter form of stationarity is a weaker stationarity condition than that of strict stationarity, since merely stationarity with respect to the first-order and second-order moments is required.

Furthermore, only *ergodic* processes will be considered. As mentioned before, it is quite common to assume ergodicity for stationary processes in engineering practice. The thorough validation of such an assumption is generally not a trivial matter.

However, this subject will not be discussed in more depth here. A stationary process $X(t)$ (with time taking values in $\mathbb{R}$) with mean μ and autocorrelation function $R_{XX}(\tau) = E\{X(t)X(t+\tau)\}$ is ergodic if for every realisation $x_k(t)$ of the process $X(t)$ the following relations hold:

$$\mu = \bar{x} = \lim_{T \to \infty} \frac{1}{2T} \int\limits_{-T}^{T} x_k(t) \, dt,$$

$$R_{XX}(\tau) = R_{x_k x_k}(\tau) = \lim_{T \to \infty} \frac{1}{2T} \int\limits_{-T}^{T} x_k(t) \, x_k(t+\tau) \, dt \quad \forall \, \tau.$$

(2.9)

Thus, an ergodic process is characterised by the fact that the time averages of the realisations equal the ensemble averages. When both stationarity and ergodicity hold, the value of a Gaussian process on a certain time instant is a random variable with a Gaussian probability density function. Furthermore, this probability density function is the same for all time instants.

Besides the information on the probability density function (or the statistical moments), we will also pursue information in the frequency domain. Consequently, the power spectral density of a stochastic process will be investigated continually. The power spectral density $S_{XX}(\omega)$ of a stochastic process $X(t)$ can be defined as the Fourier transform of the autocorrelation function:

$$S_{XX}(\omega) = \frac{1}{2\pi} \int\limits_{-\infty}^{\infty} R_{XX}(\tau) \, e^{-i\omega\tau} \, d\tau,$$

(2.10)

in which ω is the angular frequency and $i = \sqrt{-1}$. The power spectral density of a process measures its average power per unit angular frequency at a certain angular frequency.

2.2.1 White noise

Here, special attention will be given to a white noise process $\xi(t)$. In random vibration, white noise is used extensively to model excitations with a broad-banded frequency spectrum. The name 'white noise' stems from the fact that its average power is uniformly distributed in frequency, which is a characteristic of white light. Thus, it has a constant power spectral density. This means that all frequencies contribute an equal amount of energy to the stochastic process up to infinite frequencies. Consequently, a white noise process has an infinite variance. The fact that infinitely high frequencies contribute to the process implies that it has zero memory. The stationary covariance function $C_{\xi\xi}(\tau)$ of a white noise process (with zero mean μ_ξ), therefore, is a constant multiple of the Dirac delta function $\delta(t)$:

$$C_{\xi\xi}(\tau) = E\{\xi(t)\xi(t+\tau)\} = R_{\xi\xi}(\tau) = D \, \delta(t),$$

(2.11)

where D is termed the intensity of the white noise. This implies that two values of a realisation of a white noise process are uncorrelated, no matter how close they

are in time. Combination of (2.10) and (2.11) yields the following expression for the power spectral density of a white noise process:

$$S_{\xi\xi}(\omega) = \frac{1}{2\pi} \int\limits_{-\infty}^{\infty} R_{\xi\xi}(\tau)e^{-i\omega\tau}d\tau = \frac{D}{2\pi} \int\limits_{-\infty}^{\infty} \delta(t)e^{-i\omega\tau}d\tau = \frac{D}{2\pi} =: S_0. \qquad (2.12)$$

Due to the characteristics mentioned above, white noise can not be a stochastic process in the usual sense, but must be interpreted in the sense of generalised functions (like the Dirac delta function), see Kloeden and Platen [1992], Grigoriu [1995b] and Pugachev and Sinitsyn [1987].

For obvious reasons, a white noise process can not exist in practice. However, white noise can be used to model broad-banded processes. Moreover, using filtered white noise (coloured noise) one can approximate processes with a wide variety of spectral characteristics. Consequently, in such cases, the white noise modelling approach can be applied as well by interpreting the filter as a part of an augmented system, which is, then, excited by white noise. When the excitation $\underline{u}(t)$, in equation (2.1), is a white noise process, the response $\underline{x}(t)$ generally is a Markov process [Kloeden and Platen, 1992]. A Markov process possesses the Markov property. The Markov property states that the increments of a Markov process are independent. There are conditions under which such Markov modelling is appropriate and meaningful. In practice, the use of a Markov process model is (almost always) justified when the increments of the response in two non-overlapping intervals are independent. The response is Markovian if the excitation is independent at any two time instances, regardless of their distance in time. White noise is such a process. The justification of the use of white noise in the modelling is based on the comparison of two time scales: (1) the correlation time scale of the 'real' excitation process and (2) the relaxation time scale of the system. The requirement of independent increments is approximately satisfied when the correlation time scale of the excitation is much shorter than the relaxation time scale of the system.

Furthermore, a Gaussian white noise process (also called the 'Langevin process') is the formal derivative of a Wiener process $W(t)$:

$$\xi(t) = \frac{dW(t)}{dt}. \qquad (2.13)$$

A Wiener process is continuous everywhere and differentiable nowhere [Kloeden and Platen, 1992]. This again leads to the conclusion that white noise can not be a stochastic process in the usual sense. A Wiener process is a mathematical description of a Brownian motion process. A Brownian motion process is the erratic motion of a grain of pollen on a water surface due to the bombardment of the grain by water molecules. A Wiener process $W(t)$ has the following properties:

1. $W(t)$ is a Gaussian process;

2. $W(0) = 0$;

3. $E\{W(t)\} = 0$;

4. $E\{W(t_1)\,W(t_2)\} = \min(t_1, t_2) = \frac{1}{2}(\mid t_1 + t_2 \mid - \mid t_1 - t_2 \mid)$.

The fourth property means that the Wiener process possesses the Markov property. Consequently, using the fact that $E\{W(t_k) - W(t_j)\} = 0$, the autocorrelation function of the Wiener increments should be zero for non-overlapping increments:

$$
\begin{aligned}
E\{(W(t_4) - W(t_3))(W(t_2) - W(t_1))\} =& E\{W(t_4)\,W(t_2)\} + E\{W(t_3)\,W(t_1)\} - \\
& E\{W(t_3)\,W(t_2)\} - E\{W(t_4)\,W(t_1)\} \\
=& t_2 + t_1 - t_2 - t_1 = 0,
\end{aligned}
\tag{2.14}
$$

if $t_1 < t_2 < t_3 < t_4$. Note that, consequently,

$$
E\{\Delta W^2\} = E\{(W(t_2) - W(t_1))^2\} = t_2 - t_1 = \Delta t.
\tag{2.15}
$$

Moreover, it should be noted that the fourth property of the Wiener process also implies that it is a non-stationary process. In figure 2.1, an example of a realisation of a Wiener process is shown. In figure 2.2, a part of this realisation is magnified. The comparison of these figures illustrates the fourth property of the Wiener process. Furthermore, it is apparent from figure 2.2 that the random character of the process is independent of the time scale of the observation.

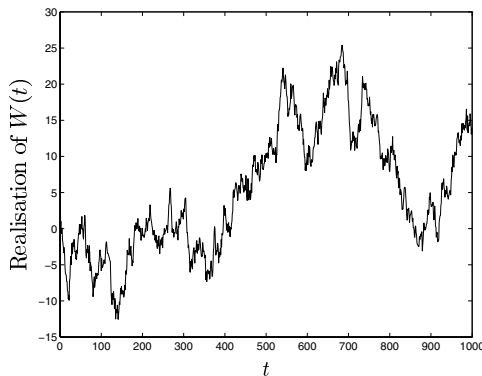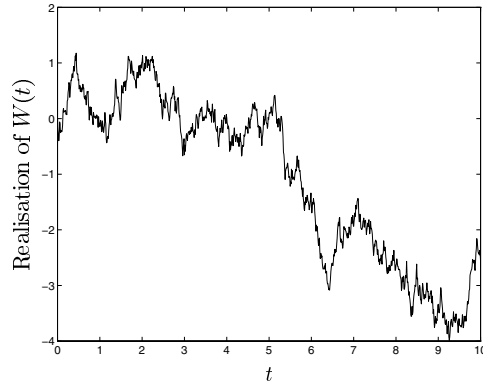Figure 2.1: An example of a realisation of a Wiener process $W(t)$.

Figure 2.2: Zoomed view of the realisation of $W(t)$ in figure 2.1.

2.3 Ito stochastic calculus

We can, now, introduce the white noise process in equation (2.1):

$$
\frac{d\underline{x}(t)}{dt} = \underline{a}(\underline{x}(t)) + \underline{b}(\underline{x}(t))\,\underline{\xi}(t), \qquad t \geq t_0,\ \underline{x}(t_0) = \underline{x}_0.
\tag{2.16}
$$

This equation is often called a nonlinear Langevin equation. This differential equation can be written as

$$d\underline{x}(t) = \underline{\breve{a}}(\underline{x}(t)) \, dt + \underline{\breve{b}}(\underline{x}(t)) \, \underline{\xi}(t) \, dt, \tag{2.17}$$

or equivalently as

$$d\underline{x}(t) = \underline{\breve{a}}(\underline{x}(t)) \, dt + \underline{\breve{b}}(\underline{x}(t)) \, d\underline{W}(t), \tag{2.18}$$

which is termed the Itô equation. Herein, $\underline{W}$ is an M-dimensional Wiener process with components $W^1, W^2, \ldots, W^M$, which are independent scalar Wiener processes. Generally, $\underline{\breve{a}}(\underline{x})$ is termed the drift coefficient and $\underline{\breve{b}}(\underline{x})$ is termed the diffusion coefficient. For $\breve{b}_{jk}$, the jk-th component of $\underline{\breve{b}}(\underline{x})$, and $\breve{a}_j$, the j-th component of $\underline{\breve{a}}(\underline{x})$, it holds that

$$\breve{b}_{jk} = \sqrt{D_k} \, b_{jk}, \qquad\qquad j = 1, 2, \ldots, N \text{ and } k = 1, 2, \ldots, M, \tag{2.19}$$

$$\breve{a}_j = a_j + \frac{1}{2} \sum_{l=1}^{N} \sum_{k=1}^{M} \breve{b}_{lk} \, \frac{\partial \breve{b}_{jk}}{\partial x_l}, \qquad\qquad j = 1, 2, \ldots, N, \tag{2.20}$$

where $a_j(\underline{x})$ is the j-th component of $\underline{a}(\underline{x})$ and b_{jk} is the jk-th component of $\underline{b}(\underline{x})$ in equation (2.16). Moreover, D_k is the intensity of the k-th component of $\underline{\xi}$.

The double summation expression is due to the Wong-Zakai correction term [Wong and Zakai, 1965]. We will briefly discuss the necessity of this correction. Let $\underline{x}^*(t)$ be the solution of the following stochastic differential equation (in the sense of Itô [1951b]):

$$d\underline{x}^*(t) = \underline{a}(\underline{x}^*(t)) \, dt + \underline{b}(\underline{x}^*(t)) \, d\underline{W}(t), \qquad t \geq t_0, \ \underline{x}^*(t_0) = \underline{x}_0. \tag{2.21}$$

Furthermore, let $\underline{x}^{(n)}$ be the solution of the *ordinary* differential equation, which can be obtained from the stochastic differential equation (2.21) by replacing the Wiener process $\underline{W}$ with $\underline{W}^{(n)}$, where $\underline{W}^{(n)}$ is a piecewise linear approximation for the Wiener process $\underline{W}$ ($\underline{W}^{(n)}$ converges to $\underline{W}$ for $n \to \infty$) on a partition $0 < t_0^{(n)} < t_1^{(n)} < \ldots < t_j^{(n)} < \ldots < t_n^{(n)} = T$, with

$$\underline{W}^{(n)}(t) = \underline{W}_{t_{j-1}^{(n)}} + (\underline{W}_{t_j^{(n)}} - \underline{W}_{t_{j-1}^{(n)}}) \, \frac{t - t_{j-1}^{(n)}}{t_j^{(n)} - t_{j-1}^{(n)}} \tag{2.22}$$

for $t_{j-1}^{(n)} \leq t \leq t_j^{(n)}$ and $j = 1, 2, \ldots, n$. In Wong and Zakai [1965], it is shown that $\underline{x}^{(n)}$ will *not* converge (for $n \to \infty$) to $\underline{x}^*$, but to the solution of (2.18). It should be noted that for external excitations (all components of $\underline{\breve{b}}$ are independent of $\underline{x}$) $\underline{\breve{a}}$ is equal to $\underline{a}$. Consequently, the Wong-Zakai correction only produces effect if the excitation is parametric.

Equation (2.17) can also be interpreted as an integral equation:

$$\underline{x}(t) = \underline{x}(t_0) + \int_{t_0}^{t} \underline{\breve{a}}(\underline{x}(\nu)) \, d\nu + \int_{t_0}^{t} \underline{\breve{b}}(\underline{x}(\nu)) \, \underline{\xi}(\nu) \, d\nu. \tag{2.23}$$

Using equation (2.13), this integral equation can be written as

$$\underline{x}(t) = \underline{x}(t_0) + \int_{t_0}^{t} \breve{\underline{a}}(\underline{x}(\nu))\, d\nu + \int_{t_0}^{t} \breve{\underline{b}}(\underline{x}(\nu))\, d\underline{W}(\nu). \tag{2.24}$$

Herein, the integrals are determined component-wise, with the j-th component being given by

$$x_j(t) = x_j(t_0) + \int_{t_0}^{t} \breve{a}_j(\underline{x}(\nu))\, d\nu + \sum_{k=1}^{m} \int_{t_0}^{t} \breve{b}_{jk}(\underline{x}(\nu))\, dW_k(\nu). \tag{2.25}$$

The first integral of (2.23) and (2.24) can be interpreted as a Riemann integral with a stochastic integrand. However, the second integral of both equations needs more attention.

Let us investigate whether the second integral of (2.23) can be interpreted as a Riemann integral too. A Riemann integral exhibits the following form:

$$I_R = \int_{A}^{B} y(s)\, ds. \tag{2.26}$$

This integral can be approximated by a Riemann sum

$$\hat{I}_R = \sum_{k=1}^{m} y(\varsigma_k^{(m)})\, (s_k^{(m)} - s_{k-1}^{(m)}), \tag{2.27}$$

where $s_{k-1}^{(m)} \leq \varsigma_k^{(m)} \leq s_k^{(m)}$ and $A \leq s_k^{(m)} \leq B$. If the Riemann sum $\hat{I}_R$ converges (for $m \to \infty$) to the same value for every choice of $\varsigma_k^{(m)}$ within the interval $[s_{k-1}^{(m)}, s_k^{(m)}]$, the Riemann integral exists (and defines I_R) and we call the function $y(s)$ Riemann integrable.

The second integral in (2.23) is not well-defined as a Riemann integral since $\breve{\underline{b}}(\underline{x}(t))\, \underline{\xi}(t)$ is not a Riemann integrable function. This is a consequence of the fact that a white noise process has zero memory. Consequently, for different choices of $\varsigma_k^{(m)}$ the Riemann sum will not converge to the same value. Moreover, a white noise process has infinite variance and an unbounded function is not Riemann integrable.

Now, let us investigate whether the second integral in (2.24) can be interpreted as a Riemann-Stieltjens integral. A Riemann-Stieltjens integral has the following form:

$$I_{RS} = \int_{A}^{B} y(s)\, dg(s). \tag{2.28}$$

Note that the second integral of equation (2.24) is of such a form. The Riemann-Stieltjens integral can be approximated by a Riemann-Stieltjens sum

$$\hat{I}_{RS} = \sum_{k=1}^{m} y(\varsigma_k^{(m)})\, (g(s_k^{(m)}) - g(s_{k-1}^{(m)})). \tag{2.29}$$

If the derivative of $g(s)$ ($g'(s) = \frac{dg(s)}{ds}$) exists, one can, of course, write the Riemann-Stieltjens integral as a Riemann integral. However, the Wiener process is differentiable nowhere. So, it can again be concluded that the second integral of equation (2.24) can not be interpreted as a Riemann integral. When the Riemann-Stieltjens sum converges to the same value for every choice of $\varsigma_k^{(m)}$, the integral (2.28) is Riemann-Stieltjens integrable. Two conditions for this property, which together are sufficient, are:

1. $y(s)$ should be Riemann integrable;

2. $g(s)$ should be of bounded variation.

In order to introduce the concept of the variation of a function $y(s)$ on the interval $s \in [A, B]$, let $A = s_0^{(m)} < s_2^{(m)} < \ldots < s_m^{(m)} = B$ an arbitrary partition of $[A, B]$ with $\Delta^{(m)} = \max_{1 \le k \le m} \Delta_k^{(m)} \to 0$ for $m \to \infty$, where $\Delta_k^{(m)} = s_k^{(m)} - s_{k-1}^{(m)}$. Then, the total variation $V_A^B(y)$ of the function y on $[A, B]$ is defined as the supremum over all such partitions of the sums of the absolute value of the increments of y:

$$V_A^B(y) = \sup_{m \to \infty, \Delta^{(m)} \to 0} \sum_{k=1}^{m} \mid y(s_k^{(m)}) - y(s_{k-1}^{(m)}) \mid . \tag{2.30}$$

If $V_A^B(y) < \infty$ we say that y is of bounded variation on $[A, B]$.

So, the question should now be whether the Wiener process is of bounded variation. In Kloeden and Platen [1992], it is stated that a function $y(s)$ is of bounded variation on $[A, B]$ if and only if its derivative $y'(s)$ exists for almost all $s \in [A, B]$. Consequently, the Wiener process can not be of bounded variation. It can, therefore, be concluded that the second integral on equation (2.24) can not be interpreted as a Riemann-Stieltjens integral either.

To overcome this problem, another definition for this kind of integrals will be introduced in the following section.

2.3.1 The Ito integral

To avoid the problem that arises when trying to interpret the second integral in (2.23) and (2.24) as Riemann or Riemann-Stieltjens integrals, respectively, the Itô integral will be introduced. For the sake of simplicity, the scalar case will be discussed here.

In order to define the Itô integral, a very important choice is made. This choice is reflected by the fact that the Itô integral $I(\check{b})$, where

$$I(\check{b}) = \int_0^T \check{b}(x(\nu)) \, dW(\nu), \tag{2.31}$$

is approximated by the Itô sum $\hat{I}(\check{b}^{(n)})$, where

$$\hat{I}(\check{b}^{(n)}) = \sum_{k=1}^{n} \check{b} \left(x(\nu_{k-1}) \right) \, (W(\nu_k) - W(\nu_{k-1})) = \sum_{k=1}^{n} \check{b}_k \, \Delta W_k. \tag{2.32}$$

The superscript n in $\check{b}^{(n)}$ expresses that $\check{b}^{(n)}$ approximates $\check{b}$ as a stochastic step function with n intervals on $[0, T]$. In order to define the stochastic step function $\check{b}^{(n)}$, consider partitions of $t = [0, T]$ of the form $0 = t_1^{(n)} < t_2^{(n)} < \ldots < t_j^{(n)} < \ldots < t_{n+1}^{(n)} = T$ with $t_{j+1}^{(n)} - t_j^{(n)} \longrightarrow 0$ for $j = 1, 2, \ldots, n$ as $n \longrightarrow \infty$. The stochastic step function can now be described by

$$\check{b}^{(n)}(t) = \check{b}(t_j^{(n)}) \ \text{ for } \ t_j^{(n)} \leq t \leq t_{j+1}^{(n)} \tag{2.33}$$

for $j = 1, 2, \ldots, n$ and $n = 1, 2, 3, \ldots$. The actual choice, mentioned above, is that the integrand $\check{b}(x(\nu))$ in (2.31) is evaluated at the left side of the integration interval, $\nu = \nu_{k-1}$, see (2.32). The thought behind this choice is the following demand:

$$E\{\check{b}(\nu)\, W(t)\} = 0 \ \text{ if } \ \nu \leq t, \tag{2.34}$$

which means that the excitation at a certain point in time should not influence the solution at earlier times. To be more specific, the integrand $\check{b}(x(\nu))$ is non-anticipative if and only if $\nu = \nu_{k-1}$ is chosen in the Itô sum.

At this point, an important question is whether $\hat{I}(\check{b}^{(n)})$ converges to a limit (for $n \to \infty$), which will then define $I(\check{b})$ for this choice of ν. Now, a condition for such convergence can be stated as follows:

$$\textit{If} \quad \int_0^T E\{(\check{b}(t) - \check{b}^{(n)}(t))^2\}\, dt \longrightarrow 0 \quad \textit{for} \quad n \to \infty$$

$$\textit{then} \quad \hat{I}(\check{b}^{(n)}) = \int_0^T \check{b}^{(n)}(t)\, dW(t) \quad \longrightarrow \quad I(\check{b}) = \int_0^T \check{b}(t)\, dW(t) \tag{2.35}$$

$$\textit{in the mean-square sense.}$$

Below, the validity of this condition will be discussed. The basic question is whether the limit $\lim_{n \to \infty} \hat{I}(\check{b}^{(n)})$ exists and in what sense it is a limit. Here, we shall use mean-square convergence. This means that we want to investigate whether a limit L_I exists, such that

$$\lim_{n \to \infty} E\{(\hat{I}(\check{b}^{(n)}) - L_I)^2\} = 0. \tag{2.36}$$

However, the limit value L_I is unknown. We now use that $\left\{\hat{I}(\check{b}^{(n)})\right\}_n$ is a Cauchy sequence [Douglass, 1996] if

$$\forall\, \varepsilon > 0 \ \exists\, n_0 \ \forall\, n \geq n_0 \ \forall\, m \geq n_0 : \ E\{(\hat{I}(\check{b}^{(n)}) - \hat{I}(\check{b}^{(m)}))^2\} \ < \ \varepsilon.$$

Consequently, for large m and n,

$$E\{(\hat{I}(\check{b}^{(n)}) - \hat{I}(\check{b}^{(m)}))^2\} \ < \ \varepsilon \tag{2.37}$$

is a necessary and sufficient condition for the existence of the limit L_I in the sense of (2.36). Due to the linearity of the operator $\hat{I}$, this condition is equivalent to

$$E\{(\hat{I}(\check{b}^{(n)} - \check{b}^{(m)}))^2\} \ < \ \varepsilon. \tag{2.38}$$

Now, the following equivalence is used:

$$E\{(\hat{I}(\check{b}^{(n)} - \check{b}^{(m)}))^2\} \;<\; \varepsilon \Longleftrightarrow \int_0^T E\{(\check{b}^{(n)} - \check{b}^{(m)})^2\}\, dt \;<\; \varepsilon. \tag{2.39}$$

To support the validity of this equivalence, consider a step function $q^{(r)}$ for which, according to (2.32),

$$E\{(\hat{I}(q^{(r)}))^2\} = E\left\{ \sum_{k=1}^r \sum_{l=1}^r (q_k^{(r)}\Delta W_k)(q_l^{(r)}\Delta W_l) \right\}. \tag{2.40}$$

Because of property (2.34), which is inherent to Itô's choice to use the left side of the integration interval for computing values for $q^{(r)}$, ΔW_k is independent of $q_k^{(r)}$ and $q_l^{(r)}$ when $k > l$ and is independent of ΔW_l for $k \neq l$, due to the Markov property of W:

$$E\left\{ q_k^{(r)} q_l^{(r)} \Delta W_k \Delta W_l \right\} = E\left\{ \Delta W_k \right\}\, E\left\{ q_k^{(r)} q_l^{(r)} \Delta W_l \right\} = 0, \tag{2.41}$$

because $E\{\Delta W_k\} = 0$. By symmetry the same holds for $l > k$:

$$E\left\{ q_k^{(r)} q_l^{(r)} \Delta W_k \Delta W_l \right\} = E\left\{ \Delta W_l \right\}\, E\left\{ q_k^{(r)} q_l^{(r)} \Delta W_k \right\} = 0. \tag{2.42}$$

The case $k = l$ provides the only non-zero contribution to $E\{(\hat{I}(q^{(r)}))^2\}$:

$$E\left\{ (\hat{I}(q^{(r)}))^2 \right\} = E\left\{ \sum_{k=1}^r (q_k^{(r)})^2\, (\Delta W_k)^2 \right\} = \sum_{k=1}^r E\left\{ (q_k^{(r)})^2 \right\}\, \Delta t_k, \tag{2.43}$$

because $q_k^{(r)}$ is independent of W_k and $E\left\{ \Delta W_k{}^2 \right\} = \Delta t_k$, see (2.15). Due to the fact that $q^{(r)}$ are step functions

$$E\left\{ (\hat{I}(q^{(r)}))^2 \right\} = \sum_{k=1}^r E\left\{ (q_k^{(r)})^2 \right\}\, \Delta t_k = \int_0^T E\left\{ (q_k^{(r)})^2 \right\}\, dt. \tag{2.44}$$

Of course, what holds for $q^{(r)}$ also holds for $\check{b}^{(n)} - \check{b}^{(m)}$, which confirms the equivalence in (2.39). Now the following conditional relation will be used:

If for a fixed $m = m_f$

$$\lim_{n \to \infty} \int_0^T E\left\{ (\check{b}^{(n)} - \check{b}^{(m_f)})^2 \right\}\, dt = \int_0^T E\left\{ (\check{b} - \check{b}^{(m_f)})^2 \right\}\, dt \;<\; \frac{1}{4}\varepsilon \tag{2.45}$$

then $\displaystyle\int_0^T E\left\{ (\check{b}^{(n)} - \check{b}^{(m)})^2 \right\}\, dt < \varepsilon$ *for* $n, m \to \infty$.

Under this condition it, thus, holds that $E\{(\hat{I}(\check{b}^{(n)} - \check{b}^{(m)}))^2\} < \varepsilon$, see (2.39). Then, $\left\{ \hat{I}(\check{b}^{(n)}) \right\}_n$ is a Cauchy sequence and is, therefore, convergent. Consequently, the limit L_I exists and (2.35) is shown to be correct. The condition, see (2.35),

$$\int_0^T E\left\{ (\check{b} - \check{b}^{(n)})^2 \right\} \, dt \longrightarrow 0 \quad \text{for} \quad n \to \infty \tag{2.46}$$

is a weak one and is easily met. When $\check{b}$ is mean-square continuous, that is when $E\{\check{b}^2\}$ is continuous, it holds that

$$E\left\{ (\check{b}^{(n)} - \check{b})^2 \right\} \longrightarrow 0 \quad \text{as} \quad n \to \infty. \tag{2.47}$$

It can be proven, see Kloeden and Platen [1992], that, consequently, (2.46) holds. The function $\check{b}$ is generally not mean-square continuous, but it can be approximated arbitrarily close by one that is [Kloeden and Platen, 1992].

It can , now, be concluded that, for general $\check{b}$, the limit of the Itô sum exists and this is what we call the Itô integral. It is important to note that the fact that the left side of the integration interval was chosen is crucial in the convergence of the Itô sum.

To compare the Itô integral with the Riemann and Riemann-Stieltjens integrals, a few properties of the Itô integral, which it shares with the conventional Riemann and Riemann-Stieltjens integrals, are given below:

1. The linearity property:

$$\int_{t_0}^{t_1} \left(c_1 \check{b}_1(\nu) + c_2 \check{b}_2(\nu) \right) \, d\nu = c_1 \int_{t_0}^{t_1} \check{b}_1(\nu) \, d\nu + c_2 \int_{t_0}^{t_1} \check{b}_2(\nu) \, d\nu; \tag{2.48}$$

2. The additivity property:

$$\int_{t_0}^{t_2} \check{b}(\nu) \, d\nu = \int_{t_0}^{t_1} \check{b}(\nu) \, d\nu + \int_{t_1}^{t_2} \check{b}(\nu) \, d\nu. \tag{2.49}$$

However, the Itô integral also has the peculiar property that

$$\int_0^t W(\nu) \, dW(\nu) = \frac{1}{2} W^2(t) - \frac{1}{2} t \tag{2.50}$$

in contrast to

$$\int_0^t y(\nu) dy(\nu) = \frac{1}{2} y^2(t) \tag{2.51}$$

from classical calculus for a differentiable function $y(t)$ with $y(0) = 0$. The origin of the extra term '$-\frac{1}{2}t$' in equation (2.50) will be explained in section 2.3.2.

It should be noted that the Itô integral (2.31) reduces to a Wiener integral $I(\check{b}) = \int_0^T \check{b} \, dW$ when $\check{b}$ is independent of x. This simplifies the evaluation of that integral considerably, since in such a case $\check{b}$ does not play any role in this integral. However, as will be set forth in section 2.4, the evaluation of the response x through the integral equation (2.24) will still involve Itô integrals when $\check{a}(x)$ is a nonlinear function of x.

Ito versus Stratonovich

In the former section, the Itô interpretation of the SDE and the stochastic integral was discussed. Actually, the Langevin equation (2.16) is meaningless without an interpretation rule, in case of parametric excitations. There are two mathematically correct interpretations, due to Itô and Stratonovich. In this thesis these interpretations will not be discussed in all detail but only a brief description of the difference between these interpretations will be given. A clarifying contribution on this subject can be found in Van Kampen [1981].

Itô's interpretation is characterised by the choice to evaluate the integrand of the stochastic integral at left side of the integration interval. In this case, the Wong-Zakai correction term, discussed earlier in this section, should be taken into account. However, equation (2.16) can also be interpreted as a Stratonovich SDE [Kloeden and Platen, 1992]. In that case, the Wong-Zakai correction is superfluous. In the Stratonovich formulation the integrand is evaluated as a halfway interpolation of the values of the integrand at the right side and left side of the integration interval. Consequently, the non-anticipativeness of the response, which was guaranteed in Itô's definition, is lost here. On the other hand, the methods of classical calculus, such as for example the chain rule, are also valid in case of Stratonovich's interpretation. This is, however, not the case for Itô SDEs. Therefore, the development of Itô stochastic calculus was necessary. In the next sections, some aspects of Itô's calculus, such as:

1. the stochastic equivalent of the classical chain rule: the Itô formula;

2. the Itô -Taylor expansions, which are the stochastic equivalents of the classical Taylor-expansions,

will be discussed. These tools of Itô calculus are essential for the development of numerical integration techniques for Itô SDEs.

Here, we have chosen to use the Itô interpretation of the SDE, because only then the non-anticipativeness of the response is guaranteed. This is physically, to say the least, desirable, since it reflects a causality condition.

2.3.2 The Ito formula

The Itô formula is the stochastic counterpart of the classical chain rule. It is of major importance for several reasons:

1. it reflects that Itô calculus differs from classical calculus and can help to understand some peculiar properties of the Itô integral, see e.g. (2.50);

2. it can be used to derive the moment equations of the response;

3. it can be used to derive the so-called Itô-Taylor expansions, which are the stochastic counterparts of the classical Taylor expansions. These expansions are of great interest, since they are commonly used to construct numerical integration schemes.

Let $y(t)$ be a stochastic process, which is defined by $y(t) = g(t, x(t))$ for $t \geq t_0$, where g has continuous second-order partial derivatives. Furthermore $x(t)$ is given by

$$dx(t) = \breve{b}(x(t))\, dW(t). \qquad (2.52)$$

Note that the drift term is omitted here for the time being. For a continuously differentiable $x(t)$ the chain rule of classical calculus would result in the following differential for $y(t)$:

$$dy(t) = \frac{\partial g(t, x(t))}{\partial t}\, dt + \frac{\partial g(t, x(t))}{\partial x}\, dx(t). \qquad (2.53)$$

In this case, only the first-order partial derivatives of g appear.

In contrast, when $x(t)$ is given by equation (2.52) we need to take into account that $(dx(t))^2 = \breve{b}^2(dW(t))^2$. Hence, $E\{(dx(t))^2\} = E\{\breve{b}^2\}\, dt$, since $\breve{b}(x(t))$ and $W(t)$ are independent by definition of the Itô integral, giving us a first order dt term coming from the second-order part of the Taylor expansion for g. To be more specific, we have

$$\begin{aligned}
\Delta y(t) =& g(t + \Delta t, x(t) + \Delta x(t)) - g(t, x(t)) = \left\{ \frac{\partial g}{\partial t}\Delta t + \frac{\partial g}{\partial x}\Delta x \right\} \\
&+ \frac{1}{2}\left\{ \frac{\partial^2 g}{\partial t^2}(\Delta t)^2 + 2\frac{\partial^2 g}{\partial t \partial x}\Delta t \Delta x + \frac{\partial^2 g}{\partial x^2}(\Delta x)^2 \right\} + \dots,
\end{aligned} \qquad (2.54)$$

where the partial derivatives are evaluated at $(t, x(t))$. It can be shown that this implies [Kloeden and Platen, 1992] that

$$dy(t) = \left\{ \frac{\partial g}{\partial t}(t, x(t)) + \frac{1}{2}\breve{b}^2(x)\frac{\partial^2 g}{\partial x^2}(t, x(t)) \right\} dt + \frac{\partial g}{\partial x}(t, x(t))\, dx(t), \qquad (2.55)$$

with the equality interpreted in the mean-square sense and with second-order and higher-order terms discarded. This is a stochastic chain rule known as the Itô formula. It contains an additional term (underlined part), which is not present in the classical chain rule (2.53). This term relates to the extra term in integrals like (2.50). For example, with $x(t) = W(t)$ and $y(t) = x^2(t)$, so $\breve{b} = 1$ and $g(t, x) = x^2$, we have

$$dy(t) = d(x^2(t)) = dt + 2x(t)\, dx(t), \qquad (2.56)$$

or

$$W(t)dW(t) = \frac{1}{2}d(W^2(t)) - \frac{1}{2}dt. \qquad (2.57)$$

This sheds light on the peculiar property of the Itô integral in equation (2.50). The Itô formula is commonly expressed in terms of the differentials dt and $dW(t)$. This is easily done in (2.55) since $dx(t) = \check{b}(x) \, dW(t)$. In general, a stochastic differential equation can also include a drift term: $dx(t) = \check{a}(x) \, dt + \check{b}(x) \, dW(t)$. Consequently, the Itô formula transforms to

$$
\begin{aligned}
dy(t) = & \left\{ \frac{\partial g}{\partial t}(t, x(t)) + \check{a}(x) \, \frac{\partial g}{\partial x} + \frac{1}{2}\check{b}^2(x) \, \frac{\partial^2 g}{\partial x^2}(t, x(t)) \right\} dt \\
& + \check{b}(x) \, \frac{\partial g}{\partial x}(t, x(t)) \, dW(t),
\end{aligned}
\tag{2.58}
$$

or in an integral formulation:

$$
\begin{aligned}
y(t_2) - y(t_1) = & \int_{t_1}^{t_2} \left\{ \frac{\partial g}{\partial t}(\nu, x(\nu)) + \check{a}(\nu, x(\nu))\frac{\partial g}{\partial x}(\nu, x(\nu)) \right. \\
& \left. + \frac{1}{2}\check{b}^2(x(\nu))\frac{\partial^2 g}{\partial x^2}(\nu, X(\nu)) \right\} d\nu \\
& + \int_{t_1}^{t_2} \check{b}(x(\nu))\frac{\partial g}{\partial x}(\nu, x(\nu)) \, dW(\nu).
\end{aligned}
\tag{2.59}
$$

For a vector stochastic process $\underline{x}$ the Itô formula can be expressed as

$$
dg(\underline{x}(t)) = \left\{ \frac{\partial g}{\partial t} + \frac{1}{2} \, \text{Trace} \, \left(\underline{\check{b}}\,\underline{\check{b}}^T g_{\underline{x}\underline{x}} \right) \right\} dt + g_{\underline{x}}{}^T d\underline{x},
\tag{2.60}
$$

where 'Trace' is the matrix operation for the summation of the diagonal elements of the matrix, T is the transpose operator, $g_{\underline{x}\underline{x}}$ is the Jacobian matrix and $g_{\underline{x}}{}^T$ is given by

$$
g_{\underline{x}}^T = \left\{ \frac{\partial g}{\partial x_1}, \frac{\partial g}{\partial x_2}, \dots, \frac{\partial g}{\partial x_j}, \dots, \frac{\partial g}{\partial x_n} \right\},
\tag{2.61}
$$

with $\underline{x} = \{x_1, x_2, \dots, x_j, \dots, x_n\}^T$. In appendix A, it is shown how the Itô formula can be used to derive the moments equations of a Markov process $x(t)$ obeying (2.18). Furthermore, in the following section, the Itô formula will be applied in order to derive the so-called Itô-Taylor expansions.

2.4   Ito-Taylor expansions

Classical numerical integration schemes, developed for deterministic differential equations, are, generally, constructed using the classical Taylor expansions, see Dormand [1996] and Butcher [1997]. These integration schemes can only be applied successfully when the integrands are sufficiently smooth. White noise is definitely not smooth. Numerical integration schemes suitable to handle SDEs are based on Itô integration. For this purpose, the Itô-Taylor expansion is developed as a stochastic counterpart of the classical Taylor expansion. This Itô-Taylor expansion can

be used to construct integration schemes, which are specifically fit to tackle SDE-problems. In this section, the Itô-Taylor expansion will be derived using the Itô formula. Furthermore, the difference with respect to the classical Taylor expansion will be clarified. Consequently, the necessity of essentially different numerical integration schemes for SDEs is illuminated.

Firstly, we will briefly discuss the classical Taylor expansion. Consider the solution $x(t)$ of a scalar ordinary differential equation:

$$\frac{dx(t)}{dt} = a(x(t)), \tag{2.62}$$

with initial value $x(t_0)$ for $t \in [t_0, T]$. This can be written as an integral formulation:

$$x(t) = x(t_0) + \int_{t_0}^{t} a(x(\nu)) \, d\nu. \tag{2.63}$$

When g is a continuously differentiable function of $x(t)$, we have, by the chain rule,

$$\frac{dg(x(t))}{dt} = \frac{\partial g(x(t))}{\partial x} \, a(x(t)), \tag{2.64}$$

which can be expressed as the integral equation

$$g(x(t)) = g(x(t_0)) + \int_{t_0}^{t} Lg(x(\nu)) \, d\nu, \tag{2.65}$$

in which the operator L (commonly known as the Lie derivative or directional derivative L_a) is defined as $L = a\frac{\partial}{\partial x}$. When $g(x) = x$, we have $Lg = a$ and $L^2 g = La$. Consequently, (2.65) reduces to (2.63). When relation (2.65) is now applied to the function $g = a$ in the integral in (2.63), we obtain

$$\begin{aligned} x(t) = x(t_0) \; &+ \int_{t_0}^{t} \left(a(x(t_0)) + \int_{t_0}^{\nu_1} La(x(\nu_2)) \, d\nu_2 \right) d\nu_1 \\ &= x(t_0) \; + \; a(x(t_0)) \int_{t_0}^{t} d\nu_1 \; + \int_{t_0}^{t} \int_{t_0}^{\nu_1} La(x(\nu_2)) \, d\nu_2 \, d\nu_1, \end{aligned} \tag{2.66}$$

which is the simplest non-trivial Taylor expansion for $x(t)$. Equation (2.65) can again be applied to the function $g = La$ in the double integral in (2.66) to derive

$$x(t) = x(t_0) + a(x(t_0)) \int_{t_0}^{t} d\nu_1 + La(x(t_0)) \int_{t_0}^{t} \int_{t_0}^{\nu_1} d\nu_2 \, d\nu_1 + Q_3, \tag{2.67}$$

with remainder term

$$Q_3 = \int_{t_0}^{t} \int_{t_0}^{\nu_1} \int_{t_0}^{\nu_2} L^2 a(x(\nu_3)) \, d\nu_3 \, d\nu_2 \, d\nu_1. \tag{2.68}$$

For a general $n + 1$ times continuously differentiable function g this method gives the classical Taylor formula in the integral form:

$$
\begin{aligned}
g(x(t)) =& g(x(t_0)) + \sum_{l=1}^{r} \frac{(t - t_0)^l}{l!} L^l g(x(t_0)) \\
&+ \int_{t_0}^{t} \ldots \int_{t_0}^{\nu_r} L^{r+1} g(x(\nu_{r+1})) \, d\nu_{r+1} \ldots d\nu_1,
\end{aligned}
\tag{2.69}
$$

for $t \in [t_0, T]$ and $r = 1, 2, 3 \ldots$.

The Taylor formula (2.69) has proven to be a very useful tool in numerical analysis. It provides approximations of a sufficiently smooth function in a neighbourhood of a given point to any desired level of accuracy. This expansion depends on the values of the function and some of its higher derivatives at the expansion point, weighted by the corresponding multiple time integral. In addition, there is a remainder term which contains the next multiple time integral, but now with a time dependent integrand.

To expand the increments of smooth functions of Itô processes, for example in the construction of numerical methods, it is advantageous to have a stochastic expansion formula with analogous properties to the deterministic Taylor formula. A stochastic Taylor formula can be based on the iterated application of the Itô formula. We will term this expansion the Itô-Taylor expansion.

This Itô formula will now be applied to derive Itô-Taylor expansions. Let $x(t)$ be the solution of a scalar Itô stochastic differential equation in integral form (2.24). Then, for any twice continuously differential function g the Itô formula (2.59) gives

$$
\begin{aligned}
g(x(t)) =& g(x(t_0)) \\
&+ \int_{t_0}^{t} \left(\breve{a}(\nu, x(\nu)) \, \frac{\partial g(x(\nu))}{\partial x} + \frac{1}{2} \, \breve{b}^2(\nu, x(\nu)) \, \frac{\partial^2 g(x(\nu))}{\partial x^2} \right) d\nu \\
&+ \int_{t_0}^{t} \breve{b}(\nu, x(\nu)) \, \frac{\partial g(x(\nu))}{\partial x} \, dW \\
=& \, g(x(t_0)) + \int_{t_0}^{t} L^0 g(x(\nu)) \, d\nu + \int_{t_0}^{t} L^1 g(x(\nu)) \, dW(\nu),
\end{aligned}
\tag{2.70}
$$

in which L^0 and L^1 are the following operators:

$$
L^0 = \breve{a} \frac{\partial}{\partial x} + \frac{1}{2} \breve{b}^2 \frac{\partial^2}{\partial x^2}, \qquad L^1 = \breve{b} \frac{\partial}{\partial x}.
\tag{2.71}
$$

In analogy with the classical Taylor expansions, we apply the Itô formula to the

function $g = \check{a}$ and $g = \check{b}$ in (2.24) and obtain

$$
\begin{aligned}
x(t) = {} & x(t_0) \\
& + \int\limits_{t_0}^{t} \left(\check{a}(x(t_0)) + \int\limits_{t_0}^{\nu_1} L^0 \check{a}(x(\nu_2)) \, d\nu_2 + \int\limits_{t_0}^{\nu_1} L^1 \check{a}(x(\nu_2)) \, dW(\nu_2) \right) d\nu_1 \\
& + \int\limits_{t_0}^{t} \left(\check{b}(x(t_0)) + \int\limits_{t_0}^{\nu_1} L^0 \check{b}(x(\nu_2)) \, d\nu_2 + \int\limits_{t_0}^{\nu_1} L^1 \check{b}(x(\nu_2)) \, dW(\nu_2) \right) dW(\nu_1) \\
= {} & x(t_0) + \check{a}(x(t_0)) \int\limits_{t_0}^{t} d\nu_1 + \check{b}(x(t_0)) \int\limits_{t_0}^{t} dW(\nu_1) + \bar{Q}_2,
\end{aligned}
$$

$$(2.72)$$

with remainder

$$
\begin{aligned}
\bar{Q}_2 = {} & \int\limits_{t_0}^{t} \int\limits_{t_0}^{\nu_1} L^0 \check{a}(x(\nu_2)) \, d\nu_2 \, d\nu_1 + \int\limits_{t_0}^{t} \int\limits_{t_0}^{\nu_1} L^1 \check{a}(x(\nu_2)) \, dW(\nu_2) \, d\nu_1 \\
& + \int\limits_{t_0}^{t} \int\limits_{t_0}^{\nu_1} L^0 \check{b}(x(\nu_2)) \, d\nu_2 \, dW(\nu_1) + \int\limits_{t_0}^{t} \int\limits_{t_0}^{\nu_1} L^1 \check{b}(x(\nu_2)) \, dW(\nu_2) \, dW(\nu_1).
\end{aligned}
$$

$$(2.73)$$

This is the simplest non-trivial Itô-Taylor expansion. We can continue it by applying the Itô formula to all the integrands of the double integrals of (2.72), which results in

$$
\begin{aligned}
x(t) = {} & x(t_0) + \check{a}(x(t_0)) \int\limits_{t_0}^{t} d\nu + \check{b}(x(t_0)) \int\limits_{t_0}^{t} dW(\nu) \\
& + L^0 \check{a}(x(t_0)) \int\limits_{t_0}^{t} \int\limits_{t_0}^{\nu_1} d\nu_2 d\nu_1 + L^1 \check{a}(x(t_0)) \int\limits_{t_0}^{t} \int\limits_{t_0}^{\nu_1} dW(\nu_2) d\nu_1 \\
& + L^0 \check{b}(x(t_0)) \int\limits_{t_0}^{t} \int\limits_{t_0}^{\nu_1} d\nu_2 dW(\nu_1) + L^1 \check{b}(x(t_0)) \int\limits_{t_0}^{t} \int\limits_{t_0}^{\nu_1} dW(\nu_2) dW(\nu_1) \\
& + \bar{Q}_3,
\end{aligned}
$$

$$(2.74)$$

with remainder $\bar{Q}_3$ as given in appendix B. The main properties of the Itô-Taylor expansion are apparent in the preceding relations. We have an expansion with the

multiple Itô integrals with constant integrands:

$$\int\limits_{t_0}^{t} d\nu, \quad \int\limits_{t_0}^{t} dW(\nu), \quad \int\limits_{t_0}^{t}\int\limits_{t_0}^{\nu_1} d\nu_2 \, d\nu_1, \quad \int\limits_{t_0}^{t}\int\limits_{t_0}^{\nu_1} dW(\nu_2) \, d\nu_1,$$

$$\int\limits_{t_0}^{t}\int\limits_{t_0}^{\nu_1} d\nu_2 \, dW(\nu_1), \quad \int\limits_{t_0}^{t}\int\limits_{t_0}^{\nu_1} dW(\nu_2) \, dW(\nu_1), \tag{2.75}$$

and a remainder term involving the next multiple Itô integrals, but now with non-constant integrands. The Itô-Taylor expansion can, in this sense, be interpreted as a generalisation of both the Itô formula and the classical Taylor formula.

It is clear that the difference between the classical Taylor expansion and the Itô-Taylor expansion gives rise to numerical stochastic integration schemes that differ essentially from the classical numerical integration schemes. An important observation is that even for external excitations the Itô-Taylor expansion for $x(t)$ involves Itô integrals for nonlinear $\breve{a}(x(t))$.

2.5   Numerical solution of stochastic differential equations

Generally, nonlinear SDEs are not solvable analytically. Therefore, the solution will have to be approximated numerically by time discrete approximations. In order to compute these time discrete approximations for the Itô process $\underline{x}$ in equation (2.18), integration schemes will have to be developed. Kloeden and Platen [1992] give an extensive survey on this subject. Commonly, these integration schemes are based on the Itô-Taylor expansions, described in section 2.4. These schemes will be termed Taylor schemes. In order to use these expansions to derive time discrete approximations, the multiple Itô integrals in (2.75) will have to be evaluated.

2.5.1   Time discrete approximation

Consider an Itô process x satisfying the stochastic differential equation

$$dx = \breve{a}(x) \, dt + \breve{b}(x) \, dW \tag{2.76}$$

on $t_0 \leq t \leq T$ with $x(t_0) = x_0$. This process will be approximated by Y, where $Y_j = Y(\tau_j)$ corresponds to a discrete time instant τ_j of the given time discretization $t_0 = \tau_1 < \tau_2 < \ldots < \tau_j < \ldots < \tau_n = T$ of $[t_0, T]$. For the sake of simplicity, here, an equidistant discretization is assumed: $\tau_{j+1} - \tau_j = \Delta t$ for $j = 1, 2, \ldots, n - 1$. In order to investigate the convergence of such approximations Y for increasing n, a convergence criterion should be introduced. Now, two different types of convergence can be distinguished for the time discrete approximation of Itô processes:

1. strong convergence;

2. weak convergence.

With respect to strong convergence we define an absolute error criterion:

$$\varepsilon_s = E\{| \, x(T) - Y(T) \, |\}, \tag{2.77}$$

which reflects a measure of pathwise closeness at the time instant T. The strong convergence criterion is used when approximation of a certain realisation of the response process is pursued. For schemes with a strong convergence order p_s the error ε_s relates to the time step Δt and the convergence order through

$$\varepsilon_s = K_s (\Delta t)^{p_s}. \tag{2.78}$$

However, we are not particularly interested in specific realisations of the response process. More important are its stochastic characteristics, such as the statistical moments. Therefore, one could also define a measure of convergence with respect to these moments. The error can then be defined by the 'mean error':

$$\varepsilon_w = \mid E\{x(T)\} - E\{Y(T)\} \mid, \tag{2.79}$$

where the error ε_w is related to a weak order of convergence p_w and Δt through

$$\varepsilon_w = K_w (\Delta t)^{p_w}. \tag{2.80}$$

Numerical integration schemes can be derived using the Itô-Taylor expansions. The desired order of convergence determines the truncation that must be used. Generally, for a certain scheme, which originates from a specific truncation of the Itô-Taylor expansion, it holds that $p_w > p_s$, since the weak convergence criterion represents a weaker type of convergence. The Itô-Taylor truncation required for a certain strong convergence order will in general involve more terms of the Itô-Taylor expansion than the Itô-Taylor truncation required for the same order of weak convergence. So, the error in the statistical moments will, generally, decrease faster (as Δt decreases) than the error on the pathwise solution.

We will, now, briefly discuss two schemes that can be derived using truncations of the Itô-Taylor expansion. When the Itô-Taylor expansion is truncated as in (2.72), the result is the Euler scheme:

$$Y_{j+1} = Y_j + \breve{a}(Y_j)\Delta t + \breve{b}(Y_j)\Delta W, \tag{2.81}$$

because

$$\int_{\tau_j}^{\tau_{j+1}} d\nu = \tau_{j+1} - \tau_j = \Delta t \ \text{ and } \ \int_{\tau_j}^{\tau_{j+1}} dW(\nu) = W(\tau_{j+1}) - W(\tau_j) = \Delta W. \tag{2.82}$$

From section 2.2 we know that the increments ΔW of the Wiener process are independent, Gaussian, random variables with zero mean and variance $E\{\Delta W^2\} = \Delta t$. For these increments we can use a sequence of independent, Gaussian pseudo-random numbers. In Kloeden and Platen [1992] it is shown that the Euler scheme has strong convergence order 0.5 and weak convergence order 1.0. Of course, when applied to a specific system the convergence order of the numerical schemes will depend on the specific $\breve{a}$ and $\breve{b}$ at hand. However, generally, in the name of a scheme the maximum attainable convergence order (for that scheme) is indicated.

Since we are merely interested in the statistical properties of the Itô response process, weak schemes will be used throughout this thesis. When all the double stochastic integrals of the Itô-Taylor expansion are included in the truncation, see (2.74), a Taylor scheme of weak order 2.0 can be derived:

$$
\begin{aligned}
Y_{j+1} =\ & Y_j + \check{a}(Y_j)\Delta t + \check{b}(Y_j)\Delta W \\
& + \frac{1}{2}\check{b}(Y_j)\check{b}'(Y_j)\{(\Delta W)^2 - \Delta t\} + \check{a}'(Y_j)\check{b}(Y_j)\Delta Z \\
& + \frac{1}{2}\left(\check{a}(Y_j)\check{a}'(Y_j) + \frac{1}{2}\check{a}''(Y_j)\check{b}^2(Y_j)\right)\Delta t^2 \\
& + \left(\check{a}(Y_j)\check{b}'(Y_j) + \frac{1}{2}\check{b}''(Y_j)\check{b}^2(Y_j)\right)\{\Delta W\Delta t - \Delta Z\},
\end{aligned}
\tag{2.83}
$$

Herein, the following weak approximations for the multiple Itô integrals of (2.75) can be given by [Kloeden and Platen, 1992]:

$$
\int_{\tau_n}^{\tau_{n+1}}\int_{\tau_n}^{\nu_1} dW(\nu_2)dW(\nu_1) = \frac{1}{2}((\Delta W)^2 - \Delta t), \quad \int_{\tau_n}^{\tau_{n+1}}\int_{\tau_n}^{\nu_1} dW(\nu_2)d\nu_1 = \Delta Z,
$$

$$
\int_{\tau_n}^{\tau_{n+1}}\int_{\tau_n}^{\nu_1} d\nu_2 dW(\nu_1) = \Delta W\Delta t - \Delta Z.
\tag{2.84}
$$

Furthermore, in (2.83) $' = \frac{\partial}{\partial x}$ while ΔZ is normally distributed with zero-mean, variance $E\{(\Delta Z)^2\} = \frac{1}{3}\Delta t^3$ and covariance $E\{\Delta Z\Delta W\} = \frac{1}{2}\Delta t^2$ [Kloeden and Platen, 1992]. Note that the peculiar property (2.50) of the Itô integral effects on the numerical integration scheme through (amongst other integrals) the first double Itô integral in (2.84). In practice, ΔZ and ΔW can be determined from two independent, Gaussian, random variables U_1 and U_2 with unit variance by means of the transformation

$$
\Delta W = U_1\sqrt{\Delta t}, \qquad \Delta Z = \frac{1}{2}\Delta t^{3/2}(U_1 + \frac{1}{\sqrt{3}}U_2).
\tag{2.85}
$$

In Kloeden and Platen [1992] it is shown that this scheme can be simplified by using the fact that we have much more freedom with the weak convergence criterion than with the strong convergence criterion as far as the generation of the noise increments is concerned. The use of the second random variable ΔZ can be avoided by replacing ΔW by $\Delta\hat{W}$ and ΔZ by $\frac{1}{2}\Delta\hat{W}\Delta t$:

$$
\begin{aligned}
Y_{j+1} =\ & Y_j + \check{a}(Y_j)\Delta t + \check{b}(Y_j)\Delta\hat{W} + \frac{1}{2}\check{b}(Y_j)\check{b}'(Y_j)\{(\Delta\hat{W})^2 - \Delta t\} \\
& + \frac{1}{2}\left(\check{a}(Y_j)\check{a}'(Y_j) + \frac{1}{2}\check{a}''(Y_j)\check{b}^2(Y_j)\right)\Delta t^2 \\
& + \frac{1}{2}\left(\check{a}'(Y_j)\check{b}(Y_j) + \check{a}(Y_j)\check{b}'(Y_j) + \frac{1}{2}\check{b}''(Y_j)\check{b}^2(Y_j)\right)\Delta\hat{W}\Delta t,
\end{aligned}
\tag{2.86}
$$

Herein, $\Delta\hat{W}$ has analogous moment properties as ΔW, which are satisfied by a Gaussian random variable with variance Δt. By using the Itô-Taylor expansions in the manner described by the former two examples many more schemes with other weak and strong convergence orders can be derived. In Kloeden and Platen [1992] it is stated that schemes of weak order p_w can be derived using truncations of the Itô-Taylor expansion, which include multiple Itô integrals up to multiplicity p_w.

Of course, these Taylor schemes can only be applied effectively when the partial derivatives of $\check{a}$ and $\check{b}$ with respect to x can be evaluated analytically. Furthermore, the implementation of such schemes can be a rather complex matter. Therefore, so-called derivative-free schemes can be derived from the Taylor schemes using finite difference approximations for the derivatives in these Taylor schemes. Platen [1987] developed an explicit, second-order weak scheme, which will be used extensively throughout this thesis:

$$Y_{j+1} = Y_j + \frac{1}{2}\left(\check{a}(\Upsilon) + \check{a}(Y_j)\right)\Delta t + \frac{1}{4}\left(\check{b}(\Upsilon^+) + \check{b}(\Upsilon^-) + 2\check{b}(Y_j)\right)\Delta\hat{W}$$
$$+ \frac{1}{4}\left(\check{b}(\Upsilon^+) + \check{b}(\Upsilon^-)\right)\left\{\left(\Delta\hat{W}\right)^2 - \Delta t\right\}\Delta t^{-\frac{1}{2}} \tag{2.87}$$

with supporting values

$$\Upsilon = Y_j + \check{a}(Y_j)\Delta t + \check{b}(Y_j)\Delta\hat{W}, \qquad \Upsilon^\pm = Y_j + \check{a}(Y_j)\Delta t \pm \check{b}(Y_j)\sqrt{\Delta t}.$$

For obvious reasons, the numerical stability of the integration schemes should be checked. This can be done by considering the numerical stability of a scheme with respect to a linear, stochastic differential test-equation of the form:

$$dx = \lambda\, x\, dt + dW. \tag{2.88}$$

where λ is a real number with $\lambda < 0$. So, $\check{a} = \lambda\, x$ and $\check{b} = 1$. Let us assume that we can write a given numerical scheme, when applied to the test-equation (2.88), in the form

$$Y_{j+1} = Y_j\, K(\lambda\Delta t) + \Delta R_j, \tag{2.89}$$

where ΔR_j represents the terms with random variables. Herein, the specific system under investigation and the applied integration scheme jointly determine the form of K. Now, the particular set of numbers $\lambda\Delta t$, for which

$$\lambda < 0 \qquad \text{and} \qquad \det(K(\lambda\Delta t)) < 1, \tag{2.90}$$

is termed the region of absolute stability of the scheme. If Δt is chosen in such a way that $\lambda\Delta t$ lies within that region, the scheme is numerically stable for the test-equation. Of course, for nonlinear systems some kind of linearised, worst-case scenario will have to be considered.

2.6 Summary

The most important conclusion of this chapter is that SDEs can not be solved numerically using classical integration techniques. Integration techniques based on

Itô calculus can be used to tackle this problem. Let us summarise the steps of reasoning towards this conclusion:

1. the excitation is modelled using a white noise process;

2. consequently, the differential equation, that describes the dynamic system, is not an ODE but an SDE;

3. the solution of the SDE (in integral formulation) cannot be expressed in terms of Riemann or Riemann-Stieltjens integrals;

4. to overcome this problem the Itô integral is defined. In this definition the fact that the response of the dynamic system should not anticipate on the excitation is crucial;

5. this specific definition of the Itô integral implies that functions of the solution of the SDE do not obey the classical chain rule, but a 'stochastic chain rule': the Itô formula. In the Itô formula an extra term appears, which is absent in the classical chain rule;

6. iterated application of this Itô formula yields the Itô-Taylor expansion. This expression is the stochastic counterpart of the classical Taylor expansion, from which it essentially differs. This difference stems from the fact that certain terms of a specific order in the Taylor expansion will contribute to terms of a lower order in the the Itô-Taylor expansion. Consequently, truncations of a specific order of the Taylor and Itô-Taylor expansions will differ;

7. the expansions mentioned above are generally used to derive numerical integration schemes. Due to the fact that the Itô-Taylor expansion differs from the classical Taylor expansion, the numerical integration schemes based on the Itô-Taylor expansion differ essentially from their classical counterparts.

In Kloeden and Platen [1992] a wide variety of numerical schemes for SDEs is presented. What kind of scheme is chosen depends on the system at hand and the information that is desired. As stated before, when path-wise approximations of realisations of the response process are sought, strong schemes should be used. However, often one is merely interested in the statistical properties of the response. Then, weak schemes should be used. As in classical numerical integration, the order of the integration scheme should be chosen based on the knowledge on the system under investigation.

3 Simulated stochastic nonlinear response phenomena

In this chapter, some characteristic phenomena in the stochastic response of a certain class of nonlinear systems will be studied. As the main computational tool we will use numerical integration using the procedures described in the previous chapter in case of white noise excitations. This study involves questions like: "what happens?" and "why does it happen?". So, the main goals of this chapter are:

1. to discover general, nonlinear, stochastic response phenomena using an inductive approach;

2. to obtain understanding on the origin of these phenomena.

In literature, the attention is, unfortunately, merely focussed on gaining information with respect to the probability distribution of the response (pdf, statistical moments). However, essential information on stochastic, nonlinear behaviour is enclosed in the frequency domain. Therefore, especially the power spectral density function of the response will be monitored repeatedly to gain insight in the roots of a wide variety of nonlinear phenomena.

A second important angle of incidence in this thesis is the proposition that the simultaneous observation of deterministic (periodic) and stochastic behaviour of nonlinear, dynamic systems can be very beneficial for gaining thorough understanding of specific aspects of stochastic, nonlinear behaviour. To illuminate this, additional investigations on the response to random excitations with a band-limited frequency spectrum are performed. Moreover, the characteristics of the response to nearly periodic, though random, excitations are studied and compared to the characteristics of periodic responses.

In order to evaluate the behaviour of a nonlinear system in case of white noise excitation, the Itô-integration techniques, discussed in chapter 2, are used. The results are compared to those obtained by the application of the far more efficient and widely-used method of statistical linearization. By definition, this method provides rather inaccurate results for (strongly) nonlinear systems. The origin of the failing of this method can be illuminated through observations of the simulated response characteristics in the frequency domain. That specific knowledge provides us with ideas for more accurate approximation methods, which will be developed, discussed and applied in the chapters 5 and 6.

3.1   The nonlinear dynamic system

The nonlinear, dynamic system, that will be used throughout this thesis, is depicted in figure 3.1. This piece-wise linear system is governed by the following, second-order differential equation:

$$m\,\ddot{x} + c\,\dot{x} + k\,x + k_{nl}\,\epsilon(x)\,x = d, \qquad \text{where}\ \ \epsilon(x) = \left\{ \begin{array}{ll} 0 & \text{if } x \geq 0 \\ 1 & \text{if } x < 0 \end{array} \right., \qquad (3.1)$$

and d is a stationary, random, Gaussian, zero-mean excitation process.
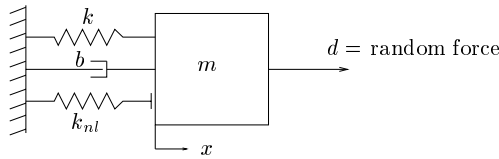
Figure 3.1: The nonlinear dynamic system.

Stiffness nonlinearities of this one-sided form can be found in many engineering systems. Some examples are elastic stops in vehicle suspensions, snubbers on solar arrays connected to satellites [Van Campen et al., 1997b], suspension bridges or models used in the offshore industry [Thompson and Stewart, 1986]. Fey [1992] and Van de Vorst [1996] used this system as a SDOF model for a beam with a nonlinear (one-sided) support. With $k = m = 1$, the differential equation can be written as

$$\ddot{x} + 2\zeta\,\dot{x} + x + \alpha\,\epsilon(x)\,x = d, \qquad (3.2)$$

where $\zeta = c/(2\sqrt{mk}) = c/2$ is the dimensionless damping parameter and $\alpha = k_{nl}/k$ the nonlinearity parameter. These parameters will be varied to examine the effect of the amount of damping and the level of nonlinearity on the stochastic behaviour of the system.

Here, a SDOF system is chosen to avoid the extra level of complexity that extra degrees of freedom impose. A strongly nonlinear, MDOF system will be investigated in chapter 4. Despite the simplicity of the nonlinearity of the system and the fact that it is a SDOF system, it exhibits very complex, nonlinear behaviour. This particular system is chosen, because it is known to exhibit a wide variety of interesting, specifically nonlinear response phenomena, when excited periodically (sinusoidal excitation) [Shaw and Holmes, 1983; Thompson and Stewart, 1986; Fey, 1992; Van de Vorst, 1996]. Some of these nonlinear, deterministic response characteristics will be discussed briefly in section 3.2. That knowledge will give us the chance to evaluate the stochastic behaviour of this system against the background of its deterministic behaviour [Van de Wouw et al., 1997].

When the random excitation is a white noise process ξ, with autocorrelation function $R_{\xi\xi}(\tau) = D\,\delta(\tau)$, the differential equation (3.2) can be transformed to the

form of an Itô equation, see (2.18). This results in the drift and diffusion coefficients

$$\check{\underline{a}} = \underline{a} = \begin{bmatrix} \dot{x} \\ -2\zeta\dot{x} - x - \alpha\epsilon(x)x \end{bmatrix} \quad \text{and} \quad \check{\underline{b}} = \underline{b} = \begin{bmatrix} 0 \\ \sqrt{D} \end{bmatrix} \quad (3.3)$$

respectively, since the Wong-Zakai correction produces no extra terms in this externally excited case.

3.2 Survey of periodic response characteristics

Extensive work on the periodic behaviour of the piece-wise linear system has been done by Shaw and Holmes [1983], Fey [1992] and Van de Vorst [1996]. In figure 3.2, the maximum absolute displacement $|x|_{max}$ is plotted as a function of the angular excitation frequency ω_e of the periodic (sinusoidal) excitation for the weakly nonlinear case of $\alpha = 1$. The periodic response data for the stronger nonlinear case $\alpha = 6$ is plotted in figure 3.3. Here, the excitation is $\cos(\omega_e t)$. To calculate these periodic responses, a time discretization method combined with a path-following technique has been used [Fey, 1992]. These figures clearly illustrate the existence
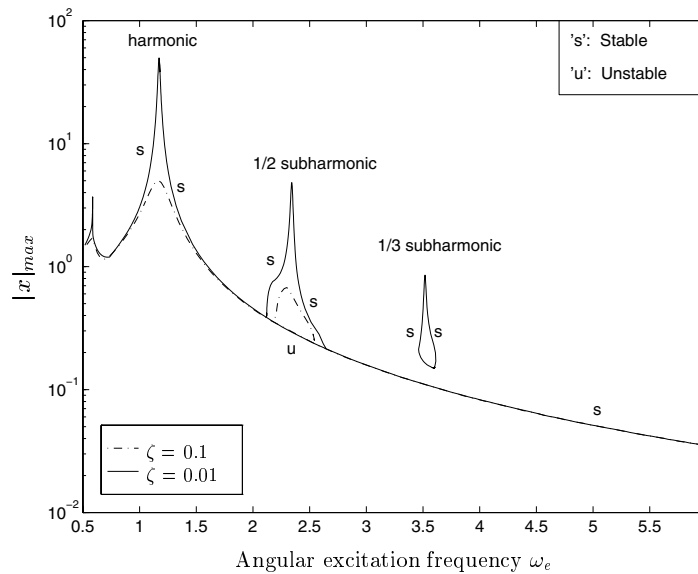
Figure 3.2: Maximum absolute displacement vs. excitation frequency for periodic excitation and $\alpha = 1$.

of harmonic (period one) and subharmonic (higher period) solutions. Furthermore, for $\omega_e \in [0.6, 0.7]$, also a superharmonic resonance exists. It should be noted that the period time of a harmonic solution equals that of the excitation. Moreover, a harmonic solution consists of the frequencies $\omega_e, 2\omega_e, 3\omega_e, \ldots$ and so on. A 1/n subharmonic solution, however, comprises the frequencies $\frac{1}{n}\omega_e, \frac{2}{n}\omega_e, \frac{3}{n}\omega_e, \ldots$, where
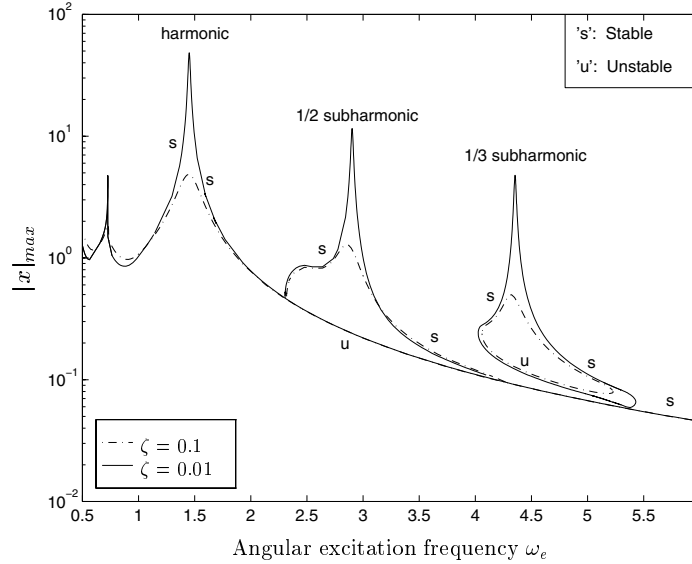
Figure 3.3: Maximum absolute displacement vs. excitation frequency for periodic excitation and $\alpha = 6$.

the response period is the n$^{\text{th}}$ multiple of the excitation period. Furthermore, in a n superharmonic resonance one or more higher harmonics cause resonance in a (sub)harmonic response. The stability of the periodic solutions is indicated by the symbols 's' and 'u' in the legend. It can be seen that in the frequency range of the 'closed loop' 1/3 subharmonic solution multiple stable solutions exist. Clearly, the subharmonic resonances become more powerful for stronger nonlinearities. More-over, higher damping gradually suppresses nonlinear effects such as subharmonic resonances.

3.3   Statistical linearization

For the evaluation of the response statistics of the piece-wise linear system, the statistical linearization method [Roberts and Spanos, 1990] will be used. The results of the linearization method will be compared to the response statistics estimated using the numerical integration techniques, discussed in chapter 2.

The basic idea of statistical linearization is to replace the original, nonlinear system by a linear model. The system parameters of the linear model are chosen in such a way that the linear model is optimal in some statistical sense with respect to the original, nonlinear system. This means that the response statistics of the linear model (which follow from a straightforward analytical procedure) are approximations for the most relevant response statistics of the nonlinear system

Let us, now, describe the method in more detail. Since the excitation is external, see section (1.2.7), the linearization will be performed on the equations of motion of

the nonlinear system. For the nonlinear system (3.2), a suitable linear model can be written as

$$\ddot{x} + 2\zeta\ \dot{x} + \beta_1\ x_E + \beta_0 = d, \tag{3.4}$$

where $x_E = x - E\{x\}$. Since $\ddot{x}_E = \ddot{x}$, $\dot{x}_E = \dot{x}$ due to stationarity and, thus, $\beta_0 = E\{d\}$, equation (3.4) can be written as

$$\ddot{x}_E + 2\ \zeta\ \dot{x}_E + \beta_1\ x_E = d_E \qquad \text{with} \qquad d_E = d - E\{d\}. \tag{3.5}$$

Throughout this thesis merely zero-mean excitation processes will be considered, implying that $\beta_0 = 0$.

The next step is the definition of an error, which embodies the difference between the nonlinear system and the linear model:

$$\varepsilon_{lin} = (x + \alpha\ \epsilon(x)\ x) - \beta_1\ x_E, \tag{3.6}$$

for some β_1. Subsequently, our goal is to minimise ε_{lin} in the mean-square sense. This minimisation of $E\{\varepsilon_{lin}^2\}$ with respect to β_0 and β_1 results in the following equations:

$$\beta_1 = \frac{E\{x_E(x + \alpha\ \epsilon(x)\ x)\}}{\sigma_x^2}, \tag{3.7}$$

$$E\{x + \alpha\ \epsilon(x)\ x\} = 0, \tag{3.8}$$

At this point, μ_x, σ_x and β_1 form the three unknowns of the linearization problem. So, for a unique solution, besides the equations (3.7) and (3.8), a third equation is necessary. This equation can be derived from frequency domain considerations. Namely, for a linear system (with frequency response function $H(i\omega)$) the relation between the auto power spectra of input d and output x obeys

$$S_{xx}(\omega) = \mid H(i\omega) \mid^2 S_{dd}(\omega). \tag{3.9}$$

The frequency response function $H(i\omega)$ is given by

$$H(i\omega) = \frac{1}{\beta_1 - \omega^2 + 2\ i\ \omega\ \zeta}. \tag{3.10}$$

Using (3.9), the variance of the response can be computed using

$$\sigma_x^2 = \int\limits_{-\infty}^{\infty} S_{xx}(\omega)\ d\omega = \int\limits_{-\infty}^{\infty} \mid H(i\omega) \mid^2 S_{dd}(\omega)\ d\omega. \tag{3.11}$$

When the excitation is a white noise process with intensity one ($S_{dd}(\omega) = \frac{1}{2\pi}$), (3.11) yields

$$\sigma_x^2 = \frac{1}{4\ \zeta\ \beta_1}. \tag{3.12}$$

The next step is to solve the equations (3.7), (3.8) and (3.12) simultaneously. In doing so, beforehand, the expected values $E\{x_0(x + \alpha\ \epsilon(x)\ x)\}$ and $E\{x + \alpha\ \epsilon(x)\ x\}$ have to expressed in terms of μ_x and σ_x^2 by assuming a Gaussian probability density function, see appendix C. It should be noted that the response of a linear system to Gaussian excitation is, generally, Gaussian too. The equations (3.7), (3.8) and (3.11) form a set of coupled, nonlinear, algebraic equations. Once the optimal values for μ_x, σ_x^2 and β_1 are computed, the probability density function of the output of the linear model is given by a normal distribution:

$$f(x) = \frac{1}{\sqrt{2\pi}\sigma_x}\exp(-\frac{(x - \mu_x)^2}{2\sigma_x^2}). \tag{3.13}$$

It should be noted that, consequently, the deviation from normality of the response of the original, nonlinear system can not be approximated using such a linear model. Moreover, one can evaluate the power spectral density of the response of the linear model using (3.9).

3.4   Response to white noise excitation

Let us consider the piece-wise linear oscillator excited by a white noise excitation with intensity one. The numerical (explicit, second-order, weak) scheme (2.87) is used to compute time-discrete approximations of realisations of the response process. An explicit scheme is chosen, because the derivatives needed in the Itô-Taylor schemes do not exist everywhere for the piece-wise linear system. The choice for a second-order scheme was based on extensive efficiency investigations between the Euler scheme, the second-order scheme and higher-order schemes (also for this application). According to the weak convergence criterion, the computed realisations converge (with the weak convergence order) to the realisations of the real response process in the sense of their statistical moments. Of course, the numerical stability of the integration scheme was checked and ensured. Moreover, time-discrete approximations using different time steps were computed to be able to guarantee convergence to a certain desired level. This desired level of accuracy is taken significantly smaller than the level of the statistical error (due to the finite sample lengths) on the estimated response statistics.

In the following sections, these realisations are used to estimate the following response statistics:

1. statistical moments up to the fourth order;

2. probability density function;

3. power spectral density (frequency domain information).

Successively, specifically nonlinear characteristics with respect to these response statistics will be observed. The results of these simulations will be compared to the results provided by statistical linearization. Doing so, the shortcomings of the linearization technique can be illuminated along with their origin.

The response statistics of the piece-wise linear system will be discussed for different levels of nonlinearity; from weakly nonlinear ($\alpha = 1$) to strongly nonlinear ($\alpha = 6$).

3.4.1 Statistical moments

The statistical moments that will be monitored are:

1. the mean μ_x;

2. the standard deviation σ_x;

3. the skewness $\gamma_x = \frac{\eta_3}{\eta_2^{3/2}}$;

4. the kurtosis $\kappa_x = \frac{\eta_4}{\eta_2^2}$,

with η_p $(p = 1, 2, 3, 4)$ defined in (2.5). The mean and the standard deviation are well-known response statistics. Together, they entirely define the probability distribution of a Gaussian process. The standard deviation is an important measure for the amount of energy in the stochastic process. The skewness is the scaled, third-order, central moment, which indicates the asymmetry in the process. For a Gaussian process the skewness is zero. Absolute values of γ in excess of about 0.5 correspond to noticeable asymmetry in the probability density function, where absolute values higher than 2 point to an extreme asymmetry. The kurtosis is the scaled, fourth-order, central moment. For a Gaussian process the kurtosis is 3. Values higher than 3 manifest a probability distribution with relatively extensive tails.

In case of simulations, these statistical moments will be approximated by so-called estimators. These estimators are computed using m independent samples of length n. In these samples the transient part of the response is omitted, since merely the steady state part of the response is of interest. The estimators for the mean, the standard deviation, the skewness and the kurtosis are

$$\bar{x} = \frac{1}{m}\sum_{j=1}^{m}\bar{x}_j = \frac{1}{mn}\sum_{j=1}^{m}\sum_{k=1}^{n}x_{jk}\,,$$

$$S_x = \frac{1}{m}\sum_{j=1}^{m}S_j = \frac{1}{mn}\sum_{j=1}^{m}\sum_{k=1}^{n}\frac{(x_{jk}-\bar{x}_j)^2}{n-1}\,,$$

$$\hat{\gamma}_x = \frac{1}{m}\sum_{j=1}^{m}\hat{\gamma}_j = \frac{1}{mn}\sum_{j=1}^{m}\sum_{k=1}^{n}\frac{(x_{jk}-\bar{x}_j)^3}{(n-1)S_j^3}\,,$$

$$\hat{\kappa}_x = \frac{1}{m}\sum_{j=1}^{m}\hat{\kappa}_j = \frac{1}{mn}\sum_{j=1}^{m}\sum_{k=1}^{n}\frac{(x_{jk}-\bar{x}_j)^4}{(n-1)S_j^4}\,,$$

(3.14)

respectively, where x_{jk} is the k-th discrete value (of the steady state part) of the j-th sample. The 95 % confidence intervals of these estimators can be determined

by

$$\left| \frac{\bar{x} - \mu_x}{\mu_x} \right| \leq \frac{1.96\, S_{\bar{x}_j}}{\bar{x}\sqrt{m}} \qquad \text{with} \qquad S_{\bar{x}_j} = \sqrt{\sum_{j=1}^{m} \frac{(\bar{x}_j - \bar{x})^2}{m-1}}, \qquad (3.15)$$

$$\left| \frac{S_x - \sigma_x}{\sigma_x} \right| \leq \frac{1.96\, S_{S_j}}{S_x\sqrt{m}} \qquad \text{with} \qquad S_{S_j} = \sqrt{\sum_{j=1}^{m} \frac{(S_j - S)^2}{m-1}}, \qquad (3.16)$$

$$\left| \frac{\hat{\gamma}_x - \gamma_x}{\gamma_x} \right| \leq \frac{1.96\, S_{\hat{\gamma}_j}}{\hat{\gamma}_x\sqrt{m}} \qquad \text{with} \qquad S_{\hat{\gamma}_j} = \sqrt{\sum_{j=1}^{m} \frac{(\hat{\gamma}_j - \hat{\gamma})^2}{m-1}}, \qquad (3.17)$$

$$\left| \frac{\hat{\kappa}_x - \kappa_x}{\kappa_x} \right| \leq \frac{1.96\, S_{\hat{\kappa}_j}}{\hat{\kappa}_x\sqrt{m}} \qquad \text{with} \qquad S_{\hat{\kappa}_j} = \sqrt{\sum_{j=1}^{m} \frac{(\hat{\kappa}_j - \hat{\kappa})^2}{m-1}}. \qquad (3.18)$$

The idea behind this is that $\bar{x}$, S_x, $\hat{\gamma}_x$ and $\hat{\kappa}_x$ are normally distributed due to the central limit theorem [Papoulis, 1965].

In figure 3.4, the estimates and confidence intervals for the mean (due to both simulation as well as linearization) are shown as a function of the nonlinearity parameter α. The confidence intervals provide information on the liability of the
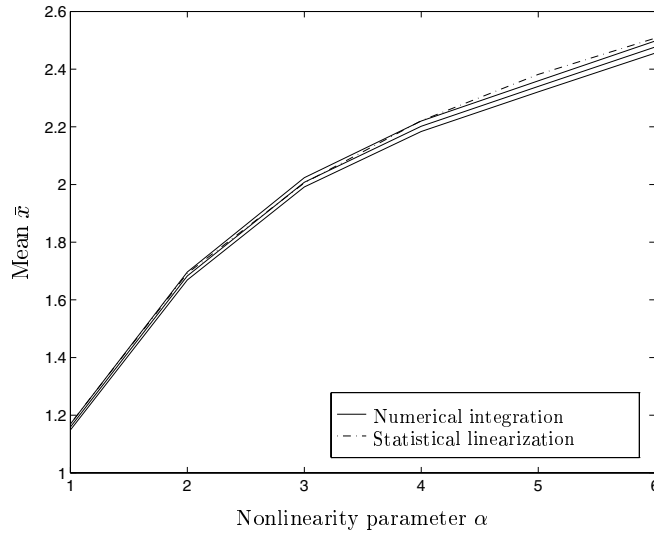
Figure 3.4: Estimation of the mean μ_x for $\zeta = 0.01$.

estimators. The mean increases with increasing nonlinearity. This is quite logical, since the asymmetry in the system increases for increasing α. Furthermore, the figure shows that the linearization results are rather accurate except for stronger nonlinearities.

In figure 3.5, the results for the standard deviation are shown. This figure shows that the error in the linearization result increases fast for an increasing nonlinearity. It should again be emphasised that the standard deviation is a very important response statistic, since it is often used in failure criteria for engineering systems. With this in mind, the error induced by the linearization approach can be considered unacceptably high for stronger nonlinearities. To be more specific, the linearization method structurally underestimates the standard deviation σ_x. This can be understood by studying the frequency domain statistics, which will be discussed in section 3.4.3.
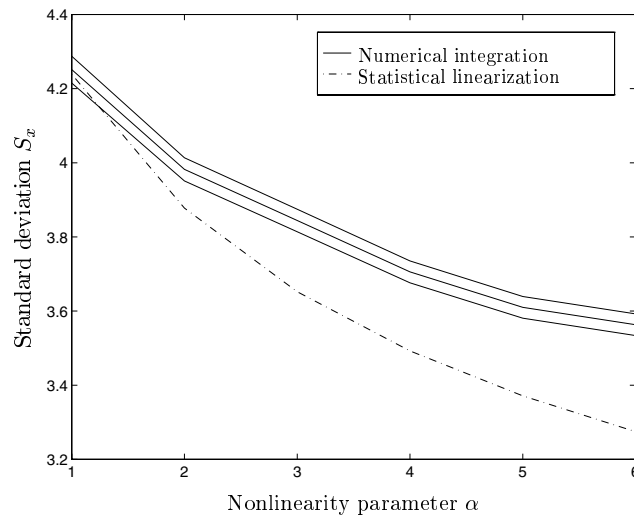
Figure 3.5: Estimation of the standard deviation σ_x for $\zeta = 0.01$.

The information with respect to the higher-order moments, like skewness and kurtosis, will also be very informative, since the response of a nonlinear system to a Gaussian excitation will generally be non-Gaussian. In figure 3.6, the estimate for the skewness is depicted (along with its 95 % confidence intervals) for an increasing nonlinearity. Clearly, a stronger nonlinearity induces a higher asymmetry in the response, indicated by a higher value for the skewness. This asymmetry clearly roots from the one-sidedness of the stiffness characteristic of the piece-wise linear system.

In figure 3.7, the estimate for the kurtosis is shown. It visualises that the estimate for the kurtosis also deviates more and more from its Gaussian value ($\kappa = 3$) for stronger nonlinearities. It can be concluded that the response diverges progressively from a normal distribution when α increases.

3.4.2 Probability density function

The deviation of the response statistics from normality will also be reflected in the probability density function. The figures 3.8 and 3.9 display the pdf for $\alpha = 1$
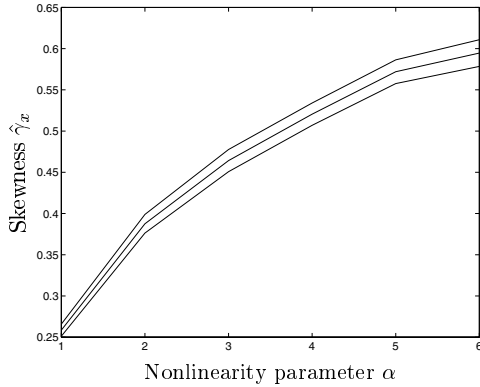
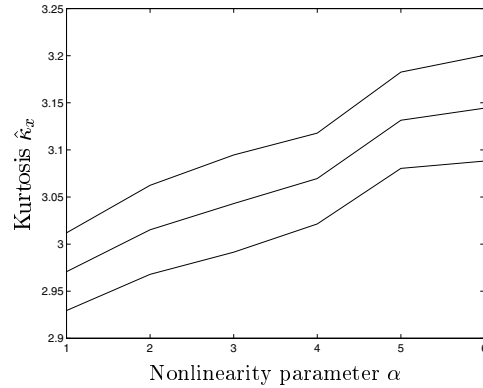Figure 3.6: Estimation of the skewness γ_x for $\zeta = 0.01$.

Figure 3.7: Estimation of the kurtosis κ_x for $\zeta = 0.01$.

and $\alpha = 6$, respectively. For the simulation estimates the 95 % confidence intervals are included. Again the simulation results are compared to the results of statistical linearization, which gives a Gaussian pdf. Figure 3.9 clearly demonstrates the asymmetry of the response for $\alpha = 6$. For $\alpha = 1$, this asymmetry is obviously less present. For $\alpha = 6$, the response characteristics indicate distinctly non-Gaussian behaviour. To test the hypothesis that the response is significantly non-Gaussian, a significance test could be performed. The test of Shapiro and Wilk [Shapiro and Wilk, 1965, 1968] is designed especially to test on normality. The application of this test to realisations of the response of the piece-wise linear system, for $\zeta = 0.01$ and $\alpha = 6$, showed that the response should be regarded as being significantly non-Gaussian (on a 99 % significance level).
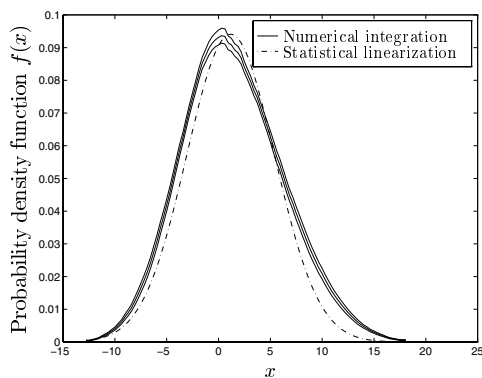
Figure 3.8: Probability density function $f(x)$ for $\alpha = 1$ and $\zeta = 0.01$.
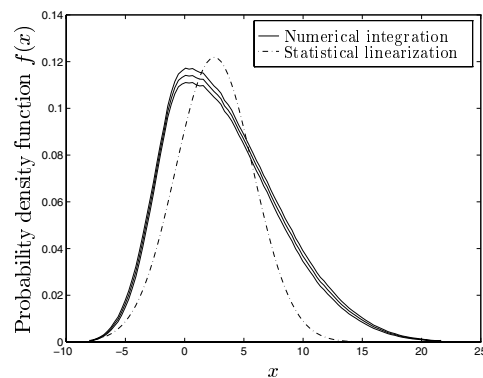
Figure 3.9: Probability density function $f(x)$ for $\alpha = 6$ and $\zeta = 0.01$.

3.4.3 Power spectral density

In literature, very little attention has been paid to the frequency domain characteristics of nonlinear, dynamic systems excited by stochastic processes. It will be shown that this information can be of great value for the understanding of the system's stochastic behaviour.

In the figures 3.10 and 3.11, the power spectral density [1] of the response, $S_{xx}(\omega)$, is plotted for two different levels of nonlinearity. The power spectral density of the response is estimated numerically using the Welch method [Oppenheim and Schafer, 1975]. The confidence levels of the estimates of the power spectral density are
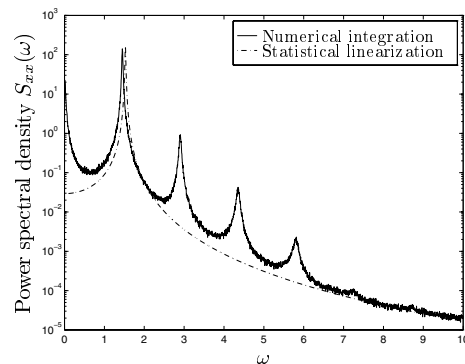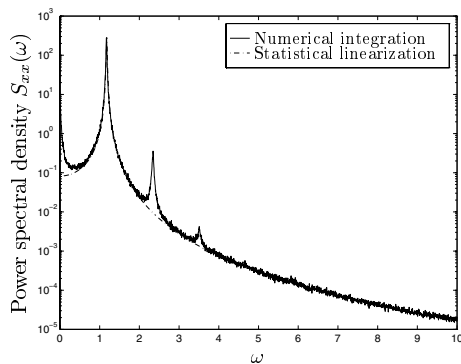
Figure 3.10: Power spectral density $S_{xx}(\omega)$ for $\alpha = 1$ and $\zeta = 0.01$.

Figure 3.11: Power spectral density $S_{xx}(\omega)$ for $\alpha = 6$ and $\zeta = 0.01$.

omitted in these figures. This is done because graphically one would not be able to distinguish the estimate of the psd from its intervals anyway. The main resonance frequency (at $\omega = 1.17$ for $\alpha = 1$ and shifting to $\omega = 1.45$ for $\alpha = 6$) is dominating these figures. The resonances at higher frequencies are situated at multiples of the main resonance frequency. These 'extra' resonances are direct consequences of the nonlinearity of the system. Since the energy in the response process can be visualised by the area beneath the graph of the power spectral density, the higher resonances contribute extra energy.

It should be noted that the presence of the 'extra' resonances becomes more evident for higher nonlinearities; for higher damping levels (for example $\zeta = 0.1$) and a weak nonlinearity ($\alpha = 1$) the higher resonances can almost disappear, see figure 3.12. The results with respect to the power spectral density (for $\alpha = 6$ and $\zeta = 0.01$) demonstrate another striking nonlinear response property; namely, the presence of a large amount of energy at low frequencies. This can be visualised by looking at a realisation of the response x, see figure 3.13. The asymmetry of the nonlinearity is the cause for this phenomenon. Namely, when such a system with an asymmetric nonlinearity is forced by an excitation comprising two frequencies ω_1

---

[1]It should be noted that throughout this thesis two-sided power spectral densities will be used. However, the power spectral densities are merely shown for positive frequencies since they are symmetric around $\omega = 0$.
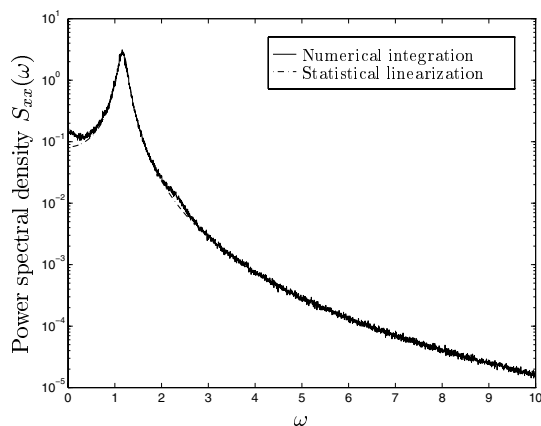
Figure 3.12: Power spectral density $S_{xx}(\omega)$ for $\alpha = 1$ and $\zeta = 0.1$.

and ω_2, the response does not only contain those two frequency components and their multiples but also the 'difference'-frequency $\omega_2 - \omega_1$. The random excitations, discussed here, consist of innumerable, close frequencies. When these frequencies lie within a resonance area, which is always the case for white noise excitations, the response contains a large amount of energy at (low) difference-frequencies.

Lang and Billings [1997] derived explicit expressions for the output frequency range of nonlinear systems with polynomial nonlinearities (so-called Volterra systems, see chapter 6). Their expression relates the output frequency range to the input frequency range and their results also supports the low-frequency spectral contents phenomenon. Furthermore, their expression implies that, for a quadratic
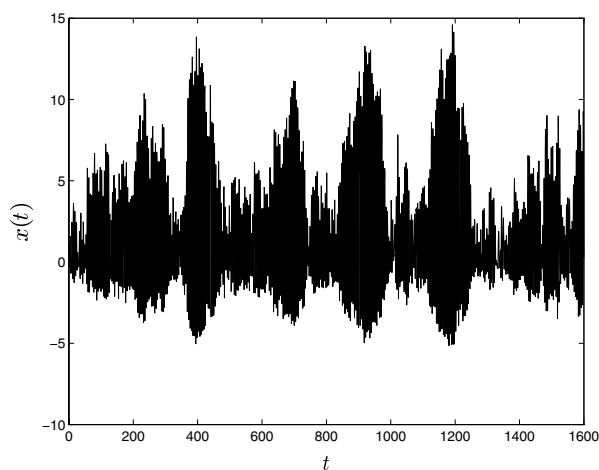
Figure 3.13: Realisation of the response $x(t)$ for $\alpha = 6$ and $\zeta = 0.01$.

stiffness nonlinearity, the response comprises twice the input frequency range besides the input frequency range itself. Following the same reasoning, a cubic stiffness nonlinearity will result in a contribution to the output frequency range of thrice the input frequency range. Moreover, the expression confirms that for asymmetric stiffness nonlinearities a low-frequency output contribution can be induced by an input that has a zero low-frequency spectral content. Of course, the nonlinearity at hand is more complex than those polynomial nonlinearities. However, the characteristics of systems with polynomial nonlinearities illustrate the existence of higher resonance frequencies as well as the large amount of low-frequency energy in the response process.

In the figures 3.10 and 3.11, also the linearization result with respect to the power spectral density is shown. The linearization technique is unable to predict the higher resonances as well as the low-frequency phenomenon. These shortcomings of such a linear model representation are the main causes for the fact that this approximation technique structurally underestimates the standard deviation. It should be noted that also the nonlinear, frequency-domain phenomena become more evident for stronger nonlinearities. For higher damping levels both effects, described above, gradually become less apparent. Summarising, we have found explanations for the inaccuracy of the linearization estimate for the standard deviation (energy measure) by observing the frequency-domain characteristics. It can be concluded that statistical linearization provides erroneous results for strongly nonlinear systems.

So, there is a strong need for the development of more accurate approximation methods for the situation where numerical integration proves (still) too time-consuming.

Next, let us compare the stochastic response characteristics (figures 3.10 and 3.11) with the periodic response characteristics (figures 3.2 and 3.3) of this system as presented in section 3.2. At first sight the figures show great similarity. However, it should be emphasised that in the figures 3.2 and 3.3 the horizontal axis embodies the angular frequency of the harmonic excitation, whereas in the figures 3.10 and 3.11 it embodies the frequencies in the response. The resonance frequencies of the harmonic and subharmonic solutions, in the periodic case, correspond with the main resonance frequency and the higher resonance frequencies of the response, in case of white noise excitations. Furthermore, for a weak nonlinearity ($\alpha = 1$) the subharmonic solution (in case of periodic excitation) is small and will even disappear for a higher level of damping ($\zeta = 0.1$), see Fey [1992]. For the same system-parameter settings, the higher resonance peaks in the power spectral density of the response to white noise will disappear too. So, there is clearly a relation between the deterministic and stochastic phenomena. To elucidate this relation and to link frequency components in the white noise excitation to frequency components in the response, we will focus on band-limited, random excitations in the next section.

Finally, in order to broaden the scope of the observed phenomena, an interesting, stochastic phenomenon is illustrated by analysing a well-known system, namely the (cubic spring) Duffing system:

$$\ddot{x} + 2\zeta\,\dot{x} + x + \alpha_D\,x^3 = \xi, \tag{3.19}$$

where α_D is the nonlinearity parameter. The stiffness term of this system is sym-

metric. Consequently, the power spectral density of the response will not have a large spectral content at low frequencies and the skewness will be zero. However, a (third harmonic) higher resonance bump is observed for weak damping ($\zeta = 0.003$), see figure 3.14. Clearly, the resonance 'peaks' are of a concave form in contrast to the convex form of the resonance peaks in the figures 3.10 and 3.11. This can be assigned to an effect, which is related to the form of the well-known back-bone curve for periodic excitations.
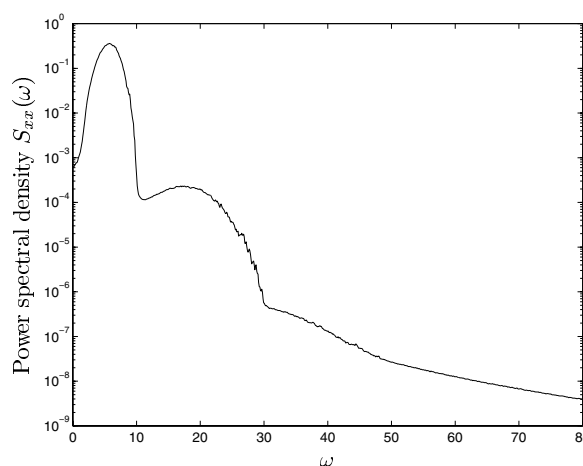
Figure 3.14: Power spectral density $S_{xx}(\omega)$ for $\mu_D = 6$ and $\zeta = 0.003$.

3.5   Response to band-limited stochastic excitation

In order to study the effect of excitation frequency components on definite characteristics in the response, simulations with Gaussian excitations with band-limited spectra are performed. The shape of the power spectral density of such an excitation is displayed in figure 3.15. In this approach, similarities between stochastic and periodic response characteristics can be illuminated.

3.5.1   Generation of realisations of a band-limited stochastic process

The energy of a band-limited random process is concentrated in the frequency band $[\omega_{min}, \omega_{max}]$ (for both positive and negative frequencies). For any shape of the power spectral density of the Gaussian process, within that frequency band, one can simulate realisations of such a process using a method, developed by Shinozuka [1972] and Yang [1972]. The idea behind the method is that a one-dimensional Gaussian, random process $d(t)$ with zero mean and a one-sided power spectral density $S_{dd}^o(\omega)$, with

$$S_{dd}^o(\omega) = \begin{cases} 2\,S_{dd}(\omega) & \text{for } \omega \geq 0 \\ 0 & \text{for } \omega < 0 \end{cases}, \tag{3.20}$$
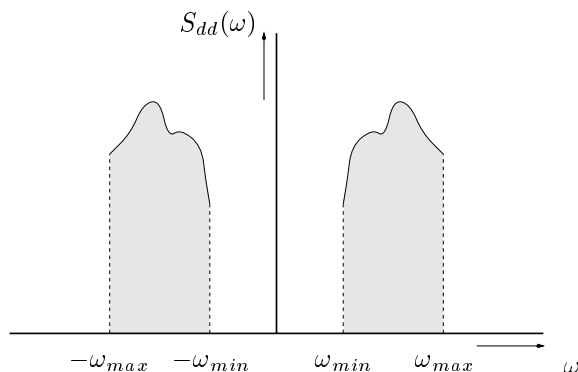
Figure 3.15: Power spectral density of a band-limited excitation $S_{dd}(\omega)$.

can be represented by a sum of cosine functions with a uniformly distributed random phase Φ. A realisation $\bar{d}(t)$ of $d(t)$ can be simulated by:

$$\bar{d}(t) = \sqrt{\Delta\omega} \ \mathrm{Re}\{Y(t)\}, \tag{3.21}$$

in which $\mathrm{Re}\{Y(t)\}$ is the real part of $Y(t)$ and

$$Y(t) = \sum_{k=1}^{N} \left\{ \sqrt{2\ S_{dd}^0(\omega_k)}\ e^{i\phi_k} \right\} e^{i\omega_k t} \tag{3.22}$$

is the finite complex Fourier transform of $\sqrt{2\ S_{dd}^o(\omega)}\ e^{i\phi}$, in which ϕ are the realisations for Φ, and $\Delta\omega = \omega_k - \omega_{k-1}$. The Fourier transform can be efficiently computed using the Fast Fourier Transform (FFT) algorithm.

Then, we can get a realisation of the response process using numerical integration techniques. Because the excitation $d(t)$ does not contain infinitely high frequencies (like white noise does), equation (3.1) is not a stochastic differential equation. Therefore, classical integration techniques can be used to solve it numerically.

3.5.2 Application to the piece-wise linear system

The response of the piece-wise linear system will be studied for excitations characterised by specific frequency bands. Here, our main goal is to obtain insight in what kind of nonlinear effects play a role in the stochastic response; in particular, a better understanding can be obtained of the appearance of the higher resonances in the case of white noise excitation. For each of the simulations, the frequency band parameters ω_{min} and ω_{max} are chosen in such a way that the excitation frequency band coincides with the major part of a specific resonance peak without overlapping adjacent resonance peaks.

Let us look at a frequency range in which the (stable) harmonic solution of the periodically excited system, with $\alpha = 6$ and $\zeta = 0.01$, exists. Accordingly, we choose a frequency band for the excitation, in which its spectrum is uniformly distributed,

with $\omega_{band} = [\omega_{min} \; \omega_{max}] = [1.13 \; 1.76]$, see figure 3.16. For such an excitation spectrum, realisations of the input process are generated. Next, realisations of the response process are computed and the estimate of the psd of the response process is depicted in figure 3.17. Recall that, for a periodic excitation with frequency ω_e,
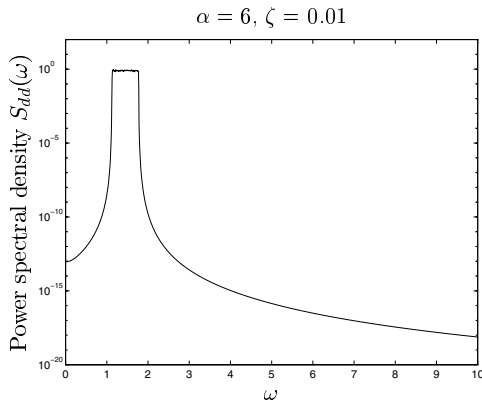

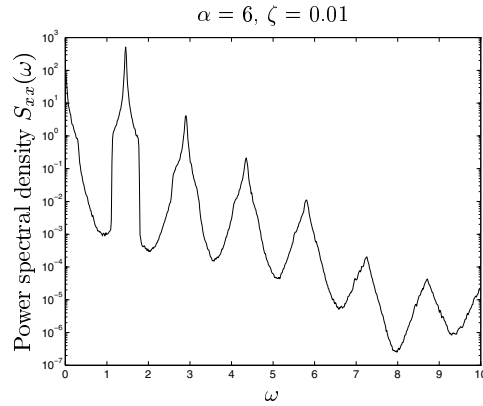Figure 3.16: Power spectral density of the excitation $S_{dd}(\omega)$ for $\omega_{band} = [1.13 \; 1.76]$.

Figure 3.17: Power spectral density of the response $S_{xx}(\omega)$ for $\omega_{band} = [1.13 \; 1.76]$.

the harmonic solutions comprise the multiple frequencies $\omega_e, 2\,\omega_e, 3\,\omega_e, \ldots$. A similar phenomenon can be observed in figure 3.17. We, therefore, term this stochastic solution a stochastic equivalent of a harmonic solution or 'stochastic harmonic' solution. Additionally, we can recognise a low-frequency energy contribution with the same origin as for white noise excitations.

In analogy with the former, an excitation with its frequency band covering the main part of the second resonance peak in figure 3.11 is applied ($\omega_{band} = [2.58 \; 3.22]$). It should be noted that, for periodic excitations, a branch of $1/2$ subharmonic solutions exists in this frequency range, see figure 3.3. The power spectral density of the response is shown in figure 3.18. A striking characteristic in this figure is that the response not only shows resonances at multiples of the frequency range of the excitation, but also at $\omega \in \omega_{band}/2$. Recall that, for periodic excitations with frequency ω_e, a $1/2$ subharmonic solution comprises the frequencies $\frac{1}{2}\,\omega_e, \omega_e, 2\,\omega_e, \ldots$. Therefore, we term such a random response a stochastic equivalent of a $1/2$ subharmonic solution or 'stochastic $1/2$ subharmonic' solution. In figure 3.19, the power spectral density of a 'stochastic $1/3$ subharmonic' solution is shown resulting from a random, band-limited excitation with $\omega_{band} = [4.03 \; 4.67]$. Fey [1992] showed that for higher levels of damping ($\zeta = 0.1$) and a relatively weak nonlinearity ($\alpha = 1$) the $1/3$ subharmonic solution can cease to exist. The same is true for its stochastic counterpart, see figure 3.20.

So, the stochastic equivalents of harmonic and subharmonic solutions appear and disappear for the same system-parameter settings as in the case of periodic excitation. Still, an explanation for the multiple resonances in case of white noise
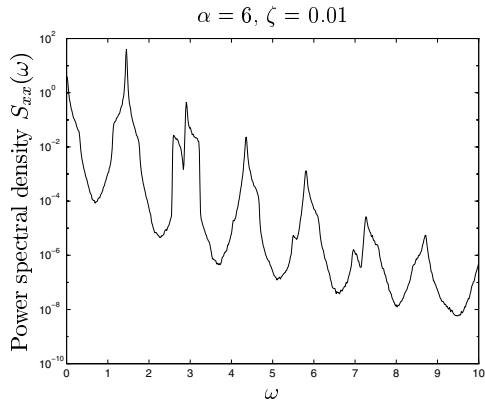
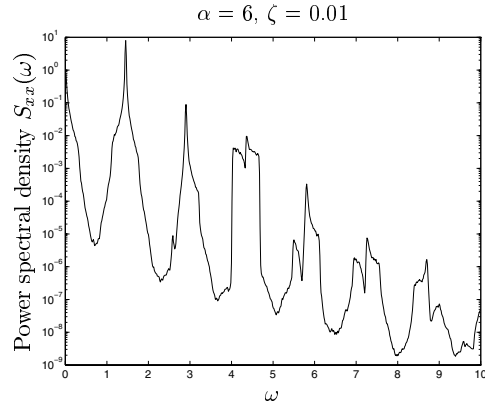Figure 3.18: Power spectral density of the response $S_{xx}(\omega)$ for $\omega_{band} =[2.58\ 3.22]$.

Figure 3.19: Power spectral density of the response $S_{xx}(\omega)$ for $\omega_{band} =[4.03\ 4.67]$.

excitations is to be found. Therefore, the results of two band-limited excitations are displayed in figure 3.21. The response psd for $\omega_{band} =[1.77\ 2.58]$ does not completely fill the convex valley (in the frequency band $[1.77\ 2.58]$) of the response psd due to an excitation in the frequency band $\omega_{band} =[1.13\ 1.77]$, see figure 3.21. This elucidates the phenomenon that the response to white noise excitations (for $\alpha = 6$ and $\zeta = 0.01$) exhibits multiple resonance peaks. The multiple resonances were shown to disappear for $\zeta = 0.01$ and $\alpha = 1$ in figure 3.12. Figure 3.22 is the equivalent of figure 3.21 for $\alpha = 1$ and $\zeta = 0.1$. Herein, the gap (near $\omega = 1.8$) in the response psd to an excitation with $\omega_{band} =[0.91\ 1.53]$ is filled by the response psd due to an excitation with $\omega_{band} =[1.53\ 2.08]$. This explains why the multiple resonance peaks are absent
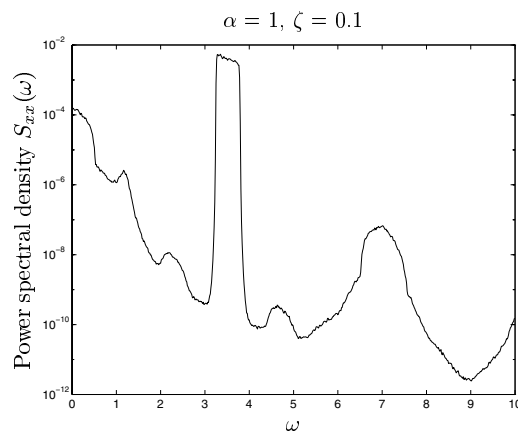

Figure 3.20: Power spectral density of the response $S_{xx}(\omega)$ for $\omega_{band} =[3.26\ 3.78]$.
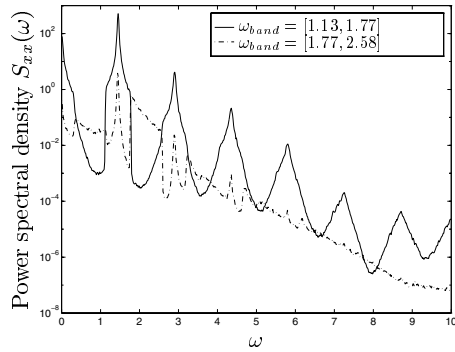
Figure 3.21: The psd of the response $S_{xx}(\omega)$ for two band-limited excitations ($\alpha = 6$ and $\zeta = 0.01$).
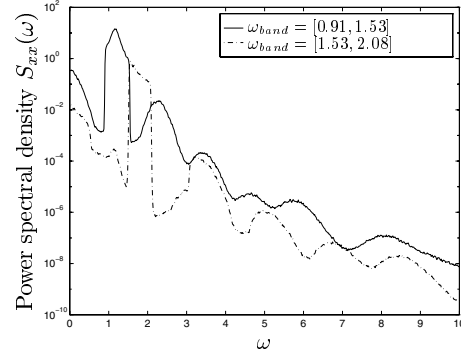
Figure 3.22: The psd of the response $S_{xx}(\omega)$ for two band-limited excitations ($\alpha = 1$ and $\zeta = 0.1$).

for these systems parameters (and white noise excitations). Resuming, it can be concluded that the response characteristics in the frequency domain are dominated by the following aspects:

- stochastic harmonic solutions;

- stochastic subharmonic solutions;

- the interaction of excitation frequencies resulting in 'difference'-frequencies' in the response. This is also the cause of the high amount of low-frequency energy in the response. Moreover, this effect also generates a psd contribution in other frequency areas.

The 'stochastic harmonic' and 'stochastic subharmonic' solutions occur simultaneously with their periodic equivalents as far as the system parameters are concerned. Therefore, a relatively short simulation with a stochastic, band-limited excitation can provide information on whether particular subharmonic solutions exist in case of periodic excitations. Furthermore, the resonance frequency of the nonlinear system can be predicted efficiently in this manner.

Finally, it should be noted that, in this section, no linearization results were discussed. The application of this method was omitted here, since a linear system will not produce any output outside the frequency range of the input. Therefore, such a linear model will not be able to predict any of the nonlinear phenomena discussed in this section.

3.6 Response to near-periodic stochastic excitation

The discussion of near-periodic, stochastic excitation can be seen as an extension of the discussion involving white noise excitations and band-limited, stochastic excitations. The near-periodic excitation is modelled as a band-limited, stochastic process

with a uniform psd. The bandwidth of the excitation $\omega_{bw} = \omega_{max} - \omega_{min}$ will be very small. Consequently, the excitation will show a dominant periodic structure, despite of its stochastic nature. For the simulations, we will use the system parameters $\alpha = 6.41$ and $\zeta = 0.0142$, for the piece-wise linear system, because this setting was also used by Van de Vorst [1996]. He showed, using harmonic excitation, that for certain excitation frequencies ($4.0 \leq \omega_e \leq 5.5$) multiple stable solutions exist, as is the case for $\alpha = 6.0$ and $\zeta = 0.01$, see figure 3.3. A stable harmonic solution coexists with a stable and an unstable $1/3$ subharmonic solution.

For harmonic excitations, the initial state of the system solely determines in which solution (or attractor) the system will settle after the transient part has died out. The set of all initial states of orbits which approaches a specific attractor is termed the basin of attraction of that attractor. The basins of attraction of this 2-dimensional state-space system are separated in the state space by 1-dimensional basin boundaries, see Van de Vorst [1996]. A saddle solution attracts within the boundary and repels across it. All the orbits that approach a saddle tangentially along the stable eigenvector for increasing time are termed *stable manifolds*. Furthermore, all the orbits that approach the saddle for decreasing time are termed *unstable manifolds*. The stable and unstable manifolds are responsible for the structure of the phase space portrait. The stable manifolds form the basin boundaries, since they do not approach an attractor, but a saddle solution.

A stroboscopic picture of the stable and unstable manifolds of this system is shown in figure 3.23 for the excitation frequency $\omega_e = 4.775$ at $t = \frac{2\pi j}{\omega_e}$, $j = 1, 2, \ldots$. Here, again the excitation is $\cos(\omega_e t)$. Note that multiple stable solutions exist. In figure 3.24, a part of figure 3.23 is magnified in order to show the main part of the basin of attraction of the stable harmonic solution clearly. The intersections of the stable and unstable manifolds correspond to the saddle solution (in this case the unstable $1/3$ subharmonic solution).
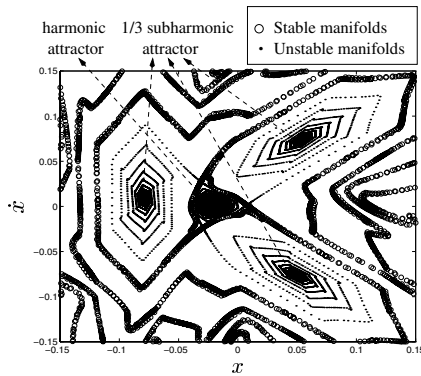

Figure 3.23: Manifolds for $\omega_e = 4.775$ ($\alpha = 6.41$ and $\zeta = 0.0142$).
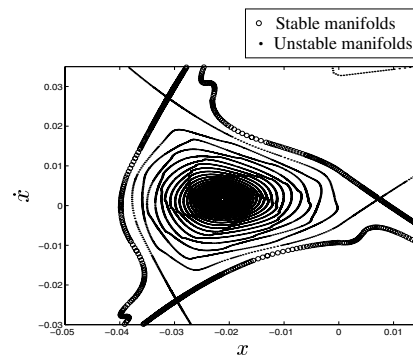
Figure 3.24: Basin of attraction of the harmonic attractor for $\omega_e = 4.775$ ($\alpha = 6.41$ and $\zeta = 0.0142$).

At this point, an interesting question is whether the concept of multiple solutions remains valid (in the practical sense) when the excitation is near-periodic, though random. Therefore, the response to a Gaussian excitation in a small band around a central frequency $\omega_c = 4.775$ will be monitored. At first, excitations are applied, for which the energy is distributed uniformly in the small frequency band. Let us consider such an excitation in the band $\omega_c - \frac{\omega_{bw}}{2} \leq \omega_e \leq \omega_c + \frac{\omega_{bw}}{2}$ with $\omega_{bw} = 0.0628$. Furthermore, the initial state $\underline{x}_0 = [0,0]^T$ is used. This initial condition lies in the basin of attraction of the harmonic solution for periodic excitations, see figure 3.24. In order to facilitate the interpretation of the simulation results, the starting-phase of the near-periodic excitation was chosen to correspond to that of the periodic excitation leading to figure 3.23[2]. In order to set up an interpretable, numerical experiment, the position and magnitude of the basins of attraction for the other excitation frequencies in the excitation bandwidth should not differ significantly from that of $\omega_c = 4.775$. This matter will be addressed later on. Simulations with stochastic excitations with such small bandwidths resulted in stochastic responses that resemble their periodic equivalents in the phase plane. A remarkable outcome is that besides the 'stochastic harmonic' solutions, see figure 3.25, also 'stochastic 1/3 subharmonic' solutions occurred, see figure 3.26.

This is remarkable, since the initial condition lies in the basin of attraction of the harmonic solution. Apparently, the randomness of the excitation induces a *'jump-phenomenon'*: a jump of the harmonic solution to the stable 1/3 subharmonic solution. One may say that a certain solution type has a certain probability of appearance, which depends on, amongst other aspects, the initial condition. For $\omega_{bw} = 0.0628$ and $\underline{x}_0 = [0,0]^T$, 300 simulations runs were performed. 61 % 'stochastic harmonic' solutions and 39% 'stochastic subharmonic' solutions occurred. For an initial condition in the basin of attraction of the 1/3 subharmonic solution, $\underline{x}_0 = [-0.1, 0]^T$ (see figure 3.23), and the same excitation bandwidth, 90% of the solutions appeared to be 'stochastic 1/3 subharmonic' solutions. So, merely 10% were 'stochastic harmonic' solutions. Clearly, not only the initial condition, but also the global stability of the stable attractors plays an important role with respect to the 'probability of occurrence' of the different solution types. The global stability of an attractor is determined by the structure of its basin boundaries, the stable manifolds. If those basin boundaries lie close to the attractor, a relatively small perturbation can cause a jump to another attractor. In this case the perturbation is a deviation from periodicity of the excitation. So, the percentage of 'stochastic harmonic' solutions will drop when the magnitude of the basin of attraction of the harmonic attractor decreases. In our example, the basin of attraction of the harmonic attractor is relatively small.

Another factor that can influence the probability of the solution types is the bandwidth of the random excitation. It is obvious that the near-periodicity assumption, which means that the stochastic excitation can be seen as a combination of a periodic excitation (with the central frequency ω_c) and disturbances due to the other frequencies in the excitation, is only useful (for the purpose of interpretation of the results) when the excitation is really very narrow-banded, as assumed until

---

[2]For an other phase of the periodic excitation, the manifolds, and thus the basins of attraction, lie differently in phase space.

Periodic response

Part random response for $[t, t + \frac{2\pi}{\omega_e}]$

Periodic response

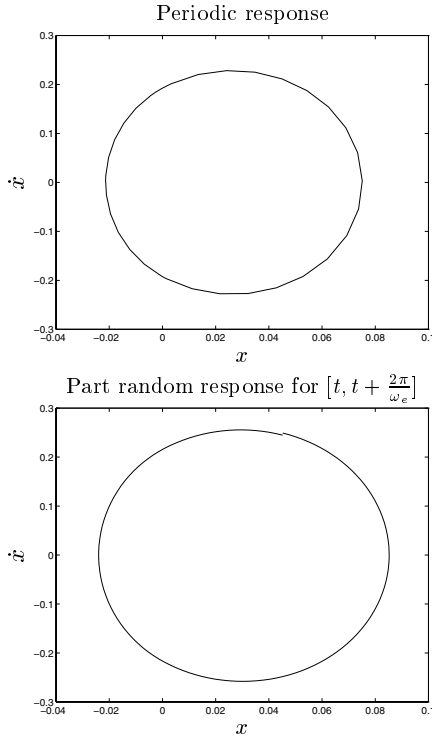Part random response for $[t, t + \frac{2\pi}{\omega_e}]$

Figure 3.25: Comparison of the form of the periodic and random harmonic solutions in the phase space ($\alpha = 6.41$ and $\zeta = 0.0142$).
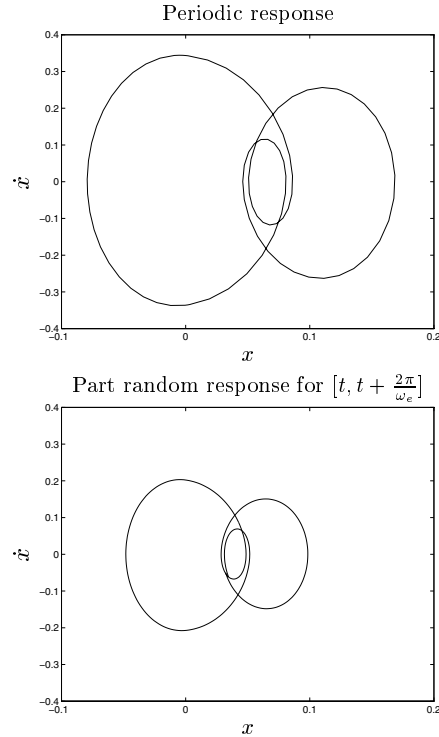
Figure 3.26: Comparison of the form of the periodic and random 1/3 subharmonic solutions in the phase space ($\alpha = 6.41$ and $\zeta = 0.0142$).

now. Here, very narrow-banded can be defined as follows: the form and magnitude of the basins of attraction for all the frequencies of the excitation bandwidth do not differ significantly. For increasing bandwidth, within this criterion of narrow-bandedness, simulations were performed (fixed $\underline{x}_0 = [0,0]^T$ and for each bandwidth 300 simulation runs). The essential result is plotted in figure 3.27. This figure clearly shows that for an increasing excitation bandwidth the appearance of 'stochastic 1/3 subharmonic' solutions increases monotonically. So, the larger the deviation from periodicity, the more jumps occur. This supports the idea of the jump-phenomenon. To illustrate the fulfilment of the narrow-bandedness criterion, we take a bandwidth $\omega_{bw} = 0.126$ and look at manifold configurations for $\omega_e = \omega_c - \frac{\omega_{bw}}{2} = 4.712$ and $\omega_e = \omega_c + \frac{\omega_{bw}}{2} = 4.838$ as shown in the figures 3.28 and 3.29, respectively. These figures show that the manifolds are already changing fairly. The basin of attraction of the harmonic remains approximately the same. When the bandwidth increases beyond $\omega_{bw} = 0.13$, the manifold configurations for the frequencies (for example for ω_{min} or ω_{max}) can become significantly different from that at ω_c. Therefore, the
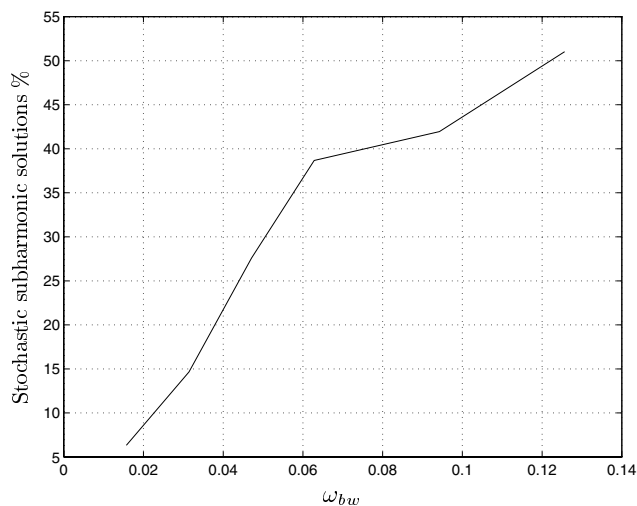
Figure 3.27: Probability of occurrence of the stochastic 1/3 subharmonic solution for increasing excitation bandwidth.

tendencies with respect to the relation between the bandwidth of the excitation and the probability of the solution types cannot be extrapolated to larger bandwidths. This is a consequence of the fact that the global stability of the two solution types are then different for different frequencies within the bandwidth. Consequently, a specific initial condition may lay in the basin of attraction of the harmonic attractor
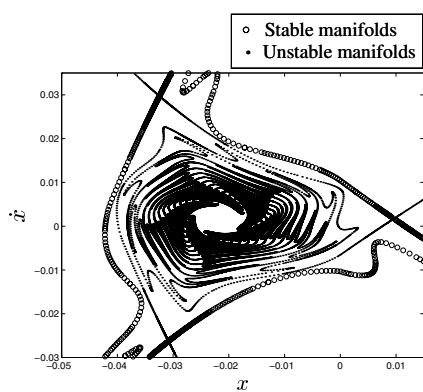

Figure 3.28: Basin of attraction of the harmonic attractor for $\omega_e = 4.712$ ($\alpha = 6.41$ and $\zeta = 0.0142$).
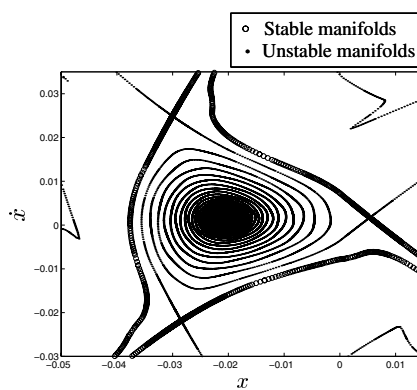
Figure 3.29: Basin of attraction of the harmonic attractor for $\omega_e = 4.838$ ($\alpha = 6.41$ and $\zeta = 0.0142$).

for one excitation frequency and in the other basin of attraction for another excitation frequency. When ω_{bw} is enlarged even further, the form of the stochastic solutions in the phase space does not resemble the form of the periodic solutions anymore. Moreover, the manifold configurations of the frequencies in the excitation bandwidth can change dramatically when other types of solutions (for example a stable 1/5 subharmonic solution, see Van de Vorst [1996]) coexist with the 1/3 subharmonic solution and the harmonic solution.

Not only the excitation bandwidth itself, but also the energy distribution within it will have effect on the probability of appearance of the solution types. According to the idea of the jump-phenomenon, the probability of the 'stochastic harmonic' solution (for $\underline{x}_0 = [0, 0]^T$) should increase when ω_c becomes more important relatively to the other frequencies in the excitation. To test this hypothesis, excitations with a non-uniform energy distribution within a fixed frequency band are applied. These excitations were ensured to exhibit a psd of the form shown in figure 3.30. Herein, S_{max} defines the value of the psd at the central frequency in the excitation bandwidth and, using the factor Q_S, the value of the psd at the boundaries of the excitation bandwidth is defined by S_{max}/Q_S. For the parameter $Q_S = 1$ (see figure 3.30), the energy distribution is uniform and for $Q_S > 10$ the distribution is almost triangular. The effect of an increasing Q_S (the excitation becomes less 'white' and the central frequency becomes relatively more important) on the probability of the solution types is clarified in figure 3.31. Clearly, less jumps occur when for higher Q_S.
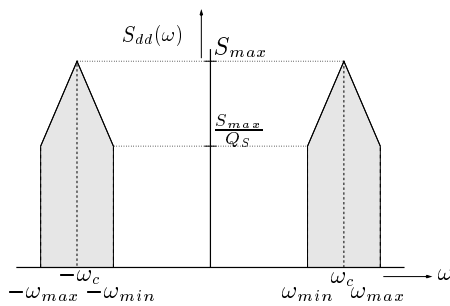
Figure 3.30: Power spectral density of a band-limited excitation $S_{dd}(\omega)$.

Figure 3.31: Probability of occurrence of the stochastic 1/3 subharmonic solution for increasing Q_S.

It can be concluded that for this kind of near-periodic, random excitation, the resulting solution type does not only depend on the initial condition of the solution, as is the case for periodic excitation. Additionally, the resulting solution type also depends on:

• the global stability of the attractors;

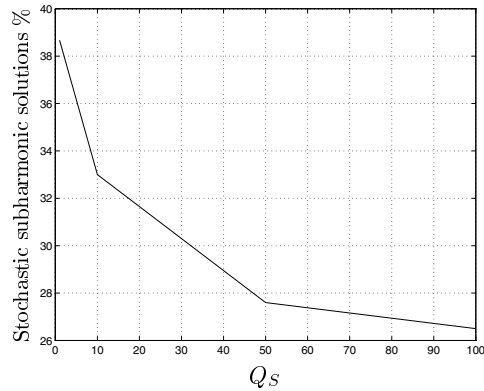- the bandwidth of the excitation;

- the energy distribution of the stochastic excitations within its frequency band.

3.7 Discussion

The stochastic behaviour of a piece-wise linear system has been studied extensively in this chapter. Hereby, a wide variety of random excitations was applied. Resuming, some important conclusions can be drawn:

- the statistical linearization technique fails to provide accurate results. This failure not only encloses the Gaussian approximation of a non-Gaussian response process. More important are the nonlinear frequency domain characteristics that cannot be predicted. Consequently, the 'linear' energy estimate appeared to be rather inaccurate;

- the frequency-domain information (psd) provides essential information on the nonlinear behaviour. This knowledge can be used to initiate ideas on the development of better approximation methods;

- the simultaneous observation of periodic and stochastic response characteristics can be very fruitful with respect to gaining understanding on the stochastic behaviour of nonlinear systems.

4 Experimental stochastic nonlinear response phenomena

In chapter 3, many typically nonlinear, stochastic response phenomena were studied and discussed based on results of numerical simulation. The main purpose of this chapter is to give the insights gained in chapter 3 *experimental* backup and to generalise these insights by studying a second, representative system. The behaviour of this MDOF, strongly nonlinear beam-impact system will be investigated under both broad-banded and small-banded, Gaussian excitations. The response of this system will be studied numerically as well as experimentally [Van de Wouw et al., 1998; De Kraker et al., 1998]. As in chapter 3, the emphasis lies on frequency domain characteristics. Furthermore, the stochastic response characteristics will again be compared to periodic response characteristics of the same system. It should be noted that, in this chapter, merely band-limited excitations will be applied. Therefore, classical integration techniques can be used for all the simulations throughout this chapter.

4.1 The nonlinear system: a base-excited beam with impact

A base-excited beam system with a nonlinear, elastic stop is investigated. Systems with elastic stops are typical examples of local (strong) nonlinearities and represent a wide range of practical, nonlinear, dynamic systems. Examples are gear rattle, ships colliding against fenders, snubbers in solar panels on satellites, safety stops in vehicle suspensions and so on. Although the nonlinearity is local, the dynamic behaviour of the entire system is strongly influenced by it.

The nonlinear, dynamic system comprises a linear elastic beam, which is clamped onto a rigid frame, and an elastic stop, see figure 4.1. The elastic stop consists of two half spheres. Figure 4.1 shows that the system is excited by a prescribed, stochastic displacement y of the rigid frame. The response x is the vertical displacement of the beam at the point of contact. Firstly, in section 4.1.1, a SDOF model for the elastic beam will be given. Secondly, in section 4.1.2, a model for the elastic stop will be presented. Finally, in section 4.1.3, a SDOF model for the total beam-impact system will be given.

4.1.1 A SDOF model of the elastic beam
The elastic beam is a continuum with an infinite number of degrees of freedom. Only transverse vibrations of the beam will be considered. For now, the beam will
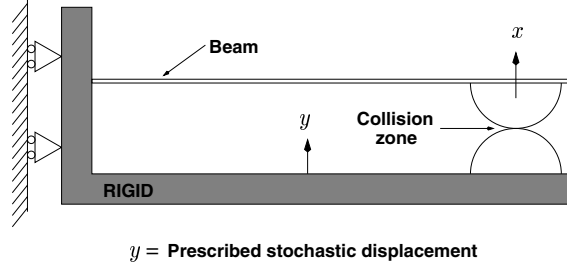
$y =$ **Prescribed stochastic displacement**

Figure 4.1: The nonlinear, base-excited beam system.

be modelled using one degree of freedom, see figure 4.2:

$$m\,\ddot{x} + c\,\dot{x} + k\,x = F_c + c\,\dot{y} + k\,y, \tag{4.1}$$

where x is the vertical displacement of the beam at contact, y the displacement of the rigid frame and F_c represents the contact force between the two half spheres. The parameters m, c and k represent the mass, damping and stiffness of the SDOF model, respectively. The model parameters are estimated by means of experiments[1] carried out on the linear beam system. The parameters m and k are related to the lowest eigenfrequency of the linear beam, whereas c represents the modal damping of the first eigenmode of the linear beam.
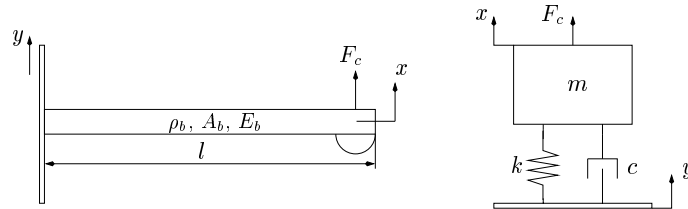

Figure 4.2: The linear, stainless steel beam (left) with Young's modulus $E_b = 1.9\ 10^{11}$ N/m^2, mass-density $\rho_b = 8000$ kg/m^3, cross-section $A_b = 58.3$ mm^2 and length $l = 259.4$ mm and the SDOF, discrete model (right) with model parameters $m = 37.75\ 10^{-3}$ kg, $k = 736.3$ N/m and $c = 0.16$ kg/s.

4.1.2 Modelling the elastic stop

The elastic stop is modelled using a Hertzian contact model [Hertz, 1895; Goldsmith, 1960]. Using this model, the following relationship holds between the contact force F_c and the relative displacement of the two colliding spheres $\delta = y - x$, see appendix D.1:

$$F_c = \frac{2}{3} E_r \sqrt{R_r}\,\delta^{1.5} = K_{\mathrm{H}}\,\delta^{1.5} \qquad \text{for} \quad \delta \geq 0. \tag{4.2}$$

---

[1]The experimental system will be discussed in section 4.4.

In equation (4.2), the reduced Young's modulus E_r represents the material properties of both colliding bodies. Furthermore, the reduced radius of curvature R_r represents the geometrical properties of the colliding bodies. These parameters are defined as

$$E_r = \frac{2}{\frac{1-\nu_1^2}{E_1} + \frac{1-\nu_2^2}{E_2}} \quad \text{and} \quad R_r = \frac{R_1 R_2}{R_1 + R_2}, \tag{4.3}$$

where R_j is the principal radius of curvature of body j, E_j is the Young's modulus of body j and ν_j the Poisson's ratio of body j. Since the collision phenomenon is in general quite complex, the following assumptions have to be made to validate equation (4.2):

- the contact area is small compared to the geometry of the colliding bodies;

- the contact areas are perfectly smooth; so, there is no friction between the colliding bodies;

- the material is isotropic and linearly elastic; so, no plastic deformation occurs;

- the contact time is long enough to establish a quasi-static state.

Furthermore, it should be noted that equation (4.2) still holds with significant deviation from the assumptions [Roozen-Kroon, 1992]. The parameter K_H was determined experimentally ($K_H = 2.1\ 10^8\ \text{N/m}^{1.5}$), see appendix D.3.

The contact model (4.2) can be refined by adding a hysteresis damping term, see Lankarani and Nikravesh [1994], accounting for energy loss during collision. The inclusion of hysteresis damping alters equation (4.2) to:

$$F_c = K_H\ \delta^{1.5} \left[1 + \frac{3(1-e^2)}{4} \frac{\dot{\delta}}{\dot{\delta}^-} \right] \quad \text{for} \quad \delta \geq 0, \tag{4.4}$$

in which e is the coefficient of restitution, a geometry and material dependent measure for energy dissipation. Moreover, $\dot{\delta}^-$ represents the velocity difference of the two colliding bodies at the beginning of the collision. Equation (4.4) is derived in appendix D.2. The coefficient of restitution e is also estimated experimentally: $e = 0.5$, see appendix D.3. The fact that e differs significantly from 1 indicates that restitution should be added to the model.

4.1.3 The SDOF nonlinear dynamic model

In the previous two subsections, the two components of the beam system, namely, the beam and the elastic stop, were discussed. The assembled, nonlinear model is visualised in figure 4.3 and its SDOF equation of motion becomes

$$m\ \ddot{\delta} + c\ \dot{\delta} + k\ \delta + K_H\ \epsilon(\delta)\ \delta^{1.5} \left[1 + \frac{3(1-e^2)}{4} \frac{\dot{\delta}}{\dot{\delta}^-} \right] = m\ \ddot{y}, \tag{4.5}$$

with

$$\epsilon(\delta) = \left\{ \begin{array}{ll} 0 & \text{for} \quad \delta \leq 0 \\ 1 & \text{for} \quad \delta > 0 \end{array} \right. . \tag{4.6}$$
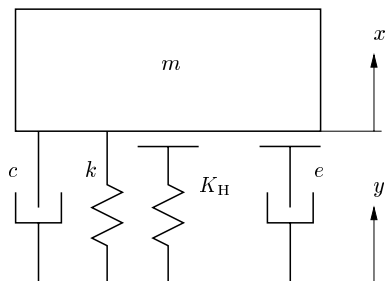
Figure 4.3: The SDOF model for the nonlinear beam-impact system.

This model can now be used to simulate (using classical, numerical integration techniques) the nonlinear response δ for different excitation forms y. The fact that $K_H \sqrt{\delta}$ (for an average δ level) considerably exceeds k up to a factor of 10^4 indicates that the system is highly nonlinear.

4.2   Survey of periodic response characteristics of the SDOF model

In order to enlarge the ability to interpret the stochastic response phenomena, discussed later on, some periodic response phenomena of the nonlinear beam-impact system will be presented first. Figure 4.4 elucidates the dependency of the maximum, absolute displacements $|\delta|_{max}$, occurring in the simulated periodic solutions,
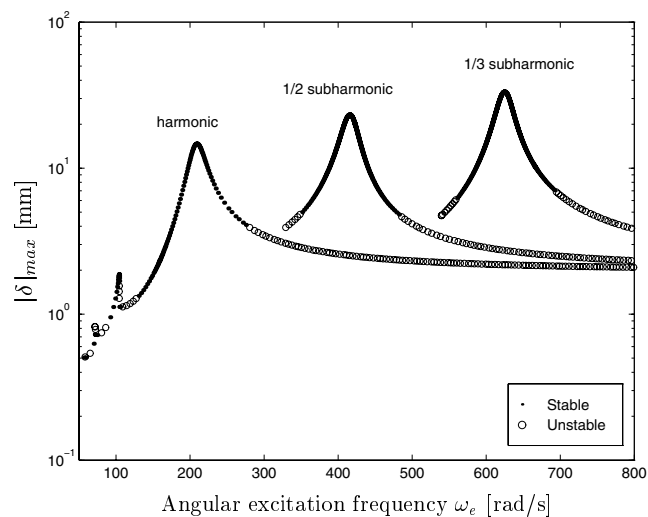
Figure 4.4: Maximum, absolute displacements $|\delta|_{max}$ of periodic solutions of the SDOF beam-impact system.

on the angular excitation frequency ω_e of the harmonic excitation. Very important nonlinear response characteristics can be extracted from figure 4.4. Firstly, besides a partly unstable harmonic resonance, subharmonic resonances exist (also with stable and unstable parts). Secondly, a remarkable feature can be found in the fact that the maximum absolute values $|\delta|_{max}$ of the subharmonic solutions are higher than those of the harmonic solutions. Moreover, the 1/3 subharmonic resonance is stronger (in terms of energy) than the 1/2 subharmonic resonance.

4.3 Simulated stochastic nonlinear response phenomena of the SDOF model

4.3.1 Simulation approach

As mentioned before, in this chapter, Gaussian, band-limited excitations are considered. Realisations of such random processes are generated using the method discussed in section 3.5.1.

Numerical integration techniques are used to compute realisations of the response process δ (and thus x). Due to the fact that the excitation process is band-limited, classical integration techniques can be used to solve the differential equation (4.5) numerically. These realisations are used to estimate the stochastic characteristics of the response process as was done in chapter 3. A constant step-size integration scheme was chosen for efficiency considerations. However, due to the major difference in stiffness between contact and non-contact situations, the minimal stepsizes, which stem from stability and convergence considerations, differ enormously for these situations. It would be very inefficient to choose one single constant step size based on contact situations. Therefore, two different step sizes are used. Consequently, the time of impact has to be determined to avoid entering contact with the large integration time step. For this purpose, the Hénon method [Hénon, 1982] is implemented within the integration routine.

The Hénon method

Let us consider the equation of motion of the beam-impact system (4.5) in a state space formulation ($\underline{f}(\delta, \dot{\delta}) = [\dot{\delta} \; \ddot{\delta}]^T$):

$$\underline{f}(\delta, \dot{\delta}) = \begin{bmatrix} \dot{\delta} \\ -\frac{c}{m}\dot{\delta} - \frac{k}{m}\delta - \frac{K_H}{m}\varepsilon(\delta)\delta^{1.5}\left(1 + \frac{3(1-e^2)}{4}\frac{\dot{\delta}}{\dot{\delta}^-}\right) + \ddot{y} \end{bmatrix}.$$
(4.7)

Now, the Hénon method can be used to determine the time of impact. Here, the method means rearranging equation (4.7) without the nonlinearities in such a way that δ becomes the independent variable, whereas t becomes one of the dependent variables. The nonlinear part of the system-description then is superfluous, since the last time interval before impact is observed. This results in the following differential equation:

$$\begin{bmatrix} \frac{d}{d\delta}(t) \\ \frac{d}{d\delta}(\dot{\delta}) \end{bmatrix} = \begin{bmatrix} \frac{1}{\dot{\delta}} \\ \frac{1}{\dot{\delta}}\left(-\frac{c}{m}\dot{\delta} - \frac{k}{m}\delta + \ddot{y}\right) \end{bmatrix}.$$
(4.8)

At the last time step before impact, this equation is integrated until $\delta = 0$. This integration step results in the known variables t_{contact}, $\dot{\delta}_{\text{contact}}$ and the condition $\delta_{\text{contact}} = 0$. Then, a switch is made to a small integration step-size in order to solve equation (4.7), continuing at t_{contact}.

4.3.2 Simulation results
Broad-band excitation

In this section, the results of simulations with stochastic excitations y are presented. The target spectrum of the excitation is taken uniformly distributed within a limited frequency band $\omega_{band} = [\omega_{min} \; \omega_{max}]$, see figure 3.15. A 0-1226.6 rad/s band excitation is applied to the system. This excitation is broad-banded relatively to the response characteristics depicted in figure 4.4. In figure 4.5, the psd of y is shown. The relative displacement of the two spheres, $\delta = y - x$, will be used as a response
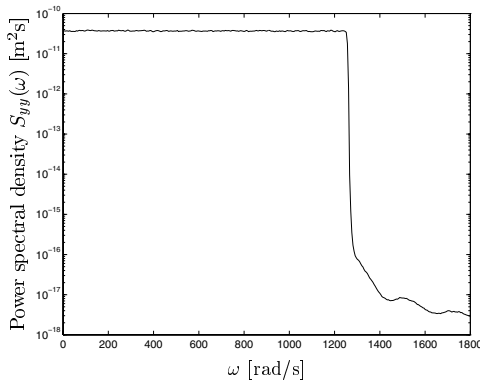

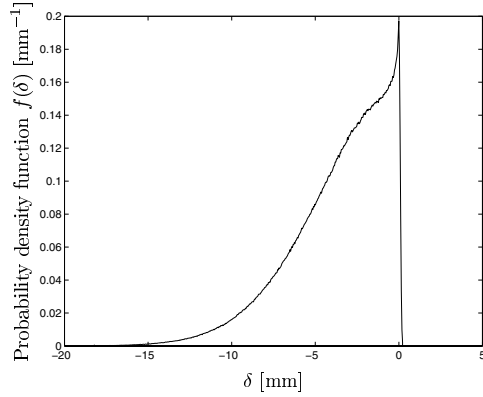Figure 4.5: Power spectral density of the excitation for $\omega_{band} = [0.0 \; 1226.6]$ rad/s.

Figure 4.6: Probability density function of the response for $\omega_{band} = [0.0 \; 1226.6]$ rad/s.

variable in the presentation of the results. The excitation is Gaussian by nature of its generation. However, as was shown in chapter 3, the response of strongly nonlinear systems to Gaussian excitations is distinctly non-Gaussian. This is clearly illustrated by the asymmetric pdf of the response variable δ, see figure 4.6. The probability density function $f(\delta)$ demonstrates an extreme asymmetry in the response. This asymmetry is a nonlinear characteristic of the system due to the elastic stop, see figures 4.7 and 4.8. Besides, the fact that the response is non-Gaussian is also indicated by higher-order moments like skewness and kurtosis. The estimates for the skewness and the kurtosis are $\hat{\gamma}_\delta = -1.01$ and $\hat{\kappa}_\delta = 3.92$, respectively; these values deviate considerably from values, that characterise a Gaussian response: $\gamma = 0.0$ and $\kappa = 3.0$. The psd of δ is shown in figure 4.9, which admits three important observations:

1. $S_{\delta\delta}(\omega)$ exhibits multiple resonance peaks;

2. the response signal contains a large amount of energy at low frequencies;
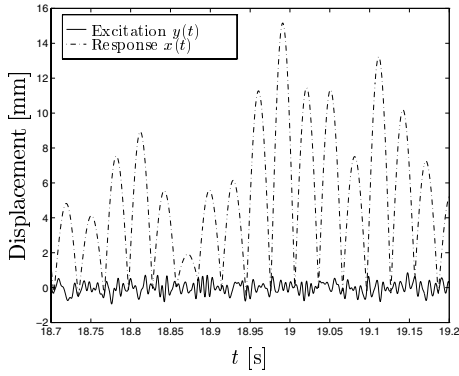
Figure 4.7: Parts of realisations of $y(t)$ and $x(t)$ for $\omega_{band} =$[0.0 1226.6] rad/s.
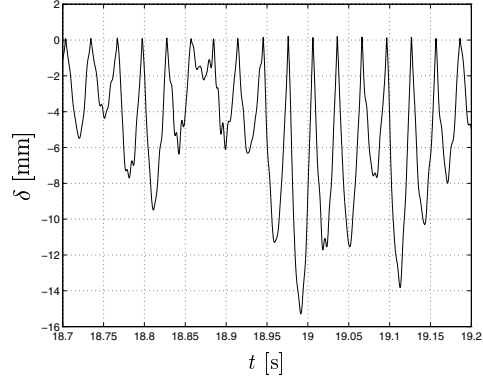
Figure 4.8: Part of a realisation of $\delta(t)$ for $\omega_{band} =$[0.0 1226.6] rad/s.

3. the level of the psd only drops with two decades at $\omega = 1226.6$, where the psd of the excitation drops with seven decades at the same frequency. So, clearly a large amount of energy in the response for $\omega > 1226.6$ is caused by energy in the excitation for $\omega < 1226.6$.

The first two response phenomena were also observed in the stochastic response of the piece-wise linear system investigated in chapter 3. Apparently, these phenomena have more general value than mere application to *one* system suggests.

Figure 4.9: Power spectral density of the response δ for $\omega_{band} =$[0.0 1226.6] rad/s.

Narrow-band excitation

In analogy with the research presented in section 3.5, three excitations with smaller bandwidths are applied:

1. a band-limited excitation with $\omega_{band} = [144.5\ 270.2]$ rad/s, that covers the major part of the harmonic resonance peak in figure 4.4;

2. a band-limited excitation, with $\omega_{band} = [351.9\ 477.5]$ rad/s, that covers the major part of the 1/2 subharmonic resonance peak in figure 4.4;

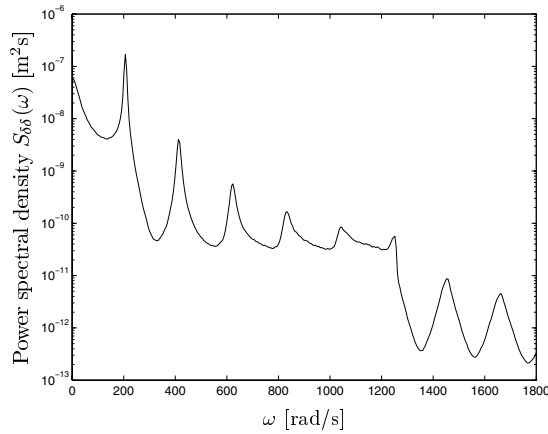3. a band-limited excitation, with $\omega_{band} = [559.2\ 684.9]$ rad/s, that covers the major part of the 1/3 subharmonic resonance peak in figure 4.4.

For these excitations the results with respect to $S_{\delta\delta}(\omega)$ are depicted in figure 4.10, figure 4.11 and figure 4.12, respectively. Clearly, a 'stochastic harmonic' response is illustrated by figure 4.10. The figures 4.11 and 4.12 illustrate a 'stochastic 1/2 subharmonic' and a 'stochastic 1/3 subharmonic' effect, respectively. Again, the
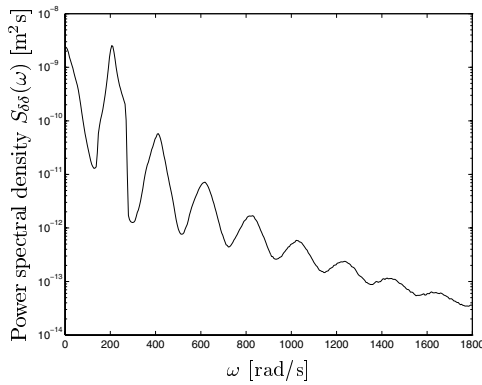

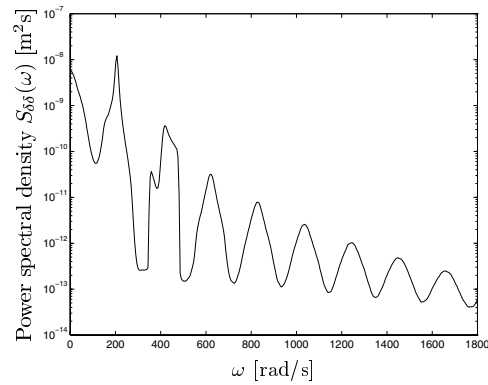Figure 4.10: Power spectral density of the response for $\omega_{band} = [144.5\ 270.2]$ rad/s.

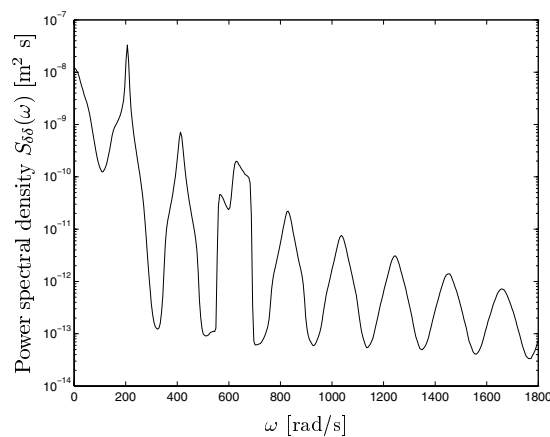Figure 4.11: Power spectral density of the response for $\omega_{band} = [351.9\ 477.5]$ rad/s.

Figure 4.12: Power spectral density of the response for $\omega_{band} = [559.2\ 684.9]$ rad/s.

ω_{band}	[rad/s]	$144.5 - 270.2$	$351.9 - 477.5$	$559.2 - 684.9$
$\hat{\sigma}_\delta^2$	[mm^2]	0.36	0.88	1.80

Table 4.1: Variance estimates of the response δ for different excitations.

similarity between stochastic and periodic response characteristics is evident. We can distinguish another interesting, nonlinear response characteristic by investigating the variance estimates $\hat{\sigma}_\delta^2$ of the response signals, see table 4.1. It should be noted that the variances of the previously defined, narrow-banded excitations are equal. From table 4.1 it is clear that the stochastic subharmonic resonances are stronger (in terms of energy) than the stochastic harmonic resonance. Furthermore, the variance estimate of the stochastic 1/3 subharmonic solution is significantly higher than the variance estimate of the stochastic 1/2 subharmonic solution. These characteristics perfectly match with their periodic equivalents, see figure 4.4.

4.4   The experimental set-up

A wide variety of *simulated*, nonlinear, stochastic response phenomena was encountered in chapter 3 and in section 4.3. In section 4.5, *experimental* results will be discussed. The experimental set-up, used in these experiments, is presented schematically in figure 4.13. A uniformly distributed, Gaussian, band-limited excitation signal is generated numerically using Shinozuka's method [Shinozuka, 1972]. This signal is sent to a controller, which controls a servovalve using feedback information from an internal displacement transducer. The servovalve provides the input for the hydraulic actuator by controlling the oil flow of the hydraulic power supply. A hydraulic service manifold connects the hydraulic power supply and the servovalve. This service manifold reduces fluctuations and snapping in the hydraulic lines during dynamic programs. All measurements are monitored using the data acquisition software package DIFA [1992]. Figure 4.14 shows the measurement equipment mounted

1. PC-486/Labview
2. Controller
3. Servovalve
4. Hydraulic power supply
5. Hydraulic service manifold
6. Hydraulic actuator
7. Beam-impact system
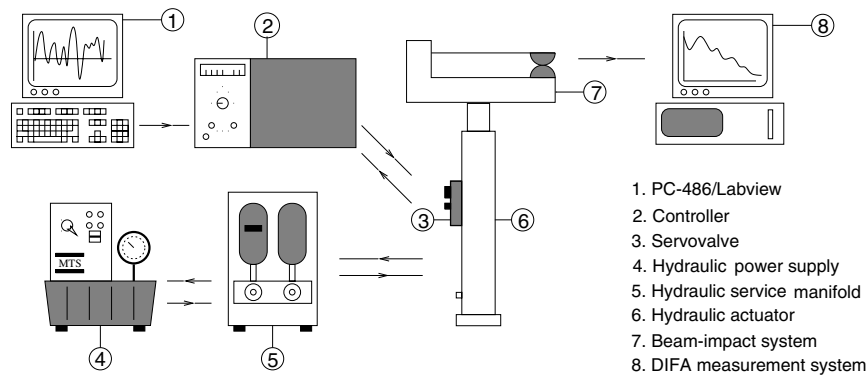8. DIFA measurement system

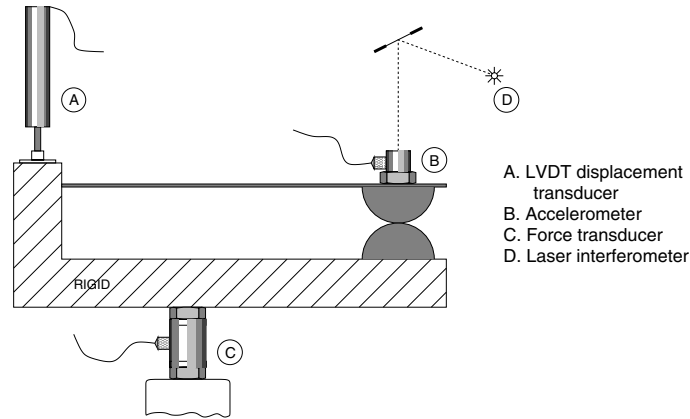Figure 4.13: The experimental set-up of the beam-impact system.

Figure 4.14: The measurement equipment mounted on the beam-impact system.

on the beam-impact system. A Linear Variable Differential Transformer (LVDT) measures the displacement of the rigid frame. The displacement and velocity of the beam, at the point of contact, are measured by a laser interferometer. Furthermore, the acceleration of the beam is measured by an accelerometer. In addition, a force transducer is used to measure the force acting on the rigid frame. The rigid frame displacement measurements are used as input for the simulations described in the following sections. Consequently, we can compare the results of these simulations to the experimental results. The specifications of the components of the experimental set-up are discussed in appendix E.

4.5   Experimental results

Several experiments were performed in order to investigate the response phenomena, observed in the former simulation results. Again, a 0-1256.6 rad/s (broad) band excitation was applied. The realised excitation spectrum is depicted in figure 4.15. In contrast with the signal offered to the controller, the power spectral density of the actual rigid frame displacement is clearly not uniformly distributed within the specified frequency range. This is due to the fact that the hydraulic actuator behaves like a first-order, low-pass filter. Therefore, it is indeed necessary to perform simulations with these rigid frame excitation spectra in order to be able to make appropriate comparisons between simulations and experiments.

Both the simulated and measured power spectral densities of the response $\delta(t)$ are shown in figure 4.16. The most important response phenomena, such as multiple resonance peaks and the presence of a large amount of low-frequency energy, are clearly visible in both the experimental and the simulation results. However, the non-uniformity of $S_{yy}(\omega)$ obstructs the observation of the second characteristic. Figure 4.16 shows that the experimental and numerical results correspond to a large extent. The experimental resonance peak around 780 rad/s is the second harmonic resonance of the beam system, which relates to the second eigenmode of the lin-
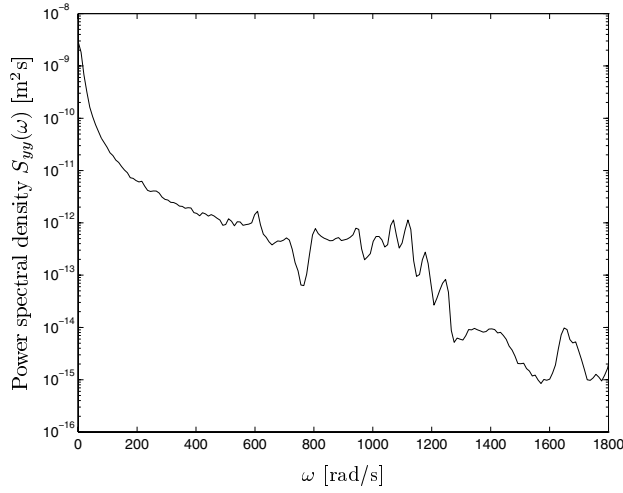
Figure 4.15: Power spectral density of the excitation for $\omega_{band} = [0.0\ 1256.6]$ rad/s.

ear beam. Of course, this resonance peak is missing in the simulation results as a consequence of the SDOF modelling approach.

In the experiments two narrow-band excitations were applied:

1. a band-limited excitation, with $\omega_{band} = [144.5\ 270.2]$ rad/s, that covers the major part of the harmonic resonance peak, see figure 4.17;
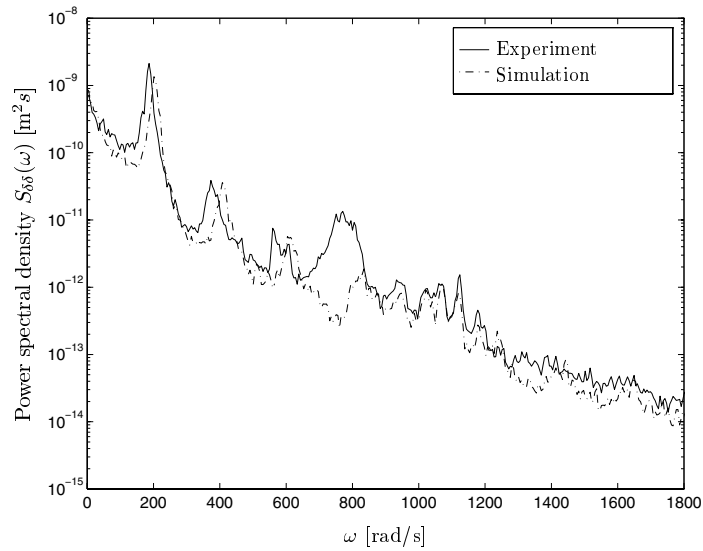
Figure 4.16: Power spectral density of the response for $\omega_{band} = [0.0\ 1256.6]$ rad/s.

2. a band-limited excitation, between $\omega_{band} = [351.9\ 477.5]$ rad/s, that covers the major part of the 1/2 subharmonic resonance peak, see figure 4.19.

The purpose of the application of these excitations is to find out whether the phenomena discussed in section 4.3 also appear in the experiments. The spectra of the response signals $\delta(t)$ are depicted in the figures 4.18 and 4.20. Apart from the absence of the second harmonic resonance in the simulations, the simulation results match the experimental results very well. Figure 4.18 clearly confirms the multiple frequency property of the nonlinear response experimentally and displays an experimental ,'stochastic harmonic' response. Furthermore, a 'stochastic 1/2 subharmonic' effect is also found in the experiments, see figure 4.20.

The estimate of the probability density function of the 144.5-270.2 rad/s band

Figure 4.17: Power spectral density of the excitation for $\omega_{band} = [144.5\ 270.2]$ rad/s.

Figure 4.18: Power spectral density of the response for $\omega_{band} = [144.5\ 270.2]$ rad/s.
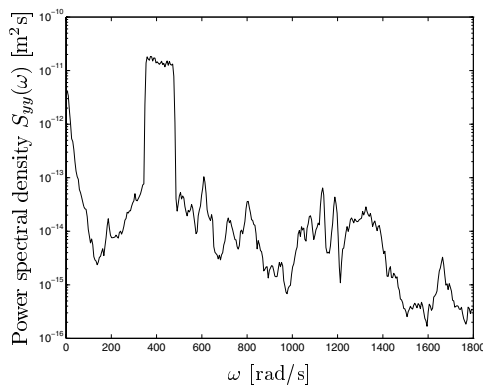
Figure 4.19: Power spectral density of the excitation for $\omega_{band} = [351.9\ 477.5]$ rad/s.

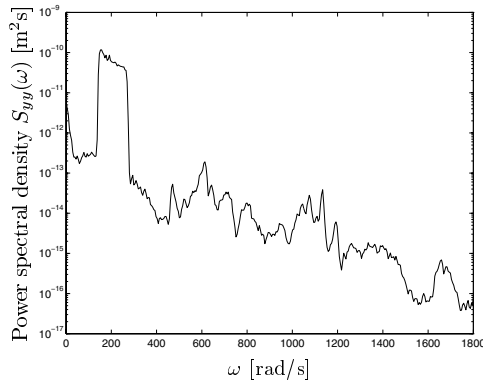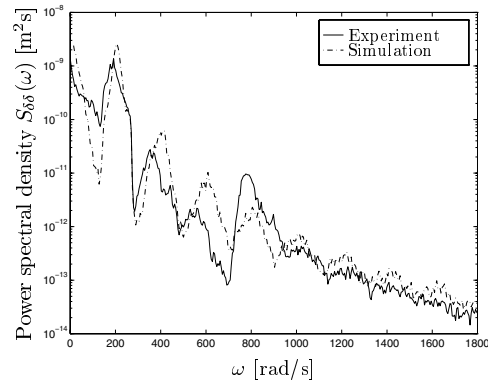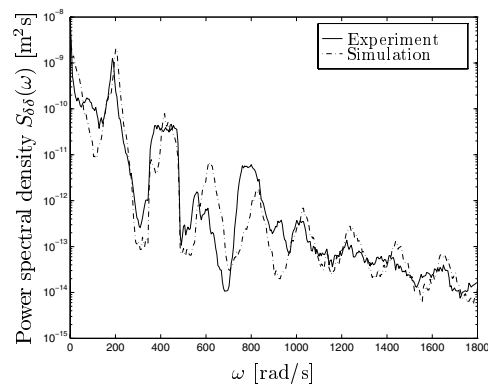

Figure 4.20: Power spectral density of the response for $\omega_{band} = [351.9\ 477.5]$ rad/s.
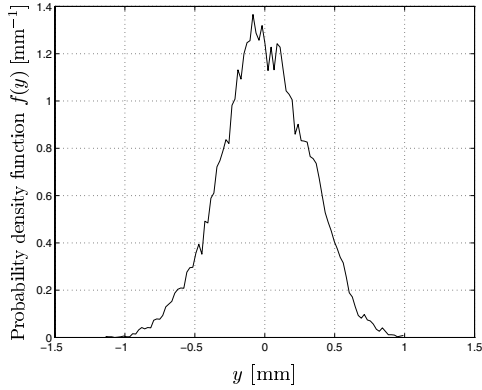
Figure 4.21: Probability density function of the excitation for ω_{band} = [144.5 270.2] rad/s.
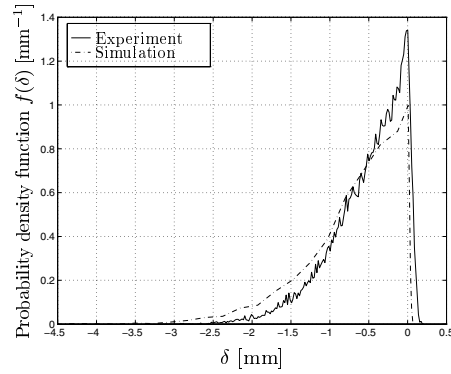
Figure 4.22: Probability density function of the response for ω_{band} = [144.5 270.2] rad/s.

excitation is depicted in 4.21. Application of a Shapiro-Wilk test on normality on these excitation data confirms that these data stem from a Gaussian distribution with 99 % probability. The probability density function of the response $\delta(t)$ to this excitation is shown in the figure 4.22. In this figure, the experimental results are compared to the simulation results. Again these results match very well. This experimental result clearly displays the fact that the response is non-Gaussian.

4.6 Response phenomena of a MDOF model

In this section, the response of a MDOF model of the beam-impact system will be investigated. The reason for this extension in modelling is twofold. Firstly, in section 4.5, it was shown that the response of the experimental system exhibits significant contributions of higher harmonic resonances. Secondly, in previous research by Van de Vorst [1996], it was shown that the extension of the model to MDOF can have a significant effect on the periodic response of the system. This effect does not limit itself to the addition of higher harmonics to the response, but also involves the fact that these higher harmonics have effect on the first harmonic resonance and its subharmonics.

4.6.1 A 2DOF model of the beam-impact system

Approximate, spatially discretized models for continuous systems can be derived using the method of Rayleigh-Ritz [Meirovitch, 1997]. The application of this method to the elastic beam is discussed in appendix F. In this way, a 4DOF model of the elastic beam is constructed. However, we are mainly interested in the influence of the second eigenmode of the elastic beam on the response of the MDOF nonlinear model. Therefore, and for efficiency reasons, the 4DOF model is reduced to a 2DOF model using a dynamic reduction method based on the lowest two eigenmodes of the beam. After adding the elastic stop to this model, the total, nonlinear, 2DOF

model can be represented by the following differential equation:

$$\underline{M}_r \underline{\ddot{n}}_r + \underline{C}_r \underline{\dot{n}}_r + \underline{K}_r \underline{n}_r + \underline{K}_{\mathrm{H}_r} \epsilon(\delta_1)\delta_1^{1.5}\left(1 + \frac{3(1-e^2)}{4}\frac{\dot{\delta}_1}{\dot{\delta}_1^-}\right) = -\underline{m}_{0_r}\ddot{y}. \quad (4.9)$$

Herein, $\underline{n}_r$ are natural coordinates and $\underline{M}_r$, $\underline{C}_r$, $\underline{K}_r$, $\underline{K}_{\mathrm{H}_r}$ and $\underline{m}_{0_r}$ are defined in appendix F. Furthermore, δ_1 is the relative displacement of the beam, with respect to the rigid frame, at the point of contact and $\dot{\delta}_1$ represents the relative velocity at the same point.

4.6.2 Survey of periodic response of the 2DOF model

Here, the periodic response characteristics of the 2DOF model will be discussed. This is done in order to, firstly, compare the periodic behaviour of the 2DOF model with that of the SDOF model and, secondly, to compare it with the stochastic behaviour of the 2DOF model.

In figure 4.23, the maximum, absolute displacements $\mid\delta_1\mid_{max}$ (of the periodic solutions) are plotted against the angular frequency of the periodic (harmonic) base-excitation y. These data were obtained using a path-following procedure [Fey, 1992]. It should be noted that this figure can be compared with figure 4.4 qualitatively as well as quantitatively, because the amplitude of the inputs y are identical for both figures.

Clearly, harmonic and subharmonic solutions are present. As was the case for the SDOF model, again, the subharmonic solutions are stronger, in terms of the 'nonlinear amplitude' $\mid\delta_1\mid_{max}$, than the harmonic solutions. A striking characteristic
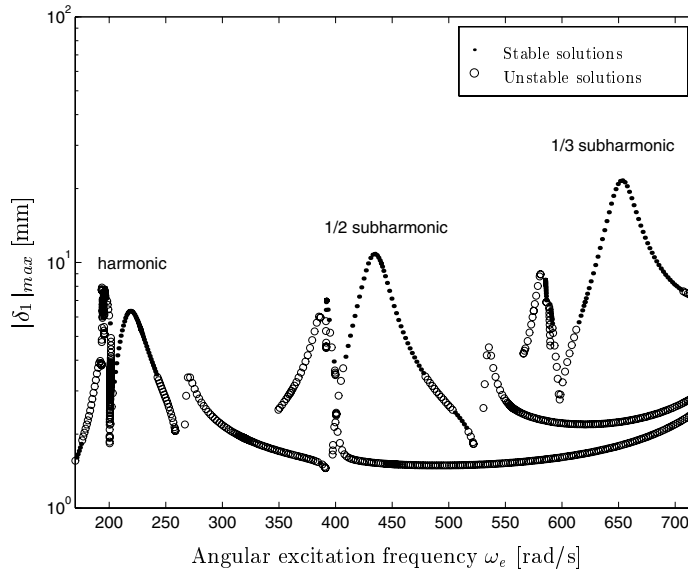
Figure 4.23: Maximum, absolute displacements $\mid\delta_1\mid_{max}$ of periodic solutions of the 2DOF beam-impact system.

is the fact that both the harmonic and the 1/2 subharmonic resonance peak exhibit large dents near their resonance frequencies. Since this effect is clearly absent in figure 4.4, it is most likely caused by the presence of the second degree of freedom in the model. Note in this respect that the second harmonic resonance frequency (780 rad/s) lies at four times the frequency at which the first harmonic resonance shows a dent (195 rad/s). Clearly, the inclusion of extra 'modes' in the model does not merely affect the response in the neighbourhood of the resonance frequency of this 'mode', but also influences the response characteristics at lower frequencies dramatically.

Furthermore, figure 4.23 is not claimed to be exhausting with respect to extremely detailed, periodic response characteristics. However, it serves its purpose within the scope of this research.

4.6.3 Simulated stochastic nonlinear response phenomena of the 2DOF model

Here, stochastic, band-limited, Gaussian excitations will be applied to the 2DOF model. These excitations correspond to the excitations applied to both the SDOF model and the experimental system in the sections 4.3.2 and 4.5.

The main goal of the following brief discussion is threefold. Firstly, the modelling extension to two degrees of freedom is evaluated through comparison of the results of the 2DOF model to those of the SDOF model. Secondly, common characteristics of the stochastic and periodic response of the 2DOF model are discussed. Finally, the simulated stochastic response of the 2DOF model is compared to the experimental results.

In figure 4.24 the psd of the response variable δ_1 of the 2DOF model, in case of a 0-1226.6 rad/s band excitation (as in figure 4.5), is shown. The contribution of the second mode of the linear beam to δ_1 is now apparent around $\omega = 780$ rad/s. This contribution of the second degree of freedom becomes even more evident when one observes the psd of the response variable δ_3 for the same excitation, see figure 4.25. Herein, δ_3 is the displacement of the beam relative to the rigid frame at a horizontal
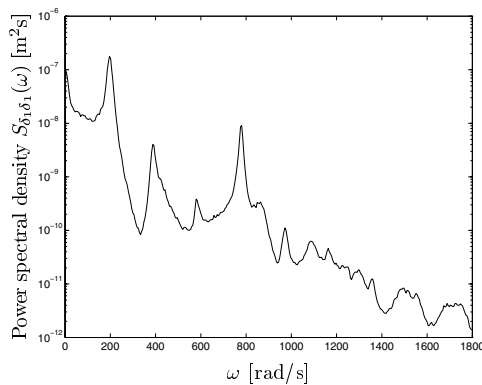
Figure 4.24: Power spectral density of δ_1 for $\omega_{band} = [0.0\ 1226.6]$ rad/s.
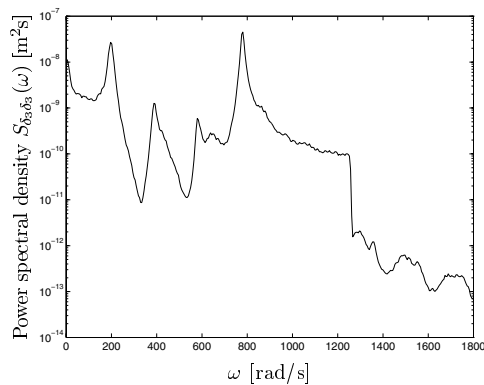
Figure 4.25: Power spectral density of δ_3 for $\omega_{band} = [0.0\ 1226.6]$ rad/s.

position $l/2$ on the beam (middle of the beam). The contribution of the second mode of the linear beam to the response of the nonlinear system appears in a more dominant way in figure 4.25, since the second mode of the linear beam contributes relatively more for the middle of the beam than for the end of the beam.

In the figures 4.26 and 4.27 estimates for the probability density functions of δ_1 and δ_3 are shown for the 0-1226.6 rad/s band excitation, mentioned above. Clearly, δ_3 tends towards a Gaussian distribution. From a physical point of view, it is clear that δ_3 should not exhibit such an extreme asymmetry as δ_1, since the beam does not encounter a contact at the horizontal position $l/2$. Therefore, δ_3 can become positive more easily than δ_1. From a more general point of view, it is known [Roberts and Spanos, 1990], that the output (in this case δ_3) of a linear system (the beam), in case of a non-Gaussian input (δ_1), will be closer to Gaussian than the input. This tendency towards a Gaussian distribution becomes stronger for lightly damped systems.
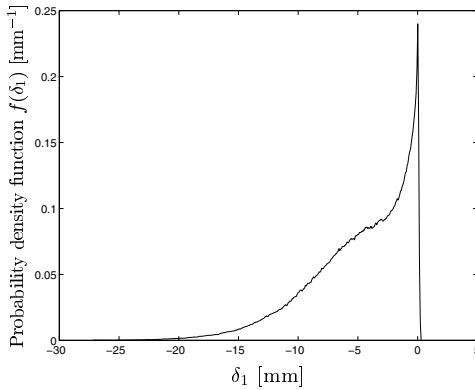
Figure 4.26: Probability density function of δ_1 for $\omega_{band} = [0.0 \quad 1226.6]$ rad/s.
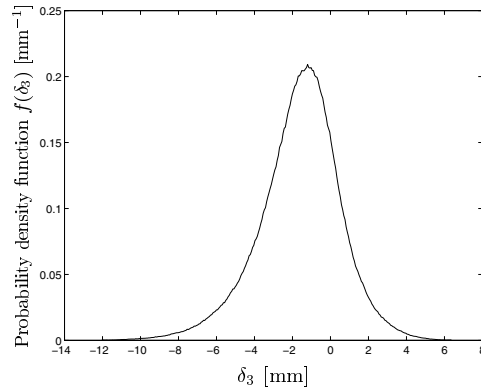
Figure 4.27: Probability density function of δ_3 for $\omega_{band} = [0.0 \quad 1226.6]$ rad/s.

In figure 4.28, the power spectral densities of the responses of the experimental system and the 2DOF model for an 'experimental' 0-1226.6 excitation (see figure 4.15) are compared. Clearly, the response of the 2DOF model exhibits the second harmonic resonance at $\omega = 780$ rad/s, which coincides with the experimental data. This represent an important modelling improvement in comparison to the SDOF model. In figure 4.29, the power spectral densities of the responses of the SDOF model an the 2DOF model for an 'experimental' 144.5-270.2 excitation (see figure 4.17) are compared. This figure shows that the addition of the extra degree of freedom has a significant effect on the stochastic response of the system: this effect does not merely express itself through the second (stochastic) harmonic resonance peak near 780 rad/s, but also affects the response characteristics in lower frequency ranges. Figure 4.30 shows that particularly this effect of the second degree of freedom makes the simulation results of the 2DOF model fit the experimental results better than the SDOF model (see figure 4.18). The fact that the extension towards
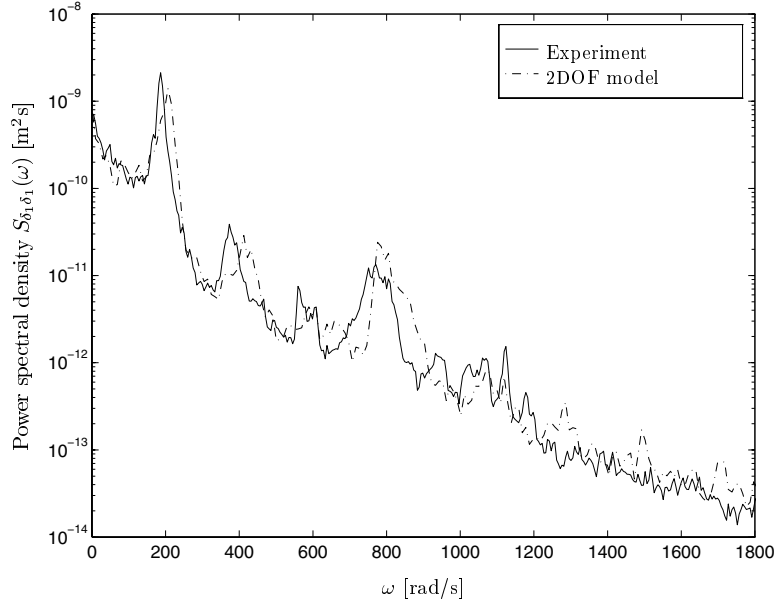
Figure 4.28: Comparison of the power spectral densities of δ_1 of the experiment and the 2DOF model for $\omega_{band} = [0.0\ 1226.6]$ rad/s.

a 2DOF model affects also the response at lower frequencies corresponds to tendencies seen in the periodic response of the 2DOF model, see figure 4.23. However, for stochastic excitations the effect of the addition of the second degree of freedom does not seem to have such a dramatic effect on the response (at lower frequencies) as for
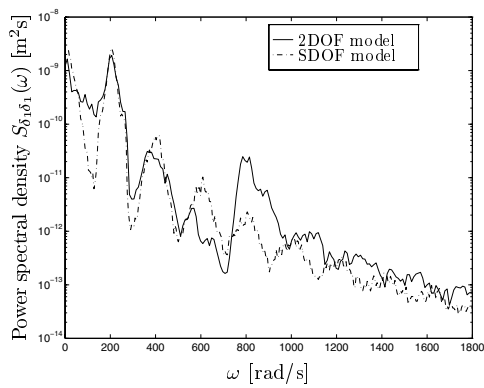
Figure 4.29: $S_{\delta_1\delta_1}(\omega)$ for the SDOF model and the 2DOF model for $\omega_{band} = [144.5\ 270.2]$ rad/s.
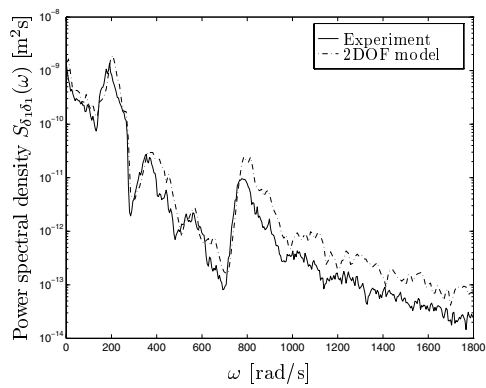
Figure 4.30: $S_{\delta_1\delta_1}(\omega)$ for the experiment and the 2DOF model for $\omega_{band} = [144.5\ 270.2]$ rad/s.

periodic excitation. Apparently, local effects (in terms of frequency) are somehow averaged for stochastic excitations.

4.7 Discussion

In this chapter the stochastic behaviour of the beam-impact system has been studied both numerically and experimentally. Summarising, some important conclusions can be drawn:

- the particularly nonlinear, stochastic response phenomena (specifically in the frequency domain) observed in the piece-wise linear system (chapter 3), were also observed in the response of the beam-impact system. So, phenomena, such as 'stochastic harmonic', 'stochastic subharmonic' responses and high-energy, low-frequency response, have more general value than application to one system suggested. Moreover, these phenomena were also observed in the experiments;

- as in chapter 3, it once more proved very fruitful to observe the deterministic (periodic) and stochastic behaviour of a system simultaneously. For many stochastic response phenomena periodic counterparts can be found. In this way, the understanding of the root of these stochastic characteristics is greatly enhanced;

- another important observation is that the addition of degrees of freedom to a model can dramatically influence the behaviour of the nonlinear system. This influence does not limit itself to the addition of extra harmonic (and subharmonic) resonances, but also influences the behaviour of the system in the lower frequency ranges. This effect has been observed in both the periodic and the stochastic behaviour of the 2DOF beam-impact model;

- it can be concluded that the extension of the model to two degrees of freedom is a significant improvement in modelling. This improvement is twofold. Firstly, the second harmonic resonance, present in the experiments, is modelled. Secondly, the inclusion of this extra mode in the linear model also affects the behaviour of the nonlinear system for lower frequencies. Consequently, the results of the 2DOF model are in better agreement with the experiments than the results of the SDOF model for this lower frequency range.

5 Higher-dimensional linear approximation

5.1 Problem motivation

In the previous two chapters, an extensive study of nonlinear, stochastic response phenomena has been performed. For that purpose, two different techniques to approximate nonlinear, stochastic response characteristics were used. Both techniques - Monte Carlo simulation and statistical linearization - have serious shortcomings. Firstly, Monte Carlo simulation, using numerical integration techniques, can provide response information to any desired level of accuracy. However, it is computationally rather inefficient when reliable estimates of stochastic response statistics are desired. This becomes even more evident when MDOF systems or a wide variety of excitations or system parameter settings are to be studied. Secondly, the statistical linearization technique is computationally very efficient, since the response statistics of the linear model can be determined analytically. However, as seen in chapter 3, the results of this method are generally very inaccurate when strongly nonlinear system are investigated.

The challenge, in this chapter, is to develop a response approximation method that can provide more accurate results than the statistical linearization technique, while exhibiting the efficiency features of a method using linear models. Such a linear model should, in contrast to that of the statistical linearization approach, model the most important, nonlinear, stochastic response phenomena, such as multiple resonance peaks and high-energy, low-frequency spectral content. Only then, the model will be able to provide estimates for the variance of the response more accurately. The extra resonance peaks, that appear in the spectrum of the output of the nonlinear system, could be modelled as 'modes' in a linear model. To do so, a suitable, linear model should be of a higher dimension than the original, nonlinear system.

The method consists of the two essential steps. The first step involves a one-off simulation, which should be performed on the nonlinear system with a reference excitation. Herein, the word one-off refers to the fact that the response has to be simulated only for this reference excitation. This provides information with respect to the power spectral density of the response of the nonlinear system for this reference excitation. The second step involves the construction of a higher-dimensional, linear model. This model should approximate the power spectral density of the output of the nonlinear system to the reference excitation accurately.

Now, such a model can be used to approximate the response statistics of the nonlinear system, when other excitations are used. Here, a white noise process will

be used as the reference excitation. Consequently, the applicability of the method is limited to sufficiently broad-banded, non-white excitations: non-white excitations are excitations with a non-uniform power spectral density. The approximation of the response statistics of the nonlinear system, now, merely involves the analytical evaluation of the response statistics of the higher-dimensional, linear model for the non-white excitations. So, no simulations are needed for the computation of the response statistics in case of the non-white excitations. The efficiency of the method enlarges when a wide variety of non-white excitations need to be studied. Namely, no computationally expensive simulations have to be performed for the non-white excited cases and the computational effort spent on the white noise excited case becomes relatively less important. In practice, such a situation may, for example, be encountered in the design of nonlinear truck suspensions, since these suspensions are expected to deal with a wide variety of road surfaces, which can be modelled as (broad-banded) random processes.

The actual construction of the higher-dimensional, linear model consist of two approximation steps:

- the first step is a non-parametric one using the method of spectral factorization [Papoulis, 1977; Overdijk et al., 1998], which will be described in the next section. Figure 5.1 expresses that this method can be used to construct a linear model with frequency response function $H_{sf}(i\omega)$ according to

$$\mid H_{sf}(i\omega) \mid^2 = \frac{S_{xx}(\omega)}{S_{\xi\xi}(\omega)} = 2\pi S_{xx}(\omega), \tag{5.1}$$

  where $S_{xx}(\omega)$ and $S_{\xi\xi}(\omega) = \frac{1}{2\pi}$ are the power spectral densities of the response of the nonlinear system x and the white noise excitation ξ, respectively. The essence of the method of spectral factorization is that it uniquely constructs the phase of $H_{sf}(i\omega)$ under the condition that $H_{sf}(i\omega)$ represents a causal, stable, minimum-phase system;

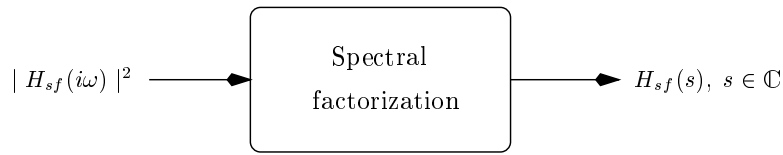Figure 5.1: Schematic representation spectral factorization procedure.

- the second step involves the construction of a parametric model. A higher-dimensional frequency response function $H_{hd}(i\omega)$ can be written in the following form:

$$H_{hd}(i\omega) = \frac{b_1 + b_2\, i\omega + b_3(i\omega)^2 + \ldots + b_{n_b+1}(i\omega)^{n_b}}{a_1 + a_2\, i\omega + a_3(i\omega)^2 + \ldots + a_{n_a+1}(i\omega)^{n_a}}, \tag{5.2}$$

with $n_b \leq n_a$ due to causality. The components of the parameter vector $\underline{\Omega} = [a_1, a_2, \ldots, a_{n_a+1}, b_1, b_2, \ldots, b_{n_b+1}]^T$ are estimated in an optimisation routine that minimises the difference between $H_{hd}(i\omega)$ and the data $H_{sf}(i\omega)$, acquired through application of the spectral factorization method, in some sense.

In section 5.2, the method of spectral factorization is described. Herein, two alternative methods for the construction of $H_{sf}(i\omega)$ are developed. The method is applied to construct a model that exhibits approximately the same spectral output (for a white noise excitation) as the piece-wise linear system (chapter 3) for a specific parameter setting. In section 5.3, the data with respect to $H_{sf}(i\omega)$ are used to estimate the parameters in $\underline{\Omega}$ of the higher-dimensional, linear frequency response function $H_{hd}(i\omega)$: the parametric modelling step. Next, in section 5.4, this model will be used to approximate the response statistics of the piece-wise linear system for a wide variety of non-white excitations. Doing so, the quality of both the model and the method are evaluated. It should be noted that, due to the linear nature of the model, the asymmetry and non-normality of the response of the piece-wise linear system can never be predicted. Here, the main goal is to construct a model that approximates the spectral information and, thus, the variance of the response accurately. Another restriction of the method is that the constructed model will, in general, only provide sensible results for one set of system parameters of the original, nonlinear system. Therefore, an analytical method to predict the variance of the response for different parameter settings, based on the knowledge of the variance for one parameter setting, is proposed in section 5.5. Finally, in section 5.6, the advantages and disadvantages of the higher-dimensional, linear approximation approach are discussed.

5.2 Non-parametric modelling: spectral factorization

Spectral factorization is a practical and efficient tool in non-parametric linear system identification. The idea of spectral factorization as described in Papoulis [1977] can be formulated as follows. One can construct the transfer function of a linear, causal, stable, minimum phase system, given merely its amplitude information.

Two different approaches are presented, resulting in two consistent expressions for the transfer function. Firstly, an approach using Fourier theory is followed. Secondly, a new approach using potential theory is presented.

The actual solution to this problem is applicable in several ways. Firstly, one can use the spectral factorization method as a modelling tool for linear systems. It can, for example, provide the complex transfer function of a practical, linear system given some measurement data. Other well-known methods in transfer function estimation are often based on input or output error minimisation (in the least squares sense). These methods make use of cross-spectra between input and output. The application of such methods requires simultaneous time series of input and output. However, situations, in which such data are not available, can easily be encountered. Fortunately, spectral factorization provides a solution that merely requires information on the autospectral density functions of input and output. Secondly, spectral factorization can be used as a design tool to create a linear, stable, causal,

minimum-phase system, given merely a set of target autospectral density functions concerning input and output. This idea gives a whole new perspective to the possible applications of the spectral factorization method. It provides, for example, the means to design a linear, stable, causal, minimum-phase system that exhibits approximately the same amplitude of the transfer function as a given linear, non-causal system. A completely different application, which will be discussed extensively here, is designing a linear system that provides approximately the same output spectrum for white noise inputs as a given nonlinear system.

In the next section, the underlying theory of the spectral factorization method is described. Two different approaches to construct the complex transfer function are derived and presented. Firstly, an approach based on Fourier theory is presented, see also Papoulis [1977] and Priestley [1981]. Secondly, a new approach is presented based on results from potential theory [Overdijk et al., 1998]. In section 5.4, the method is applied to construct a linear, stable, causal, minimum-phase model for the piece-wise linear system (3.2), see chapter 3.

5.2.1 Alternative methods for the construction of the transfer function

Let $H(s)^1$, $s \in \mathbb{C}$, be the Laplace transform of the impulse response $h(t)$, $t \in \mathbb{R}$, of a

$$\text{causal and stable,} \tag{5.3}$$

linear, time-invariant system. Furthermore, the system satisfies the

$$\text{minimum phase} \tag{5.4}$$

property, i.e. the inverse system is causal and stable as well. So, a negative real number α exists such that $H(s)$ is analytic and has no zeros in the domain

$$G = \{s \in \mathbb{C} \mid \text{Re}(s) > \alpha\}. \tag{5.5}$$

Let us introduce the function

$$A(\omega) := H(i\omega)H^*(i\omega) = \mid H(i\omega) \mid^2, \quad \omega \in \mathbb{R}, \tag{5.6}$$

where H^* is the complex conjugate of H. In the following sections we show that the transfer function $H(s)$ of a system satisfying conditions (5.3) and (5.4) is uniquely determined by the value of $\arg(H(0))$ and the function $A(\omega)$ in (5.6) provided that $A(\omega)$ satisfies the Paley-Wiener condition

$$\int_{-\infty}^{\infty} \frac{\mid \ln A(\omega) \mid}{1 + \omega^2} \, d\omega \neq \infty. \tag{5.7}$$

We discuss two alternative constructions of $H(s)$, given the function $A(\omega)$ and $\arg(H(0))$. Firstly, we describe a construction using Fourier theory and, secondly, a construction based on two-dimensional potential theory is presented.

---

[1] The subscript '*sf*' will be omitted here.

Construction of H(s) using Fourier theory

Consider the function

$$W(s) = H^{'}(s)/H(s), \quad s \, \epsilon \, G, \tag{5.8}$$

which is analytic on the domain G, see (5.5), and wherein $' = d/ds$. So for $s \, \epsilon \, G$ the integral

$$V(s) = \int\limits_0^s W(\xi) \, d\xi \tag{5.9}$$

is independent of the contour of integration within G from zero to $s \epsilon G$. The function $V(s)$ is analytic on G and

$$V^{'}(s) = W(s), \quad s \, \epsilon \, G. \tag{5.10}$$

It can be easily verified that for the function

$$\hat{H}(s) = H(0)\frac{e^{V(s)}}{H(s)} \tag{5.11}$$

we obtain

$$\hat{H}(0) = 1, \quad \hat{H}^{'}(s) = 0, \quad s \, \epsilon \, G. \tag{5.12}$$

Hence, $\hat{H}(s) = 1$ for $s \, \epsilon \, G$ and, therefore,

$$H(s) = e^{V(s) + \ln|H(0)| + i \arg(H(0))}, \quad s \, \epsilon \, G. \tag{5.13}$$

So, an analytic function $c(s)$ on G exists such that

$$H(s) = e^{c(s)}, \quad s \, \epsilon \, G. \tag{5.14}$$

The function $c(s)$ is unique modulo $2\pi i$. Furthermore,

$$A(\omega) = H(i\omega)H^{*}(i\omega) = e^{c(i\omega) + c^{*}(i\omega)} = e^{2\text{Re}(c(i\omega))}, \quad \omega \, \epsilon \, \mathbb{R}. \tag{5.15}$$

Hence,

$$\text{Re}(c(i\omega)) = \frac{1}{2}\ln(A(\omega)), \quad \omega \, \epsilon \, \mathbb{R}. \tag{5.16}$$

In view of (5.14) the problem to be solved can be formulated as follows: Construct an analytic function $c(s)$ on G satisfying (5.16) and, additionally,

$$\text{Im}(c(0)) = \arg(H(0)). \tag{5.17}$$

We show that $c(s)$ on G is uniquely determined by (5.16) and (5.17) modulo $2\pi i$. As stated in the introduction, this is done in the present section using Fourier theory.

Let us transform the complex s-plane into the complex z-plane using the Möbius transformation

$$z = \frac{1-s}{1+s} \;\; ; \;\; s = \frac{1-z}{1+z}. \tag{5.18}$$

The imaginary axis in the s-plane corresponds to the unit circle in the z-plane such that

$$s = i\omega \;\; \leftrightarrow \;\; z = e^{-2i\arctan(\omega)}, \;\; \omega \, \epsilon \, \mathbb{R},$$

$$z = e^{i\theta} \;\; \leftrightarrow \;\; s = -i\tan\frac{\theta}{2}, \;\; -\pi < \theta < \pi. \tag{5.19}$$

Furthermore, the half plane $\mathrm{Re}(s) > 0$ corresponds to the interior domain $\mid z \mid < 1$ of the unit circle.

We translate the problem described in (5.16) and (5.17) from the s-plane to the z-plane as follows. Construct a function $C(z)$ of the complex variable z, which is analytic for $\mid z \mid < 1$, such that

$$r(\theta) := \mathrm{Re}(C(e^{i\theta})) = \frac{1}{2}\ln\left(A\left(\tan\frac{\theta}{2}\right)\right), \;\; -\pi < \theta < \pi,$$

$$\arg(H(0)) = \mathrm{Im}(C(1)), \tag{5.20}$$

see (5.16) and (5.17). The relation between $c(s)$ and $C(z)$ follows from (5.18) and (5.19):

$$c(s) = C\left(\frac{1-s}{1+s}\right), \qquad \mathrm{Re}(s) > 0,$$

$$C(z) = c\left(\frac{1-z}{1+z}\right), \qquad \mid z \mid < 1,$$

$$c(i\omega) = C\left(e^{-2i\arctan(\omega)}\right), \qquad \omega \, \epsilon \, \mathbb{R}, \tag{5.21}$$

$$C(e^{i\theta}) = c\left(-i\tan\frac{\theta}{2}\right), \qquad -\pi < \theta < \pi.$$

It follows from the Paley-Wiener condition (5.7) that

$$\int\limits_{-\pi}^{\pi} \mid r(\theta) \mid d\theta = \int\limits_{-\infty}^{\infty} \frac{\mid \ln A(\omega) \mid}{1+\omega^2} \, d\omega \neq \infty. \tag{5.22}$$

So, we can write $r(\theta)$ as a Fourier series:

$$r(\theta) = \sum_{n=-\infty}^{\infty} r_n \, e^{in\theta}, \;\; -\pi < \theta < \pi, \tag{5.23}$$

where the Fourier coefficients r_n, $n = 0, \pm 1, \pm 2, \ldots$, are given by

$$r_n = \frac{1}{2\pi} \int_{-\pi}^{\pi} r(\theta) e^{-ni\theta}\, d\theta = \frac{1}{\pi} \int_{0}^{\pi} r(\theta) \cos(n\theta)\, d\theta, \tag{5.24}$$

since $r(\theta)$ is real and even. Hence,

$$r_n = r_{-n} \,\epsilon\, \mathbb{R}, \quad n = 0, \pm 1, \pm 2, \ldots . \tag{5.25}$$

The function

$$C(z) = r_0 + 2 \sum_{n=1}^{\infty} r_n\, z^n + i \arg(H(0)), \quad \mid z \mid < 1, \tag{5.26}$$

is analytic for $\mid z \mid < 1$ and

$$\begin{aligned}
\mathrm{Re}(C(e^{i\theta})) &= \frac{1}{2} \left[C(e^{i\theta}) + C^*(e^{i\theta}) \right] \\
&= \frac{1}{2} \left[r_0 + 2 \sum_{n=1}^{\infty} r_n\, e^{in\theta} + r_0 + 2 \sum_{n=1}^{\infty} r_n^*\, e^{-in\theta} \right] \\
&= \sum_{n=-\infty}^{\infty} r_n\, e^{in\theta} = r(\theta),
\end{aligned} \tag{5.27}$$

$$\mathrm{Im}(C(1)) = \arg(H(0)).$$

So, the function $C(z)$ in (5.26) satisfies (5.20) and, therefore, $C(z)$ is the unique solution of the problem described in (5.20).

We now summarise the result of this section. Using (5.14), (5.21) and (5.26), we conclude that

$$H(s) = \exp\left(\left[r_0 + 2 \sum_{n=1}^{\infty} r_n \left(\frac{1-s}{1+s} \right)^n + i \arg(H(0)) \right] \right), \quad \mathrm{Re}(s) > 0. \tag{5.28}$$

Using (5.19) and (5.28), we obtain

$$H(i\omega) = \exp\left(\left[r_0 + 2 \sum_{n=1}^{\infty} r_n e^{-2in\arctan(\omega)} + i \arg(H(0)) \right] \right), \quad \omega \,\epsilon\, \mathbb{R}. \tag{5.29}$$

Finally, from (5.20) and (5.24) we get, for $n = 0, 1, 2, \ldots$,

$$r_n = \frac{1}{2\pi} \int_{0}^{\pi} \ln\left(A\left(\tan \frac{\theta}{2} \right) \right) \cos(n\theta)\, d\theta. \tag{5.30}$$

The numerical calculation of the coefficients r_n can be performed efficiently using the Fast-Fourier-Transform (FFT) algorithm.

Resuming, the steps to do are summarised below:

- firstly, compute the coefficients r_n using the information on $A(\omega)$, relation (5.30) and the FFT-algorithm;

- secondly, use the information on r_n to compute $H(i\omega)$ through (5.29).

In the following section, a new approach to construct the transfer function is presented. In this approach, results from potential theory are used in a straightforward manner. Consequently, the approach will appear to be much more transparent than the approach using Fourier theory.

Construction of H(s) using methods from potential theory

In this section, we discuss an alternative construction of the transfer function $H(s)$ starting with the problem formulated in (5.16) and (5.17). To this end, we write

$$c(s) = c(x + iy) = u(x,y) + iv(x,y), \quad (x,y) \, \epsilon \, \mathbb{R}^2, \tag{5.31}$$

where

$$u(x,y) = \mathrm{Re}(c(s)), \; v(x,y) = \mathrm{Im}(c(s)). \tag{5.32}$$

So, according to (5.16) and (5.17) we have

$$\begin{aligned} u(0,y) &= \frac{1}{2}\ln(A(y)), \quad y \, \epsilon \, \mathbb{R} \\ v(0,0) &= \arg(H(0)). \end{aligned} \tag{5.33}$$

Since $c(s)$ is analytic for $\mathrm{Re}(s) > 0$, the function $u(x,y)$ is harmonic in the domain

$$D = \left\{ (x,y) \, \epsilon \, \mathbb{R}^2 \mid x > 0 \right\}, \tag{5.34}$$

i.e. u satisfies the two-dimensional potential (Laplace) equation on D [Schwartz et al., 1960]. The harmonic function u is given on the boundary of D, i.e. on the y-axis; see (5.33). Using Green's function, we can solve the Dirichlet problem to calculate the harmonic function u on D from its values on the boundary of D. From standard calculations we obtain

$$u(x,y) = -\int\limits_{-\infty}^{\infty} u(0,\eta) \, \frac{\partial G_r}{\partial \xi}(0,\eta; x, y) \, d\eta, \tag{5.35}$$

for $(x,y) \, \epsilon \, D$. Here, Green's function $G_r(\xi,\eta; x,y)$ in the point (ξ,η), corresponding to the source point $(x,y) \, \epsilon \, D$ and vanishing on the boundary of D, is given by

$$G_r(\xi,\eta; x,y) = \frac{1}{4\pi} \ln\left(\frac{(\xi - x)^2 + (\eta - y)^2}{(\xi + x)^2 + (\eta - y)^2} \right), \quad (x,y) \, \epsilon \, D. \tag{5.36}$$

From (5.33), (5.35) and (5.36) we get

$$u(x,y) = \frac{1}{2\pi} \int\limits_{-\infty}^{\infty} \frac{x \ln(A(\eta))}{x^2 + (\eta - y)^2} \, d\eta, \quad (x,y) \, \epsilon \, D. \tag{5.37}$$

It follows from the Paley-Wiener condition (5.7) that the integral in (5.37) converges for all $(x, y) \; \epsilon \; D$. Using the Cauchy-Riemann differential equations

$$\frac{\partial u}{\partial x} = \frac{\partial v}{\partial y}, \quad \frac{\partial u}{\partial y} = -\frac{\partial v}{\partial x} \tag{5.38}$$

to calculate $v(x, y) = \mathrm{Im}(c(s))$ from $u(x, y) = \mathrm{Re}(c(s))$, we obtain

$$v(x, y) = \frac{1}{2\pi} \int\limits_{-\infty}^{\infty} \frac{(\eta - y) \ln(A(\eta))}{x^2 + (\eta - y)^2} \, d\eta + \beta, \quad (x, y) \; \epsilon \; D, \tag{5.39}$$

where the value of the constant β follows from (5.33), i.e.

$$\beta = \arg(H(0)). \tag{5.40}$$

So, we conclude that $c(s)$ can be expressed as

$$c(s) = c(x + iy) = \frac{1}{2\pi} \int\limits_{-\infty}^{\infty} \frac{(x + i(\eta - y)) \ln(A(\eta))}{x^2 + (\eta - y)^2} \, d\eta + i \arg(H(0)). \tag{5.41}$$

By elementary calculations the above expression can be put in the form:

$$\begin{aligned} c(s) = c(x + iy) &= \frac{1}{2\pi} \int\limits_{-\infty}^{\infty} \frac{\ln(A(x\eta + y))}{1 + \eta^2} d\eta + \\ &+ \frac{i}{2\pi} \int\limits_{-\infty}^{\infty} \frac{\eta}{x^2 + \eta^2} \ln\left(\frac{A(y + \eta)}{A(y - \eta)}\right) d\eta \\ &+ i \arg(H(0)), \quad (x, y) \; \epsilon \; D. \end{aligned} \tag{5.42}$$

From (5.14) and (5.42) we conclude

$$\begin{aligned} H(i\omega) = e^{c(i\omega)} &= \\ &= \sqrt{A(\omega)} \exp\left(\frac{i}{2\pi} \int\limits_{0}^{\infty} \frac{1}{\eta} \ln\left(\frac{A(\omega + \eta)}{A(\omega - \eta)}\right) d\eta + i \arg(H(0))\right), \end{aligned} \tag{5.43}$$

where $\omega \; \epsilon \; \mathbb{R}$.

When this approach is used, the information on $A(\omega)$ has to be used in relation (5.43) in order to compute data concerning frequency response function $H(i\omega)$.

Numerical aspects of the alternative methods in spectral factorization

The fact that, in practice, the relations (5.29) and (5.43) will be evaluated for discrete values of ω is a common characteristic of the two approaches discussed above. The application of the methods requires information on $A(\omega)$ in (5.30) and (5.43). Clearly, for each discrete value of ω, information on $A(\omega)$ is needed for $\omega \in [0 \, \infty>$.

It appears that the information on $A(\omega)$ for large values of ω is important. However, in practice, only amplitude information up to a certain finite frequency will be available. Consequently, if information on $A(\omega)$ for higher frequencies is needed for the accurate evaluation of the relations (5.30) and (5.43), one could 'create' extra data for $A(\omega)$ by extending these data with a certain order. This order should be determined from the data for the highest frequencies available.

For the approach based on Fourier theory, the integral in (5.30) is evaluated through application of the Fast Fourier Transform algorithm. In the approach based on potential theory, the integral in (5.43) also has to evaluated numerically. Some aspects concerning the efficient, numerical evaluation of this integral are discussed in appendix G. Both approaches were applied to data on $A(\omega)$ descending from known, linear systems. In such a way, the accuracy and efficiency of the alternative spectral factorization methods could be compared. These tests showed that, in general, the approach based on potential theory was computationally more efficient when comparing equally accurate results of the method based on Fourier theory. Due to its computational advantages and its theoretical transparency the approach based on potential theory deserves preference.

5.2.2 Application to the piece-wise linear system

In this section, the spectral factorization method is applied to construct a linear, causal, stable, minimum-phase model for the the piece-wise linear system (3.2), for $\alpha = 6.41$ and $\zeta = 0.0142$. Therefore, a one-off simulation is performed with a white noise process ξ with $S_{\xi\xi}(\omega) = \frac{1}{2\pi}$. This results in data concerning the power spectral density of the response $S_{xx}(\omega)$. This simulation is performed using the numerical integration techniques for stochastic differential equations, discussed in chapter 2. The quotient $S_{xx}(\omega)/S_{\xi\xi}(\omega) = 2\pi S_{xx}(\omega)$, see figure 5.2, represents
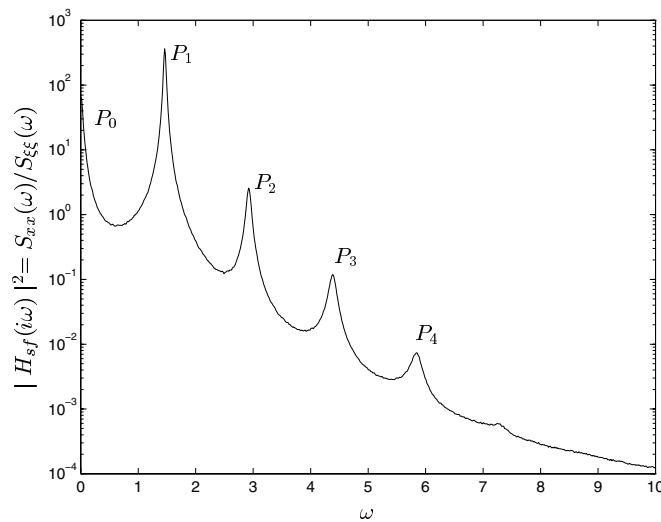
Figure 5.2: Simulated input data for the spectral factorization routine.

the input data for the spectral factorization routine. Namely, this quotient equals $\mid H_{sf}(i\omega)\mid^2$. Note that the multiple resonance peaks are indicated by P_j, $j = 1, 2, 3, 4$, whereas P_0 indicates the high-energy, low-frequency spectral component. It should be noted that the alternative methods in spectral factorization, resulting in expressions (5.29) and (5.43), provide the same results. Here, (5.43) is used, because it is computationally more efficient than (5.29) (in the numerical sense). Application of relation (5.43) results in data concerning $H_{sf}(i\omega)$ ensuring that it is causal, stable and minimum-phase, see figure 5.3. Herein, $\arg(H(0)) = 0$ is used,
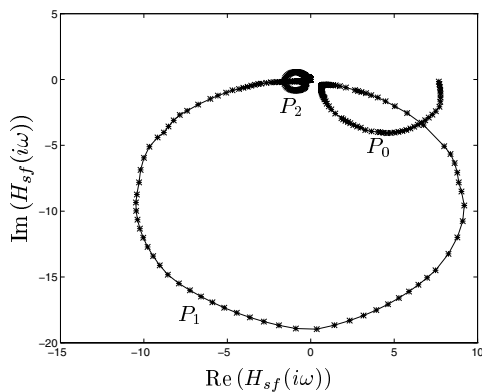
Figure 5.3: Nyquist plot of $H_{sf}(i\omega)$.
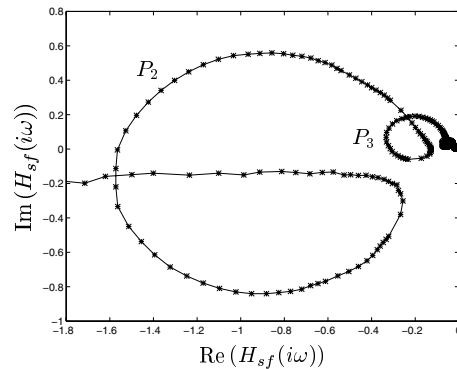
Figure 5.4: Zoomed view of the Nyquist plot of $H_{sf}(i\omega)$.

since a real model is desired. The integral in (5.43) is evaluated numerically for discrete values of ω: $\underline{\omega} = [\omega_1, \ldots, \omega_m]^T$. In figure 5.3, the low-frequency component P_0 and the loops representing the first and second resonance peak P_1 and P_2 are clearly visible. Figure 5.4 shows a zoomed view of figure 5.3 in order to display the reflection the higher resonances P_2 and P_3 in $S_{xx}(\omega)$ on $H_{sf}(i\omega)$. Note that the identifiers P_j, $j = 0, 1, 2, 3$ in the figures 5.3 and 5.4 correspond with those in figure 5.2. It should be noted that the amplitude data of this frequency response function exactly matches the data in figure 5.2, see equation (5.43).

Now, we have complex data concerning concerning the frequency response function of a linear, stable, causal, minimum-phase model, that exhibits approximately the same spectral output for white noise excitation as the piece-wise linear system (for $\alpha = 6.41$ and $\zeta = 0.0142$). The accuracy of $H_{sf}(i\omega)$ is only limited by, firstly, the statistical accuracy of the simulated power spectral density $S_{xx}(\omega)$ and, secondly, the accuracy of the numerical evaluation of the integral in (5.43). Here, the statistical accuracy of the one-off simulation is dominating the accuracy of $H_{sf}(i\omega)$. The 95 % confidence intervals of $S_{xx}(\omega)$ lie at 2.5 % from the power spectral density estimate.

5.3   Building a parametric model

The next step towards the construction of an analytical, higher-dimensional, linear model is the estimation of the parameters a_j and b_k ($j = 1, 2, \ldots, n_a + 1$, $k =$

$1, 2, \ldots, n_b + 1$) in a parametric model $H_{hd}(s)$ of the form:

$$H_{hd}(s) = \frac{b_1 + b_2 \, s + b_3 s^2 + \ldots + b_{n_b+1} s^{n_b}}{a_1 + a_2 \, s + a_3 s^2 + \ldots + a_{n_a+1} s^{n_a}}, \quad s \in \mathbb{C}. \tag{5.44}$$

Hereto, a target function $O(\underline{\Omega})$, which measures the quality of a parameter estimate $\underline{\Omega} = [a_1, \ldots, a_{n_a+1}, b_1, \ldots, b_{n_b+1}]^T$, has to be defined. Here, a least squares estimate form for $O(\underline{\Omega})$ is chosen:

$$
\begin{aligned}
O(\underline{\Omega}) = \frac{1}{2} \Bigg[& \sum_{l=1}^{m} q_{1,l} \left(\mid H_{hd}(i\omega_l) - H_{sf}(i\omega_l) \mid \right)^2 \\
& + q_2 \, 2\pi \int_{-\infty}^{\infty} \left(\mid H_{hd}(i\omega) \mid^2 - \mid H_{hd}(i\omega) \mid^2 \right) d\omega \Bigg].
\end{aligned}
\tag{5.45}
$$

Herein, besides the difference between $H_{hd}(i\omega)$ and $H_{sf}(i\omega)$, the difference in output variance for a white noise input is incorporated in the weighted target function (with weighting factors $q_{1,l}$ and q_2). Note that also a weighting over the frequency is incorporated in order to ensure accurate modelling of the higher resonance peaks, which occur at a significantly lower energy level. In order to give the model $H_{hd}(i\omega)$ any validity, m, the number of data points, should be much greater than $n_a + n_b + 1$, the number of parameters to be estimated. A Gauss-Newton method [Gill et al., 1981] is used to find an optimum for the parameters $\underline{\Omega}$ of $H_{hd}(s)$. Before we apply these optimisation tools to find optimal parameters a_j and b_k ($j = 1, 2, \ldots, a_{n_a+1}$ and $k = 1, 2, \ldots b_{n_b+1}$), which fit $H_{hd}(i\omega)$ to $H_{sf}(i\omega)$, certain restrictions have to be imposed on these parameters. These restrictions are related to the fact that $H_{hd}(s)$ should be a stable and minimum-phase transfer function, as is $H_{sf}(s)$. Firstly, the stability condition implies that the poles of $H_{hd}(s)$ lie in the left half of the complex plane ($\text{Im}(s) < 0$), which imposes a restriction on the parameters a_j, $j = 1, 2, \ldots, n_a + 1$. Secondly, the minimum-phase condition implies that the zeros of $H_{hd}(s)$ lie in the left half of the complex plane, which imposes a restriction on the parameters b_k, $k = 1, 2, \ldots, n_b + 1$. The optimisation procedure was executed for different orders n_a and n_b (under the restriction that $n_b \leq n_a$) of the numerator polynomial and the denominator polynomial, respectively. In choosing values for n_a and n_b it was regarded that the linear model should approximate four resonance peaks (P_1 to P_4) and and the low-frequency component (P_0), see figure 5.2. Hereto, n_a should be at least 9. Of course, the maximum values for n_a and n_b are taken limited to 20, because very high values for n_a and n_b cause a unacceptable increase in optimisation complexity and cannot be expected to necessarily improve the resulting model. From the limited set of values for n_a and n_b, the best optimum was selected, which was attained using $n_a = 11$ and $n_b = 9$. Clearly, $H_{hd}(s)$ represents a system of a rather high dimension. The fact that 21 parameters have to be estimated makes the actual optimisation quite complex. The corresponding $H_{hd}(i\omega)$ is compared to $H_{sf}(i\omega)$ in the figures 5.5 and 5.6. These figures show that $H_{hd}(i\omega)$ describes $H_{sf}(i\omega)$ very well. Even the higher resonances are modelled accurately. Consequently, $H_{hd}(i\omega)$ represents a linear, causal, stable, higher-dimensional,
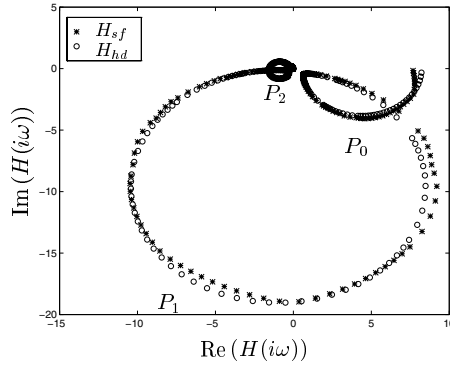
Figure 5.5: Comparison of $H_{hd}(i\omega)$ with $H_{sf}(i\omega)$.
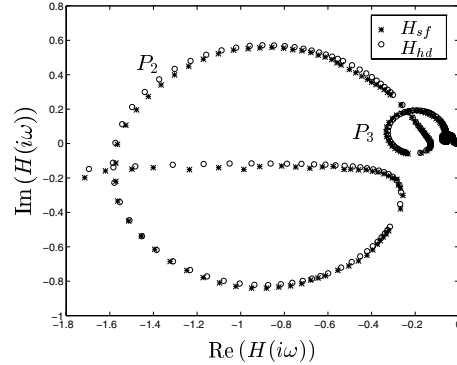
Figure 5.6: Comparison of $H_{hd}(i\omega)$ with $H_{sf}(i\omega)$: zoomed view.

minimum-phase system, whose autospectral density approximates that of the piece-wise linear system ($\alpha = 6.41$ and $\zeta = 0.0142$) for the white noise input. In the next section, this model will be used to approximate the stochastic response characteristics of the piece-wise linear system for a wide variety of non-white excitations.

5.4 Application to the piece-wise linear system

Consider non-white excitations d, that can be defined as filtered white noise processes. Here, a second-order filter will be used. Consequently, the filter output spectrum $S_{dd}(\omega)$ can be written as

$$S_{dd}(\omega) = \frac{S_{\xi\xi}(\omega)}{(\omega_f^2 - \omega^2)^2 + (2\zeta_f\omega_f\omega)^2}, \tag{5.46}$$

where ω_f and ζ_f are parameters of the second-order filter and $S_{\xi\xi}(\omega)$ is the white noise input spectrum. By varying ω_f and ζ_f, different non-white excitations can be created. Note that the filter represents a linear system; so, the non-white excitation still is a zero-mean, Gaussian process. Note that in practice these non-white excitations are known and do not have to be modelled as a filtered white noise processes.

For the piece-wise linear system the magnitude of the excitation influences its response in a purely linear fashion [Shaw and Holmes, 1983]. Therefore, one and the same higher-dimensional, linear model can be applied to excitations with significantly differing energy levels.

For $\omega_f = 2\omega_{nl}$ and $\zeta_f = 0.5$, the the power spectral density of the non-white excitation and the estimate for the psd of the response are shown in the figures 5.7 and 5.8, respectively. It can be concluded that the higher-dimensional model describes the nonlinear phenomena in the frequency domain more accurately than the statistical linearization technique. In figure 5.9, the absolute value of the relative error of the estimate of the variance of the response (relative to the simulation results) is depicted for varying ω_f. Parameter ζ_f is fixed at 0.5 and $\omega_{nl} =$

Figure 5.7: Power spectral density of the non-white excitation for $\omega_f = 2\,\omega_{nl}$ and $\zeta_f = 0.5$.

Figure 5.8: Power spectral density of the response for $\omega_f = 2\,\omega_{nl}$ and $\zeta_f = 0.5$.

$2\sqrt{1+\alpha}/(1+\sqrt{1+\alpha}$ is the harmonic resonance frequency of the piece-wise linear system, where $\alpha = 6.41$ is the stiffness of the one-sided spring. Herein, the results of the higher-dimensional model are also compared to those obtained through application of the statistical linearization technique. Furthermore, the 95 % confidence interval of the simulations is incorporated in this figure. It should be noted these simulations are performed using the integration techniques discussed in chapter 2. Clearly, the higher-dimensional model provides better results than the statistical linearization technique. Moreover, the accuracy of the results of the higher-dimensional
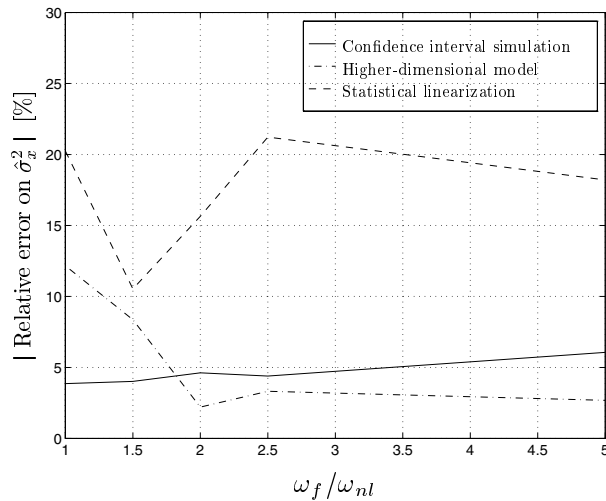
Figure 5.9: Relative error on the estimate of the variance of the response for varying ω_f and $\zeta_f = 0.5$.
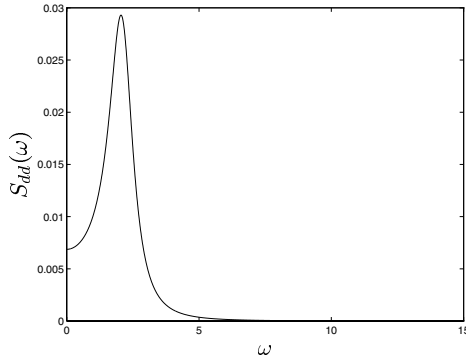
Figure 5.10: Power spectral density of the non-white excitation for $\omega_f = 1.5\,\omega_{nl}$ and $\zeta_f = 0.25$.
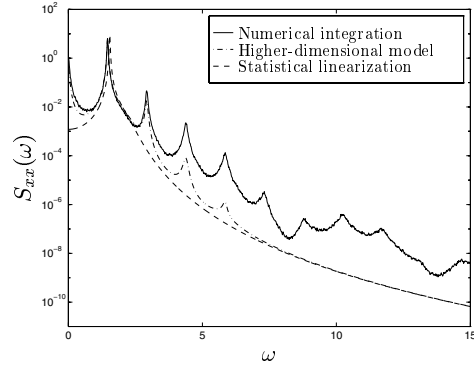
Figure 5.11: Power spectral density of the response for $\omega_f = 1.5\,\omega_{nl}$ and $\zeta_f = 0.25$.

model lies for the greater part within the confidence limits of the simulations. In the figures 5.10, 5.11 and 5.12, some results for $\zeta_f = 0.25$ are depicted. Note that a lower value for ζ_f indicates a more narrow-banded excitation (for the same ω_f).

For these excitations the higher-dimensional model again provides more accurate results than the statistical linearization technique. For $\zeta_f = 0.1$ some results are displayed in the figures 5.13, 5.14 and 5.15. Note that for $\zeta_f = 0.1$ the assumption of broad-bandedness of the excitation is clearly violated. Consequently, the results of the higher-dimensional model will be less accurate than for higher values of ζ_f.
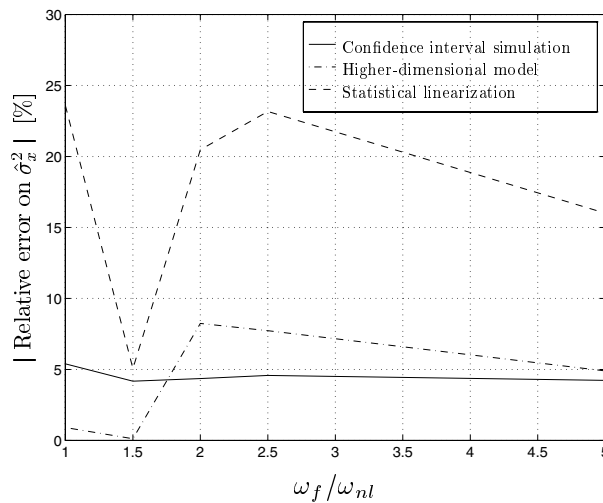
Figure 5.12: Relative error on the estimate of the variance of the response for varying ω_f and $\zeta_f = 0.25$.
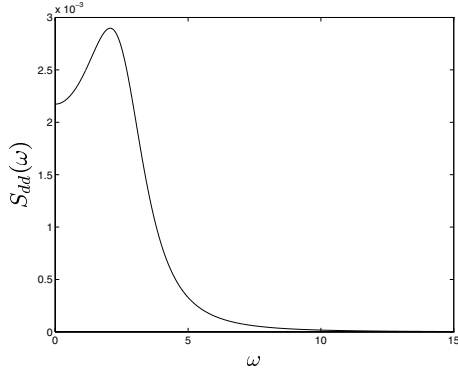
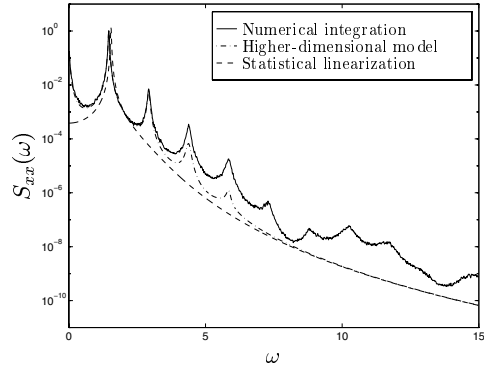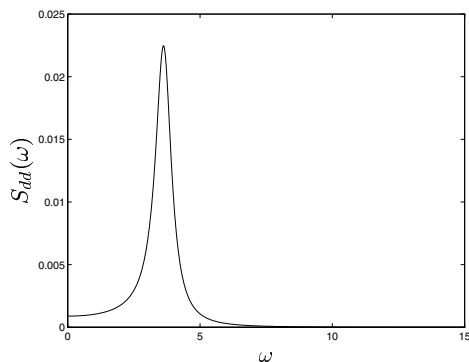Figure 5.13: Power spectral density of the non-white excitation for $\omega_f = 2.5\,\omega_{nl}$ and $\zeta_f = 0.1$.
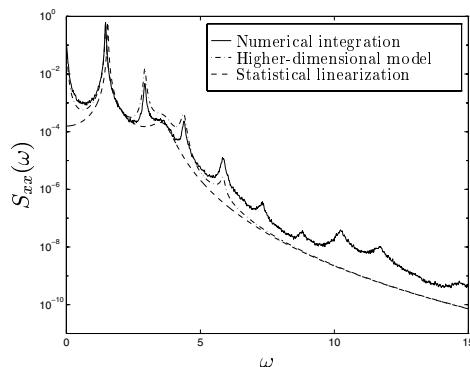
Figure 5.14: Power spectral density of the response for $\omega_f = 2.5\,\omega_{nl}$ and $\zeta_f = 0.1$.

However, figure 5.14 shows that the higher-dimensional model still provides quite accurate information with respect to the spectral energy distribution of the response.

For all the values of ζ_f, the error on the variance estimates of the higher-dimensional model (and the statistical linearization procedure) are, in general, markedly higher for $\omega_f = \omega_{nl}$ and $\omega_f = 2\,\omega_{nl}$ than for other values of ω_f. This can be explained by the fact that for $\omega_f = \omega_{nl}$ and $\omega_f = 2\,\omega_{nl}$ the non-white excitations are concentrated exactly in the frequency area of the harmonic and subharmonic resonances of the piece-wise linear system, respectively. Typically, nonlinear en-
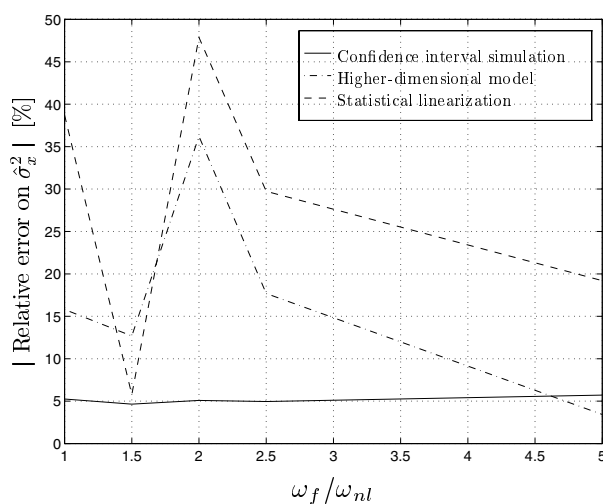
Figure 5.15: Relative error on the estimate of the variance of the response for varying ω_f and $\zeta_f = 0.1$.

ergy shifts (in the frequency domain) occur in these resonances. The effect of this nonlinear phenomenon on the variance of the response is difficult to model linearly.

Furthermore, it should be noted that the statistical linearization provides estimates for the variance that are generally too low, as was the case in chapter 3.

5.5 System parameter variation

For general, nonlinear, dynamic systems the higher-dimensional linear model is only valid for the system parameter setting for which is was designed. As mentioned before, the magnitude of the excitation influences the response of the piece-wise linear system in a purely linear fashion [Shaw and Holmes, 1983]. Therefore, one and the same higher-dimensional, linear model can be applied for excitations with significantly differing energy levels. However, in general this can lead to very inaccurate results.

In this section, a method is proposed that can predict the variance of the response for a range of parameter settings of a nonlinear system given an accurate estimate of the variance of the response for one specific parameter setting. So, as was the case for the construction of the higher-dimensional linear model, a one-off simulation will be the starting point.

Here, the method will be illustrated through application to the Duffing system (3.19). As in the statistical linearization approach, a replacing linear system can be defined:

$$\ddot{x} + 2\zeta\,\dot{x} + \beta_1\,x = \xi. \tag{5.47}$$

As a consequence of the fact that the nonlinearity of the Duffing system is a symmetric one, the mean of the response will be zero. We can define an error, that reflects the difference between the Duffing system and the linear model (5.47):

$$\varepsilon_{lin} = (x + \alpha_D\,x^3) - \beta_1 x. \tag{5.48}$$

Minimising $E\{\varepsilon_{lin}^2\}$ with respect to β_1 gives

$$\beta_1 - \left(1 + 3\alpha_D E\{x^2\}\right) = 0. \tag{5.49}$$

A second equation can be derived from energy considerations:

$$E\{x^2\} - \frac{1}{4\zeta\beta_1} = 0. \tag{5.50}$$

The equations (5.49) and (5.50) determine the statistical linearization result for the Duffing system and can be written as

$$\underline{g}\left(E\{x^2\}, \beta_1, \alpha_D\right) = \left[\begin{array}{c} \beta_1 - \left(1 + 3\alpha_D E\{x^2\}\right) \\ E\{x^2\} - \frac{1}{4\zeta\beta_1} \end{array} \right] = \underline{0}, \tag{5.51}$$

in which $\underline{0}$ is a column with zeros. Assume that the one-off simulation and the statistical linearization procedure are performed for $\alpha_D = \alpha_D^s$ and that, thus, $E\{x^2\}\mid_{\alpha_D^s}$

and $\beta_1 \mid_{\alpha_D^s}$ are known. Then, estimates for $E\{x^2\}$ and β_1 for other values of α_D can be estimated using

$$E\{x^2\} \mid_{\alpha_D^{new}} = E\{x^2\} \mid_{\alpha_D^{old}} + \frac{\partial E\{x^2\}}{\partial \alpha_D} \mid_{\alpha_D^{old}} \Delta\alpha_D$$

$$\beta_1 \mid_{\alpha_D^{new}} = \beta_1 \mid_{\alpha_D^{old}} \quad + \frac{\partial\beta_1}{\partial\alpha_D} \mid_{\alpha_D^{old}} \Delta\alpha_D, \tag{5.52}$$

in which estimates for $\frac{\partial E\{x^2\}}{\partial\alpha_D} \mid_{\alpha_D^{old}}$ and $\frac{\partial\beta_1}{\partial\alpha_D} \mid_{\alpha_D^{old}}$ are determined from the, in this case linear, algebraic equations

$$\frac{d\underline{g}}{d\alpha_D}(\frac{\partial E\{x^2\}}{\partial\alpha_D} \mid_{\alpha_D^{old}}, \frac{\partial\beta_1}{\partial\alpha_D} \mid_{\alpha_D^{old}}, E\{x^2\} \mid_{\alpha_D^{old}}, \beta_1 \mid_{\alpha_D^{old}}, \alpha_D^{old}) =$$

$$= \begin{bmatrix} \frac{\partial\beta_1}{\partial\alpha_D} \mid_{\alpha_D^{old}} -3E\{x^2\} \mid_{\alpha_D^{old}} -3\alpha_D^{old}\frac{\partial E\{x^2\}}{\partial\alpha_D} \mid_{\alpha_D^{old}} \\ \\ \frac{\partial E\{x^2\}}{\partial\alpha_D} \mid_{\alpha_D^{old}} + \frac{\partial\beta_1}{\partial\alpha_D} \mid_{\alpha_D^{old}} \frac{1}{4\zeta(\beta_1\mid_{\alpha_D^{old}})^2} \end{bmatrix} = \underline{0}. \tag{5.53}$$

In order to follow the path of the true solution with respect to the variance of the response as accurate as possible, the steps $\Delta\alpha_D$ should be taken small: here $\Delta\alpha_d = 0.01$ was used.

This procedure (termed path-followed statistical linearization) was applied to the Duffing system with a starting value $\alpha_D = 4$. The results are shown in figure 5.16. This figure shows that the procedure, described above, provides very accurate results.
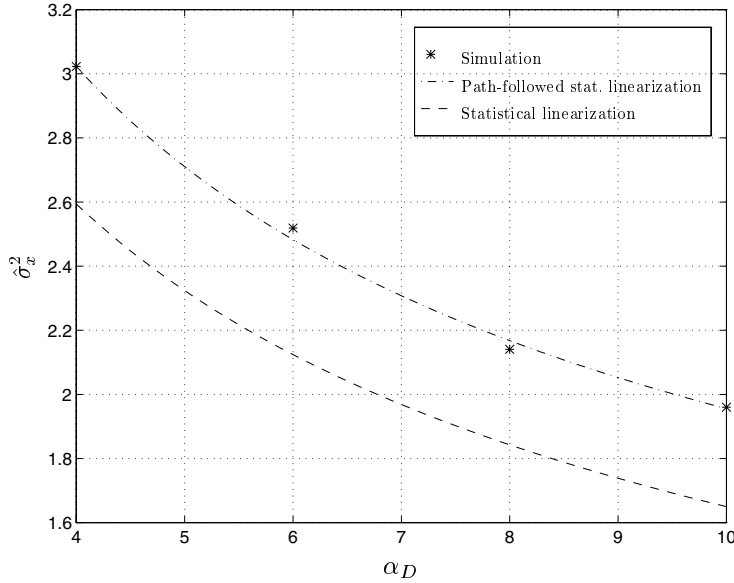
Figure 5.16: Estimates of the variance of the response for varying α_D and $\zeta = 0.003$.

5.6   Discussion

In section 5.2.2, it was shown that the higher-dimensional approximation approach can provide more accurate results than statistical linearization. This is specifically a direct consequence of the fact that nonlinear frequency domain phenomena, such as multiple resonances and high-energy, low-frequency spectral content, are approximated in the higher-dimensional approach. Of course, this results in enhanced variance estimates.

It should be noted, however, that these phenomena are approximated using a linear model. Such a linear model cannot model energy-shifts in the frequency domain, which are characteristic for a nonlinear system and cause the nonlinear phenomena mentioned above. Examples of such energy-shifting can be found in harmonic and subharmonic solutions and the high-energy, low-frequency spectral content. Thus, these phenomena are approximated in a rather artificial way; namely by building a higher-order model which approximates the above phenomena by linear resonances (modes).

Furthermore, it should be stated once more that application of the higher-dimensional approximation approach should be justified (in terms of computational efficiency) by the fact that a wide range of excitations are to be studied. Only then the computational effort spent on the one-off simulation, needed for the construction of the model, can become insignificant in comparison with the situation, in which the responses to all the excitations are evaluated through simulation.

In order to overcome some of the disadvantages of this higher-dimensional approximation approach, in the next chapter the leap towards nonlinear approximation is taken.

6 Nonlinear approximation using finite-order Volterra systems

6.1 Introduction

In chapter 5, a linear, higher-dimensional approximation technique was developed. In this technique, the stochastic, nonlinear response phenomena in the frequency domain are approximated in a linear and, thus, rather artificial way. These response phenomena can be approximated in a more natural way using nonlinear approximation. Moreover, the linear, higher-dimensional approximation technique exhibits another disadvantage; a simulation with a reference excitation is needed to construct the linear model. This model can be used to approximate the response statistics of the original, nonlinear system for other stochastic excitations. The computational efficiency of the method is, therefore, merely guaranteed when the response to many of such excitations is to be investigated. So, it is desirable to develop a method that, firstly, incorporates truly nonlinear approximation and, secondly, is also computational efficient when the application of only a few excitations need to be studied.

In order to tackle these problems, in this chapter, a technique based on nonlinear approximation is developed and applied to the piece-wise linear system. Herein, specific, nonlinear models will be used to approximate the response statistics of the original, nonlinear system. Of course, the computation of the response statistics for such a nonlinear model should be far more efficient than that for the original, nonlinear system. Therefore, finite-order Volterra systems will be used as model form. Finite-order Volterra systems are systems with polynomial nonlinearities. A nonlinear approximation technique using polynomial nonlinearities can be seen as a natural extension of linearization. Besides the fact that the replacement of the original system by a finite-order Volterra model gives us the advantage of computational efficiency, the gradual extension of the replacing models from linear towards polynomial will enhance our understanding of the nonlinear response phenomena of the original system.

A brief description of the basic ideas behind Volterra theory is described in section 6.2. In section 6.3, a technique called bilinearization (or Carleman linearization) is used to construct a finite-order Volterra model. In section 6.4, a statistical bilinearization technique is proposed and applied to the piece-wise linear system (3.2). Herein, the parameters of the Volterra model are determined in such a way that the model approximates the original, nonlinear system optimally in a statistical sense. In section 6.5, some results of the application of the statistical bilinearization technique

to the piece-wise linear system are discussed.

6.2 Volterra systems

In Volterra [1959] the following relation between the input $u(\nu)$, $\nu \in [-\infty, \infty]$ and the output $y(t)$ of a (time-invariant) Volterra system was first considered:

$$
\begin{aligned}
y(t) = & \int_{-\infty}^{\infty} h_1(\tau_1) \, u(t - \tau_1) \, d\tau_1 \, + \\
& + \int_{-\infty}^{\infty} \int_{-\infty}^{\infty} h_2(\tau_1, \tau_2) \, u(t - \tau_1) \, u(t - \tau_2) \, d\tau_1 \, d\tau_2 \\
& + \int_{-\infty}^{\infty} \ldots \int_{-\infty}^{\infty} h_k(\tau_1, \ldots, \tau_k) \, u(t - \tau_1) \ldots u(t - \tau_k) \, d\tau_1 \ldots d\tau_k \, + \ldots,
\end{aligned}
\tag{6.1}
$$

where $k = 1, 2, \ldots$ and $u(-\infty) = 0$. Herein, $h_k(\tau_1, \tau_2, \ldots, \tau_k)$, $k = 1, 2, \ldots$ is called the kth order Volterra kernel with $h_k(-\infty, -\infty, \ldots, -\infty) = 0$, $k = 1, 2, \ldots$. Notice that an expression, such as $u(-\infty) = 0$, means that the input $u(\nu)$ is zero for ν sufficiently small. The first term in (6.1) corresponds to the well-known convolution representation of linear systems. The subsequent terms in (6.1), for $k = 2, 3, \ldots$, represent natural extensions of the linear system using polynomial, nonlinear terms. In this chapter, a polynomial system (or truncated Volterra system) of order p will be used as nonlinear model form:

$$
y(t) = \sum_{k=1}^{p} \int_{-\infty}^{\infty} h_k(\tau_1, \ldots, \tau_k) \, u(t - \tau_1) \ldots u(t - \tau_k) \, d\tau_1 \ldots d\tau_k,
\tag{6.2}
$$

where p is the order of the polynomial system. Note that the polynomial nature of this representation enters through the input. The main issue in the characterisation of such system is the determination of $h_k(\tau_1, \tau_2, \ldots, \tau_k)$, $k = 1, 2, \ldots, p$.

6.3 Bilinearization

In this section, a method called bilinearization or Carleman linearization [Rugh, 1981] is described. The idea is that an affine, nonlinear system with analytic non-linearities can be approximated by a system with bilinear state equation of the form [Lesiak and Krener, 1978]:

$$
\begin{aligned}
\dot{\underline{x}}(t) &= \underline{A}(t) \, \underline{x}(t) + \underline{D}(t) \, \underline{x}(t) \, u(t) + \underline{e}(t) \, u(t) \\
y(t) &= \underline{C}(t) \, \underline{x}(t), \qquad t \geq 0, \; \underline{x}(0) = \underline{0},
\end{aligned}
\tag{6.3}
$$

where $\underline{x}(t)$ is an N_b-dimensional column-vector with state variables, while $u(t)$ and $y(t)$ are scalar inputs and outputs, respectively. Furthermore, $\underline{A}(t)$ is an $N_b \times N_b$

matrix, $\underline{D}(t)$ is an N_b-dimensional column-vector, $\underline{e}(t)$ is an N_b-dimensional column-vector and $\underline{C}(t)$ is an N_b-dimensional row-vector. This is called an affine system since the input appears linearly in the state equations. Here, it is assumed that $\underline{x}(0) = \underline{0}$. Moreover, it is important to note that analytical expressions for the Volterra kernels of such a bilinear system are available [Bruni et al., 1971]. One can truncate the resulting Volterra system at a specific order to obtain a finite-order Volterra system description as in (6.2). This system description can then be used to approximate the response statistics of the bilinear system and, thus, to approximate the response statistics of the original, nonlinear system.

6.3.1 The bilinearization technique

Here, the bilinearization technique will be described briefly. Consider an affine, nonlinear system with the following state equations:

$$
\begin{aligned}
\underline{\dot{x}}(t) &= \underline{a}(t, \underline{x}(t)) + \underline{b}(t, \underline{x}(t))\, u(t) \\
y(t) &= \underline{c}(t)\, \underline{x}(t), \qquad t \geq 0,\ \underline{x}(0) = \underline{0},\ \underline{a}(t, \underline{0}) = \underline{0}\ \forall\, t,
\end{aligned}
\tag{6.4}
$$

where again $\underline{x}(t)$ is an N-dimensional state column-vector, while $u(t)$ is a scalar input and $y(t)$ a scalar output. Furthermore, $\underline{a}(t, \underline{x}(t))$ and $\underline{b}(t, \underline{x}(t))$ are time-dependent vectorfields on $\mathbb{R}^N$ and $\underline{c}(t)$ is an N-dimensional row-vector. It is assumed that $\underline{a}$, $\underline{b}$ and $\underline{c}$ are analytic functions of $\underline{x}$ and continuous in t.

In Rugh [1981], it is stated that, when a solution of the state equation (6.4) exists for $u(t) = 0$ ($t \in [0, T]$) and initial condition $\underline{x}(0) = \underline{x}_0$, there is a Volterra system representation for the state equation that converges on $[0, T]$ when $\mid u(t) \mid\, < \epsilon$ for some sufficiently small $\epsilon > 0$. So, this means that the convergence of the Volterra representation is only guaranteed on a limited time interval and for an input signal which is sufficiently small. We, now, aim to determine a polynomial input-output expression for (6.4) up to order p, as in (6.2), which approximates (6.4) sufficiently close. To do so, first, bilinear state equations are constructed, which have the same Volterra kernels (up to order p) as the system in (6.4). Next, the input-output relation for that bilinear system can be determined. Then, an approximation for the input-output relation of (6.4) is available and can be used to approximate the response statistics of this system.

The right-hand side of (6.4) can be replaced by a power series representation:

$$
\begin{aligned}
\underline{a}(t, \underline{x}(t)) &= \underline{A}_1(t)\, \underline{x}(t) + \underline{A}_2(t)\, \underline{x}^{(2)}(t) + \ldots + \underline{A}_p(t)\, \underline{x}^{(p)}(t) + \ldots \\
\underline{b}(t, \underline{x}(t)) &= \underline{B}_0(t) + \underline{B}_1(t)\, \underline{x}(t) + \ldots + \underline{B}_{p-1}(t)\, \underline{x}^{(p-1)}(t) + \ldots,
\end{aligned}
\tag{6.5}
$$

where the Kronecker product notation is used:

$$
\underline{x}^{(2)}(t) = \underline{x}(t) \otimes \underline{x}(t).
\tag{6.6}
$$

For matrices $\underline{P}$ and $\underline{Q}$ with dimensions $n_p \times m_p$ and $n_q \times m_q$, respectively, the Kronecker product is defined as

$$
\underline{P} \otimes \underline{Q} = \begin{bmatrix} P_{11}\underline{Q} & \ldots & P_{1m_p}\underline{Q} \\ \vdots & \vdots & \vdots \\ P_{n_p 1}\underline{Q} & \ldots & P_{n_p m_p}\underline{Q} \end{bmatrix}.
\tag{6.7}
$$

Note that $\underline{x}^{(p)}(t)$ is an N^p-dimensional column-vector and $\underline{A}_p(t)$ is an $N \times N^p$ matrix. Using (6.5), (6.4) can be rewritten as

$$\dot{\underline{x}}(t) = \sum_{k=1}^{p} \underline{A}_k(t)\, \underline{x}^{(k)}(t) + \underline{B}_k(t)\, \underline{x}^{(k)}(t)\, u(t) + \dots$$

$$y(t) = \underline{c}(t)\, \underline{x}(t), \qquad \underline{x}^{(k)}(0) = \underline{0},\ t \geq 0. \tag{6.8}$$

In order to determine the first p kernels corresponding to (6.8), differential equations are developed for $\underline{x}^{(j)}(t)$ [Rugh, 1981]:

$$\frac{d}{dt}[\underline{x}^{(j)}(t)] = \sum_{k=1}^{p-j+1} \underline{A}_{j,k}(t)\, \underline{x}^{(k+j-1)}(t) + \sum_{k=0}^{p-j} \underline{B}_{j,k}(t)\, \underline{x}^{(k+j-1)}(t) + \dots, \tag{6.9}$$

with $\underline{x}^{(j)}(0) = 0$ (for $j = 1, \dots, p$), $\underline{A}_{1,k} = \underline{A}_k$ and, for $j > 1$,

$$\underline{A}_{j,k}(t) = \underline{A}_k(t) \otimes \underline{I}_N \otimes \cdots \otimes \underline{I}_N + \underline{I}_N \otimes \underline{A}_k(t) \otimes \dots \otimes \underline{I}_N +$$

$$\dots + \underline{I}_N \otimes \dots \otimes \underline{I}_N \otimes \underline{A}_k(t). \tag{6.10}$$

It should be noted that there are $j - 1$ Kronecker products in each term and j terms. The notation for $\underline{B}_{j,k}(t)$ is likewise. Note that $\underline{I}_N$ represents an $N \times N$ identity matrix. Now, by setting

$$\underline{x}^{\otimes}(t) = \begin{bmatrix} \underline{x}^{(1)}(t) \\ \underline{x}^{(2)}(t) \\ \vdots \\ \underline{x}^{(p)}(t) \end{bmatrix}, \tag{6.11}$$

(6.9) can be written as a bilinear state equation (plus higher-order terms):

$$\frac{d}{dt}\underline{x}^{\otimes}(t) = \begin{bmatrix} \underline{A}_{11} & \underline{A}_{12} & \cdots & \underline{A}_{1p} \\ \underline{0} & \underline{A}_{21} & \cdots & \underline{A}_{2,p-1} \\ \underline{0} & \underline{0} & \cdots & \underline{A}_{3,p-1} \\ \vdots & \vdots & \vdots & \vdots \\ \underline{0} & \underline{0} & \cdots & \underline{A}_{p1} \end{bmatrix} \underline{x}^{\otimes}(t)$$

$$+ \begin{bmatrix} \underline{B}_{11} & \underline{B}_{12} & \cdots & \underline{B}_{1,p-1} & \underline{0} \\ \underline{B}_{20} & \underline{B}_{21} & \cdots & \underline{B}_{2,p-2} & \underline{0} \\ \underline{0} & \underline{B}_{30} & \cdots & \underline{B}_{3,p-3} & \underline{0} \\ \vdots & \vdots & \vdots & & \vdots \\ \underline{0} & \underline{0} & \cdots & \underline{B}_{p0} & \underline{0} \end{bmatrix} \underline{x}^{\otimes}(t)u(t) + \begin{bmatrix} \underline{B}_{10} \\ \underline{0} \\ \underline{0} \\ \vdots \\ \underline{0} \end{bmatrix} u(t) + \dots,$$

$$y(t) = \begin{bmatrix} \underline{c}(t) & \underline{0} & \cdots & \underline{0} \end{bmatrix} \underline{x}^{\otimes}(t) + \dots, \quad \underline{x}^{\otimes}(0) = \underline{0},$$

$$\tag{6.12}$$

where $\underline{x}^{\otimes}(t)$ is an N_b-dimensional column-vector of state variables ($N_b = \sum_{l=1}^{p} N^l$). This equation is called a Carleman linearization or the bilinearization of the linear-analytic state equation (6.4).

6.3.2 Input-output relation for bilinear state equations

Here, the Volterra representation of (6.12) will be described. Since the Volterra representation of (6.12) coincides with that of (6.4) up to order p, we can now use (6.12) to evaluate the input-output behaviour of (6.4). Note that (6.12) is a bilinear system as in (6.3).

It can be derived that the input-output relation of the bilinear state equations (6.3) can be written as [Rugh, 1981]:

$$y(t) = \sum_{k=1}^{\infty} \int_0^t \int_0^{\tau_1} \cdots \int_0^{\tau_{k-1}} \underline{C}(t) \; \underline{\Phi}(t,\tau_1) \; \underline{D}(\tau_1) \; \underline{\Phi}(\tau_1,\tau_2) \; \underline{D}(\tau_2)$$

$$\cdots \underline{D}(\tau_{k-1}) \; \underline{\Phi}(\tau_{k-1},\tau_k) \; \underline{e}(\tau_k) \; u(\tau_1) \ldots u(\tau_k) \; d\tau_k \ldots d\tau_1, \tag{6.13}$$

where $\underline{\Phi}(t,\tau)$ is the transition matrix of $\underline{A}(t)$ defined by the Peano-Baker series:

$$\underline{\Phi}(t,\tau) = \underline{I} + \int_\tau^t \underline{A}(\tau_1) \; d\tau_1 + \int_\tau^t \underline{A}(\tau_1) \int_\tau^{\tau_1} \underline{A}(\tau_2) \; d\tau_2 \; d\tau_1$$

$$+ \ldots + \int_\tau^t \underline{A}(\tau_1) \int_\tau^{\tau_1} \underline{A}(\tau_2) \ldots \int_\tau^{\tau_{k-1}} \underline{A}(\tau_k) \; d\tau_k \ldots d\tau_1 + \ldots . \tag{6.14}$$

Note that in (6.13) causality is implied through the integration limits of the multiple integrals: for each t, $y(t)$ merely depends on $\{u(\nu), \; \nu \in [-\infty, t]\}$. We once more assume that $\underline{x}(0) = \underline{0}$ in equation (6.13). As a consequence, the contribution with respect to the initial condition $\underline{x}(0)$ can be omitted in (6.13). For a stationary system $\underline{A}(t)$ is a constant matrix. Consequently, it can be shown that in that case

$$\underline{\Phi}(t_1, t_2) := \underline{\Phi}(t_1 - t_2) = e^{\underline{A}(t_1 - t_2)}. \tag{6.15}$$

Combining (6.13), (6.12), (6.3) and (6.2) gives the Volterra kernels of the bilinear system (6.12). The kernels up to order p also represent the kernels of (6.4).

6.4 Statistical bilinearization: application to the piece-wise linear system

In this section, the bilinearization technique will be used within a technique that will be termed statistical bilinearization. The statistical bilinearization technique will be applied to the piece-wise linear system (3.2). Hereto, this system will be approximated using polynomial nonlinearities. Here, only terms up to order two ($p = 2$) will be used. The replacing system can, therefore, be written as

$$\ddot{x} + 2\zeta \; \dot{x} + \beta_1 \; x_E + \beta_2 \; x_E^2 - \beta_2 \; E\{x_E^2\} = d, \tag{6.16}$$

where $x_E = x - E\{x\}$ and $\ddot{x}_E = \ddot{x}$, $\dot{x}_E = \dot{x}$ due to stationarity. Equivalent to the procedure followed in statistical linearization, see section 3.3, an error has to be defined. This error embodies the difference between the piece-wise linear system and the quadratic system (6.16):

$$\varepsilon_{bilin} = (x + \alpha \ \epsilon(x) \ x) - \beta_1 \ x_E - \beta_2 \ x_E^2 + \beta_2 \ E\{x_E^2\}, \tag{6.17}$$

for given β_1 and β_2. Subsequently, our goal is to minimise $E\{\varepsilon_{bilin}^2\}$ with respect to β_1 and β_2. This results in the following equations:

$$\beta_1 = \frac{E\{x_E(x + \alpha \ \epsilon(x) \ x)\}}{\sigma_x^2}, \tag{6.18}$$

$$\beta_2 = \frac{E\{x_E^2(x + \alpha \ \epsilon(x) \ x)\} - E\{x + \alpha \ \epsilon(x) \ x\}\sigma_x^2}{E\{x_E^4\} - \sigma_x^4}. \tag{6.19}$$

At this point we have four unknown quantities (μ_x, σ_x, β_1 and β_2) and two equations. A third equation can be found through the averaging of equation (3.1):

$$E\{x + \alpha \ \epsilon(x) \ x\} = 0. \tag{6.20}$$

In order to find a necessary fourth equation to solve for the unknowns the bilinearization procedure will be applied. This will yield an expression for σ_x^2 for given values of β_1 and β_2.

By choosing a replacing Volterra system as in (6.16), the power series representation of the original nonlinear system as required in (6.5) is readily defined. Consequently, the matrices in equation (6.12) can be determined. Since this equation is a bilinear state equation of the form of (6.3), the matrices of (6.3) are also known:

$$\underline{A} = \begin{bmatrix} 0 & 1 & 0 & 0 & 0 & 0 \\ -\beta_1 & -2\zeta & -\beta_2 & 0 & 0 & 0 \\ 0 & 0 & 0 & 1 & 1 & 0 \\ 0 & 0 & -\beta_1 & -2\zeta & 0 & 1 \\ 0 & 0 & -\beta_1 & 0 & -2\zeta & 1 \\ 0 & 0 & 0 & -\beta_1 & -\beta_1 & -4\zeta \end{bmatrix}, \tag{6.21}$$

$$\underline{D} = \begin{bmatrix} 0 & 0 & 0 & 0 & 0 & 0 \\ 0 & 0 & 0 & 0 & 0 & 0 \\ 0 & 0 & 0 & 0 & 0 & 0 \\ 1 & 0 & 0 & 0 & 0 & 0 \\ 1 & 0 & 0 & 0 & 0 & 0 \\ 0 & 2 & 0 & 0 & 0 & 0 \end{bmatrix}, \ \underline{e} = \begin{bmatrix} 0 \\ 1 \\ 0 \\ 0 \\ 0 \\ 0 \end{bmatrix}, \ \underline{C} = \begin{bmatrix} 1 \\ 0 \\ 0 \\ 0 \\ 0 \\ 0 \end{bmatrix}^T. \tag{6.22}$$

Next, (6.13) can be used to compute the kernels of this bilinear system. However, first $\underline{\Phi}(t - \tau) = e^{\underline{A}(t-\tau)}$ is computed. This can be done using the relation

$$e^{\underline{A}t} = \mathcal{L}^{-1}\left\{(s\underline{I}_N - \underline{A})^{-1}\right\}, \tag{6.23}$$

where $\mathcal{L}$ is the Laplace operator and $s \in \mathbb{C}$. This expression is very lengthy due to the fact that it is a function of the parameters ζ, β_1 and β_2. Therefore, it is not given here and the elements of $\underline{\Phi}(t, \tau)$ will be denoted by $\Phi_{jk}(t - \tau)$, $j, k = 1, \ldots, 6$. Now, the Volterra kernels of the bilinear system can be evaluated. Firstly, the first-order (linear) kernel can be determined from (6.13):

$$h_1(t, \tau_1) = \underline{c}\,\underline{\Phi}(t, \tau_1)\underline{e} = \Phi_{12}(t, \tau_1). \tag{6.24}$$

Due to the stationarity of $\underline{A}(t)$, $h_1(t, \tau_1)$ can be written as $h_1(t - \tau_1) = \Phi_{12}(t - \tau_1)$. Secondly, the observation of (6.13) admits the determination of the second-order kernel:

$$\begin{aligned}
h_{2\,tri}(t, \tau_1, \tau_2) = [&\Phi_{12}(\tau_1 - \tau_2)\ (\Phi_{14}(t - \tau_1) + \Phi_{15}(t - \tau_1)) \\
&+ 2\ \Phi_{16}(t - \tau_1)\ \Phi_{22}(\tau_1 - \tau_2)]\ \theta(t - \tau_1)\ \theta(\tau_1 - \tau_2),
\end{aligned} \tag{6.25}$$

where

$$\theta(t) = \left\{ \begin{array}{ll} 1 & \text{if } t \geq 0 \\ 0 & \text{if } t < 0 \end{array} \right. . \tag{6.26}$$

The presence of the θ terms in (6.25) implies that $t > \tau_1 > \tau_2$, which means that $h_{2\,tri}$ is a triangular kernel, indicated by the subscript *tri*. The fact that $h_{2\,tri}$ is a triangular kernel follows from the integration limits in (6.13). Since $h_{2\,tri}(t, \tau_1, \tau_2) = h_{2\,tri}(t + \Delta t, \tau_1 + \Delta t, \tau_2 + \Delta t)$, $h_{2\,tri}$ is a stationary kernel. In case of stationarity, the kernel $h_{2\,tri}$ can be written as

$$\begin{aligned}
h_{2\,tri}(\tau_1, \tau_2) := h_{2\,tri}(0, -\tau_1, -\tau_2) = [&\Phi_{12}(\tau_2 - \tau_1)\ (\Phi_{14}(\tau_1) + \Phi_{15}(\tau_1)) \\
&+ 2\Phi_{16}(\tau_1)\ \Phi_{22}(\tau_2 - \tau_1)]\ \theta(\tau_1)\ \theta(\tau_2 - \tau_1).
\end{aligned} \tag{6.27}$$

At this point, we have information on the first-order and second-order Volterra kernels of the bilinear system. It should be noted that a second-order Volterra system is entirely determined through its first-order and second-order kernels.

This information can be used to compute the variance of the output of the bilinear system $\sigma_y^2 (= \sigma_x^2$ when $\underline{c} = [1\ 0])$ using

$$\sigma_y^2 = \int\limits_{-\infty}^{\infty} S_{yy}(\omega)\ d\omega. \tag{6.28}$$

For a second-order Volterra system, such as (6.16), the power spectral density $S_{yy}(\omega)$ obeys

$$\begin{aligned}
S_{yy}(\omega) = &\ |\ H_1(i\omega)\ |^2\ S_{dd}(\omega) \\
&+ 2 \int\limits_{-\infty}^{\infty} H_{2\,symm}(i(\omega - \gamma), i\gamma)\ H_{2\,symm}(i(-\omega + \gamma), -i\gamma) \\
&\qquad S_{dd}(\gamma)S_{dd}(\omega - \gamma)d\gamma,
\end{aligned} \tag{6.29}$$

where $H_1(s)$, $s \in \mathbb{C}$ is the first-order transfer function, which can be determined by taking the one-dimensional Laplace transform of $h_1(t)$. Moreover, $H_2(s_1, s_2)$, with $s_1 \in \mathbb{C}$ and $s_2 \in \mathbb{C}$, is the second-order, symmetric transfer function, which can be found by, firstly, performing a two-dimensional Laplace transform on $h_{2tri}(\tau_1, \tau_2)$ and, secondly, performing a symmetrizing operation on the result. This procedure is described in appendix H. It should be noted that a term with a Dirac delta pulse at $\omega = 0$ is omitted in expression (6.29) for $S_{yy}(\omega)$, since that term does not contribute to σ_y^2 but relates to μ_y^2. Now, using (6.29), the power spectral density of the output can be computed. Consequently, the variance of the output can be evaluated through (6.28) for specific values of β_1 and β_2 and, thus, we have defined the fourth equation needed in the statistical bilinearization technique.

Since $\sigma_y^2 = \sigma_x^2$ is now known, a new estimate for the mean of the response of the piece-wise linear system can be determined using (6.20). New values for β_1 and β_2 can be computed by solving the equations (6.18) and (6.19). In order to be able to evaluate the expected values in these equations, a functional form for the probability density function of the response has to be chosen. Here, for the sake of efficiency, a Gaussian pdf is used, see equation (3.13). The expressions for $E\{x + \alpha \, \epsilon(x) \, x\}$ and $E\{x_0(x + \alpha \, \epsilon(x) \, x)\}$ can be found in appendix C. The expressions for $E\{x_0^4\}$ and $E\{x_0^2(x + \alpha \, \epsilon(x) \, x)\}$ can be found in appendix I.

The procedure, described before, has to be applied recursively in an optimisation loop, which consists of the following steps:

1. choose initial values for β_1 and β_2;

2. use equations (6.20), (6.28) and (6.29) to compute estimates for μ_x and σ_x, given β_1 and β_2;

3. compute new values for β_1 and β_2 using the information gained in step 2 and the equations (6.18) and (6.19);

4. go back to step 2 until both β_1 and β_2 have converged.

6.5 Results

The statistical bilinearization technique is applied to the piece-wise linear system. Hereby, we investigate the white-noise excited case with $S_{dd}(\omega) = S_{\xi\xi}(\omega) = \frac{1}{2\pi}$.

In figure 6.1, the estimates for the standard deviation of the response of the piece-wise linear system, obtained by application of the statistical bilinearization technique, are displayed. In this figure, these results are compared to the results of the statistical linearization technique and simulation (using the numerical integration techniques discussed in chapter 2) for varying α and $\zeta = 0.01$. Clearly, the statistical bilinearization technique estimates the standard deviation of the response very accurately, in contradiction to the statistical linearization technique. The source of this accurate approximation can be found by observing the frequency domain information, see figure 6.2. This figure shows that two important nonlinear frequency domain phenomena, namely, the multiple resonance peaks (two in this case) and the high-energy, low-frequency spectral content, are modelled very well by the bilinearization procedure. These phenomena represent important contributions to the
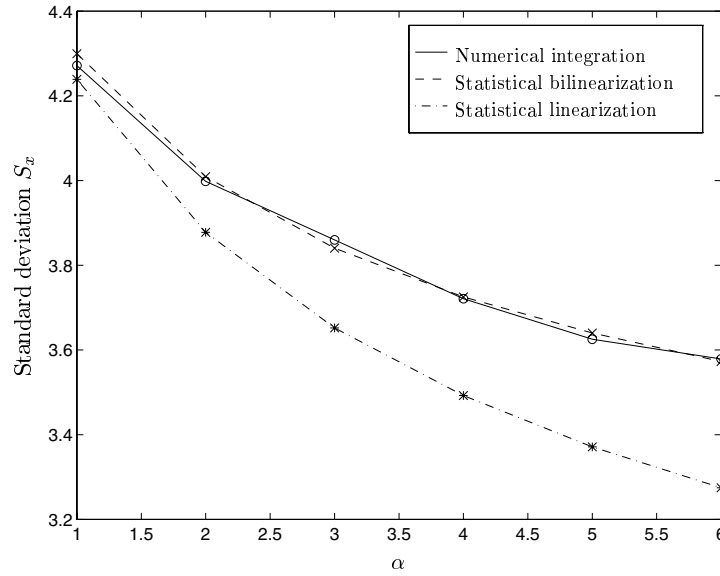
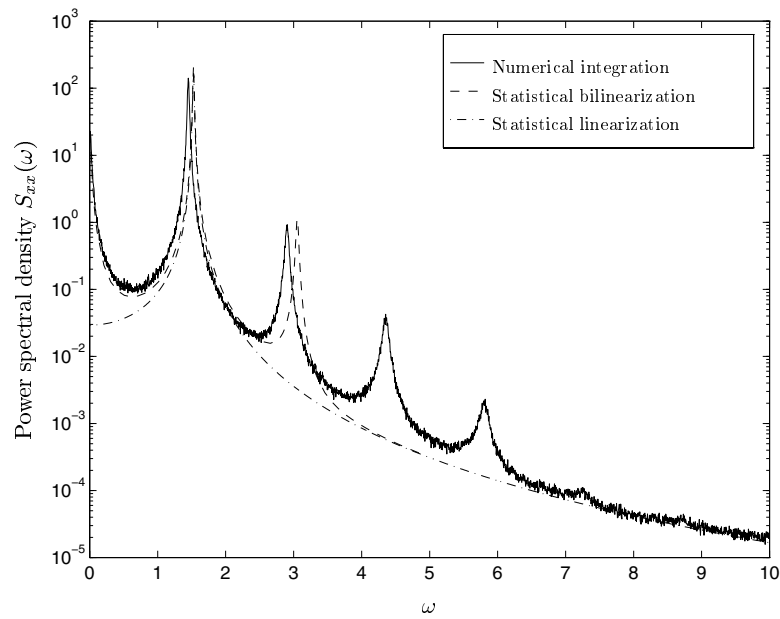Figure 6.1: Estimation of the standard deviation σ_x for $\zeta = 0.01$.

Figure 6.2: Estimation of the power spectral density $S_{xx}(\omega)$ for $\alpha = 6$ and $\zeta = 0.01$.

energy in the response. As a consequence, the variance of the response can only be estimated accurately when these phenomena are modelled. Clearly, only the second resonance frequency appears, whereas higher resonances are absent in the output of the Volterra model. This is a consequence of the fact that we only incorporated a second-order polynomial nonlinearity in our nonlinear model. Higher resonances could be approximated by including higher-order polynomial terms in our Volterra model.

In this form, the statistical bilinearization technique is computationally very efficient (in the same order as the statistical linearization technique). Moreover, the bilinearization approach provides much more accurate results than the statistical linearization technique (in the application to the piece-wise linear system). This is a consequence of the fact that in the statistical bilinearization technique the most important, nonlinear, frequency-domain response phenomena are modelled. The statistical bilinearization procedure is so efficient because it can provide very accurate results using only a second-order Volterra system. In this respect it distincts itself from the bilinearization procedure as proposed in Lesiak and Krener [1978]. Namely, in the bilinearization procedure a bilinear system is pursued, whose output $y_b(t)$ converges to the output of the original, nonlinear system $y(t)$. The system parameters of the bilinear system are determined by minimising the error on the output through $| y_b(t) - y(t) |$ for all t in the time interval of interest. In the statistical bilinearization procedure the parameters of the bilinear system are determined by minimising an error that represents a weighted closeness of the original, nonlinear system and bilinear system; namely, the parameters are determined by minimising $E\{\varepsilon_{bilin}^2\}$ with ε_{bilin} given in (6.17). As a consequence, accurate results can be obtained using a low-order Volterra model.

The third resonance peak could be predicted by extending the polynomial model (6.16) with a third-order nonlinearity (in this case a cubic stiffness nonlinearity). However, this would result in an expression for the power spectral density of the output (see (6.29) for the second-order system), which includes double integrals. The computation of the variance would then include the numerical evaluation of triple integrals and would, therefore, be very laborious. Consequently, the computational efficiency of the method would be seriously compromised. Furthermore, due to the fact that the second-order model already provides highly accurate variance estimates, these variance estimates can hardly be improved by this extension. Moreover, an extension of the model with one order does not automatically lead to an improvement of the prediction of all response characteristics. This is due to the fact that one has little insight into the rate of convergence of the Volterra series of the bilinear system [Rugh, 1981; Schetzen, 1980]. Furthermore, when the statistical bilinearization procedure would be applied to the piece-wise linear system using a third-order polynomial model, the resulting parameter estimates β_1 and β_2 will most likely differ from those of the second-order model. Predictions on accuracy improvements of response characteristics related to model extensions to higher orders are, therefore, difficult to make.

In this context, it should also be remarked that the piece-wise linear system is not analytic everywhere. Therefore, the Volterra series (up to order p) of the bilinear system will not exactly represent that of the piece-wise linear system. However, it

will represent the best finite-order, polynomial model in some statistical sense (as defined before).

Another extension of the method concerns the choice of another form of the probability density function of the response. In Spanos and Donley [1991], a method called quadratization is proposed. This method is in essence the same as the statistical bilinearization technique, when a second-order polynomial model is used in the bilinearization procedure. In Spanos and Donley [1991], a non-Gaussian, truncated Gram-Charlier expansion is used for the probability density function of the response. In such a model, higher-order statistical moments play a role. Non-Gaussian characteristics of the response, such as the skewness, can then be approximated. In Spanos and Donley [1991], systems with relatively small asymmetry are investigated. In such cases, the skewness can be predicted accurately. In the application to the piece-wise linear system, the statistical bilinearization technique was also extended using such a non-Gaussian form for the probability density function. However, due to the fact that the piece-wise linear system is significantly asymmetric, the skewness was not estimated accurately. Moreover, the variance estimates were not improved due to this extension. Another drawback of this extension is the fact that the estimation of the third-order moment of the output of the bilinear system involves the numerical evaluation of triple integrals. Once more, this dramatically reduces the computational efficiency of the method.

6.6 Discussion

In this chapter, a method called statistical bilinearization was developed. The strength of the method can be recognised in the combination of two features. Firstly, the response statistics of the bilinear model can be computed very efficiently (as long as the order of the polynomial model is low). Secondly, a truly nonlinear approximation approach is followed, which makes it possible to model some typically nonlinear phenomena in the original, nonlinear system in accordance to (the nonlinear) reality.

The statistical bilinearization technique was applied successfully to the piece-wise linear system. This application resulted in very accurate variance estimates for the response. Furthermore, typically nonlinear, frequency-domain response phenomena, such as multiple resonance peaks and high-energy, low-frequency spectral content, are modelled correctly. Furthermore, it should be noted that the method is numerically far more efficient than simulation and can even compete with the statistical linearization technique in this respect, as long as the polynomial model used in the bilinearization technique is of a low order.

7 Conclusions, discussion and recommendations

In this chapter, the conclusions with respect to the main lines of research of this thesis will be presented. Moreover, some recommendations for future research will be given.

7.1 Conclusions and discussion

In this thesis, stochastically excited nonlinear dynamic systems were investigated. Within the scope of this research theme, the work can be characterised by two main lines of research. The first line of research focuses on the study, development and qualification of response approximation methods. Herein, characteristics of these methods, such as efficiency, accuracy and applicability, jointly determine the quality of the method. Once such response approximation methods are available, attention can be given to the second line of research. Herein, the focus lies on gaining thorough understanding of specifically nonlinear, stochastic response phenomena.

The main conclusions are summarised below:

- classical integration schemes should not be used to compute (approximate) time-discrete solutions of stochastic differential equations. For this purpose, so-called Ito-Taylor schemes are developed;

- frequency-domain response information is essential for the thorough understanding of the behaviour of stochastically excited, nonlinear, dynamic systems;

- the simultaneous study of periodic and stochastic behaviour of nonlinear, dynamic systems has proven to be very fruitful with respect to gaining insight into nonlinear system behaviour;

- statistical bilinearization can be used as an efficient tool to accurately approximate the stochastic, nonlinear response characteristics of the piece-wise linear system;

- spectral factorization is a very effective tool for constructing linear models for both linear and nonlinear systems based on merely data for the autopower spectra of input and output.

Next, a discussion of the most important observations with respect to the main lines of research are presented.

As far as the investigation and development of the response computation methods are concerned, the following conclusions can be drawn:

- in the literature a wide variety of successful methods were proposed, such as closure techniques and stochastic averaging. However, an important, common shortcoming of these methods is reflected by the fact that these methods only provide information on the probability distribution of the response. Note that this information represents only partly the information on the response statistics; frequency domain information is not provided by the methods mentioned above. Furthermore, the applicability of these methods, in terms of the variety of systems and stochastic excitations that can be investigated by application of these methods, is rather limited (chapter 1);

- existing methods that do provide information on both the probability density function and frequency domain response statistics are, firstly, Monte Carlo simulation and, secondly, statistical linearization. Moreover, these methods can tackle a wide variety of problems (chapter 1);

- using Monte Carlo simulation principally any system and any excitation form can be handled. As a consequence, the method is widely applicable. In Monte Carlo simulation the response statistics are estimated from a finite number of samples of the response, which can be computed using numerical integration. Consequently, any desired level of accuracy can be attained. High levels of accuracy can, however, only be obtained at the cost of computational efficiency. It can be concluded that Monte Carlo simulation can provide very accurate results for a wide variety of problems, though is computationally rather inefficient (chapters 1, 3 and 4);

- when nonlinear, dynamic systems are excited by broad-banded stochastic processes, these processes are generally modelled as white noise processes. Consequently, these systems can be described by stochastic differential equations. Due to the specific properties of the white noise process, these stochastic differential equations cannot be solved numerically using classical, numerical integration techniques. In such cases, other numerical integration techniques should be used. Suitable numerical integration techniques are based on Itô stochastic calculus and differ essentially from the classical integration schemes (chapter 2);

- the statistical linearization technique can also tackle a wide variety of problems and also provides approximate information on the frequency domain characteristics of the stochastic response. In this technique, a linear model, which optimally fits the original, nonlinear system (in some statistical sense), is constructed. Due to the fact that response statistics of such a model can, in general, be evaluated analytically, statistical linearization is computationally very efficient. However, it only provides accurate approximation of the response statistics for weakly nonlinear systems. In chapter 3, it is shown that the statistical linearization technique structurally underestimates the variance

of the response of the piece-wise linear system (even for a moderate nonlinearity). This is dangerous when these estimates are used in failure criteria for practical systems. The cause for this underestimation of the variance can be found by comparing accurate, simulated frequency domain characteristics with those determined using the linear model;

- due to the efficiency-related shortcomings of Monte Carlo simulation and the accuracy-related shortcomings of statistical linearization, other response computation methods are needed. Therefore, in this thesis, two methods are proposed: a method using higher-dimensional, linear approximation (chapter 5) and a method based on nonlinear approximation, termed statistical bilinearization (chapter 6). These methods are developed for handling problems with broad-banded excitations. When narrow-banded, stochastic excitations or near-periodic stochastic excitations are applied, Monte Carlo simulation should be preferred to obtain accurate results;

- the method based on higher-dimensional, linear approximation makes use of a one-off simulation concerning the original, nonlinear system excited by a stochastic reference excitation. Based on the information obtained through this simulation, a higher-dimensional linear model is constructed. This model can then be used to approximate the response statistics of the original, nonlinear system for other stochastic excitations. In contrast to the statistical linearization method, in this method, a linear model is constructed, which has a higher dimension than the original, nonlinear system. This is done in order to model some specifically nonlinear response phenomena (in the frequency domain) in a linear fashion. The method is shown to provide more accurate results than the statistical linearization technique in the application to the piece-wise linear system. The efficiency of the method is greatly enhanced when the response statistics to a wide variety of stochastic excitations are approximated. A shortcoming of the method is reflected by the fact that, in general, the higher-dimensional, linear model can only be used to approximate the response statistics of the original, nonlinear system accurately for stochastic excitations, which are similar to the reference excitation, in terms of energy. However, for the piece-wise linear system this shortcoming is vanishing, since the energy level of the excitation merely represents a scaling factor on the response [Shaw and Holmes, 1983; Fey, 1992]. The energy levels of the excitation and the response of the piece-wise linear system are, therefore, linearly coupled. Consequently, once a higher-dimensional model for this system is constructed, it can be used to approximate the response statistics of the piece-wise linear system for stochastic excitations with different spectra and energy levels (chapter 5);

- the spectral factorization method has been shown to be an effective tool to construct a causal, stable, minimum-phase transfer function using only 'measurement' data on the autospectral densities of the input and output of a specific system. In this thesis, the method is applied successfully to construct a linear model for a nonlinear system. However, the method is pre-eminently suit-

able to construct linear models using measurement data of linear systems. In this respect, it can certainly compete with the commonly used modal analysis tools. Moreover, it has the advantage that no information on the cross-spectral density between the input and output is needed (chapter 5);

- in order to attain higher levels of accuracy than provided by higher-dimensional, linear approximation, a method based on nonlinear approximation was developed in chapter 6. The method, termed statistical bilinearization, is shown to provide very accurate results for the piece-wise linear system. The accuracy is that high because the response phenomena of the original, nonlinear system can be approximated in a truly nonlinear manner. Furthermore, it is computationally very efficient due to the use of Volterra models of a low order. Such high accuracy could be obtained using low-order Volterra models, due to the statistical nature of the criterion according to which the parameters of the model are estimated. In general, higher-order Volterra systems might be necessary to obtain such levels accuracy;

- in figure 7.1, the accuracy and efficiency of the response computation methods, discussed in this thesis, are compared qualitatively by application to the piece-wise linear system. It can be concluded that the statistical bilinearization
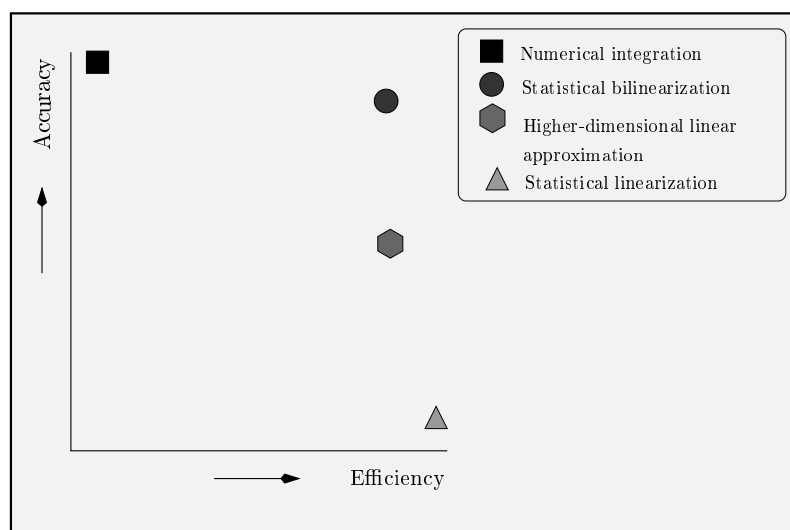

Figure 7.1: Qualitative comparison of the accuracy and efficiency of response approximation methods.

technique should be preferred based on efficiency and accuracy considerations, when the response statistics of a nonlinear system for broad-banded excitations are pursued.

As far as the investigation of nonlinear, stochastic phenomena is concerned, the following conclusions can be drawn:

- in general, the response of a strongly nonlinear system to a Gaussian excitation is essentially non-Gaussian (chapters 3 and 4);

- when investigating the stochastic response of a nonlinear system, it is extremely important to incorporate the frequency domain statistics of the response, such as its power spectral density, in this investigation. Namely, several specifically nonlinear response phenomena can be recognised by looking at the power spectral density of the response. Firstly, multiple resonance peaks can appear in a nonlinear, SDOF system, where in a linear, SDOF system only one resonance peak will appear in the power spectral density of the response. This nonlinear phenomenon was observed in the response of the piece-wise linear system, the beam-impact system and the Duffing system. Furthermore, this phenomenon was observed in both simulation and experiment. For systems with an asymmetric stiffness nonlinearity, such as in the piece-wise linear system and the beam-impact system, another specifically nonlinear, stochastic, frequency domain phenomenon can be observed: the power spectral density of the response exhibits a large amount of energy at low frequencies. This phenomenon is due to the asymmetry of the nonlinearity and can be seen as an interaction phenomenon between different frequencies in the stochastic excitation. It was observed in the response of the piece-wise linear system and the beam-impact system and in both simulation and experiment.

  Both phenomena (multiple resonance frequencies and high-energy, low-frequency response) cannot be predicted by the statistical linearization technique. This is the cause for the fact that this technique underestimates the variance of the response. Namely, these phenomena represent 'extra' energy in the nonlinear response. It can, thus, be concluded that the observation of frequency domain phenomena is very important for two reasons. Firstly, the peculiarities of the energy distribution of the response over the frequency range are illuminated. Secondly, insight can be gained on the effect that these phenomena have on the variance of the response (chapters 3, 4, 5 and 6);

- in order to gain thorough understanding of nonlinear stochastic system behaviour, it is very fruitful to investigate the deterministic (in this case periodic) and stochastic system behaviour simultaneously.

  While investigating the periodic response of the piece-wise linear system and the beam-impact system, harmonic and subharmonic resonances were encountered. When exciting these systems with band-limited, stochastic excitations, stochastic equivalents of harmonic and subharmonic solutions were found. These stochastic resonances appear at the same frequencies as their periodic equivalents. Furthermore, 'stochastic, subharmonic' resonances appear and disappear for the same system parameter settings as for periodic excitations. Consequently, a relatively short simulation with a stochastic excitation can provide information on the existence (and place in the frequency domain) of harmonic and subharmonic resonances. It should be noted that these 'stochastic equivalents' of harmonic and subharmonic solutions were found in both simulation and experiment. In the periodic response of the piece-wise lin-

ear system and the beam-impact system many interesting, nonlinear, local (in terms of excitation frequency) phenomena, such as superharmonic resonances, occur. The variety of such detailed phenomena increases dramatically when a MDOF system is studied. When relatively broad-banded, stochastic excitations are applied, these phenomena seem to be averaged out somehow. However, when relatively small-banded, stochastic excitations are applied some periodic phenomena, such as multiple, stable solutions, appear to have stochastic equivalents too. Another observation, which is made for both periodically and stochastically excited systems, is that the extension of a model from SDOF to MDOF has the following effect: firstly, extra resonances appear for higher frequencies, related to the higher 'modes', and, secondly, the addition of extra degrees of freedom also has a dramatic effect on the response in the lower frequency range of the first 'mode'.

Summarising, it can be concluded that many similarities can be found while observing the periodic and stochastic response of a nonlinear, dynamic system simultaneously. The recognition of mutual phenomena greatly enhances the understanding of nonlinear, stochastic behaviour (chapters 3 and 4).

The two main lines of research, as described above, are intertwined to a great extent. For example, the notion that frequency domain information is essential to understand nonlinear, stochastic behaviour led to, firstly, understanding of the inaccuracy of the variance estimates of the statistical linearization method and, secondly, to the idea of the development of the higher-dimensional, linear approximation method in chapter 5. The other way around, the development and application of the statistical bilinearization method led to more understanding on the origin of the multiple resonance peaks in the power spectral density of the response of the systems investigated in this thesis when excited by broad-banded inputs.

7.2   Recommendations

The scope of the research in this thesis should be extended in different directions. Firstly, non-Gaussian excitations could be considered. Non-Gaussian excitations can be encountered in many fields of engineering [Grigoriu, 1995a]. It is, therefore, important to study the behaviour of both linear and nonlinear systems for such excitations. Secondly, the non-stationarity of either the excitation or the system can add an extra dimension of complexity, which is interesting for future work. Monte Carlo simulation becomes computationally even less efficient in such cases (in comparison with stationary problems), since ergodicity can not be assumed anymore. The need for the development of alternative response approximation methods, then, becomes even more important.

In this thesis, the combination of stochasticity and nonlinearity has given rise to many interesting and challenging problems. However, a wide variety of interesting, practical problems can already be encountered when the level of complexity concerning the nonlinearity of the system is released. In the practice of mechanical engineering many examples of continuous structures exhibiting linear relations between force and displacement and force and velocity exist. For deterministic forc-

ings, such problems are often tackled using the well-known finite element method. Of course, such structures can be excited by forces that vary randomly in time or space (or both). Then, a finite element method for stochastic differential equations [Sun, 1979] could be used to tackle such problems numerically. Further research in this direction seems to be very important since structures are loaded by such random forces in many fields of engineering, such as acoustics, off-shore engineering etc.

Another interesting topic for future work would be to consider such systems (as above) with deterministic loading, but with random system parameters or random boundary conditions, where the system parameters are random variables (not random processes). In many practical systems a level of uncertainty in the system parameters or boundary conditions is quite common due to, for example, production imperfections. Within this topic, then again, the leap towards nonlinear systems could be taken. Another level of complexity is imposed onto these kind of problems when an optimised design is pursued. Then, the problem at hand is twofold; firstly, the response statistics of these systems (with random system parameters) need to be determined accurately and efficiently and, secondly, the optimisation procedure should be able to effectively cope with the randomness in the design variables and response characteristics.

A final recommendation concerns the application of the spectral factorization method, as described in chapter 5. In this thesis, this method is merely used to construct a linear model with which the stochastic response of a nonlinear system can be approximated. However, the method of spectral factorization is pre-eminently suitable to be applied as a non-parametric modelling tool for linear systems. An advantage over commonly used modal analysis methods is that it can also be used to tackle problems, in which the input and output can not be measured simultaneously. Namely, in the commonly used modal analysis methods often the cross-spectral density between input and output, which can only be estimated using simultaneous information on input and output, is needed.

A The moment equations

The Itô formula can be used to derive the appropriate moment equations belonging to a response process obeying a certain SDE. Therefore, the Itô formula (2.60) can be applied to a function $\psi(\underline{x}) = (x_1^{q_1} x_2^{q_2} \ldots x_j^{q_j} \ldots x_n^{q_n})$:

$$d\psi(\underline{x}) = \left[\frac{\partial\psi(\underline{x})}{\partial\underline{x}}\right]^T d\underline{x} + \frac{1}{2}\,\mathrm{Trace}\{\check{\underline{b}}\check{\underline{b}}^T\psi_{\underline{x}\underline{x}}(\underline{x})\}dt. \qquad (A.1)$$

By substituting equation (2.18) for $d\underline{x}$, equation (A.1) can be written as

$$d\psi(\underline{x}) = \left[\frac{\partial\psi(\underline{x})}{\partial\underline{x}}\right]^T \left(\check{\underline{a}}(\underline{x})\,dt + \check{\underline{b}}(\underline{x})\,d\underline{W}(t)\right) + \frac{1}{2}\,\mathrm{Trace}\{\check{\underline{b}}\check{\underline{b}}^T\psi_{\underline{x}\underline{x}}(\underline{x})\}dt. \qquad (A.2)$$

Taking the expected value of both sides yields

$$\begin{aligned} E\{d\psi(\underline{x})\} = &E\left\{\left[\frac{\partial\psi(\underline{x})}{\partial\underline{x}}\right]^T \left(\check{\underline{a}}(\underline{x})dt + \check{\underline{b}}(\underline{x})d\underline{W}(t)\right)\right\} \\ &+ \frac{1}{2}\,E\left\{\mathrm{Trace}\{\check{\underline{b}}\check{\underline{b}}^T\psi_{\underline{x}\underline{x}}(\underline{x})\}dt\right\}. \end{aligned} \qquad (A.3)$$

This equation can be written as a set of differential equations governing the statistical moments of $\underline{x}$:

$$\dot\mu_p = \frac{d}{dt}E\left\{\psi(\underline{x})\right\} = E\left\{\left[\frac{\partial\psi(\underline{x})}{\partial\underline{x}}\right]^T \check{\underline{a}}(\underline{x})\right\} + \frac{1}{2}\,E\left\{\mathrm{Trace}\{\check{\underline{b}}\check{\underline{b}}^T\psi_{\underline{x}\underline{x}}(\underline{x})\}\right\}, \quad (A.4)$$

where $\dot\mu^p$ is the time derivative of the p-th order response moment

$$\mu_p = \mu_{q_1,q_2,\ldots,q_j,\ldots,q_n} = E\left\{x_1^{q_1} x_2^{q_2} \ldots x_j^{q_j} \ldots x_n^{q_n}\right\}. \qquad (A.5)$$

Furthermore $\left[\frac{\partial\psi(\underline{x})}{\partial\underline{x}}\right]^T$ and $\psi_{\underline{x}\underline{x}}(\underline{x})$ are given by

$$\begin{aligned} \left[\frac{\partial\psi(\underline{x})}{\partial\underline{x}}\right]^T = \Big[&q_1 x_1^{q_1-1} x_2^{q_2} \ldots x_j^{q_j} \ldots x_n^{q_n},\ q_2 x_1^{q_1} x_2^{q_2-1} \ldots x_j^{q_j} \ldots x_n^{q_n},\ \ldots,\\ &q_j x_1^{q_1} x_2^{q_2} \ldots x_j^{q_j-1} \ldots x_n^{q_n},\ \ldots,\ q_n x_1^{q_1} x_2^{q_2} \ldots x_j^{q_j} \ldots x_n^{q_n-1}\Big] \end{aligned} \qquad (A.6)$$

$$\psi_{\underline{xx}}(\underline{x}) = \frac{\partial^n \psi(\underline{x})}{\partial x_1 \, \partial x_2 \ldots \partial x_j \ldots \partial x_n} \qquad \text{(Jacobian Matrix)}. \qquad (A.7)$$

A difficulty in using the moment equations (A.4), when dealing with non-linear systems, is that the moments are generally governed by an infinite hierarchy of coupled equations. Thus, in order to obtain a solution it is necessary to introduce a 'closure approximation', which can provide a soluble set of equations. Closure techniques are discussed in section 1.2.6.

B Remainder of the second-order Ito-Taylor expansion

The remainder $\bar{Q}_3$ of the Itô-Taylor expansion (2.74) can be expressed as

$$
\begin{aligned}
\bar{Q}_3 = & \int_{t_0}^{t} \int_{t_0}^{\nu_1} \int_{t_0}^{\nu_2} L^0 L^0 \breve{a}(x(\nu_3)) \, d\nu_3 \, d\nu_2 \, d\nu_1 \\
& + \int_{t_0}^{t} \int_{t_0}^{\nu_1} \int_{t_0}^{\nu_2} L^1 L^0 \breve{a}(x(\nu_3)) \, dW(\nu_3) \, d\nu_2 \, d\nu_1 \\
& + \int_{t_0}^{t} \int_{t_0}^{\nu_1} \int_{t_0}^{\nu_2} L^0 L^1 \breve{a}(x(\nu_3)) \, d\nu_3 \, dW(\nu_2) \, d\nu_1 \\
& + \int_{t_0}^{t} \int_{t_0}^{\nu_1} \int_{t_0}^{\nu_2} L^1 L^1 \breve{a}(x(\nu_3)) \, dW(\nu_3) \, dW(\nu_2) \, d\nu_1 \\
& + \int_{t_0}^{t} \int_{t_0}^{\nu_1} \int_{t_0}^{\nu_2} L^0 L^0 \breve{b}(x(\nu_3)) \, d\nu_3 \, d\nu_2 \, dW(\nu_1) \\
& + \int_{t_0}^{t} \int_{t_0}^{\nu_1} \int_{t_0}^{\nu_2} L^1 L^0 \breve{b}(x(\nu_3)) \, dW(\nu_3) \, d\nu_2 \, dW(\nu_1) \\
& + \int_{t_0}^{t} \int_{t_0}^{\nu_1} \int_{t_0}^{\nu_2} L^0 L^1 \breve{b}(x(\nu_3)) \, d\nu_3 \, dW(\nu_2) \, dW(\nu_1) \\
& + \int_{t_0}^{t} \int_{t_0}^{\nu_1} \int_{t_0}^{\nu_2} L^1 L^1 \breve{b}(x(\nu_3)) \, dW(\nu_3) \, dW(\nu_2) \, dW(\nu_1).
\end{aligned}
\tag{B.1}
$$

C Evaluation of the expected values of nonlinear functions for statistical linearization

The expected values in the equations (3.7) and (3.8), concerning the nonlinearity of the piece-wise linear system, need to be evaluated in terms of μ_x and σ_x. For this purpose, we use the fact that the response of a linear system to a Gaussian excitation is also Gaussian. Consequently, the expected values

$$E\{x + \alpha\epsilon(x)x\} = \int_{-\infty}^{\infty} (x + \alpha\epsilon(x)x)f(x)dx$$

$$E\{x_E(x + \alpha\epsilon(x)x)\} = \int_{-\infty}^{\infty} (x_E(x + \alpha\epsilon(x)x))f(x)dx, \tag{C.1}$$

(with $f(x)$ given by equation (3.13)) can be transformed to

$$E\{x + \alpha\epsilon(x)x\} = \frac{1}{\sqrt{2\pi}\sigma_x} \int_{-\infty}^{\infty} (x + \alpha\epsilon(x)x)\exp\left(-\frac{(x-\mu_x)^2}{2\sigma_x^2}\right) dx$$

$$E\{x_E(x + \alpha\epsilon(x)x)\} = \frac{1}{\sqrt{2\pi}\sigma_x} \int_{-\infty}^{\infty} (x_E(x + \alpha\epsilon(x)x))\exp\left(-\frac{(x-\mu_x)^2}{2\sigma_x^2}\right) dx. \tag{C.2}$$

Straightforward calculations concerning these integrals yield the following expressions:

$$E\{x + \alpha\epsilon(x)x\} = \mu_x + \frac{\alpha\mu_x}{2}\left(1 - \text{erf}\left(\frac{\mu_x}{\sqrt{2}\sigma_x}\right)\right) - \frac{\alpha\sigma_x}{\sqrt{2\pi}}\exp\left(-\frac{\mu_x^2}{2\sigma_x^2}\right)$$

$$E\{x_E(x + \alpha\epsilon(x)x)\} = \sigma_x^2 + \frac{\alpha\sigma_x^2}{2}\left(1 - \text{erf}\left(\frac{\mu_x}{\sqrt{2}\sigma_x}\right)\right), \tag{C.3}$$

in which erf represents the error function.

D Hertzian contact and hysteresis damping

D.1 The Hertzian contact force law

The Hertzian contact model [Hertz, 1895] can be used to describe the collision be-
tween two bodies. When two spherical bodies collide, with their centres of gravity
moving in opposite directions, the contact area can generally be modelled as circu-
lar. A relation between the force on the contacting bodies and a measure for the
deformation in the contact area (the indentation of the contacting bodies) will be
derived. This relation is called the contact force law of Hertz. It is assumed that
the surfaces of both bodies can be approximated by paraboloids. In case of the
beam-impact system, described in chapter 4, the contacting bodies are half spheres,
which validates the latter assumption. Consequently, planes, in which the axes of
rotation of the colliding bodies lie, can be defined (see figure D.1). The radius of
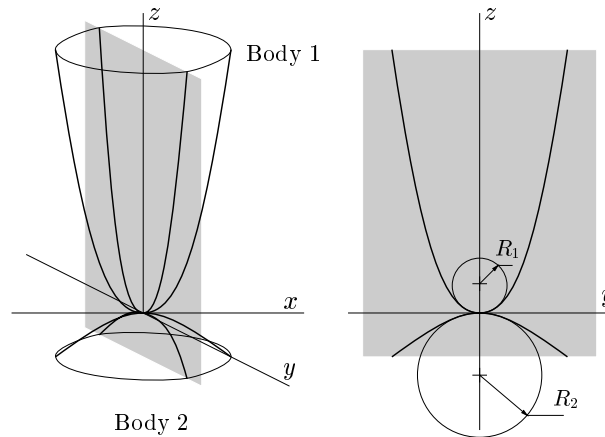
Figure D.1: Two contact bodies represented as paraboloids.

the circle, that approximates the paraboloid in such a plane, is termed the radius of
curvature R_j for body j. Both bodies have a maximum and a minimum radius of
curvature: the main radii of curvature. In case of a circle-contact (as in the contact
between the two half spheres) the two main radii of curvature are equal.

In order to construct the contact force law of Hertz for a circle-contact a few
assumptions have to be made. The most important ones are:

- the radius of the contact area is small compared with the geometry of the colliding bodies;

- there are no shear-stresses on the contact area;

- the deformation is purely linearly elastic;

- the period of time, in which the bodies are in contact, is long enough to establish a quasi-static state.

The approach $h(r)$ of two opposite points P_1 and P_2 on the surface of the contacting bodies (see figure D.2) can be described by

$$h(r) = \delta - \frac{1}{2}kr^2, \text{ with } k = \frac{1}{R_1} + \frac{1}{R_2}, \tag{D.1}$$

where k is the reciprocal of the reduced radius of curvature, δ is a measure for the deformation of the spheres (see figure D.2) and R_1 and R_2 represent the radii of curvature of the two spheres. Note that r is defined in figure D.2 as the horizontal distance between the axis of rotation of the body and the observed point on the surface of the body. When the approach $h(r)$ is positive, the two bodies are in contact

Figure D.2: Geometry of the contact area.

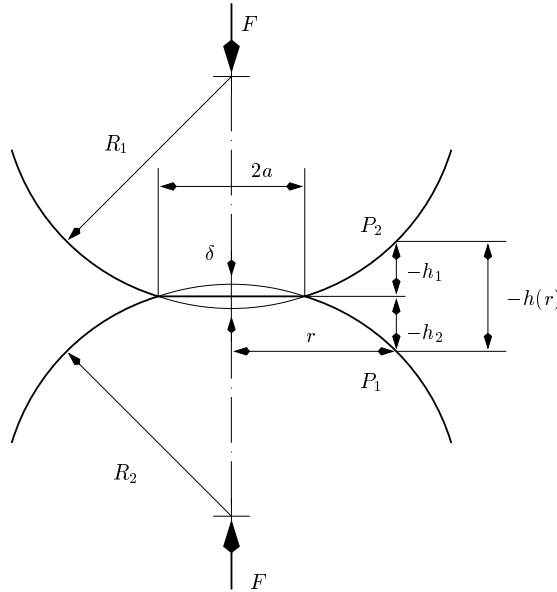for points P_1 and P_2 at r. The distance $h(r)$ between two points consists of two parts: the indentation δ and minus the distance between two opposite points P_1 and P_2 on the surfaces of the spheres in case of point-contact between the two bodies. The

indentation δ does not merely lead to deformation of the two bodies in the contact area, but also results in deformation outside the contact area. The total deformed area is called the zone of influence. It should be noted that relation (D.1) for $h(r)$ only holds outside the the zone of influence. The second part of the expression for $h(r)$ ($h_p(r) = \frac{kr^2}{2}$) can be found using geometrical considerations:

$$r^2 = 2R_j h_{p_j} - h_{p_j}^2, \qquad j = 1, 2. \tag{D.2}$$

Near the contact area ($R_j \gg h_j$), $h_p(r)$ can be given by

$$h_p(r) = h_{p_1} + h_{p_2} = \frac{r^2}{2R_1} + \frac{r^2}{2R_2} = \frac{kr^2}{2}. \tag{D.3}$$

Three integral equations (D.4), (D.6) and (D.7) form the basis of the contact force law of Hertz:

$$\bar{h}(r) = \frac{d}{dr} \int_{s=0}^{r} \frac{s\, h(s)}{\sqrt{r^2 - s^2}}\, ds = -A \int_{s=r}^{a} \frac{s\, p(s)}{\sqrt{s^2 - r^2}}\, ds, \tag{D.4}$$

with a the radius of the contact area and

$$A = 2\left(\frac{1 - \nu_1^2}{E_1} + \frac{1 - \nu_2^2}{E_2}\right) = \frac{4}{E_r}. \tag{D.5}$$

The second integral is the so-called 'Abel'-integral:

$$p(r) = -\frac{1}{r}\frac{d}{dr} \int_{t=r}^{a} \frac{t\, n(t)}{\sqrt{t^2 - r^2}}\, dt, \quad r \le a, \tag{D.6}$$

and its inverse represents the last integral:

$$n(t) = \frac{2}{\pi} \int_{r=t}^{a} \frac{r p(r)}{\sqrt{r^2 - t^2}} dr. \tag{D.7}$$

These equations express the connection between the approach $h(r)$ and the pressure $p(r)$. The integral equations can be derived from mechanical equilibria [Hills et al., 1993].

Substituting $h(r)$ from equation (D.1) in the first part of equation (D.4) results in

$$\begin{aligned}
\bar{h}(r) &= \frac{d}{dr} \int_{s=0}^{r} \frac{s(\delta - \frac{1}{2}ks^2)}{\sqrt{r^2 - s^2}} ds \\
&= \frac{d}{dr} \left| -\delta\sqrt{r^2 - s^2} - \frac{1}{6}k(r^2 - s^2)^{\frac{3}{2}} + \frac{1}{2}kr^2\sqrt{r^2 - s^2} \right|_0^r \\
&= \frac{d}{dr}\left(\delta r - \frac{1}{3}kr^3\right) \\
&= \delta - kr^2.
\end{aligned} \tag{D.8}$$

Equating this result with the second part of equation (D.4) gives

$$\int\limits_{s=r}^{a} \frac{s\,p(s)}{\sqrt{s^2 - r^2}}\,ds = -\frac{\delta - kr^2}{A}. \tag{D.9}$$

Substituting this result in equation (D.7) results in

$$n(t) = -\frac{2\left(\delta - kt^2\right)}{\pi A}. \tag{D.10}$$

Using (D.10), (D.6) can be written as

$$\begin{aligned}
p(r) &= -\frac{1}{r}\frac{d}{dr}\int\limits_{t=r}^{a} \frac{-2\,t\,(\delta - kt^2)}{\pi A\sqrt{t^2 - r^2}}\,dt, \quad r \le a, \\
&= -\frac{1}{r}\frac{d}{dr}\frac{2}{\pi}\left(-\int\limits_{t=r}^{a}\frac{t\delta}{A\sqrt{t^2 - r^2}}dt + \int\limits_{t=r}^{a}\frac{kt^3}{A\sqrt{t^2 - r^2}}dt\right), \quad r \le a, \\
&= -\frac{1}{r}\frac{d}{dr}\frac{2}{\pi}\left(-\frac{\delta}{A}\sqrt{a^2 - r^2} + \frac{ka^2}{A}\sqrt{a^2 - r^2} - \frac{2k}{3A}(a^2 - r^2)^{1.5}\right).
\end{aligned} \tag{D.11}$$

Straightforward calculations transform expression (D.11) to

$$\frac{\pi A p(r)}{2} = -\frac{\delta}{\sqrt{a^2 - r^2}} - k\left[\frac{-a^2}{\sqrt{a^2 - r^2}} + 2\sqrt{a^2 - r^2}\right]. \tag{D.12}$$

Using the boundary condition at $r = a : p(a) = 0$, δ can be expressed through

$$\delta = ka^2. \tag{D.13}$$

This result differs from the result that can be obtained using equation (D.1), which was derived using geometrical considerations. For this reason, (D.1) only holds outside the zone of influence.

Substituting (D.13) in (D.12) yields the following expressions for the pressure:

$$p(r) = -\frac{4k}{\pi A}\sqrt{a^2 - r^2}. \tag{D.14}$$

In a static situation, the pressure $p(r)$ and the contact force F_c are in balance according to

$$-F_c = \int\limits_{r=0}^{a}\int\limits_{\phi=0}^{2\pi} p(r)\,r\,d\phi\,dr = -\frac{8k}{A}\int\limits_{r=0}^{a} r\sqrt{a^2 - r^2}\,dr = -\frac{8k}{3A}a^3. \tag{D.15}$$

Rewriting (D.14) results in an equation that contains an expression for the maximum pressure p_0:

$$p(r) = -p_0\sqrt{1 - \left(\frac{r}{a}\right)^2}, \text{ with } p_0 = \frac{4ka}{\pi A}. \tag{D.16}$$

Combining the former expression for p_0 with (D.15) yields

$$p_0 = \frac{3}{2\pi} \frac{F_c}{a^2}. \tag{D.17}$$

One of the assumptions was that of linear elasticity. As a boundary between elasticity and plasticity the stress $\sigma_{0.2}$, at which 0.2 % irreversible deformation occurs, can be used. Thus, the maximum force that can be applied can be computed using (D.17):

$$F_{c\,max} = \frac{2\pi\,a^2}{3}\sigma_{0.2}. \tag{D.18}$$

The combination of (D.15), (D.13) and (D.5) results in the contact force law of Hertz:

$$F_c = \frac{2E_r}{3\sqrt{k}}\,\delta^{1.5} = K_\mathrm{H}\,\delta^{1.5}. \tag{D.19}$$

D.2 Hysteresis damping

Hysteresis damping is an extension to the contact model of Hertz [Lankarani and Nikravesh, 1994]. Hysteresis damping accounts for the loss of energy as a result of the collision. This energy is dissipated by means of sound and heat.

In case of hysteresis damping, equation (D.19) transforms to

$$F_c = K_\mathrm{H}\,\delta^{1.5} + \mu\,\delta^{1.5}\dot{\delta}, \tag{D.20}$$

with μ the *hysteresis damping factor*, a measure for energy dissipation. This model is valid for low impact velocities; i.e. those impact situations for which impact velocities are negligible compared to the propagation speed of deformation waves across the solids. Equation (D.20) looks like a Kelvin-Voigt model (a spring, parallel to a damper), with the difference that the speed dependent part also is indentation dependent.

The velocities of the two colliding bodies before and after the collision, $V_\mathrm{before} = V^-$ and V_after respectively, are related through the coefficient of restitution e:

$$V_\mathrm{after} = e\,V_\mathrm{before}. \tag{D.21}$$

The kinetic energy of the two colliding bodies before and after the collision can, therefore, be written as

$$\begin{aligned}
T_\mathrm{before} &= \frac{1}{2}m_1(V_1^-)^2 + \frac{1}{2}m_2(V_2^-)^2 \\
T_\mathrm{after} &= \frac{1}{2}m_1(eV_1^-)^2 + \frac{1}{2}m_2(eV_2^-)^2,
\end{aligned} \tag{D.22}$$

and, thus,

$$T_\mathrm{after} = e^2\,T_\mathrm{before}. \tag{D.23}$$

Herein, m_1 and m_2 are the masses of the colliding bodies and V_1^- and V_2^- are the relative initial approach velocities, which are defined by

$$V_1^- = \frac{m_2}{m_1 + m_2} V_a \ \text{ and } V_2^- = -\frac{m_1}{m_1 + m_2} V_a,$$ (D.24)

where the approach velocity V_a is the difference between the absolute velocities V_1 and V_2 of the bodies. Consequently, the expression for the kinetic energy loss $\Delta T = T_{\text{before}} - T_{\text{after}}$ is:

$$\Delta T = \frac{1 - e^2}{2(m_1 + m_2)} \left((m_1^2 + m_1 m_2)(V_1^-)^2 + (m_2^2 + m_1 m_2)(V_2^-)^2 \right).$$ (D.25)

The initial relative impact velocity, $\dot{\delta}^-$, can be defined by

$$\dot{\delta}^- \equiv V_1^- - V_2^-.$$ (D.26)

Consequently, equation (D.25) can be rewritten to

$$\begin{aligned}
\Delta T = {} & \frac{1}{2} \frac{m_1 m_2}{m_1 + m_2} (\dot{\delta}^-)^2 (1 - e^2) \\
& + \left(\frac{m_1 m_2 V_1^- V_2^-}{m_1 + m_2} + \frac{1}{2} \frac{m_1^2 (V_1^-)^2}{m_1 + m_2} + \frac{1}{2} \frac{m_2^2 (V_2^-)^2}{m_1 + m_2} \right) (1 - e^2).
\end{aligned}$$ (D.27)

The momentum balance equation can be written as

$$m_1 V_1^- + m_2 V_2^- = 0.$$ (D.28)

This can be rewritten to

$$\frac{m_1 m_2 V_1^- V_2^-}{m_1 + m_2} + \frac{1}{2} \frac{m_1^2 (V_1^-)^2}{m_1 + m_2} + \frac{1}{2} \frac{m_2^2 (V_2^-)^2}{m_1 + m_2} = 0.$$ (D.29)

Substitution of equation (D.29) in equation (D.27) yields

$$\Delta T = \frac{1}{2} m_{\text{eff}} (\dot{\delta}^-)^2 (1 - e^2) \ \text{ with } \ m_{\text{eff}} = \frac{m_1 m_2}{m_1 + m_2}.$$ (D.30)

During the collision, two phases can be distinguished: a phase of compression and a phase of restitution. During both phases the kinetic energy of the colliding bodies is dissipated in the form of heat and sound. In the (δ, F_c) curve (see figure D.3), the dissipated energy equals the surface within the hysteresis-loop. The upper curve represents the compression phase, whereas the lower curve represents the restitution phase.

In order to obtain an estimate for the energy dissipated during the collision, we assume that the amount of energy dissipated during the compression phase equals the amount of energy dissipated during the restitution phase. Using this assumption, ΔT can be computed as follows:

$$\Delta T = \oint \mu \, \delta^{1.5} \dot{\delta} \, d\delta \approx 2 \int_{\delta=0}^{\delta_m} \mu \, \delta^{1.5} \dot{\delta} \, d\delta,$$ (D.31)
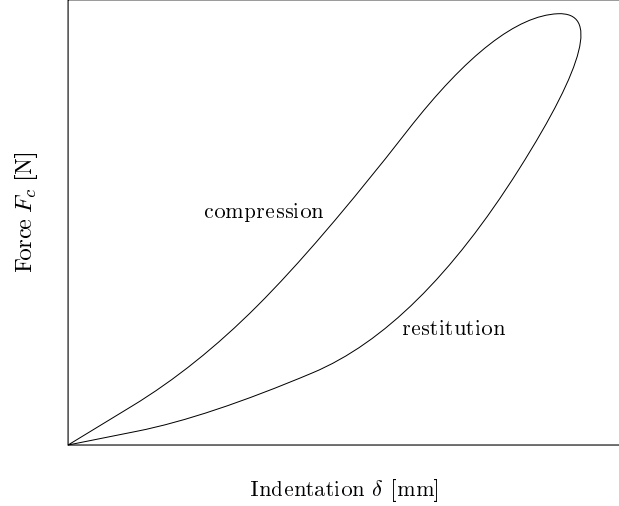
Figure D.3: Example of a hysteretic (δ, F_c)-curve of one collision.

where, δ_m is the maximum indentation. Through geometrical equivalence, a collision between two sphere halves can be reduced to a collision between a half sphere with radius

$$\frac{1}{R} = \frac{1}{R_1} + \frac{1}{R_2},\tag{D.32}$$

and a semi-infinite surface. Analogous, the effective mass m_{eff} of the half sphere can be written as

$$\frac{1}{m_{\text{eff}}} = \frac{1}{m_1} + \frac{1}{m_2} = \frac{m_1 m_2}{m_1 + m_2}.\tag{D.33}$$

The mass m_{eff} represents the mass of the half sphere with radius R. The semi infinite surface has infinite mass. When the indentation δ attains its maximum δ_m, the indentation velocity $\dot{\delta}$ equals zero. Therefore, damping is absent at that moment and the hysteresis model equals to the contact force model of Hertz. For the contact force it then holds that

$$F_c = K_{\text{H}} \delta^{1.5} = -m_{\text{eff}}\, \ddot{\delta}.\tag{D.34}$$

This equation can be integrated with respect to time to obtain the variation of the indentation velocity during the compression phase:

$$-K_{\text{H}} \frac{\delta^{2.5}}{2.5} = \frac{1}{2} m_{\text{eff}} (\dot{\delta}^2 - (\dot{\delta}^-)^2),\tag{D.35}$$

using the boundary condition $\dot{\delta} = \dot{\delta}^-$ for $\delta = 0$. Rewriting (D.35) results in

$$\dot{\delta} = \sqrt{(\dot{\delta}^-)^2 - \frac{2\,K_{\text{H}} \delta^{2.5}}{2.5\,m_{\text{eff}}}}.\tag{D.36}$$

At maximum indentation ($\delta = \delta_m$, $\dot{\delta} = 0$), this equation transforms to

$$\delta_m = \left[\frac{5 \; m_{\text{eff}}(\dot{\delta}^-)^2}{4 \; K_{\text{H}}} \right]^{\frac{2}{5}}.$$ (D.37)

Substituting equation (D.36) in equation (D.31) results in

$$
\begin{aligned}
\Delta T =& 2 \int\limits_{\delta=0}^{\delta_m} \mu \; \delta^{1.5} \sqrt{(\dot{\delta}^-)^2 - \frac{2 \; K_{\text{H}} \; \delta^{2.5}}{2.5 \; m_{\text{eff}}}} \; d\delta \\
=& -2 \left[\frac{1}{3} \frac{\mu \; m_{\text{eff}}}{K_{\text{H}}} \left((\dot{\delta}^-)^2 - \frac{4 \; K_{\text{H}} \delta^{2.5}}{5 \; m_{\text{eff}}} \right)^{\frac{3}{2}} \right]_{\delta=0}^{\delta_m} \\
=& \frac{2}{3} \frac{\mu \; m_{\text{eff}}}{K_{\text{H}}} (\dot{\delta}^-)^3 - 2 \left(\frac{1}{3} \frac{\mu \; m_{\text{eff}}}{K_{\text{H}}} \left((\dot{\delta}^-)^2 - \frac{4 \; K_{\text{H}} \delta_m^{2.5}}{5 \; m_{\text{eff}}} \right)^{\frac{3}{2}} \right).
\end{aligned}
$$ (D.38)

Then, substituting equation (D.37) in equation (D.38) results in

$$\Delta T = \frac{2}{3} \frac{\mu \; m_{\text{eff}}}{K_{\text{H}}} (\dot{\delta}^-)^3.$$ (D.39)

Equating this equation to (D.30) gives an expression for the dissipation coefficient μ:

$$\mu = \frac{3 \; K_{\text{H}} \; (1 - e^2)}{4 \; \dot{\delta}^-}.$$ (D.40)

Substituting this equation in (D.20) results in the final expression for the contact force F_c, the modified contact force law of Hertz with hysteresis damping:

$$F_c = K_{\text{H}} \; \delta^{1.5} \left[1 + \frac{3(1 - e^2)}{4} \frac{\dot{\delta}}{\dot{\delta}^-} \right].$$ (D.41)

The determination of the Hertzian stiffness parameter K_{H} and the coefficient of restitution e is discussed in section D.3.

D.3   Estimation of the Hertzian contact parameter K_{H} and the coefficient of restitution e

Both K_{H} and e were estimated by means of a single experiment. In this experiment several collisions were observed in order to accumulate information regarding the indentation δ, the indentation velocity $\dot{\delta}$ and the contact force F_c during these collisions. The dependency of F_c on δ is visualised in figure D.4 for a few collisions. The parameter K_{H} can be estimated by comparing the contact force F_c and the indentation δ at maximum indentation, assuming that the static contact force is proportional to $\delta^{1.5}$, see equation (D.19). This resulted in $K_{\text{H}} = 2.1 \; 10^8$ N/m$^{1.5}$.
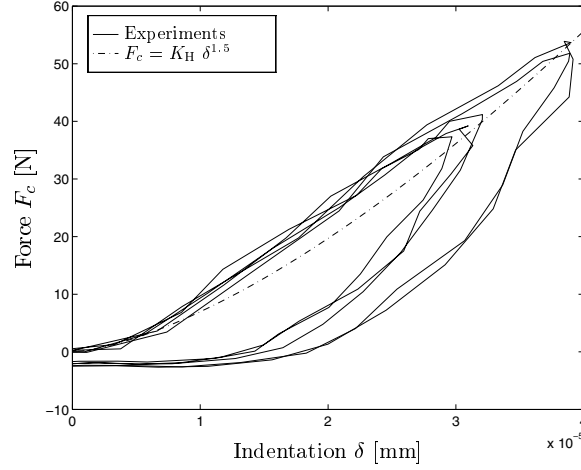
Figure D.4: Measured contact force vs. indentation for several collisions.

The coefficient of restitution e can be estimated by considering the amount of energy loss ΔT during a collision. ΔT is equal to the surface within the hysteresis loop:

$$\Delta T = \oint \mu \, \delta^{1.5} \, \dot{\delta} \, d\delta. \tag{D.42}$$

Therefore, μ can be estimated from

$$\mu = \frac{\Delta T}{\oint \delta^{1.5} \, \dot{\delta} \, d\delta}. \tag{D.43}$$

The coefficient of restitution can now be obtained from

$$e = \sqrt{1 - \frac{4 \, \mu \, \dot{\delta}^{-}}{3 \, K_{\mathrm{H}}}}, \tag{D.44}$$

see equation (D.40). This resulted in $e = 0.5$. Both K_{H} and e are least-squares estimates in which the information obtained from several collisions is accounted for.

E Specifications of the components of the experimental set-up

In this appendix, the components of the experimental set-up are discussed briefly. This includes the measuring equipment, which is discussed in section E.2.

E.1 Components of the experimental set-up

Signal generator

The input signals for the controller are generated through application of the method of Shinozuka (see section 3.5.1). For this purpose, the method is implemented in the numeric computation software package MATLAB [1992]. The software package LabVIEW [1992] is used to provide for the transfer of the signal to the controller. This signal is a staircase signal. It is, therefore, constant during a time interval, that equals the reciprocal of the sample frequency. Due to the filtering characteristics of the controller-servovalve-actuator part of the experimental set-up (see figure 4.13), the signal, that represents the actual excitation on the beam-impact system (i.e. the displacement of the rigid frame), is delayed with respect to the signal, that is sent to the controller. Consequently, an extreme high sample frequency is of no use. A sample frequency of 800 Hz (5026.5 rad/s) appeared to be a good compromise.

Controller

The controller receives an input signal from the signal generator and subsequently sends it to the servovalve. The controller is a MTS model 406.11. It controls the servovalve using a feedback from a Linear Variable Differential Transformer (LVDT), that measures the actual position of the hydraulic actuator. The system controller-servovalve-actuator behaves like a first-order system (see figure E.1) up to a frequency of approximately 75 Hz (470 rad/s). This first-order system is determined by its amplification factor and its time constant. The amplification factor can be modified manually by the controller. However, the time constant is dictated by the experimental set-up. Experiments have shown that this time constant equals 0.833 s^{-1}. A signal with frequency $\frac{2\pi}{0.833} = 7.54$ rad/s as input, thus, results in a signal with a 3 dB amplitude loss and a 45 degrees phase differential on the output of the first-order system. For more information on the controller see MTS [1975b].
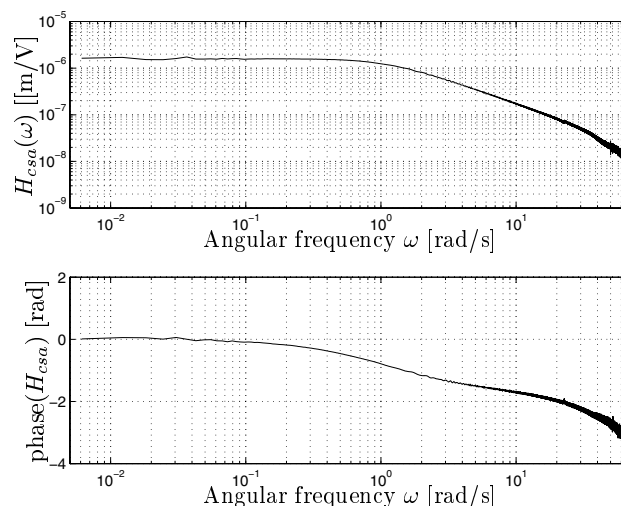
Figure E.1: Amplitude and phase of the frequency response function H_{csa} of the controller-servovalve-actuator system.

Servovalve

The servovalve receives a signal from the controller to regulate the oil flow in the hydraulic actuator in such manner that the desired displacement is generated by the hydraulic actuator. The servovalve is a MTS model 252.23. For more information on the servovalve see MTS [1975c].

Hydraulic actuator

The rigid frame of the beam-impact system is coupled to the hydraulic actuator. Consequently, the actuator dictates the displacement of the rigid frame and, thus, provides the excitation. The hydraulic actuator is a MTS model 244.12. It can deliver a maximum force of 25 kN and has a dynamic stroke of 254 mm. The actuator is powered by a hydraulic service manifold. For more information on the hydraulic actuator see MTS [1975e].

Hydraulic service manifold

The hydraulic service manifold is connected to the hydraulic lines between the hydraulic power supply and the servovalve. The hydraulic service manifold is a MTS model 288.15. Accumulators in both the pressure and the return line of the manifolds supply the surges of the hydraulic fluid demanded by the servovalve and reduce fluctuations and snapping in the hydraulic lines during dynamic programs. A additional function of the manifold is to accumulate energy for peak supplies. The manifold also holds a 5-micron filter to collect contaminants in the fluid to help prevent servovalve wear. For more information on the hydraulic actuator see MTS [1975d].

Hydraulic power supply

The hydraulic power supply supplies the pressure needed by the hydraulic actuator to move. The hydraulic power supply is a MTS model 507.01. It can supply a pressure of 21 MPa at a flowrate of 12.3 l/min.. It requires 380 V 3-phase AC electric power supply. For more information on the hydraulic power supply see MTS [1975a].

Data acquisition

All the measuring instruments, mounted on the the beam system, produce electrical potential inputs for the DIFA Dynamic Signal Analyser (DSA) [DIFA, 1992]. The DIFA DSA is a high performance, 12 channel, PC-based measuring system. The data acquisition hardware is from DIFA's DSA series, model DSA 230. The software is of DIFA's Transfer, Analysis and Control software D-TAC 200, which controls all acquisition functions.

E.2 Measuring equipment

Here, the measuring equipment, mounted on the beam-impact system, see figure 4.14, is discussed.

Linear variable differential transformer (LVDT)

A LVDT is a contactless measuring instrument. An iron core which is attached to a moving object influences a magnetic field in a spool. This results in a change of potential, which is a measure for the displacement of the core. The LVDT, mounted on the beam, is a Lucas Control Systems model DC-E 500. It has a measuring range of ± 12.5 mm, a sensitivity of 0.787 V/mm and a linearity of less than 0.25% of the full range.

Accelerometer

The mounted accelerometer produces an electric charge, which is transformed to a potential by a charge amplifier. This potential is a measure for the acceleration of the accelerometer. The accelerometer is a Brüel & Kjær model 4367. It can measure a maximum continuous sinusoidal acceleration of 30 km/s^2 (100 km/s^2 maximum shock acceleration). It has a charge sensitivity of 2.41 pC/ms^{-2} and a maximum transverse sensitivity of 1.5% at 30 Hz.

Force transducer

The force transducer produces an electric charge, which is transformed to a potential by a charge amplifier. This potential is a measure for the force applied to the force transducer. The force transducer is a Kistler model 9321A. It has a measuring range of ± 10 kN, a sensitivity of -3.94 pC/N and 3.90 pC/N in the negative and in the positive direction, respectively, and a linearity of less than 0.3% of the full range.

Laser interferometer

A laser interferometer is used to measure the displacement and the velocity of the right side of the beam. This laser interferometer is a Polytec series 3000 vibrometer system. The main components of the system are a laser interferometer, model

OFV-302 and a controller processor, model OFV-3000. The measuring range of the displacement is set to ± 5.2 mm and the sensitivity is, therefore, set to 320 μm/V. The calibration accuracy of the displacement measurement of the laser interferometer is $\pm$ 1% of reading $\pm$ 1 step, due to the digital nature of the output. The linearity of the displacement measurement is $\pm$ 1 step. The step is set to 1.3 μm as a result of the measuring range setting. The measuring range of the velocity is set to ± 500 mm/s and the sensitivity is therefore set to 25 (mm/s)/V. The calibration accuracy of the velocity measurement of the laser interferometer is ± 1% of rms (root mean square) reading. The laser interferometer is used instead of a LVDT, since the varying angle at the end of the beam obstructs the use of an LVDT. This introduces, in this case, too much friction between the LVDT and its core.

Charge amplifier

A charge amplifier is used to transform the electric charge from the force transducer and the accelerometer to an electrical potential. The charge amplifier is a Kistler model 5007. It has a linearity of less than 0.5% of its full range. The range and sensitivity can be set manually to meet the needs of the specific experiment.

F MDOF model of the beam-impact system

The beam-impact system is depicted in figure F.1. The beam is made of stainless steel, with the following material properties: modulus of elasticity $E_b = 1.9 \, 10^{11} \, \text{N/m}^2$ and mass-density $\rho_b = 8000 \, \text{kg/m}^3$. Other characteristics of the system are the mass of the ptfe half sphere, which is attached to the beam, $m_s = 12.4 \, 10^{-3} \, \text{kg}$ and the mass of the accelerometer $m_a = 13 \, 10^{-3} \, \text{kg}$. The part of the system, for which a MDOF model is to be constructed, can be specified by the following components: the elastic beam, the half sphere and the mounted accelerometer. The accelerometer is a cylindrical body with radius R_a. The half sphere and the accelerometer introduce a dramatic increase in stiffness in the region of their attachment to the beam. Therefore, for modelling purposes, the elastic beam is split into an elastic part (of length l_e) and a rigid part (of length $l - l_e$), see figure F.1. It should be noted that the point of contact between the two half spheres is assumed to lie at a horizontal position $z = \frac{l + l_e}{2}$.
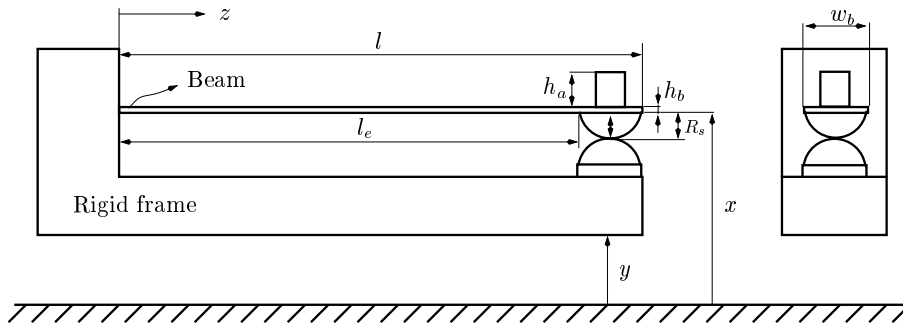
Figure F.1: The nonlinear base-excited beam system, where $l = 259.9$ mm, $l_e = 229$ mm, $w_b = 29.9$ mm, $h_b = 1.95$ mm, $R_s = 15.15$ mm and $h_a = 17.75$ mm.

F.1 Application of the method of Rayleigh-Ritz

The elastic beam (including rigid part) is a continuum with an infinite number of degrees of freedom. The method of Rayleigh-Ritz [Meirovitch, 1997] will be used to construct a model for the beam with a finite number of degrees of freedom. It should be noted that only transverse vibrations of the beam will be considered.

The rigid attachment of the elastic beam to the rigid frame imposes two boundary conditions. Furthermore, extra boundary conditions are necessary due to the division of the beam into an elastic part and a rigid part. These boundary conditions are found through the compatibility of these parts of the beam.

For the elastic beam including the rigid part, which encloses the rigid part of the beam, the half sphere attached to the beam and the accelerometer, the expression for the kinetic energy is given by

$$
\begin{aligned}
T = & \frac{1}{2} \int_{z=0}^{l_e} \rho_b \, A_b \, \left(\dot{x}(z) \right)^2 dz + \frac{1}{2} m_{tot} \left(\dot{x} \left(z = \frac{l + l_e}{2} \right) \right)^2 \\
& + \frac{1}{2} J_{tot} \left(\frac{\partial \dot{x}}{\partial z} \left(z = \frac{l + l_e}{2} \right) \right)^2,
\end{aligned}
\tag{F.1}
$$

where is the cross-sectional area of the beam $A_b = w_b h_b = 59.8 \text{ mm}^2$, $\dot{x} = \frac{\partial x}{\partial t}$. Furthermore, in (F.1),

$$
\begin{aligned}
m_{tot} = & \rho_b \, A_b \, (l - l_e) + m_a + m_s, \\
J_{tot} = & J_r + J_a + J_s \\
= & \frac{1}{12} \rho_b \, A_b \, (l - l_e)^3 + \rho_b \, A_b \, (l - l_e) \, \left(\frac{1}{2} h_b - h_m \right)^2 \\
& + \frac{1}{12} \, m_a \, \left(3 R_a^2 + h_a^2 \right) + m_a \, \left(\frac{1}{2} h_a + h_b - h_m \right)^2 \\
& + m_s \, \left(\frac{83}{320} \, R_s^2 + \left(h_m + \frac{3}{8} R_s \right)^2 \right).
\end{aligned}
\tag{F.2}
$$

Herein, J_r, J_a and J_s are the moments of inertia of the rigid part of the beam, the accelerometer and the half sphere, respectively. Moreover, h_m is the vertical position of the centre of gravity of the rigid part of the beam system (including rigid part of the beam, the accelerometer and the half sphere) relative to the bottom-side of the beam (h_m is positive in upward direction):

$$
h_m = \frac{m_a (\frac{1}{2} h_a + h_b) - \frac{3}{8} m_s R_s + \frac{1}{2} \rho_b A_b (l - l_e) h_b}{m_a + m_s + \rho_b A_b (l - l_e)}.
\tag{F.3}
$$

Define $\delta(z) = x(z) - y$ as the vertical displacement of the beam relative to the rigid frame, which has vertical displacement y. Consequently, the potential energy of the beam V can be expressed as

$$
V = \int_{z=0}^{l_e} E_b \, I_b \, \left(\frac{\partial^2 \delta}{\partial z^2} \right)^2 (z) \, dz,
\tag{F.4}
$$

in which the second moment of area for the cross-section of the beam is determined by $I_b = \frac{1}{12} w_b h_b{}^3$.

The relative displacement of the beam $\delta(z)$ obeys the following two boundary conditions:

$$\begin{cases} \delta(z = 0) = & 0 \\ \frac{\partial \delta}{\partial z}(z = 0) = & 0. \end{cases} \tag{F.5}$$

Using the method of Rayleigh-Ritz, $\delta(z)$ will be expressed as a polynomial function of z. Substitution of the boundary conditions (F.5) in a fifth-order polynomial[1] gives

$$\delta(z, t) = r_2 z^2 + r_3 z^3 + r_4 z^4 + r_5 z^5 = \begin{bmatrix} r_2 & r_3 & r_4 & r_5 \end{bmatrix} \begin{bmatrix} z^2 \\ z^3 \\ z^4 \\ z^5 \end{bmatrix} = \underline{r}^T \underline{z}. \tag{F.6}$$

This description can be used to construct a 4DOF model for the elastic part of the beam ($0 \leq z \leq l_e$). For the rigid part,

$$\delta(z, t) = \delta(l_e, t) + \frac{\partial \delta}{\partial z}(l_e, t)(z - l_e) \qquad \text{for } l_e \leq z \leq l. \tag{F.7}$$

The coefficients in $\underline{r}$ are considered to be degrees of freedom of the Rayleigh-Ritz model. Consider a description in terms of physical degrees of freedom $\underline{\delta}^T = [\delta_1 \ \delta_2 \ \delta_3 \ \delta_4]$ as defined by

$$\begin{aligned}
\delta_1 &= -\delta\left(z = \frac{l + l_e}{2}\right) = -\delta(z = l_e) - \left(\frac{l - l_e}{2}\right)\frac{\partial \delta}{\partial z}(z = l_e), \\
\delta_2 &= -\delta(z = \frac{3l}{4}), \\
\delta_3 &= -\delta(z = \frac{l}{2}), \\
\delta_4 &= -\delta(z = \frac{l}{4}).
\end{aligned} \tag{F.8}$$

The relation between $\underline{\delta}$ and $\underline{r}$ is, consequently, governed by a transformation matrix P:

$$\underline{r} = \underline{P}\,\underline{\delta} \Rightarrow \delta = \underline{r}^T \underline{z} = \underline{\delta}^T \underline{P}^T \underline{z}, \tag{F.9}$$

with

$$P^{-1} = - \begin{bmatrix} l_e l & \frac{1}{2}(3l_e^2 l - l_e^3) & 2l_e^3 l - l_e^4 & \frac{1}{2}(5l_e^4 l - 3l_e^5) \\ (\frac{3l}{4})^2 & (\frac{3l}{4})^3 & (\frac{3l}{4})^4 & (\frac{3l}{4})^5 \\ (\frac{l}{2})^2 & (\frac{l}{2})^3 & (\frac{l}{2})^4 & (\frac{l}{2})^5 \\ (\frac{l}{4})^2 & (\frac{l}{4})^3 & (\frac{l}{4})^4 & (\frac{l}{4})^5 \end{bmatrix}. \tag{F.10}$$

---

[1]The validation for the choice for a fifth-order polynomial will be given later.

Recall that for the absolute displacement of the beam it holds that $x = \delta + y$ with

$$\begin{cases} \delta = & \underline{\delta}^T \underline{P}^T \underline{z} & \text{for } 0 \le z \le l_e, \\ \delta = & \underline{\delta}^T \underline{P}^T \underline{z}(z = l_e) + (z - l_e)\underline{\delta}^T \underline{P}\frac{\partial z}{\partial z}(z = l_e) & \text{for } l_e \le z \le l. \end{cases} \quad \text{(F.11)}$$

Substituting this in relation (F.1) for the kinetic energy yields

$$T = \frac{1}{2}(\rho_b A_b l_e + m_{tot})\dot{y}^2 + \dot{y}\,\underline{\dot{\delta}}^T\,\underline{m}_0 + \frac{1}{2}\,\underline{\dot{\delta}}^T\,(\underline{M} + \underline{m}_1 + \underline{J})\,\underline{\dot{\delta}}, \quad \text{(F.12)}$$

where

$$\underline{m}_0 = \rho_b\,A_b\,\underline{P}^T \int\limits_0^{l_e} \underline{z}\,dz + m_{tot}\,\left(\underline{P}^T\underline{z}(z = l_e) + \frac{1}{2}(l - l_e)\,\underline{P}^T\frac{\partial \underline{z}}{\partial z}(z = l_e)\right),$$

$$\underline{M} = \rho_b\,A_b\,\underline{P}^T \int\limits_0^{l_e} \underline{z}\,\underline{z}^T dz\,\underline{P},$$

$$\underline{m}_1 = m_{tot}\,\underline{P}^T \left(\underline{z}(z = l_e) + \frac{1}{2}(l - l_e)\,\frac{\partial \underline{z}}{\partial z}(z = l_e)\right)$$
$$\left(\underline{z}^T(z = l_e) + \frac{1}{2}(l - l_e)\,\frac{\partial \underline{z}}{\partial z}^T(z = l_e)\right)\underline{P},$$

$$\underline{J} = J_{tot}\,\underline{P}^T\,\frac{\partial \underline{z}}{\partial z}(z = l_e)\frac{\partial \underline{z}}{\partial z}^T(z = l_e)\,\underline{P}. \quad \text{(F.13)}$$

Using (F.11), (F.4) yields

$$V = \frac{1}{2}\underline{\delta}^T\underline{K}\,\underline{\delta}, \quad \text{(F.14)}$$

with

$$\underline{K} = E_b\,I_b\,\underline{P}^T \int\limits_0^{l_e} \left(\frac{\partial^2 \underline{z}}{\partial z^2}\right)\,\left(\frac{\partial^2 \underline{z}}{\partial z^2}\right)^T dz\,\underline{P}. \quad \text{(F.15)}$$

The expressions for the kinetic and potential energies can be used in Lagrange's equations [Meirovitch, 1997]:

$$\frac{d}{dt}\frac{\partial T}{\partial \dot{q}_s} - \frac{\partial T}{\partial q_s} + \frac{\partial V}{\partial q_s} = 0, \quad \text{(F.16)}$$

where q_s are the generalised coordinates. Applying this to the beam-impact system yields

$$\underline{M}_{tot}\,\underline{\ddot{\delta}} + \underline{K}\,\underline{\delta} = -\underline{m}_0\,\ddot{y}, \quad \text{(F.17)}$$

where $\underline{M}_{tot} = \underline{M} + \underline{J} + \underline{m}_1$.

At this point, we have a 4DOF model at our disposal. However, we are merely interested in the influence of the inclusion of the second eigenmode in the model. Therefore, the first two eigenfrequencies of the Rayleigh-Ritz model should be accurate. In order to check the latter, Rayleigh-Ritz models with one, two, three, four and finally five degrees of freedom were constructed. It could be observed that the lowest two eigenfrequencies of the model did not change significantly by the extension of the model from 4DOF to 5DOF. Therefore, the 4DOF was accepted as being accurate enough.

In order to check the quality of this 4DOF model, its lowest two eigenfrequencies are compared to the eigenfrequencies of the experimental system in table F.1.

Eigenfrequencies [Hz]	
Experimental	Model
16.16	17.36
124.40	125.84

Table F.1: Lowest two eigenfrequencies of the 4DOF model vs. experimental eigenfrequencies.

F.2 Modelling of the damping of the elastic beam

The linear damping of the elastic beam will be modelled using proportional damping. Firstly, the equations of motion (F.17) are transformed to equations of motion in terms of natural coordinates $\underline{n}$:

$$\underline{U}^T \underline{M}_{tot} \underline{U}\, \ddot{\underline{n}} + \underline{U}^T \underline{K}\, \underline{U}\, \dot{\underline{n}} = -\underline{U}^T \underline{m}_0 \ddot{y}, \tag{F.18}$$

where $\underline{\delta} = \underline{U}\, \underline{n}$ and $\underline{U}$ is a matrix, whose columns represent the eigenvectors of the 4DOF model. It should be noted that $\underline{U}^T \underline{M}_{tot} \underline{U}$ and $\underline{U}^T \underline{K}\, \underline{U}$ are diagonal matrices. When proportional damping is assumed, the damping matrix $\underline{U}^T \underline{C}\, \underline{U}$ is also a diagonal matrix with diagonal terms $2\zeta_j\, \sqrt{k_j\, m_{tot_j}}$, $j = 1, 2, 3, 4$. Herein, m_{tot_j} and k_j are the jj-th elements of $\underline{M}_{tot}$ and $\underline{K}$, respectively. Furthermore, ζ_j are the dimensionless damping parameters related to mode j. Simulations confirmed that this form of damping can be effectively used to model the damping in the experimental system ($\zeta_1 = 0.015$ and $\zeta_2 = 0.005$). The inclusion of this type of damping transforms (F.18) to

$$\underline{U}^T \underline{M}_{tot} \underline{U}\, \ddot{\underline{n}} + \underline{U}^T \underline{C}\, \underline{U}\, \ddot{\underline{n}} + \underline{U}^T \underline{K}\, \underline{U}\, \dot{\underline{n}} = -\underline{U}^T \underline{m}_0 \ddot{y}. \tag{F.19}$$

F.3 A 2DOF model of the beam-impact system

When the nonlinearity of the beam-impact system (see section 4.1.2 and appendix D for a description of the nonlinearity) is incorporated in the model (F.19) and the

transformation to physical coordinates $\underline{\delta}$ is effectuated, the nonlinear equations of motion are

$$\underline{M}_{tot}\ddot{\underline{\delta}} + \underline{C}\,\dot{\underline{\delta}} + \underline{K}\,\underline{\delta} + \underline{K}_{\mathrm{H}}\epsilon(\delta_1)\delta_1^{\ 1.5}\left(1 + \frac{3(1-e^2)}{4}\frac{\dot{\delta}_1}{\dot{\delta}_1^-}\right) = -\underline{m}_0\ddot{y}, \qquad (\mathrm{F}.20)$$

in which $\dot{\delta}_1^- = \underline{\delta}[1]$ is the relative velocity of the beam at the point of contact at the beginning of a collision and

$$\begin{aligned}
\underline{K}_{\mathrm{H}} &= \left[\begin{array}{cccc} K_{\mathrm{H}} & 0 & 0 & 0 \end{array}\right]^T, \\
\epsilon(\delta_1) &= \left\{\begin{array}{ll} 1 & \text{for } \delta_1 > 0 \\ 0 & \text{for } \delta_1 \leq 0 \end{array}\right. .
\end{aligned} \qquad (\mathrm{F}.21)$$

A nonlinear 4DOF model is now available. However, as stated before, our interest focusses on the lowest two eigenfrequencies of the model. Moreover, simulations using a 4DOF model are unnecessarily inefficient (due to the relatively high third and fourth eigenfrequency) when merely the information with respect to the lowest two eigenfrequencies is needed. Therefore, the 4DOF model is reduced to a 2DOF model, without any loss of modelling accuracy as far as the first two eigenmodes are concerned. The reduced 2DOF model can be written in terms of natural coordinates:

$$\underline{M}_r\ddot{\underline{n}}_r + \underline{C}_r\dot{\underline{n}}_r + \underline{K}_r\underline{n}_r + \underline{K}_{\mathrm{H}_r}\epsilon(\delta_1)\delta_1^{\ 1.5}\left(1 + \frac{3(1-e^2)}{4}\frac{\dot{\delta}_1}{\dot{\delta}_1^-}\right) = -\underline{m}_{0_r}\ddot{y},$$

$$(\mathrm{F}.22)$$

in which

$$\begin{aligned}
\underline{n}_r &= [\underline{n}[1], \underline{n}[2]]^T = [n_1, n_2]^T, \\
\delta_1 &= \underline{U}[1,1]n_1 + \underline{U}[1,2]n_2, \\
\underline{U}_r &= \underline{U}[:, 1:2], \\
\underline{M}_r &= \underline{U}_r^T\underline{M}_{tot}\underline{U}_r, \\
\underline{C}_r &= \underline{U}_r^T\underline{C}\underline{U}_r, \\
\underline{K}_r &= \underline{U}_r^T\underline{K}\underline{U}_r, \\
\underline{K}_{\mathrm{H}_r} &= \underline{U}_r^T\underline{K}_{\mathrm{H}}, \\
\underline{m}_{0_r} &= \underline{U}_r^T\underline{m}_0.
\end{aligned} \qquad (\mathrm{F}.23)$$

G Some numerical aspects of the spectral factorization approach based on potential theory

Let us consider the approach using potential theory in spectral factorization. This resulted in expression (5.43) for the frequency response function. Herein, an integral of the following form is encountered:

$$\int_0^\infty f(\eta)\, d\eta = \int_0^\infty \frac{1}{\eta} \ln\left(\frac{A(\omega+\eta)}{A(\omega-\eta)}\right) d\eta. \tag{G.1}$$

Note that the integrand $f(\eta)$ of the integral (G.1) is apparently singular at $\eta = 0$. Namely, the limit

$$\lim_{\eta \downarrow 0} \frac{1}{\eta} \ln\left(\frac{A(\omega+\eta)}{A(\omega-\eta)}\right) = \frac{2A'(\omega)}{A(\omega)} + \mathcal{O}(\eta^2) \tag{G.2}$$

does exist. However, in practice $A'(\omega)$ is not known, since the data concerning $A(\omega)$ are discrete data resulting from data concerning autospectral density functions of input and output. However, using the fact that $f(\eta)$ is an even function and the fact that $f'(0)$ exists it can be concluded that $f'(0) = 0$. Therefore, $f(0)$ can be accurately estimated by $f(\epsilon)$, in which ϵ is small.

Now, we consider the numerical evaluation of the integral in (G.1). We suppose that there exists an integer n and a positive real number C such that

$$A(\omega) = C\, \omega^n \left(1 + \mathcal{O}(\frac{1}{\omega})\right), \quad \text{for } \omega \to \infty. \tag{G.3}$$

Substitute this into $f(\eta)$ to obtain

$$\lim_{\eta \to \infty} \frac{1}{\eta} \ln\left(\frac{A(\omega+\eta)}{A(\omega-\eta)}\right) = \lim_{\eta \to \infty} \frac{1}{\eta} \ln\left(1 + \mathcal{O}(\frac{1}{\eta})\right) = \mathcal{O}(\frac{1}{\eta^2}). \tag{G.4}$$

Hence, the integral in (G.1) converges for $\eta \to \infty$. However, equation (G.4) shows that this integral converges rather slowly. This would lead to a numerically rather inefficient integration routine. Therefore, it is desirable to estimate the tail of the integral. Let h be a continuous real function on $[0, \infty>$ such that

$$h(\eta) = \mathcal{O}(\frac{1}{\eta^2}), \quad \text{for } \eta \to \infty. \tag{G.5}$$

We would like to evaluate the tail on the integral (G.1) numerically through

$$I = \int_0^\infty h(\eta) \, d\eta. \tag{G.6}$$

Choose $S > 0$ and define

$$I_n = \int_0^{nS} h(\eta) \, d\eta, \quad n = 1, 2, 3, \ldots. \tag{G.7}$$

Now, we have

$$I = I_n + \int_{nS}^\infty h(\eta) \, d\eta \approx I_n + \int_{nS}^\infty \frac{C}{\eta^2} \, d\eta = I_n + \frac{C}{nS} \tag{G.8}$$

for some constant C. Hence,

$$I_{n-1} + \frac{C}{S(n-1)} = I_n + \frac{C}{Sn} \tag{G.9}$$

and, therefore,

$$\frac{C}{S} = n(n-1) \left[I_n - I_{n-1} \right]. \tag{G.10}$$

So, an improved estimate of the integral can be evaluated through

$$\hat{I}_n = I_n + (n-1) \left[I_n - I_{n-1} \right]. \tag{G.11}$$

Numerical studies also confirm that $\hat{I}_n$ converges much faster than I_n.

H Determination of the second-order symmetric transfer function

In this appendix, the second-order, symmetric transfer function $H_{2sym}(s_1, s_2)$ for the Volterra system (6.16) is determined from the second-order, triangular kernel $h_{2tri}(\tau_1, \tau_2)$. The expression for this kernel is very lengthy and, therefore, not given here. However, all contributions $h_{2tri}^j(\tau_1, \tau_2)$, $j = 1, \ldots, m$, to $h_{2tri}(\tau_1, \tau_2)$ according to

$$h_{2tri}(\tau_1, \tau_2) = \sum_{j=1}^{m} h_{2tri}^j(\tau_1, \tau_2), \qquad j = 1, \ldots, m, \tag{H.1}$$

obey the form:

$$h_{2tri}^j(\tau_1, \tau_2) = \exp\left(Z_1^j \tau_1\right) \exp\left(Z_2^j (\tau_2 - \tau_1)\right) \; \theta(\tau_1)\theta(\tau_2 - \tau_1), \tag{H.2}$$

for $j = 1, \ldots, m$ and with $\theta(t)$ defined in (6.26). It should be noted that Z_1^j and Z_2^j are functions of the system parameters of the second-order Volterra system (6.16) and $Z_1^j \in \mathbb{C}$ and $Z_2^j \in \mathbb{C}$. The 2-dimensional Laplace transformations of these contributions are defined by

$$H_{2tri}^j(s_1, s_2) = \int\limits_{-\infty}^{\infty} \int\limits_{-\infty}^{\infty} h_{2tri}^j(\tau_1, \tau_2) \exp\left(-(\tau_1 s_1 + \tau_2 s_2)\right) \; d\tau_1 \, d\tau_2, \tag{H.3}$$

with $s_1 \in \mathbb{C}$ and $s_2 \in \mathbb{C}$. Due to linearity of (H.3),

$$H_{2tri}(s_1, s_2) = \sum_{j=1}^{m} H_{2tri}^j(s_1, s_2), \qquad j = 1, \ldots, m. \tag{H.4}$$

Evaluation of expression (H.3) yields

$$H_{2_{tri}^j}(s_1, s_2) = \int\limits_{\tau_1=-\infty}^{\infty} \int\limits_{\tau_2=-\infty}^{\infty} \exp\left(Z_1^j \tau_1\right) \exp\left(Z_2^j(\tau_2 - \tau_1)\right) \theta(\tau_1)$$

$$\theta(\tau_2 - \tau_1) \exp\left(-(\tau_1 s_1 + \tau_2 s_2)\right) d\tau_2 \, d\tau_1$$

$$= \int\limits_{\tau_1=0}^{\infty} \exp\left(-\tau_1(s_1 + Z_2^j - Z_1^j)\right) \tag{H.5}$$

$$\left\{ \int\limits_{\tau_2=\tau_1}^{\infty} \exp\left(-\tau_2(s_2 - Z_2^j)\right) d\tau_2 \right\} d\tau_1,$$

where

$$\int\limits_{\tau_2=\tau_1}^{\infty} \exp\left(-\tau_2(s_2 - Z_2^j)\right) d\tau_2 = \frac{1}{Z_2^j - s_2} \left[\exp\left(-\tau_2(s_2 - Z_2^j)\right) \big|_{\tau_2=\tau_1}^{\infty} \right]$$

$$= \frac{1}{s_2 - Z_2^j} \exp\left(-\tau_1(s_2 - Z_2^j)\right). \tag{H.6}$$

Using (H.6), one should realise that $H_{2_{tri}^j}(s_1, s_2)$ will be used with $\mathrm{Re}(s_1) = 0$ and $\mathrm{Re}(s_2) = 0$, see equation (6.29). Equation (H.6) will then only hold for $Re(Z_2^j) < Re(s_2) = 0$ (for $j = 1, \ldots, m$), since only then the imaginary plane $Re(s_1) = Re(s_2) = 0$ will lie in the convergence region of the two-dimensional La-Place transformation. For all contributions $h_{2_{tri}^j}(\tau_1, \tau_2)$ and corresponding Z_2^j this condition is satisfied here. Inserting (H.6) in (H.5) leads to

$$H_{2_{tri}^j}(s_1, s_2) = \frac{1}{s_2 - Z_2^j} \int\limits_0^{\infty} \exp\left(\tau_1(Z_1^j - s_1 - s_2)\right) d\tau_1$$

$$= \frac{1}{(Z_2^j - s_2)(Z_1^j - s_1 - s_2)}. \tag{H.7}$$

This equation only holds for $Re(Z_1^j) < 0$, for $j = 1, \ldots, m$, (for the same reason as $Re(Z_2^j) < 0$). This condition is also satisfied for all contributions $h_{2_{tri}^j}(\tau_1, \tau_2)$ and corresponding Z_1^j.

Next, the symmetric, second-order transfer function will be determined. In general, for a symmetric (second-order) transfer function it holds that

$$H_{2_{sym}}(s_1, s_2) = H_{2_{sym}}(s_2, s_1). \tag{H.8}$$

From equation (H.7) it is clear that all contributions to $H_{2_{tri}}(s_1, s_2)$ are asymmetric. The contributions to the second-order, symmetric transfer function can be determined from the contributions to the second-order, triangular transfer function

using

$$H_{2_{sym}^j}(s_1, s_2) = \frac{1}{2} \left[H_{2_{tri}^j}(s_1, s_2) + H_{2_{tri}^j}(s_2, s_1) \right]$$

$$= \frac{1}{2(Z_1^j - s_1 - s_2)} \left(\frac{1}{(Z_2^j - s_2)} + \frac{1}{(Z_2^j - s_1)} \right).$$

(H.9)

I Evaluation of the expected values of nonlinear functions for statistical bilinearization

The expected values $E\{x_E^4\}$ and $E\{x_E^2(x + \alpha\ \epsilon(x)\ x)\}$ in the equation (6.19), concerning the nonlinearity of the piece-wise linear system, need to be evaluated in terms of μ_x and σ_x. Here, we assume that the response x is Gaussian. Consequently, the expected values

$$E\{x_E^4\} = \int\limits_{-\infty}^{\infty} x_E^4\ f(x)\ dx,$$

$$E\{x_E^2(x + \alpha\epsilon(x)x)\} = \int\limits_{-\infty}^{\infty} (x_E^2(x + \alpha\epsilon(x)x))\ f(x)\ dx,$$

(I.1)

(with $f(x)$ given by equation (3.13)) can be transformed to

$$E\{x_E^4\} = \frac{1}{\sqrt{2\pi}\sigma_x} \int\limits_{-\infty}^{\infty} x_E^4\ \exp\left(-\frac{(x - \mu_x)^2}{2\sigma_x^2}\right) dx,$$

$$E\{x_E^2(x + \alpha\epsilon(x)x)\} = \frac{1}{\sqrt{2\pi}\sigma_x} \int\limits_{-\infty}^{\infty} (x_E^2(x + \alpha\epsilon(x)x))\ \exp\left(-\frac{(x - \mu_x)^2}{2\sigma_x^2}\right) dx.$$

(I.2)

Straightforward calculations concerning the integrals in (I.2) yield the following expressions:

$$E\{x_E^4\} = 3\ \sigma_x^4,$$

$$E\{x_E^2(x + \alpha\epsilon(x)x)\} = \frac{\alpha\mu_x\sigma_x^2}{2}\left(1 - \mathrm{erf}\left(\frac{\mu_x}{\sqrt{2}\sigma_x}\right)\right) -$$

$$\alpha\sqrt{\frac{2}{\pi}}\sigma_x^3\ \exp\left(-\frac{\mu_x^2}{2\sigma_x^2}\right),$$

(I.3)

in which erf represents the error function.

Bibliography

Arnold, L. (1974). *Stochastic differential equations: theory and applications*. John Wiley, New York.

Arnold, L. (1998). *Random dynamical systems*. Springer-Verlag, Berlin.

Bruni, C., Di Pillo, G., and Koch, G. (1971). On the mathematical models of bilinear systems. *Richerche di Automatica*, **2(1)**, 11–26.

Butcher, J. C. (1997). *The numerical analysis of ordinary differential equations: Runge-Kutta and general linear methods*. John Wiley & Sons, New York.

Cai, G. Q. and Lin, Y. K. (1988a). A new approximate solution technique for randomly excited non-linear oscillators. *Int. J. Non-Linear Mech.*, **23(5/6)**, 409–420.

Cai, G. Q. and Lin, Y. K. (1988b). On exact stationary solutions of equivalent non-linear stochastic systems. *Int. J. Non-Linear Mech.*, **23(4)**, 315–325.

Cai, G. Q., Lin, Y. K., and Elishakoff, I. (1992). A new approximate solution technique for randomly excited non-linear oscillators 2. *Int. J. Non-Linear Mech.*, **27(6)**, 969–979.

Caughey, T. K. (1963a). Derivation and application of the Fokker-Planck equation to discrete non-linear systems subjected to white random excitation. *J. Acoust. Soc. Em.*, **35(11)**, 1683–1692.

Caughey, T. K. (1963b). Equivalent linearization technique. *J. Acoust. Soc. Am.*, **35(11)**, 1706–1711.

Caughey, T. K. (1964). On the response of a class of nonlinear oscillators to stochastic excitations. *Proc. Collog. Int. du Centre National de la Recherche Scientifeque*, **148**, 392–402.

Caughey, T. K. (1971). Nonlinear theory of random vibrations. In *Advances in Applied Mechanics*, vol. 11. Academic Press, New York.

Caughey, T. K. and Dienes, J. K. (1961). Analysis of a non-linear first-order system with a white noise input. *J. Appl. Phys.*, **23**, 2476–2479.

Caughey, T. K. and Ma, F. (1983). The exact steady-state solution of a class of nonlinear stochastic systems. *Int. J. Non-Linear Mech.*, **17**, 137–142.

Chen, G., Chen, G., and Hsu, S.-H. (1995). *Linear stochastic control systems*. CRC Press, Boca Raton.

Crandall, S. H. (1985). Non-Gaussian closure techniques for stationary random vibration. *Int. J. Non-Linear Mech.*, **20(1)**, 1–8.

Crandall, S. T. (1963). Perturbation techniques for random vibration of nonlinear systems. *J. Acoust. Soc. Am.*, **35(11)**, 1700–1705.

De Kraker, A., Van de Wouw, N., and Van Campen, D. H. (1998). Identification of nonlinear phenomena in a stochastically excited beam system with impact. In *Proc. of ISMA23, 1998 International Conference on Noise and Vibration Engineering, Leuven (Belgium), Vol. 1, 16-18 Sep. 1998*, pp. 321–328. eds. P. Sas.

Den Hartog, J. P. (1956). *Mechanical vibrations*. McGraw-Hill, New York.

DIFA (1992). *FA100 User Manual*. DIFA Measuring Systems, Breda, The Netherlands.

Dimentberg, M. F. (1982). An exact solution to a certain non-linear random vibration problem. *Int. J. Non-Linear Mech.*, **17(4)**, 231–235.

Dormand, J. R. (1996). *Numerical methods for differential equations: a computational approach*. CRC Press, Boca Raton.

Douglass, S. A. (1996). *Introduction to mathematical analysis*. Addison-Wesley Publishinf Company, Reading Massachusetts.

Elishakoff, I. and Cai, G. Q. (1992). Approximate solution for nonlinear random vibration problems by partial linearization. In *Nonlinear Vibrations*, pp. 117–122. ASME.

Falsone, G. (1992). Stochastic linearization of MDOF systems under parametric excitations. *Int. J. Non-Linear Mech.*, **27(6)**, 1025–1037.

Fey, R. H. B. (1992). *Steady-state behaviour of reduced dynamic systems with local nonlinearities*. Ph.D. thesis, Eindhoven University of Technology, The Netherlands.

Fey, R. H. B., Van Campen, D. H., and De Kraker, A. (1996). Long term structural dynamics of mechanical systems with local nonlinearities. *Trans. ASME, J. Vibration and Acoustics*, **118(2)**, 147–153. Also publ. in: Proc. Winter Annual Meeting ASME, Anaheim (Calif., USA), 8-13 Nov., DE-Vol. 50, AMD-Vol. 44, eds. R.A. Ibrahim and N.S. Namachchivaya, 1992, pp. 159-167.

Gill, P. E., Murray, W., and Wright, M. H. (1981). *Practical optimization*. Academic press, London.

Goldsmith, W. (1960). *Impact: the theory and physical behaviour of colliding solids*. E. Arnold Ltd., London.

Grigoriu, M. (1995a). *Applied non-Gaussian processes : examples, theory, simulation, linear random vibration, and MATLAB solutions*. PTR Prentice Hall, Englewood Cliffs.

Grigoriu, M. (1995b). White noise processes in random vibration. In W. Kliemann and N. S. Namachchivaya, eds., *Nonlinear dynamics and stochastic mechanics*, CRC mathematical modelling series, chap. 9, pp. 231–257. CRC Press, Inc., Florida.

Hampl, N. C. and Schuëller, G. I. (1989). Probability densities of the response of nonlinear structures under stochastic dynamic excitation. *Probabilistic Engineering Mechanics*, **4(1)**, 2–9.

Hénon, M. (1982). On the numerical computation of poincaré maps. *Journal of Applied Mechanics*, **47**, 931 − 939.

Hertz, H. (1895). *Gesammelte Werke, vol. 1: Schriften Vermischten Inhalts*. J.A. Barth, Leipzig, Germany (German).

Hills, D. A., Nowell, D., and Sackfield, A. (1993). *Mechanics of elastic contacts*. Butterworth-Heinemann, Oxford.

Ibrahim, R. A. (1985). *Parametric random vibration*. John Wiley and Sons, New York.

Ibrahim, R. A., Soundararajan, A., and Heo, H. (1985). Stochastic response of nonlinear dynamic systems based on a non-Gaussian closure. *Journal of Applied Mechanics*, **52**, 965–970.

Itô, K. (1944). Stochastic integral. *Proc. Imperial Academy Tokyo*, **20**, 519–524.

Itô, K. (1951a). On a formula concerning stochastic differentials. *Nagoya Math. Journal*, **3**, 55–65.

Itô, K. (1951b). On stochastic differential equations. *Memoirs of the American Mathematical Society*, **4**, 51–89.

Iyengar, R. N. (1988). Higher order linearization in non-linear random vibration. *Int. J. Non-Linear Mech.*, **23**, 385–391.

Khasminskii, R. Z. (1966). A limit theorem for the solutions of differential equations with random right-hand sides. *Theory of Probability and Applications*, **11(3)**, 390–405.

Kloeden, P. E. and Platen, E. (1992). *Numerical solution of stochastic differential equations*. Springer-Verlag, Berlin.

Kramer, H. A. (1940). Brownian motion in a field of force and diffusion of chemical reactions. *Physica*, **7**, 284–304.

Krylov, N. and Bogoliubov, N. (1943). *Introduction to nonlinear mechanics*. Princeton University Press, Princeton.

Kwakernaak, H. and Sivan, R. (1972). *Linear optimal control systems*. Wiley-Interscience, New York.

LabVIEW (1992). *User Manual*. National Instruments, Austin, TX, USA.

Lang, Z.-Q. and Billings, S. A. (1997). Output frequencies of nonlinear system. *International Journal of Control*, **67(5)**, 713–730.

Lankarani, H. M. and Nikravesh, P. E. (1994). Continuous contact force models for impact analysis in multibody sytems. *Nonlinear Dynamics*, **5**, 193 − 207.

Lesiak, C. and Krener, A. J. (1978). The existence and uniqueness of volterra series for nonlinear systems. *IEEE Transactions on Automatic Control*, **AC-23(6)**, 1090–1095.

Lin, Y. K. (1967). *Probabilistic theory of structural dynamics*. McGraw-Hill, New York.

Lin, Y. K. (1986). Some observations on the stochastic averaging method. *Probabilistic Engineering Mechanics*, **1(1)**, 23–27.

Lin, Y. K. and Cai, G. Q. (1988). Exact stationary-response solution for second order non-linear systems under parametric and external white-noise excitations, part 2. *J. Appl. Mech. ASME*, **55**, 702–705.

MATLAB (1992). *User's Guide*. The MathWorks Inc., Natick, Mass., USA.

Meirovitch, L. (1997). *Principles and techniques of vibrations*. Prentice-Hall International, New Jersey.

Melsa, J. L. and Sage, A. P. (1973). *An Introduction to probability and stochastic processes*. Prentice-Hall,Inc., New Yersey.

MTS (1975a). *Product manual hydraulic power supply series 507*. Minneapolis, MN, USA.

MTS (1975b). *Product manual model 406.11 controller*. Minneapolis, MN, USA.

MTS (1975c). *Product manual series 252 servovalves*. Minneapolis, MN, USA.

MTS (1975d). *Product manual series 288 hydraulic service manifolds*. Minneapolis, MN, USA.

MTS (1975e). *Product specification series 204 hydraulic actuators*. Minneapolis, MN, USA.

Nayfeh, A. H. (1973). *Perturbation methods*. Wiley-Interscience, London.

Nayfeh, A. H. (1981). *Introduction to perturbation techniques*. Wiley-Interscience, London.

Nayfeh, A. H. and Balachandran, B. (1995). *Nonlinear dynamics: analytical, computational and experimental methods*. John Wiley & Sons, New York.

Nayfeh, A. H. and Mook, D. T. (1979). *Nonlinear oscillations*. Wiley-Interscience, New York.

Nikias, C. L. and Petropulu, A. P. (1993). *Higher-order spectra analysis, a nonlinear signal processing framework*. PTR Prentice-Hall, Inc., Englewood Cliffs.

Oksendal, B. (1998). *Stochastic differential equations*. Springer-Verlag, Berlin.

Oppenheim, A. V. and Schafer, R. W. (1975). *Digital signal processing*. Prentice-Hall Inc., Englewood Cliffs.

Overdijk, D. A., Van de Wouw, N., and De Kraker, A. (1998). Alternative methods in spectral factorization: a modelling and design tool. *ZAMM*. submitted.

Papanicolaou, G. C. and Kohler, W. (1974). Asymptotic theory of mixing stochastic ordinary differential equations. *Communication on Pure and Applied Mathematics*, **27**, 641–668.

Papoulis, A. (1965). *Probability, random variables and stochastic processes*. McGraw-Hill Book Company, New York.

Papoulis, A. (1977). *Signal analysis*. McGraw-Hill Book Company, New York.

Parker, T. S. and Chua, L. O. (1989). *Practical numerical algorithms for chaotic systems*. Springer-Verlag, New York.

Platen, E. (1987). Derivative free numerical methods for stochastic differential equations. In H. Engelbert and W. Schmidt, eds., *Lecture Notes in Control and Information Sciences*, vol. 96, pp. 187–193. Springer, Berlin.

Priestley, M. B. (1981). *Spectral analysis and time series, Volume 2: Multivariate series, prediction and control*. Academic Press, London.

Pugachev, V. S. and Sinitsyn, I. N. (1987). *Stochastic differential systems*. John Wiley & sons, New York.

Richard, K. and Anand, G. V. (1983). Non-linear resonance in strings under narrow-band random excitation, part i: Planar response and stability. *Journal of Sound and Vibration*, **86(1)**, 85–98.

Roberts, J. B. (1978). First passage time for oscillators with non-linear damping. *J. Appl. mech.*, **45**, 175–180.

Roberts, J. B. (1981). Transient response of non-linear systems to random excitation. *Journal of Sound and Vibration*, **74**, 11–29.

Roberts, J. B. and Spanos, P. D. (1986). Stochastic averaging: an approximate method of solving random vibration problems. *Int. J. Non-Linear Mech.*, **21(2)**, 111–134.

Roberts, J. B. and Spanos, P. D. (1990). *Random vibration and statistical linearization*. John Wiley and Sons, New York.

Roozen-Kroon, P. J. M. (1992). *Structural optimization of bells*. Ph.D. thesis, Eindhoven University of Technology, The Netherlands.

Rubinstein, R. Y. (1981). *Simulation and the Monte Carlo method*. John Wiley, New York.

Rugh, W. J. (1981). *Nonlinear system theory*. John Hopkins university Press, London.

Schetzen, M. (1980). *The Volterra and Wiener theories of nonlinear systems*. John Wiley, New York, N.Y.

Schwartz, M., Green, S., and Rutledge, W. A. (1960). *Vector analysis*. Harper, New York.

Shapiro, S. S. and Wilk, M. B. (1965). An analysis of variance test for normality (complete samples). *Biometrika*, **52(3 and 4)**, 591–611.

Shapiro, S. S. and Wilk, M. B. (1968). Approximations for the null distribution of the W statistic. *Technometrics*, **10(4)**, 861–866.

Shaw, S. W. and Holmes, P. J. (1983). A periodically forced piecewise linear oscillator. *Journal of Sound and Vibration*, **90(1)**, 129–155.

Shinozuka, M. (1972). Monte Carlo solution of structural dynamics. *Computers & Structures*, **2**, 855–874.

Spanos, P. D. and Donley, M. G. (1991). Equivalent statistical quadratization for nonlinear systems. *Journal of Engineering Mechanics*, **117(6)**, 1289–1310.

Spanos, P. D. and Donley, M. G. (1992). Non-linear multi-degree-of-freedom system random vibration by equivalent statistical quadratization. *Int. J. Non-linear Mechanics*, **27(5)**, 735–748.

Spanos, P. D. and Mignolet, M. D. (1989). Arma Monte Carlo simulation in probabilistic structural analysis. *Shock Vib. Digest*, **21**, 3–10.

Sri Namachchivaya, N. and Lin, Y. K. (1988). Application of stochastic averaging for systems with high damping. *Prob. Engin. Mech.*, **3(3)**, 185–196.

Stratonovich, R. L. (1963). *Topics in the theory of random noise*. Gordon and Breach, New York.

Sun, J. Q. and Hsu, C. S. (1987). Cumulant-neglect closure method for nonlinear systems under random excitations. *Journal of Applied Mechanics, Transactions ASME*, **54(3)**, 649–655.

Sun, T.-C. (1979). Finite element method for random differential equations. In A. Bharucha-Reid, ed., *Approximate solution of random equations*, vol. XII of *North-Holland series in probability and applied mathematics*, pp. 223–237. North-Holland, Amsterdam.

Thompson, J. M. T. and Stewart, H. B. (1986). *Nonlinear dynamics and chaos; geometrical methods for engineers and scientists*. John Wiley and Sons Ltd., New York.

Van Campen, D. H., De Kraker, A., Fey, R. H. B., Van de Vorst, E. L. B., and Van der Spek, J. A. W. (1997a). Long-term dynamics of nonlinear MDOF engineering systems. *Chaos, Solitons and Fractals; Special Issue on Nonlinearities in Mechanical Engineering*, **8(4)**, 455–477.

Van Campen, D. H., Fey, R. H. B., Van Liempt, F. P. H., and De Kraker, A. (1997b). Steady-state behaviour of a solar array system with elastic stops. In *Proc. IUTAM Symp. on New Applications of Nonlinear and Chaotic Dynamics in Mechanics*, pp. 303–312. Kluwer, Dordrecht.

Van de Vorst, E. L. B. (1996). *Long term dynamics and stabilization of nonlinear mechanical systems*. Ph.D. thesis, Eindhoven University of Technology, The Netherlands.

Van de Wouw, N., De Kraker, A., and Van Campen, D. H. (1997). Nonlinear phenomena in a stochastically excited dynamic system. In *Proc. 1997 ASME Int. Mechanical Engineering Congress and Exposition, Dallas (USA), DE-Vol. 95, AMD-Vol. 223, 16-21 Nov. 1997*, pp. 151–158. eds. W.C. Xie, N.S. Namachchivaya and O.M. O'Reilly.

Van de Wouw, N., Van den Bosch, H. L. A., De Kraker, A., and Van Campen, D. H. (1998). Experimental and numerical analysis of nonlinear phenomena in a stochastically excited beam system with impact. *Choas, Solitons & Fractals*, **9(8)**, 1409–1428.

Van Kampen, N. G. (1981). Itô versus Stratonovich. *Journal of Statistical Physics*, **24(1)**, 175–187.

Volterra, V. (1959). *Theory of functionals and of integral and integro-differential equations*. Dover Publications Inc., New York.

Wiener, N. (1942). Response of a nonlinear device to noise. MIT Radiation Laboratory Report 165, MIT.

Wong, E. and Zakai, M. (1965). On the relation between ordinary and stochastic differential equations. *Int. J. Eng. sci.*, **3(2)**, 213–229.

Wu, W. F. and Lin, Y. K. (1984). Cumulant-neglect closure for non-linear oscillators under random parametric and external excitations. *Int. J. Non-Linear Mech.*, **19(4)**, 349–362.

Yang, J.-N. (1972). Simulation of random envelope processes. *Journal of Sound and Vibration*, **21(1)**, 73–85.

Yong, Y. and Lin, Y. K. (1987). Exact stationary-response solution for second order non-linear systems under parametric and external white-noise excitations. *J. Appl. Mech. ASME*, **54**, 414–418.

Zadeh, L. A. and Desoer, C. A. (1963). *Linear system theory: the state space approach*. McGraw-Hill, New York.

Zhu, W. Q. (1988). Stochastic averaging methods in random vibration. *Appl. Mech. Rev.*, **41(5)**, 189–199.

Zhu, W. Q., Lu, M. Q., and Wu, Q. T. (1993). Stochastic jump and bifurcation of a duffing oscillator under narrow-band excitation. *Journal of Sound and Vibration*, **165(2)**, 285–304.

Acknowledgements

Hereby, I would like to thank the following persons for their contribution to this thesis:

- my supervisors Dick van Campen and Jan Kok for their faith in me and for the many fruitful discussions;

- my coach Bram de Kraker for his support and valuable comments during the past few years;

- Henk Nijmeijer, Douwe Overdijk and Malo Hautus for their help on the subjects of Volterra theory, spectral factorization and Itô calculus, respectively;

- Eric van den Bosch and Tinka Verhagen; their work has proven to be a valuable contribution to this thesis;

- Rob Fey and Remco Leine for their support on the subject of the path-following technique;

- Bert Verbeek and René van de Molengraft for their willingness to provide helpful reflections on parts of my work;

- my room-mates Ad Goijaerts, Niels Geerts, Marco Moens and Harold van Melick for their daily support on practical problems and especially for all the gibberish;

- Goswijn Simons for designing the cover-artwork;

- my girl-friend Dorien for her everlasting support and love; this has given me the energy to complete all this;

- my father, Kees van de Wouw, for all the inspirational talks, his open arms and breadth of mind;

- and last but not least, my mother, Mijntje Broeren, for her tremendous contribution to the person I have become.

Dorien, Kees and Mijntje, all three of you; thanks a lot for your unconditional faith, love and support.

Nathan van de Wouw,
Weert, July 1999.

Curriculum vitae

December 9th, 1970   Born in Eindhoven, The Netherlands.

1983-1989   Atheneum-B, Bisschoppelijk College, Weert.

1989-1994   Study Mechanical Engineering, Eindhoven University
of Technology.

1994-1999   Research assistant, Eindhoven University of Technology,
Department of Mechanical Engineering.